



Università
Ca' Foscari
Venezia

**Scuola Dottorale di Ateneo
Graduate School**

**Dottorato di ricerca
in Scienze Ambientali
Ciclo XXXII
Anno di discussione 2020**

***EVOLUZIONE TEMPORALE DEI FONDALI DI DUE
AMBIENTI MOLTO DINAMICI DEL NORD
ADRIATICO***

***SEAFLOOR EVOLUTION OF TWO HIGHLY
DYNAMIC NORTH ADRIATIC COASTAL SETTINGS***

SETTORE SCIENTIFICO DISCIPLINARE DI AFFERENZA: GEO/02

Tesi di Dottorato di Stefano Fogarin, matricola 829521

**Coordinatore del Dottorato
Prof. Enrico Bertuzzo**

**Supervisor del Dottorando
Prof.ssa Emanuela Molinaroli
Ph.D. Fantina Madricardo**

Abstract

The research of this PhD concerns the seafloor settings and short-time evolution of two highly dynamic coastal environments in the North Adriatic Sea (Italy): the Chioggia inlet in the Venice Lagoon and the Po river prodelta. In this thesis, I applied a semi-automatic and repeatable method to describe in detail the shallow water seafloors of these two valuable areas, which were partly unexplored before. Starting from multibeam echosounding (MBES) and ground truth data, I provide seabed morpho-bathymetry, substrate composition and benthic habitat mapping of the study areas. Although this methodological approach was designed specifically for these study areas, it can be applied to other shallow coastal environments. This work fits in the innovative benthic habitat mapping researches and can contribute to monitor and protect coastal regions and habitats as required by the European Marine Strategy Framework Directive (MSFD – EC 2008-56-EC).

Moreover, through the comparison of repeated morpho-bathymetric surveys over time I highlighted the changes of the seafloor geomorphology, sediment and habitat distribution. The interpretation of the assessed changes allowed me to highlight natural and human induced active coastal processes.

The Chioggia inlet is a highly human-altered tidal inlet and it has been strongly modified by the recent construction of the mobile barriers (MoSE), a project intended to defend the City of Venice and its lagoon from flood events (“Acqua Alta”). In the thesis, I document how these new hard structures are markedly influencing the inlet, modifying the water circulation and changing the sediment distribution. We found a diffused thick shell substratum in the inlet channel linked to the increased currents in the restricted section of the inlet. The same currents seem to be responsible for the migration of large dunes (up to 12 cm day⁻¹) and the shrinking of smaller dune fields over time. Another direct consequence of the human imprint is the formation of two large erosive depressions (scour holes) that we found around the new built breakwater (completed in 2006) that implied the erosion of about 476,000 m³ of seafloor sediments. These features are very active and almost doubled their extension from the first MBES survey in 2011 (62,500 m² and 35,500 m²) to the last in 2016 (105,100 m² and 61,700 m²), endangering the stability of the concrete structure itself. I finally mapped the seabed biocoenosis and documented the presence of a human-made hard-substrata habitat in correspondence of the breakwater and MoSE rip-rap revetments. This new

habitat hosts a diversified and structurally complex biological communities, in marked contrast with the adjacent soft-sedimentary habitats.

The asymmetric Po river prodelta shape depends on the Adriatic longshore current that sets a constant sediment transport toward south. On a smaller scale, this study document that the recognized morphological features (especially those in shallow water) underwent rapid shifts and alternating phases of construction/obliteration over a short period of time (2013-2016). These changes reflect the interplay between the river sediment discharge and the reworking action of the sea that contribute to sediment resuspension and dispersal. Except for a thick muddy sedimentary lobe deposited in the northern part of the study area after short-time flood events, we generally documented a lowering of the prodelta front. This deepening is only marginally due to the well-known subsidence. The presence of muddy sediments rich of water and organic content probably enhances the methanogenesis processes and the formation of collapse and gravity instability features.

Acknowledgments

Firstly, I would like to thank both my supervisors, Dr. Fantina Madricardo and Prof. Emanuela Molinaroli, for their support during my PhD studies and for giving me the opportunity to work independently on this interesting topic. I had the possibility to work in a competent and forefront research group that gave me the possibility to publish scientific papers increasing the current knowledge in coastal seafloor morphodynamics.

Thanks to Marco Sigovini and Luca Zaggia for their scientific guidance through all these years at the ISMAR - CNR, for the fruitful discussions and their help either at the last minute or from far distances.

Thanks to Giuliano Lorenzetti and Giorgia Manfé for their availability to answer at each my environmental/geological doubts. Thanks also to Alessandro Bosman, Aleksandra Kruss and all the other members of CNR for giving me the possibility to work with their data. Thanks to Flavia Visin, and the other scientists of DAIS laboratories, for their assistance during sediment analyses. Thanks for the welcoming and amicable atmosphere, which made it easier to start this new job experience.

I am also very grateful to the crew of the CNR research vessel Litus, for their skillful help during the survey, and to Loris Dametto for his technical help on the ground truth sampling.

Thanks to all my old-time friends and to the new ones who have been always on my side and helped me to distract from the heavy days.

A special thanks to my beloved Concetta for her love, support and faith in me through these years.

Finally, I want to thank my parents, my sister and all my relatives for their patience and constant encouragement. Words cannot express how grateful I am.

Preface

The research leading to the results of this cumulative thesis was conducted between September 2016 and September 2019 and is the outcome of a scientific collaboration between Ca' Foscari University and the Institute of Marine Sciences of the Italian National Research Council (CNR-ISMAR). Within the Italian National Flagship Project RITMARE, more than 25 CNR-ISMAR scientists, including the author of this thesis, contributed to acquire an extensive and high-resolution MBES datasets in the Venice Lagoon and in the Po di Pila delta between 2013 and 2016. These areas are very shallow and morphologically complex, causing challenges for traditional acoustic or optical surveys. Additional ground-truth surveys, composed of grab samples and underwater video collection, was performed to check the recorded acoustic data and cross-validate the results.

The thesis consists of a brief introduction, including an overview of the main goals and a characterization of the study areas, followed by the core dissertation consisting in three scientific studies. The first study was published in an international peer-reviewed journal and the third one is submitted and under review. The second paper is ready to be submitted. The thesis is then concluded with a chapter of summary discussions.

Contents

Summary

1. Introduction and background	1
1.1. General overview.....	1
1.2. Research objectives	3
1.3 Benthic Habitat Mapping and MultiBeam EchoSounder	4
2. Study area – North Adriatic Sea	9
2.1. Chioggia inlet (study I and II)	14
2.2. Po delta (study III).....	18
3. Study I: Tidal inlets in the Anthropocene: geomorphology and benthic habitats of the Chioggia inlet, Venice Lagoon (Italy)	23
3.1. Introduction.....	24
3.2. Geographical setting.....	26
3.3. Materials and methods	29
3.3.1. High resolution MultiBeam EchoSounder Data.....	29
3.3.1.1. Seafloor features	30
3.3.1.2. Backscatter classification.....	31
3.3.2. Ground-truth data	32
3.3.2.1. Sediment samples.....	32
3.3.2.2. Underwater images (Drop frames).....	32
3.4. Results	33
3.4.1. Bathymetry and seafloor features classification	33
3.4.1.1. Erosional features.....	34
3.4.1.2. Depositional Features.....	36
3.4.1.3. Anthropogenic features.....	38
3.4.1.4. Biogenic features	39
3.4.2. Ground truth samples analysis	39
3.4.2.1. Sediment grain size.....	39
3.4.2.2. Seafloor images	40
3.4.3. Backscatter classification.....	40
3.4.4. Backscatter classification accuracy.....	41
3.4.5. Benthic habitat classification.....	42
3.4.5.1. Class 1 – Coarse shell detritus	44
3.4.5.2. Class 2 – Sand with sparse shell detritus.....	45
3.4.5.3. Class 3 – Bare sand	45

3.4.5.4. Class 4 – Lagoon mudflat	45
3.4.5.5. Class 5 – Muddy sediment.....	46
3.4.5.6. Class 6 – Artificial rock bed	46
3.4.5.7. Class 7 – Seagrass meadow	47
3.4.6. Anthropogenic objects	47
3.5. Discussion	48
3.5.1. Tidal inlet seafloor features and sediment distribution	48
3.5.2. The anthropogenic impact on tidal inlet benthic habitats	52
3.6. Conclusions.....	56
3.7. References	58
3.8. Appendix.....	69
4. Study II: Bathymetric and backscatter data of seafloor change of the Chioggia inlet (Venice Lagoon) as a result of human intervention	74
4.1. Introduction.....	75
4.2. Study area.....	76
4.3. Material and Methods.....	78
4.3.1. Data acquisition	78
4.3.2. Ground-truth analysis.....	80
4.3.2.2. Surficial sediment samples	80
4.3.2.2. Underwater videos (Drop frames).....	80
4.3.3. Backscatter classification.....	81
4.3.4. Change assessment	81
4.3.5. Seafloor features analysis.....	82
4.4. Results	83
4.4.1 Bathymetric DEMs	83
4.4.2. Bathymetric change assessment and volume differences	84
4.4.3. Ground-truth analyses.....	87
4.4.3.1. Grain size	87
4.4.3.2. Drop-frames.....	88
4.4.4. Backscatter mosaics and classification	89
4.4.5. Backscatter change assessment	92
4.4.6. Seafloor features analysis.....	94
4.4.6.1. Scour holes	94
4.4.6.2. Dunes and dune fields	97
4.4.6.3. MoSE area.....	101
4.5. Discussion	102

4.6. Conclusions.....	108
4.7. References.....	109
4.8. Appendix.....	115
5. Study III: Short-term evolution of Po della Pila delta lobe from high-resolution multibeam bathymetry (2013-2016).....	120
5.1. Introduction.....	121
5.2. Data and methods.....	123
5.2.1. Multibeam data acquisition and processing.....	123
5.2.2. Seismic survey.....	127
5.2.3. Ground-truth data.....	127
5.2.4. Backscatter intensity classification.....	128
5.3. Results.....	128
5.3.1. Morphological characterization of Po della Pila submarine lobe.....	128
5.3.2. Morphological changes over time.....	131
5.3.3. Sedimentological characteristics of the submerged delta.....	134
5.3.3.1. Sediment grain sizes.....	134
5.3.3.2. Backscatter classification and sediment distribution changes over time.....	135
5.3.5. Seismic facies analysis of the delta front.....	137
5.4. Discussion.....	139
5.4.1. Distribution and variability of submarine morphological features in the 2013-2016 frame.....	140
5.4.2. Collapse and gravity instability features.....	142
5.5. Conclusions.....	143
5.6. References.....	144
5.7 Appendix.....	150
6. Discussion and conclusions.....	155
7. References.....	162
A. Appendix.....	176
A.1. Declaration of contributions.....	176
A.2. List of publications (not included in this thesis).....	177
A.3. Conference contribution as presenting author.....	178

Acronyms

AD	Anno Domini
ARPA	Agenzia Regionale per la Prevenzione e Protezione Ambientale
AVG	Angle Varying Gain
BC	Before Christ
BHM	Benthic Habitat Mapping
BP	Before Present
BPI	Bathymetric Position Index
BR	Bathymetric Residual
BS	Backscatter
BTM	Benthic Terrain Model
CNR	Consiglio Nazionale delle Ricerche
CVN	Consorzio Venezia Nuova
DEM	Digital Elevation Model
DGPS	Differential Global Positioning System
EC	European Community
FAO	Food and Agriculture Organization
GIS	Geographic Information System
GPS	Global Positioning System

IIM	Istituto Idrografico della Marina
IMAGE	Ingegneria Idraulica, Marittima, Ambientale e Geotecnica (Padova)
IPCC	Intergovernmental Panel on Climate Change
ISMAR	Istituto di Science Marine
MAV	Magistrato alle Acque di Venezia
MBES	MultiBeam EchoSounder
MESH	Mapping Seabed European Habitat
MoSE	Modulo Sperimentale Elettromeccanico
MRU	Motion Sensor Unit
MSFD	Marine Strategy Framework Directive
NOAA	National Oceanic and Atmospheric Administration
ROV	Remotely Operated Vehicle
RSLR	Relative Sea Level Rise
SAR	Synthetic Aperture Radar
SLR	Sea Level Rise
TPU	Total Propagated Uncertainty
WACC	Western Adriatic Coastal Current

1. Introduction and background

1.1. General overview

Since historical ages, coastal areas have played a crucial role in the human geography: they host an intense agriculture and industrial activity, dense population and several hard infrastructures (Elliot and Cutts, 2004). Littorals are also important environments because provide habitats of many organisms and support important biological, physical and chemical cycles that balance ocean and marine systems (Costanza et al., 1998; Barbier et al., 2011). About the 40-50 % of the world population resides at less than 100 km from the coasts, grouped into large cities such as Tokyo, Shanghai, New York, etc. (Crossland et al., 2005). In particular, estuaries and lagoon are the most productive environments (e.g. source of fishery), but are also among the most susceptible to anthropogenic influences (Chapman, 2012); they indeed constitute a particularly important place for human settlements and for the development of productive activities.

Studying the morphodynamics of seafloor bedforms can provide a better understanding of substrata composition and sediment transport pathways in littoral regions; this can help to recognize the active coastal processes and to identifying and mitigate the navigation hazards that are particularly important in tidal inlet which usually serve as commercial shipping channels (Bruun, 1986).

It is known that coastal lagoons and estuaries account for 13 % of the coastal zone worldwide (Kjerfve, 1994), but the associated human pressure on these habitats are not yet completely understood. The impacts indeed involve different sector of the environments (e.g. water column, soil, biota), transmitting each other at different velocities and for long distances (Knights et al., 2013). Several times, these impacts reflect on the morpho-bathymetry and the substrate composition of the seafloor (Madricardo et al., 2017); other times the benthic habitats are altered, losing its initial setting (Pister, 2009). Our ability to monitor and quantify these changes, such as the identification of the drivers that induce the modification, is central to understand the spatio-temporal behavior of the marine seafloors and the ecosystems (Montereale-Gavazzi et al., 2018). The complexity of the seafloor is a fundamental structural propriety of the benthic marine ecosystems (Lecours et al., 2016) and it has been demonstrated to be positively correlated with biodiversity (Ferrari et al., 2016). This complexity is far from being understood given that only the 0.05 % of seafloor of the ocean and about 5 % of the coastal and transitional environments have been mapped in high resolution (Blondel, 2010; NOAA, 2014). This is also very important to protect the ecosystem services, as indicates by the European Marine Strategy Framework Directive (MSFD

– EC 2008-56-EC) that consider the seafloor health an indicator of the “Good Environment Status”. Preservation of coastal ecosystems requires an understanding of the delicate equilibrium that these sites maintains during its existence (Filatova et al., 2011).

In this perspective, the study of the evolution of the seafloors is relevant to understand, not only the hydrodynamic circulation and sediment transport, but also the benthic habitat distribution. The recent development of innovative acoustic remote sensing techniques allows today to study the geomorphology, the textural sediment composition and the benthic habitats of the seabed, also in coastal areas with low depth and high turbidity. It has been observed that repeated morpho-bathymetric surveys over time can highlight the change of the seabed, in geomorphological, sedimentological and habitat distribution terms (Rattray et al., 2013; Fraccascia et al., 2016; Montereale-Gavazzi et al., 2018).

Today, these methodologies have been seldom applied in environments characterized by shallow waters (< 10 m depth), such as those typical of the North Adriatic Sea. In 2012, Hughes Clarke et al. (2012) as first applied multi-temporal MBES surveys to describe the temporal morpho-bathymetric progression of mass wasting events on the Squamish prodelta through several acoustic surveys. In 2016, Montereale-Gavazzi et al. (2016) applied, for the first time, similar methods to those adopted in this thesis in an extremely shallow tidal channel in the northern Venice lagoon (e.g. Scannello channel). Testing several clustering analyses, the authors classified automatically the backscatter to recognize biogenic features (such as sponges and macrophytes). Fraccascia et al. (2016) described the migration of small bedforms in a natural tidal inlet (Knudedyb). Mascioli et al. (2017) studied the subtidal sector of the southwest German Wadden Sea, introducing some morphometric codes to semi-automatic map the features of the seabed. Kruss et al. (2019) applied with success a procedure to identify macroalgae patches in a shallow water fjord of the Svalbard Archipelago. Homrani et al. (2019) analyzed the morphological evolution of shelly sand banks in a shallow water tidal system (South Brittany, France) through multiple acoustic surveys. All these researches however focus on a single aspect of the seafloor (e.g. backscatter signatures, bedforms migration, macroalgae coverage, submarine slides, etc.) whereas an integrate and interdisciplinary approach that considers all the seabed elements undertaken herein to fully define the environmental dynamics. The information collected in this PhD project can also be useful to integrate modeling studies: the high resolution data showed herein can be used to cross-validate the prevision of morphological and sedimentological evolution of seafloors in the short-term span.

1.2. Research objectives

The overall aim of this thesis is to understand the temporal evolution of the coastal seafloor of the North Adriatic Sea through repetitive acoustic surveys.

This thesis proposes a new approach to analyze the seafloor morpho-bathymetry, sediment and habitat distribution. Two study areas of the North Adriatic Sea have been selected to develop this method: the Chioggia inlet and the Po di Pila delta. These dynamic regions were analyzed with repeated bathymetric surveys to assess their spatio-temporal evolution in the short-term taking into account the hydrodynamics, geomorphological and ecological characteristics. The surveys were carried out with the latest MultiBeam EchoSounder (MBES) generation, a Kongsberg EM2040 Dual-Compact. Simultaneously, a ground-truth survey accompanied the recorded acoustic data with the collection of surficial sediment samples and underwater videos. Where available, satellite images were used to support the studies of emerged areas.

In order to test the thesis, several research goals were defined:

1. Describe in detail the properties of the seafloor in the study areas;
2. Qualitatively assess the change over time of seafloor morphologies and sediment distribution;
3. Understand the processes that induce these changes;
4. Develop of a semi-automatic, effective and repeatable method to study the shallow water coastal seafloors.

Study I: Tidal inlets in the Anthropocene: geomorphology and benthic habitats of the Chioggia inlet, Venice Lagoon (Italy). PUBLISHED in Earth Surface Processes and Landforms

The aim of this study is to investigate the Chioggia inlet seafloors with MBES survey, throughout the recognition of the main features (erosional, depositional, biogenic and anthropogenic) and the sediment distribution. A classification of benthic habitats and a mapping of the engineering structures have been performed. Finally, a possible interpretation of the anthropogenic alterations of the seafloor due to human pressures, especially the recent MoSE construction, has been proposed.

Study II: Bathymetric and backscatter data of seafloor change of the Chioggia inlet (Venice Lagoon) as a result of human intervention. READY TO BE SUBMITTED.

The aim of the second study is to analyze the changes in Chioggia Inlet seafloor during a span of 5 years. The evolution of the morpho-bathymetry such as the substrata variation have been studied, especially focusing on the main seafloor features (i.e. scour holes, dune fields). Development of a standard protocol to describe the evolution of a seafloor starting from multiple MBES datasets.

Study III: Short-term evolution of Po della Pila delta lobe from high-resolution multibeam bathymetry (2013-2016). SUBMITTED in Estuarine, Coastal and Shelf Science

The aim of the last study is to map the Po prodelta seabed (morpho-bathymetry and substrata composition) and its evolution during a time span of three years. A particular focus was given to the interpretation of the sedimentological features, also in relation of the Po river influence and the Adriatic meteo-marine conditions. The support of satellite images was used to define the changes of emerged areas and the prodelta mouth bar.

1.3 Benthic Habitat Mapping and MultiBeam EchoSounder

There are different definitions of habitat and there is no general agreement in the scientific community knowledge of the uniqueness of this term. In ecology, two main approaches are possible to describe the "space" used by a species or community.

1. Habitat as abiotic, including the physical characteristics of the substrate and the surrounding environment (such as the water column) or comprising the substrate of biotic origin (e.g. coral structures).
2. Habitat defined by the community itself which insists and/or characterizes it. This approach overlaps with similar concepts of community and biocoenosis.

The meaning introduced by the seabed mapping discipline is still different. It is mainly based on geological/sedimentological concepts and it focuses on "patterns on the seafloor", i.e. the patterns observed in the seabed using oceanographic tools, including physical sampling and remote sensing surveys (e.g. ROV). A possible standardize definition is "the physical and environmental conditions that support a particular biological community" (MESH, 2008).

In the terrestrial mapping, habitats are usually easily to recognize because dominated by vegetation or anthropogenic structures. Conversely, in the marine habitats the geomorphology and hydrodynamic are mixed together to define a particular habitat (Brown et al., 2011).

To produce an effective classification of these habitats it is necessary to apply Benthic Habitat Mapping (BHM) procedures. The BHM is a recent branch of the marine sciences, with multidisciplinary influences of geology, biology and ecology. It is defined as “representation of the distribution and extension of the habitats in the seabed and identification of the separation borders” (MESH, 2008). The objective of this mapping is a quantitative description of the submerged habitats, considering biotic (organisms, community, etc.) and abiotic (textural composition, morphology, etc.) components (Brown and Blondel, 2009).

The classification of the seabed can be performed visually, mechanically or acoustically (Kostylev et al., 2001). All visual (underwater videos/photos) and mechanical (grabbing, coring) methods are punctual, so they require a lot of time and energy to be performed. Besides, these solutions are not suitable to investigate large areas. Conversely, acoustic methods (SideScan Sonar, Single Beam and MultiBeam EchoSounder) can survey large areas in a short time, saving energy and money. The BHM permit to combine acoustic data with ground-truth data (i.e. collection of information in-situ), obtaining an effective classification and description of the seabed (Brown et al., 2011). Summarizing, the BHM process involves acoustic surveys, ground-truth sampling, data analyses and finally derivation of a descriptive model. This last step is generally performed with GIS software that permit an effective representation of the spatial data with thematic maps (Fig. 1).

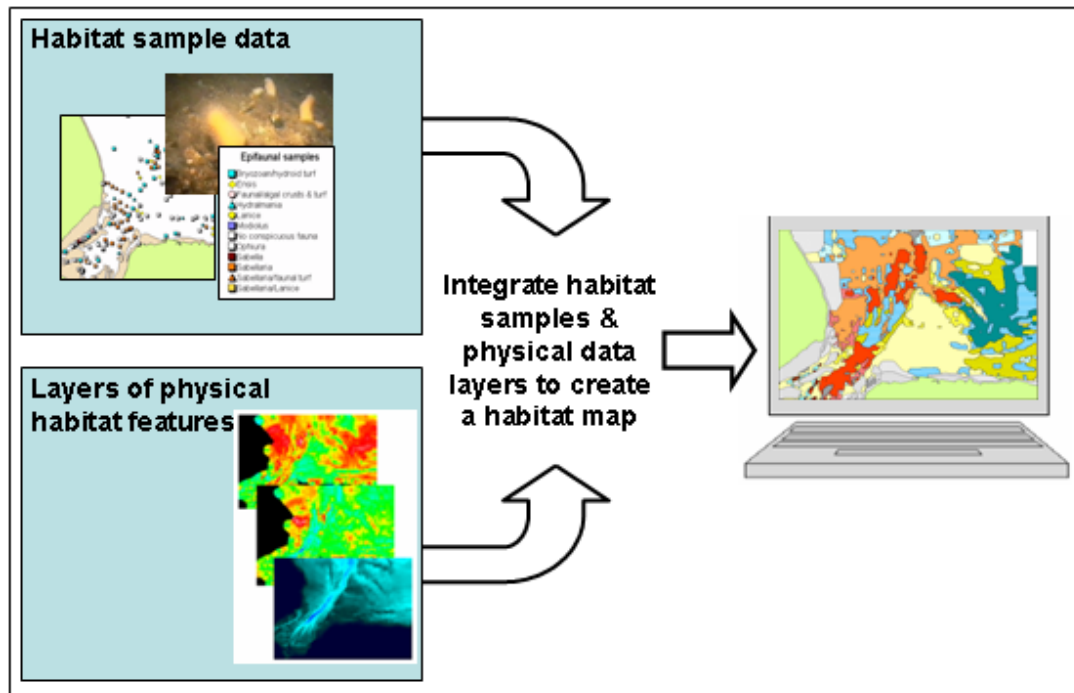


Figure 1: processing methodology for Benthic Habitat Mapping. Source: Foster-Smith et al. (2007).

The most effective solution to obtain continuous seabed information where the light does not penetrate is based on acoustic waves because they propagate well through the water column. The preferred instrument used to perform this task is the MultiBeam EchoSounder which can co-register simultaneously the morpho-bathymetry and the backscatter of the seafloor (Brown and Blondel, 2009).

The MBES is a sonar, i.e. an instrument that transmits acoustic waves towards the seabed and analyzes the returning signal (echo) reflected from the bottom or from other objects (fishes, submerged vegetation, etc.). Transducer and receiver are installed on vessel's hull, so the ship's position can be integrated into the data collection. With a differential position system (DGPS) and a motion sensor unit (MRU) the ship's motion can be recorded at the time of each pulse and a highly accurate bathymetric record can be produced. The MBES can collect continuous data from the seabed along a band (swath) of variable width depending of instrument setup and depth of investigated area. The MBES estimates the depth by producing an acoustic pulse and recording the time it takes for the signal to return to the receiver once it has been reflected from the seabed. The velocity of propagation of the sound depends from the density of the water (i.e. salinity, temperature and pressure) so a constant monitoring with a sound probe is required. The transducer ensonifies the seabed with a series of swaths perpendicular to the navigation motion and records the reflection echoes in a region parallel to the motion and perpendicular to the direction of the ensonification (Fig. 2).

Using the two-way travel time ΔT , the water sound velocity c and the incident angle Ψ , the water depth D at the across-track position for each sounding y can be calculated as follows (Jong et al., 2010; Lütjens, 2018):

$$D = \frac{1}{2} c \Delta T \cos \Psi$$

$$y = \frac{1}{2} c \Delta T \sin \Psi$$

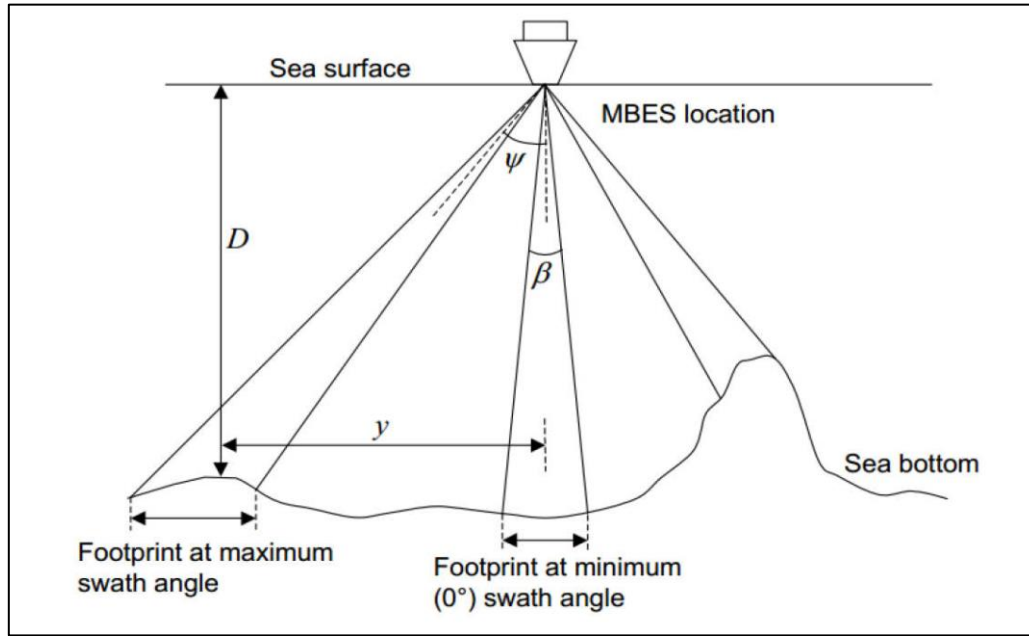


Figure 2: bathymetric measurement and footprint size depending on the swath. Source: Lütjens (2018).

The instrumental frequency influences the resolution of the data: typical frequencies used in the surveys range from 10 kHz to 400 kHz. It shall further be highlighted, that to achieve high accuracy, a high resolution as well as a narrow beam is needed. The higher the frequency, the shorter is the wavelength and the narrower the beam width. However, the higher the frequency the higher is also the absorption (Lurton and Augustin, 2010; Vandelli, 2013).

MBES do not only measure the travel-time of the sound waves to estimate the bathymetry, it also registers the intensity of the reflected signal (acoustic backscatter). When a sound pulse hits the seabed, most of the signal is scattered in all direction and some parts also penetrate into the substrata, depending on the impedance (Fig. 3). The signal with the highest strength that returns to the receiver is called backscatter (Lurton and Augustin, 2010). Each substrata type has a different acoustic impedance: the type of sediment (or rock) and its grain-size, roughness, compaction and slope define the acoustic response of the seabed (Lurton, 2003; Ferrini and Flood, 2006; Sutherland et al., 2007; Le Bas and Huvenne, 2009). Generally hard substrata scatter acoustic energy stronger than soft ones (Lucieer et al., 2013; Neves et al., 2014). Also, the biological coverage (underwater vegetation, megazoobenthos, etc.) can influence the signal of backscatter (Fonseca et al., 2002;

Urgeles et al., 2002; Holmes et al., 2008; De Falco et al., 2010; McGonigle and Collier, 2014; Monterale-Gavazzi et al., 2016). Acquiring backscatter information and classifying it into acoustic intensity classes, can therefore be used to study the seafloor characteristics and benthic habitats (Lurton et al., 2015).

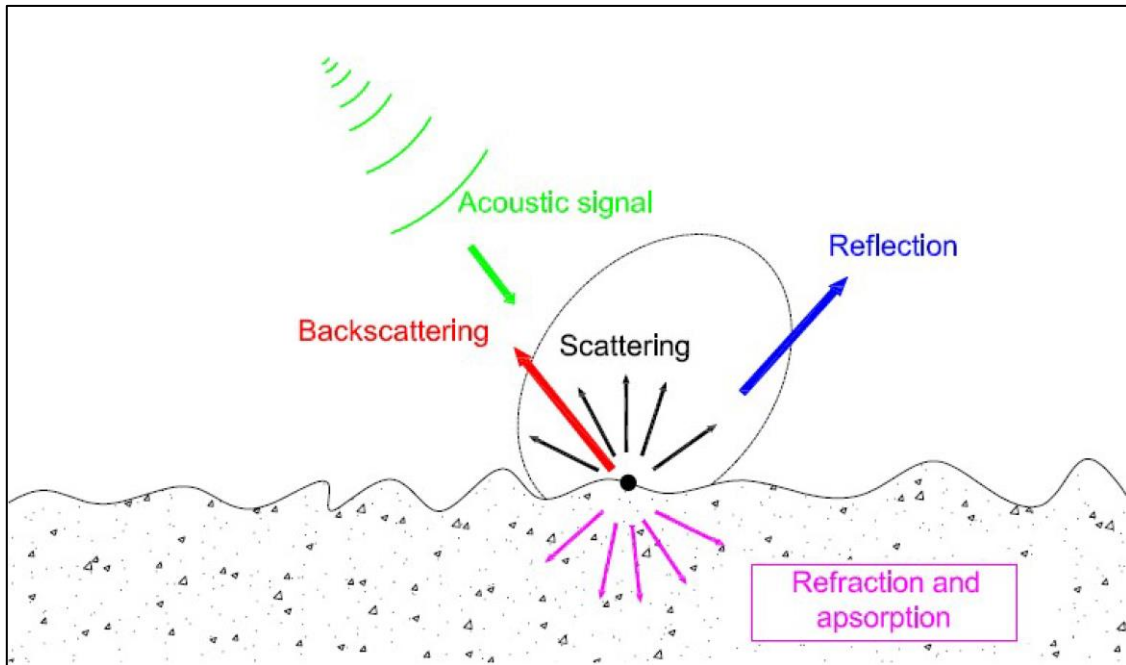


Figure 3: reflection and scattering of an incident acoustic pulse by a rough surface. Source: Pribičević et al. (2016).

In summary, the MBES is able to co-register bathymetric and acoustic backscatter data. The bathymetry is derived from the time that the acoustic signal takes to return to the receiver and describes the morphology of the seabed (morpho-bathymetry); the backscatter instead is a measure of the intensity of the retro-diffused beam and provides some information on the physical characteristics of the substrate.

2. Study area – North Adriatic Sea

The Adriatic Sea is a closed sea 800 km long and 150 km large. It is the northernmost part of the Mediterranean Sea, spreading from the Strait of Otranto (where it connects to the Ionian Sea) to the northeast Po Valley. Different countries have coasts on the Adriatic, such as Italy, Croatia, Slovenia, Bosnia and Herzegovina, Albania and Montenegro. The average's depth is 259.5 m and the maximum depth is 1,233 m (near Dubrovnik). The Adriatic Sea sits on the Adriatic Microplate (Apulian), which departed from the African Plate during the Mesozoic era (Battaglia et al., 2004). The plate's motion concurred to the rise of the neighbor mountain chains after its impact with the Eurasian plate (Weber et al., 2010; Zecchin et al., 2017). In the final part of the Oligocene, the Apennine Peninsula was created, separating the Adriatic basin from the rest of the Mediterranean (Zecchin et al., 2017). The main water fluxes of the Adriatic flow counterclockwise from the Strait of Otranto along the eastern coast and back to the Mediterranean along the Italian coasts (Artegiani et al., 1997): this southward current branch is known as Western Adriatic Coastal Current (WACC). The salinity is generally lower than Mediterranean's because the Adriatic receives about a third of the fresh water flowing into the Mediterranean (Artegiani et al., 1997). The water surface temperatures range from 30°C in summer to 12° in winter. There are several marine protected areas in the Adriatic, designed to protect the sea habitats and biodiversity (e.g. Tegnue di Chioggia, Delta del Po, Torre del Cerrano, Torre Guaceto, etc.). The sea hosts an abundant flora and fauna, with more than 7,000 species, some of which endemic and threatened (Coll et al., 2010).

Since historical ages, the Adriatic Sea has been a very important source of food for the neighbor countries and an important junction for trade, industry and touristic/recreational activities. Besides, their coasts are strongly populated, hosting more than 3.5 million of people and several important cities such as Venice, Bari, Trieste, Durrës, Split, etc. Consequently, the Adriatic Sea is a very impacted and anthropized sea, where management and administration of the waters and the coasts is a fundamental objective, especially in prevision of the global climatic change and mean sea level rise.

The Adriatic Sea is characterized by a very low-gradient profile in the northern and central part (about 40 m per 100 km) and by steeper gradients in the southern part (Correggiari et al., 1996). For this reason, the Adriatic is subdivided in three different sectors: north, middle and south (Fig. 4). The north basin is the shallower, rarely exceeding the depth of 100 m and it gradually deepens from

north to south. It extends between Venice and Trieste towards a line connecting Ancona and Zadar. This basin is the largest continental shelf of the entire Mediterranean.

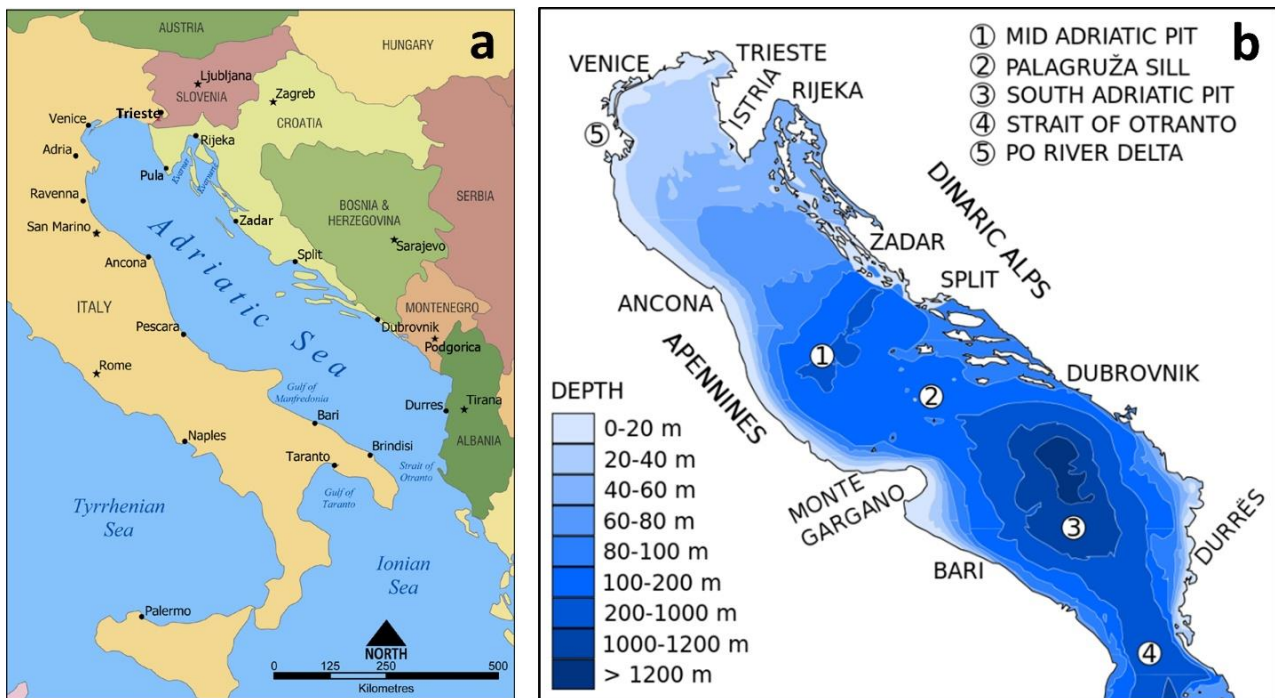


Figure 4: (a) eastern Italy and adjacent seas; (b) sub-division of the Adriatic Sea and its bathymetry. Source: FAO, 2012.

From the Italian coast to the open sea, the seabed is composed by a different sequence of sediments (Brambati, 1983). Close to the peninsula, the first encountered sediments are typically coastal sands (Frignani et al., 2005). The grain size ranges from fine to coarse sand. Moving away from the land, at a depth of about 8/10 m, a muddy belt surrounds the coasts (Brambati, 1983; Albani, 1998). These materials are particularly concentrated in the northernmost part of the basin (e.g. in front of Venice coasts). Toward the depth ≥ 20 m the seafloor is composed by relict sands formed during the last Adriatic post-glacial transgression when the water level was lower (Simonini et al., 2005). The relict sands have been intensely exploited during the last century for beach protection (Preti, 2000; ARPA Emilia-Romagna, 2002; Correggiari et al., 2012). Finally, the sediments return to be muddy toward south at depths of about 100 m (Brambati, 1983). Conversely the seafloor of the eastern part (Croatia) is terraced and rocky (Dinaric limestone).

The salinity of the North Adriatic is the lowest of the entire Mediterranean because of the high discharge of fresh water (Marini et al., 2010). The north basin indeed hosts some of the major Italian rivers, such as Po, Adige, Tagliamento, etc. All these rivers contribute to the transportation of sediments and nutrients in the sea, but also pollutants and litter (Cozzi and Giani, 2011).

Concerning the tides, four semidiurnal (M2, S2, N2 and K2) and three diurnal (K1, O1 and P1) constituents give a significant contribution to the evolution of sea surface elevation (see Book, 2009 for tide constituents' details), resulting in a mixed, mainly semidiurnal tidal regime. For the intrinsic characteristics of an elongated and enclosed basin, the tides in the North Adriatic result amplified respect with the Mediterranean Sea, reaching values up to 1 m (Malačić et al., 2000).

Considering the active tide increased by the sea level rise (SLR) the flood risks for the Italian coasts of the North Adriatic Sea are very high (Antonioli et al., 2017; Marsico et al., 2017), such as already demonstrated in the extreme flood event of November 1966. Most of the coastland regions indeed lays below the mean sea level and the territory is very sensitive to relative sea level rise (RSLR) due to land subsidence and eustatism (Tosi et al., 2016). In particular, some important cities, such as Venice and Ravenna, and valuable ecosystems, such as the Po delta and Marano-Grado lagoon, are extremely vulnerable (Fig. 5). For example, in the last decades the number of high water events (Acqua Alta) is increased causing several problems to the historical city of Venice (Gugliuzzo, 2018; <https://www.comune.venezia.it>).

Considering that SLR has been increasing at a rate of 1.2 mm/year (Carbognin et al., 2011), subsidence is the main component of the increased flood risk. Ground subsidence in the North Adriatic territory is caused by both natural and anthropogenic factors, acting on different time scales. The role played by natural causes includes tectonics, glacio-isostasy and compaction of alluvial fine-material deposits (Tosi et al., 2016), whereas the anthropogenic subsidence is the result of mainly groundwater withdrawal, activity largely conducted during the 19th century (Da Lio and Tosi, 2019). In this perspective, the policies and strategies for the safeguard of the littoral from the floods cover a fundamental role in the management of the territory.



Figure 5: the flood risk areas in the Italian territory in preview of the worst SLR scenario (updated map on July 2018). The entire northeast Italian littoral such as part of the Po Valley are clearly threatened by flood risk. Source: <https://www.enea.it>.

Inside the North Adriatic environment, two seafloors have been selected to be investigated: the Chioggia inlet and the Po di Pila delta. The two areas are located on the Veneto coast about 40 km from each other; they present similarities and differences and have been chosen for their academic interest which represents a challenge for remote sensing data acquisition. Primarily, both areas are shallow and very dynamic, changing their morphology in the times as witnessed by the numerous historical nautical charts available. These changes that often occur in the short-time span, can be effectively identified with repeated MBES surveys. If other coastal Adriatic areas had been selected, the seafloor evolution would not have been assessed with short-time surveys.

Secondly, both regions are characterized by complex sediment dynamics and are frequently interested by storm events. In the Chioggia inlet (and in the other inlets of Venice Lagoon) an important net sediment transport toward the sea has been attested in previously researches (e.g.

Amos et al., 2010; Defendi et al., 2010; Ferrarin et al., 2010; Villatoro et al., 2010). This transport, firstly driven by tide currents, means a general sediment loss in the lagoon basin. The Chioggia Inlet, such as the central-south Venice Lagoon and northern Venetian coasts, are indeed suffering a well documented erosion (e.g. Sfriso et al., 2005a; Pousa et al., 2007; Sarretta et al., 2010; Torresan et al., 2012) that is recently enhanced by human interventions. The Venice Lagoon has been subject to human pressures since historical times but from the second half of the last century their magnitude considerably increased (i.e. excavation of Malamocco channel, inlets' jetties modification, MoSE project construction, etc.). Conversely, in the Po delta the sediment dynamics are primarily driven by the river behavior. The frequently Po flood events are indeed responsible of the seabed features and sediment accumulation on the prodelta region (Correggiari et al., 2005; Stefani and Vincenzi, 2005). Sediment movimentation and bedforms migration are also governed by meteo-marine conditions which occasionally generate fast changes during strong storm events. Compare to the Chioggia inlet, the overall erosion of the region is uncertainty; Ninfo et al. (2018) showed even a deposition and progradation of the area. Moreover, the Po prodelta also differs from the Chioggia inlet because it is more natural and the human-induced seabed evolution is probably less relevant.

Both the Chioggia inlet and the Po di Pila prodelta lack of a morphological and sedimentological characterization of the seafloor, high-resolution data of morpho-bathymetry and bottom sediment distribution are neglected. The majority of the studies are related to test models, for example, several modeling researches focused on the morphological evolution (e.g. Cappucci et al., 2004; Simeoni et al., 2007 Ferrarin et al., 2008; Carniello et al., 2009), on the water circulation (e.g. Cucco and Umgiesser, 2006; Bellafiore et al., 2008; Ferrarin et al., 2010; Maicu et al., 2018) and on the sediment transport (e.g. Friedrichs and Scully, 2007; Ferrarin et al., 2010; Carniello et al., 2012; Carniello et al., 2014; Braga et al., 2017). The MBES and ground-truth data collected during this PhD project will be able to contribute to validate the accuracy of these modeling studies.

Finally, both regions are protected environments, hosting a high biodiversity and endemic species, and their protection is essential as indicates by the European Marine Strategy Framework Directive (MSFD – EC 2008-56-EC).

2.1. Chioggia inlet (study I and II)

The Chioggia inlet (45°13'54 "N, 12°18'3"E WGS84, geographic coordinates) is the southernmost inlet that connects the Venice Lagoon to the Adriatic Sea (Fig. 6). It has a maximum discharge of 5,000/6,000 m³/s and a tidal prism of 82 x 10⁶ m³ (Consorzio Venezia Nuova, 1989; Fontolan et al., 2007). The mean water current through the inlet channel varies with tide reaching a peak value of 0.5 ms⁻¹ during syzygy (Gačić et al., 2004). However, during extreme excursion of the water level driven by meteo-marine conditions (storm surges), the current speed increases up to 2 ms⁻¹ (Zaggia, personal communication).

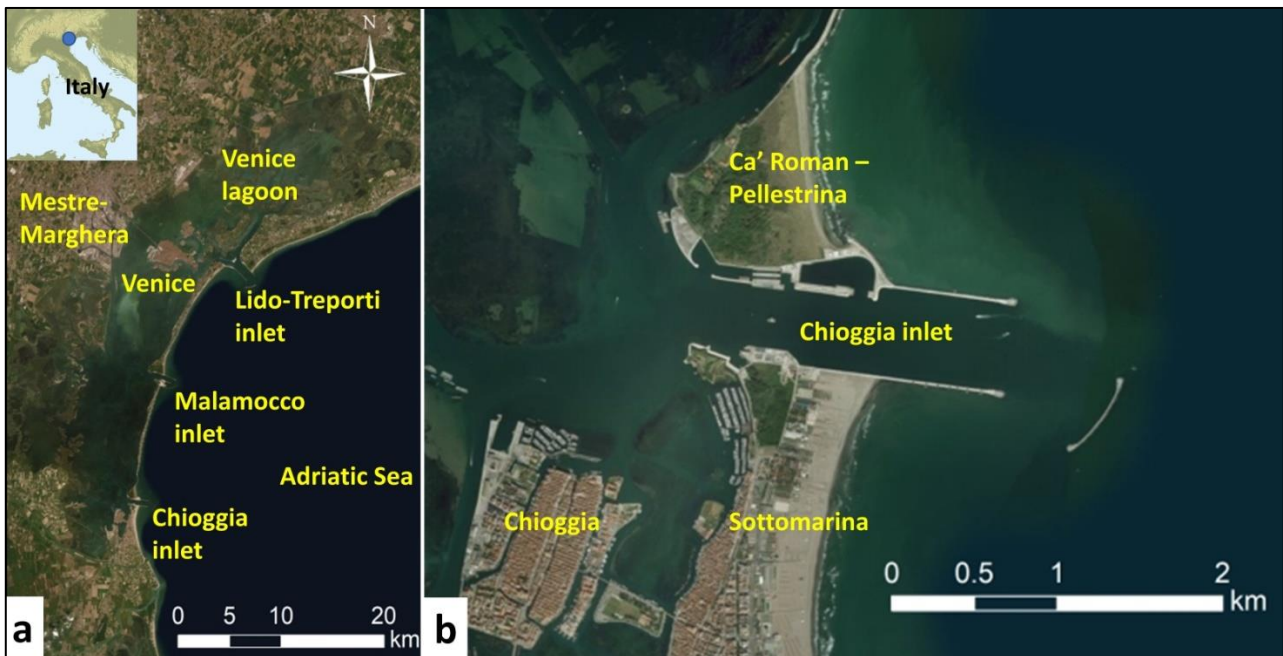


Figure 6: (a) the Venice Lagoon and its three tidal inlets; (b) the study area of Chioggia Inlet.

The Venice Lagoon, including the Chioggia inlet, has been influenced by anthropogenic pressures since historical times, dating as far back as 900 BP (Molinaroli et al., 2007). However, the significant human modification in the area started only in the 18th century, with the stabilization of the inlet by the construction of the jetties and the removing of the dunes in the adjacent beaches. These processes altered completely the natural regime that the Chioggia inlet had acquired (Zunica, 1971). The Chioggia inlet has the typical morphology of tidal inlets (Fig. 7), in agreement with Hayes (1980) and Smith (1984): there is an ebb-tidal delta with its terminal lobe, a central tidal channel that hosts the major flux exchanges and two lateral subaqueous spits that develop from the neighboring beaches. Previously studies did not recognize the flood-tidal delta in the Chioggia inlet, but during

our research we confirmed its existence (see study N.1). Conversely, the shape and composition of the ebb-tidal delta have been studied in the past (e.g. Zecchin et al., 2008; Villatoro et al., 2010).

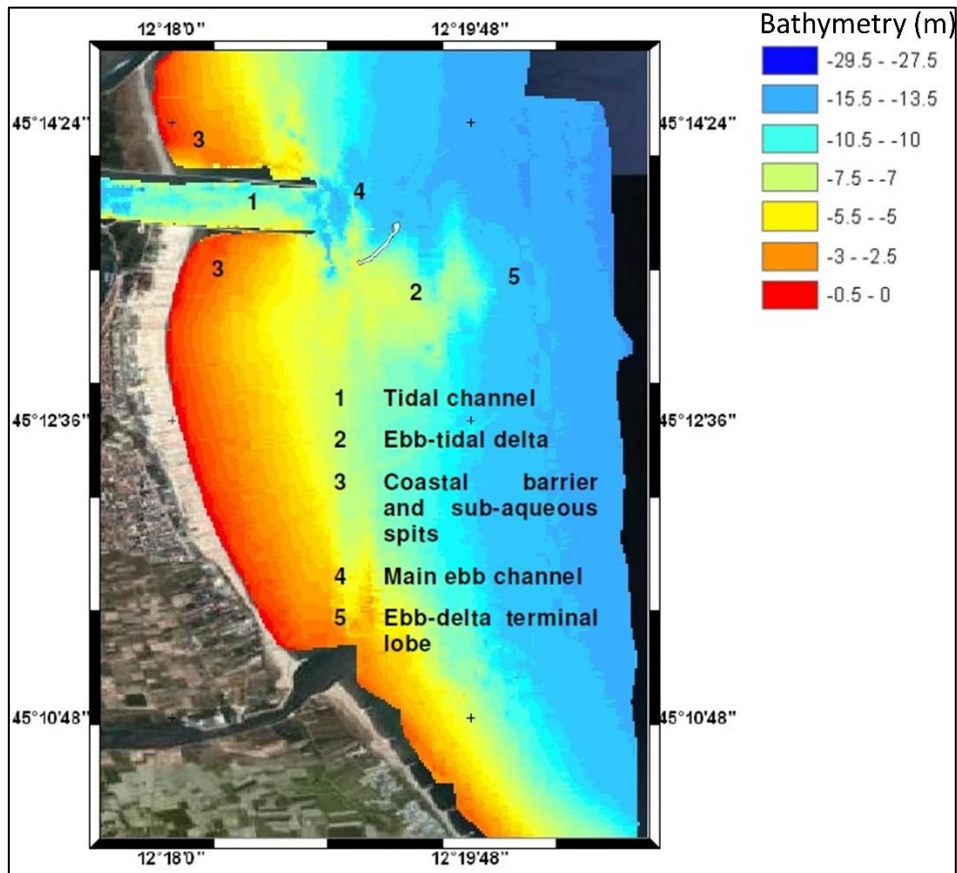


Figure 7: low-resolution morphology and physiography of the Chioggia inlet and Sottomarina littoral. Source: Villatoro (2010).

In this region, the water current circulation, such as the sources, the transportation and the deposition of sediments is very complex. The main current (and transport of sediments) observed at Sottomarina moves northwards, i.e. it has the opposite direction of WACC present generally in the North Adriatic (Brambati et al., 1978; Bellafiore and Umgiesser, 2010). This characteristic is due to the establishment of an anticyclonic movement for the presence of the inlet's jetties and the influence of the Brenta and Adige rivers that flow into the Adriatic with southwest-northeast outflows (Bellafiore and Umgiesser, 2010). Even the littoral sediment transportation gives an important contribution on the deposition nearby the inlet. The result is a progradation of the Sottomarina beach of about 9 m/year and an accretion of the subaqueous ebb-tidal delta of about 50,000 m³/year (Villatoro et al., 2010).

The region, such as the Veneto coast, is interested by winds from first and second quadrant (Bora and Scirocco). In particular, the bora propagates in the gulf of Venice with a front of 25 km, keeping its direction and velocity unaltered also after a path of 130 km (IMAGE, 2006). However, the

strongest storm surges, occur in presence of scirocco that causes an anomalous raising of the sea level, especially if in correspondence of baric and tidal summing conditions.

In the central-southern lagoon sub-basin, including the Chioggia inlet, the seafloor sediments are exclusively lagoon materials, mostly silt-sandy: the finer materials are found close to the internal margin, whereas coarse sands are present along the tidal channel and in the beaches of Sottomarina and Ca' Roman (Fig. 6). The mud content of the sediment in the inlet channel is commonly lower than 50 % (Molinaroli et al., 2007). The D50 of the sediment ranges between 100 μm and 400 μm (Villatoro et al., 2010). Bonardi et al. (2005) found that the southern part of the Venice lagoon (including Chioggia) is characterized by silicate-rich sediments.

To cope with the flood risks, the city of Venice started in 2003 the construction of the MoSE (Modulo Sperimentale Elettromeccanico), a project intended to protect the city of Venice and its lagoon by the high water events. The MoSE is an *“integrated system consisting of rows of mobile gates installed at the Lido, Malamocco, and Chioggia inlets that are able to isolate the Venetian Lagoon temporarily from the Adriatic Sea during acqua alta high tides”* (<http://www2.comune.venezia.it/mose-docprg>). Together with other interventions, such as the reinforcements of the coasts and the rise of the pavements and banks, the mobile barriers should defend the Venice Lagoon from tides of up to 3 m (sea level higher than 110 cm). After several delays, the project is expected to be fully completed in 2022. The MoSE consists of rows of mobile gates at the three inlets, Lido-Treporti, Malamocco and Chioggia from north to south, which can temporarily separate the lagoon from the Adriatic Sea during events of a significant high tide (Fig. 8). The number of gates depends on the section of each inlet (41 elements at Lido-Treporti separated by an artificial island, 19 at Malamocco and 18 at Chioggia) and each gate can be operated independently. The gates are composed of metallic hollow structures connected with hinges to the concrete housing installed on the seabed (Fig. 8). During normal conditions, the gates are full of water and sunk in their housing structures. When an extreme tide is forecast, the gates are filled with compressed air and they arise from the water rotating around the axis of the hinges, separating the lagoon from the sea. When the tide level returns to normality, the gates are filled again with water and returned to their housing. To guarantee the navigability in the port of Venice when the gates are operating, a refuge lock have been constructed in each inlet that permits vessel transit. Moreover, an arcuate breakwater (*“Lunata Frangiflutti”*) was built on seaside in each inlet to protect the MoSE gates from the waves during storms (Fig. 8).

The effects caused by the infrastructures to the surrounding seafloors and ecosystems have not yet been fully quantified and documented (Temmerman et al., 2013; Perkins et al., 2015).

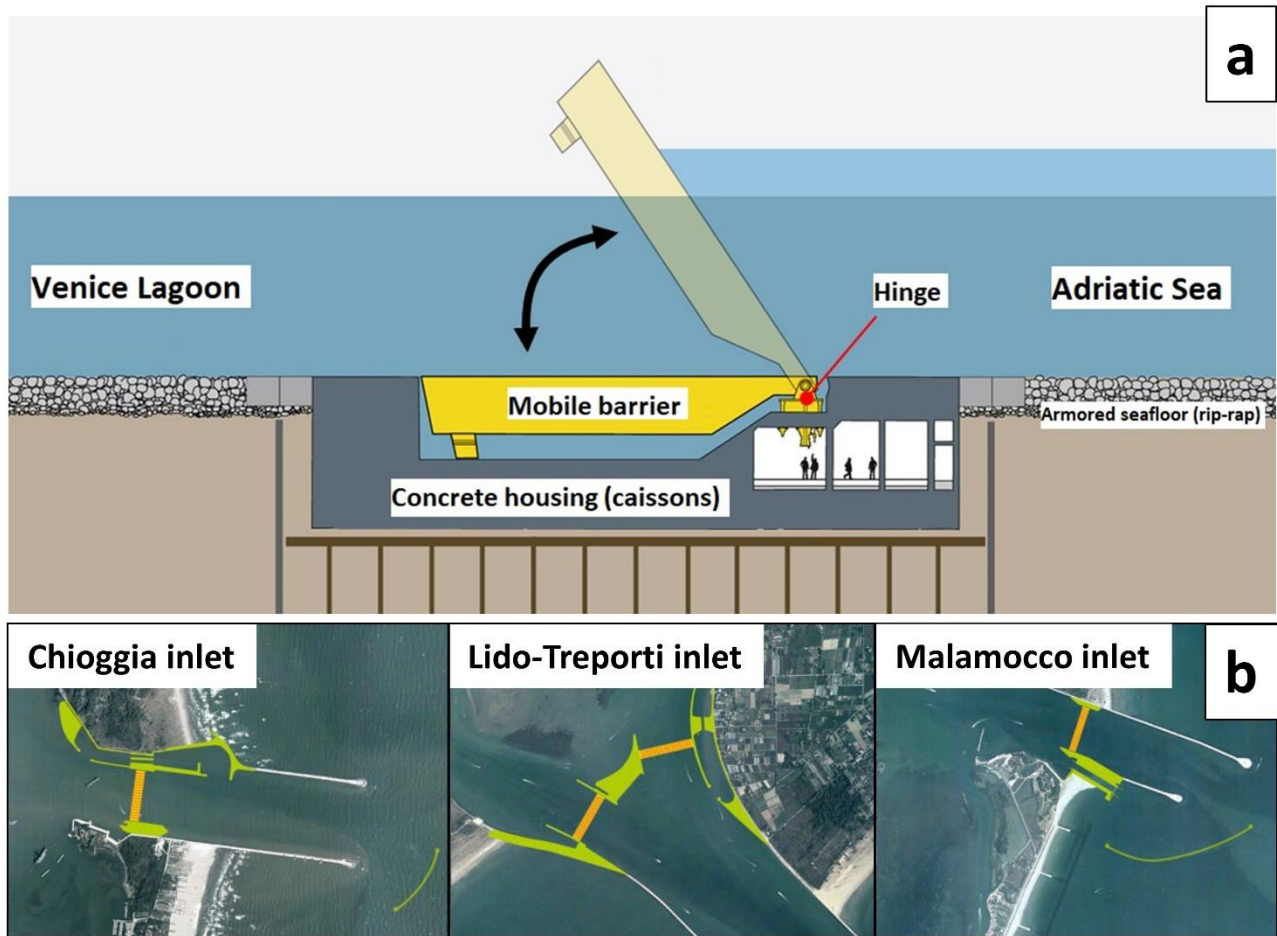


Figure 8: (a) the MoSE system functioning; (b) the modification introduced by the MoSE at the three inlets. It is possible to distinguish the MoSE trench, the refuge harbor, the changes at the jetties and the artificial island (only at Lido-Treporti). Source: <https://www.mosevenezia.eu>.

In the Chioggia inlet the MoSE works reduced the inlet cross-section from 500 to 350 m and the seafloor depth changed significantly due to dredging (Villatoro et al., 2010). So far, the MoSE project has required: (I) the construction of a 500 m long breakwater on the seaside, southeast of the inlet, (II) the reinforcement of the jetties, (III) the creation of a refuge harbor with a double navigation lock, (IV) the excavation of a 24 m deep and 50 m wide recess for hosting the mobile gates and their concrete housing structures, (V) the stabilization of the seabed near the recess with the deposition of stones and concrete artefacts and (VI) the dredging and deepening of the channels close to the inlet.

2.2. Po delta (study III)

The Po river is the longest Italian river (about 652 km) with a median flow of 1,540 m³/s and a total watershed of 71,000 km² (Syvitski et al., 2005). The Po originates in the western Alps, near the city of Cuneo, passes through the entire Po Valley and flows into the North Adriatic after a subdivision in five branches: Po di Maestra, Po di Pila, Po di Tolle, Po di Gnocca and Po di Goro (from north to south). According to Syvitski et al. (2005), Po di Pila is the major branch, transporting about the 61 % of fresh water and about the 74 % of sediment load to the delta. Almost 15 x 10⁹ kg / year of suspended sediment load flows into the sea (Catteneo et al., 2007), making the Po river the largest source of sediments of the entire Adriatic. The Po flows through many large anthropized areas, including the cities of Turin, Piacenza and Ferrara, and the same Po Valley hosts more than 16 million of people, about 1/5 of the Italian population. For this reason, the river is a high source of contaminants and litter to the Adriatic Sea.

The Po delta (45° 57' N, 12° 25' E, WGS84, geographic coordinates; Fig. 9) is the largest delta of the Adriatic Sea (about 180 km²), with the largest liquid and solid discharge (Amorosi et al., 2016). It is located at south of the Venice Lagoon between the city of Chioggia and Ravenna.



Figure 9: (a) the delta of the Po river and its terminal branches; (b) zoom on the Po di Pila delta (main branch).

Over the centuries the delta changed its shape and dimension (Fig. 10), incorporating several lobes built during the last 5,000 years (Amorosi and Milli, 2001; Trincardi et al., 2004). The entire Po system has indeed been under heavy human alteration for land use and freshwater management in historical time.

The growth rate of the delta is estimated on 47 m/year after 1886 AD, when the artificial straightened of the Po di Pila was realized to protect the plain from the floods (Visentini and Borghi, 1938). However, since the 1950, the delta was subject to a strong degradation and retreat, mainly due to the lack of sediment supply caused by channelization of watercourses and exploitation of the seabed (Stefani and Vincenzi, 2005). Only recently a restart of progradation for the northern part of the delta was hypothesized integrating satellite images and meteo-marine data (Ninfo et al., 2018).

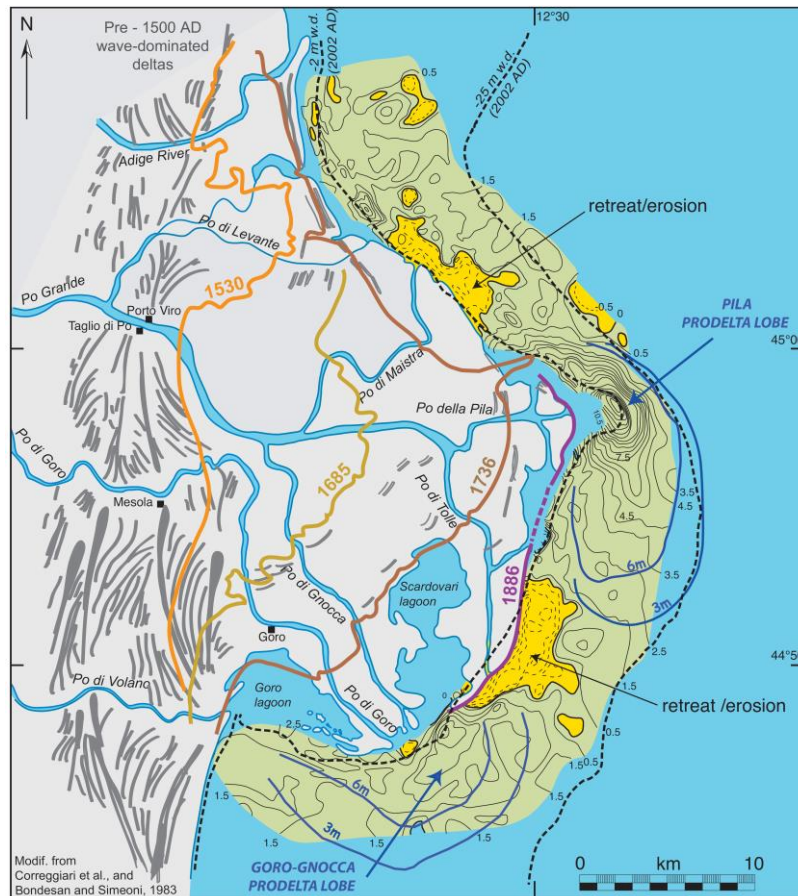


Figure 10: the map shows the main evolution phases of the modern Po delta. The coast lines were obtained with the comparison of bathymetry acquired in 1905 and 1953 (Bondesan and Simeoni, 1983). The yellow areas indicate net offshore erosion, whereas green ones indicate lobe construction. Source: Trincardi et al. (2004).

Besides the freshwater input, the circulation of water in the delta is also influenced by the Adriatic Sea littoral current, tidal cycles and winds. Due to the relatively low tide excursion, mainly winds, waves and WACC affect the dispersal of sediments (Trincardi et al., 2004; Friedrichs and Scully, 2007; Amorosi et al., 2016). The dominant winds, that generate the incoming waves, are the cold Bora, coming from northeast, and the warm Scirocco, coming from southeast (Orlić et al., 1994).

Today the modern delta is a multi-lobe, supply-dominated system, mainly driven by river discharge (Fig. 11), as opposed to the wave-dominated system of earlier periods (Trincardi et al., 2004).

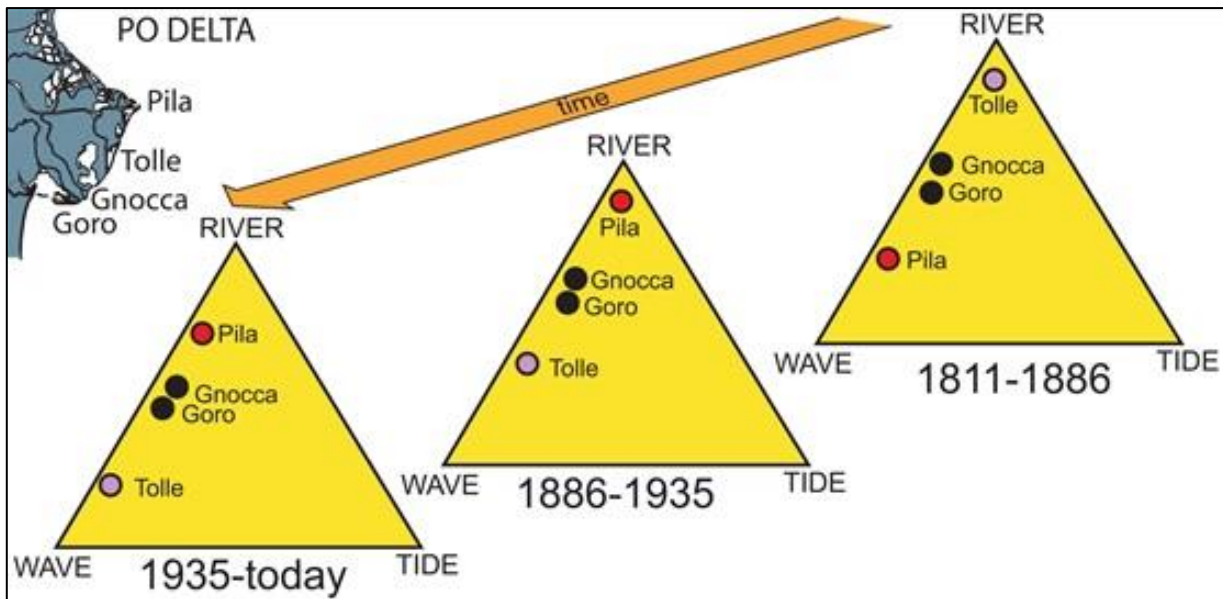


Figure 11: the main three factors influencing the major Po branches during the times. The Po di Pila delta changed its status from wave-dominated delta (1811-1886) to river-dominated delta (after 1886), likely due to anthropogenic intervention. Source: Trincardi et al. (2004).

The general lowlands of the Po region summed with subsidence make the area a high-risk flood region especially in view of SLR. The subsidence is very strong (rates up to -15 mm/year) and has a non-homogeneous spatial distribution in the last 25 years. It is due both to natural (e.g. sediment compaction) and anthropogenic (e.g. extraction of methane) factors. Although the subsidence is well documented for the subaerial Po delta (Tosi et al., 2016; Fiaschi et al., 2018) it is not completely understood for the submerged parts (i.e. prodelta). Antonioli et al. (2017), provided a relative SLR projection at 2100 for the region ranging from 594 mm to 1.4 m. These previsions show clearly the risks of flood in the area, requiring a continuous monitoring of the land and the artificial structures (jetties, piers, etc.).

The sediment distribution inside the Po delta region is very complex (e.g. Amorosi et al., 2003; Fox et al., 2004; Simeoni et al., 2007). Generally high-density sandy mouth bars prograde over fine-grained prodelta deposits, resulting in a coarsening-up grain size sequence. The type of sediment on the prodelta surface varies widely depending on the dispersal of the precipitation over the catchment (Tesi et al., 2013; Braga et al., 2017). The sediment pattern distribution is however not regular in the delta. Moreover, the morphologies and the sediments are continuously reworked by river diversion, meteo-marine drivers and anthropogenic activities (Trincardi et al., 2004; Maselli and Trincardi, 2013).

In general, the sands prevail above the 3 m isobath, such as in the neighboring beaches and over the mouth bar and spits (Simeoni et al., 2007). These beaches are continuously reshaped.

Conversely, the muddy sediments are present below the 8-m isobath. However, local deposits of fine materials are present on shallower waters due to flocculation (Braga et al., 2017). The sediment inputs are sufficient to contrast the erosive processes of waves, currents and tides, allowing an accumulation of mud up to the 4 m isobath close to the main distributary mouth (Fox et al., 2004).

3. Study I: Tidal inlets in the Anthropocene: geomorphology and benthic habitats of the Chioggia inlet, Venice Lagoon (Italy)

Stefano Fogarin^{1,2}, Fantina Madricardo², Luca Zaggia², Marco Sigovini², Giacomo Montereale-Gavazzi^{3,4}, Aleksandra Kruss², Giuliano Lorenzetti², Giorgia Manfé², Antonio Petrizzo², Emanuela Molinaroli¹ and Fabio Trincardi²

¹ Department of Environmental Sciences, Informatics and Statistics (DAIS), Università Ca' Foscari Venezia, Campus Scientifico, Via Torino 155, Mestre, VE, Italy

² Istituto di Scienze Marine-Consiglio Nazionale delle Ricerche, Arsenale - Tesa 104, Castello 2737/F, 30122 Venezia, Italy

³ Royal Belgian Institute of Natural Sciences, Operational Directorate Natural Environment, Gulledele 100, 1200 Brussels, Belgium

⁴ Renard Centre of Marine Geology, Department of Geology and Soil Science, University of Ghent

Abstract

Adopting a multidisciplinary approach, we mapped with unprecedented detail the seafloor morphology, sediment distribution and benthic habitats of a tidal inlet in the Venice Lagoon, Italy, which has been greatly impacted by human activity. Thanks to very high resolution multibeam data, we identified ebb and flood-tidal deltas, a tidal point bar, active dune fields, pools and scour holes. The seafloor substrate of the inlet was investigated by integrating automatically classified multibeam backscatter data with sediment samples and underwater seafloor images. The sediment composition comprises four textural classes with 75 % overall thematic accuracy. The particle size distribution of each morphological feature was assessed distinguishing, in particular, sediments over crests and troughs of small-dune fields with wavelengths and heights of less than 4 m and 0.2 m, respectively.

Adopting state-of-the-art benthic habitat mapping procedures, we found seven distinctive benthic habitats that reflect spatial variability in hydrodynamics and sediment transport pathways. The dominant classes were *Sand with sparse shell detritus* (46 %) and *Bare sand* (32 %). The rip-rap revetment used for the inlet jetties and for the hard structures, built in the inlet channel to protect

Venice from flooding, created a new habitat that covers 5.5 % of the study area. This study shows how combining geomorphological and ecological analyses is crucial for the monitoring and management of tidal inlets and coastal infrastructures.

Keywords: Tidal inlet, MultiBeam Echosounder, sedimentary dynamics, benthic habitat mapping, Venice Lagoon

3.1. Introduction

Coastal barrier systems are elongated coastal landforms, parallel to the shoreline that shelter lagoons from the open sea (Bird, 2008). They include marine deposits with shoreface, beach and sub-aerial dunes on the seaward side, and a back-barrier lagoon connected to the sea by one or more inlets. Coastal barrier systems fringe about 13 % of the world's coastlines (Bird, 1994; Kjerfve, 1994; Oertel, 1985; Bird, 2008) and are an important part of the world ecological heritage (Costanza et al., 1997; Luisetti et al., 2014). Historically, coastal barrier systems have played a crucial role in human geography: these sites usually host intensive agricultural and industrial plants, dense population and hard infrastructures (Gönenç and Wolflin, 2005).

Most of present-day coastal barrier systems formed early in the middle Holocene (8500-7500 yr BP) when a rapid sea level rise induced flooding of the continental shelves and the coast lines shifted landward approaching their current position (e.g. Stanley and Warne, 1994; Smith et al., 2011; Stutz and Pilkey, 2011; Hijma et al., 2012; De Haas et al., 2018). These systems reflect a complex interaction between the local geological and physiographic structure, sea-level variations and tidal currents, sediment availability and sediment dispersal processes (Fruergaard et al., 2015). Understanding the evolution of coastal barrier systems is the key to predicting coastal adaptation to future sea level rise and, more generally, to climate change (Miselis and Lorenzo-Trueba, 2017; Moore and Murray, 2018).

In the recent evolution of coastal barrier systems human interventions often play a major role inducing rapid morphological changes (Williams, 2013; Miselis and Lorenzo-Trueba, 2017). This anthropogenic forcing can radically shift the dynamics that the system would normally follow under natural conditions (Oost et al., 2012).

Humans are altering the planet, including long-term global surface geologic processes, in such a way that a new geological epoch called the Anthropocene has been introduced, although still waiting to be officially recognized (Hamilton, 2016; Finney and Edwards, 2016). While the study of land-use changes in the Anthropocene has considerably advanced (Tarolli et al., 2014; Brown et al., 2017), much less is known about the human impact on the seafloor, particularly in coastal areas (Madricardo et al., 2019).

In this work, we investigate in detail the seafloor morphology of a tidal inlet and the impact induced by recent human modifications. Inlets play a key role in the evolution of coastal barrier systems (Kjerfve, 1994; Tambroni and Seminara, 2006; De Swart and Zimmermann, 2009; Reddy et al., 2015) given that they: (i) control hydrodynamics, i.e. the rate of water exchange which influences the chemical-physical properties of the lagoon; (ii) are responsible for the sediment transport from the lagoon to the open sea and vice versa; (iii) affect the morphodynamics of the adjacent coast; (iv) allow the migration of different species at different life stages. In addition, tidal inlets are often subject to intense maritime traffic and human modification.

We focus on the Venice Lagoon (Italy), the largest lagoon of the Mediterranean, surrounding the historical city of Venice. This lagoon has undergone strong changes in the Anthropocene era and can be considered as a “human-oriented ecosystem” (Cima and Ballarin, 2013). In the Venice Lagoon, the shift from the Holocene to the Anthropocene social-ecological system states (as defined in Renaud et al., 2013) could be set at the time of Serenissima Repubblica of Venice (starting from the end of 7th century), when the urbanization and regulation of the lagoon environment radically modified its natural evolution. To avoid its silting up, the major rivers flowing into the lagoon were diverted between the 12th and 19th century.

The natural inlets were radically reshaped by the construction of long jetties between 1808 and 1933 (Fontolan et al., 2007; Balletti et al., 2006). They were dredged and deepened from 5 m to 15 m with a consequent increase in tidal flow and erosive processes in the whole lagoon (Gatto and Carbognin, 1981; Tambroni and Seminara, 2006). The still ongoing construction of a system of mobile barriers at the lagoon inlets during the past 15 years (the MoSE Project, Ministero dell’Ambiente-Magistrato alle Acque, 1997) is one of the major engineering interventions at the inlets. These barriers have been built to defend the city of Venice and the other islands in the lagoon from extreme flood events (see Trincardi et al., 2016 for the background). The mobile barriers represent a paradigmatic example of grey infrastructure in response to flooding in view of global

mean sea level rise (Temmerman et al., 2013; Perkins et al., 2015). The changes caused by grey infrastructure to surrounding ecosystems have not yet been fully quantified and documented in most cases all over the world (Powell et al., 2018).

In this study we provide not only a very high resolution mapping of a tidal inlet seafloor morphologies and habitats, but we also quantitatively assess the most recent physical changes (e.g. morpho-bathymetry and sedimentary dynamics) induced by the construction of the mobile barriers and their impact on the tidal inlet habitats. This work aims to increase the knowledge about the benefits or unintended negative impacts of grey infrastructures in view of the knowledge-based management coastal zones.

3.2. Geographical setting

The Venice Lagoon is about 50 km long and 8-14 km wide, with a surface area of about 550 km² (Fig. I1). It is separated from the Adriatic Sea by a system of barrier islands aligned in a NE-SW direction and exchanges water with the sea through three inlets: Lido, Malamocco and Chioggia (from north to south).

The lagoon has a mean depth of about 1.2 m, with only 5 % of its area deeper than 5 m (Molinaroli et al., 2009). The area includes shallows, tidal flats, channels and canals, salt marshes, islands, fish ponds, and reclaimed areas. The main navigation channels are up to 20 m deep. The deepest point of the lagoon is close to the Malamocco Inlet where the bottom reaches a depth of 48 m (Madricardo et al., 2017). Inside the inlets the water velocities can be more than 1 ms⁻¹ (Gačić et al., 2004).

The Venice back-barrier system started to form during the Holocene marine transgression that reached the southern Venice area from 8000 to 9000 yr BP and the central-northern lagoon sector from 5000 to 6000 yr BP (Tosi et al., 2007; Zecchin et al., 2009; Zecchin et al., 2014). Fluvial, back-barrier, deltaic, shoreface and tidal channel deposits characterize the Holocene sequence in the Venice Lagoon forming a transgressive-regressive cycle (Zecchin et al., 2008; Zecchin et al., 2009).

The Venice Lagoon is a microtidal environment (mean tidal range less than 1 m) and it can be considered a “restricted” lagoon (as defined in Kjerfve and Magill, 1989), where tide and wind are the main forcing factors of circulation. Four semidiurnal (M2, S2, N2 and K2) and three diurnal (K1,

O1 and P1) tidal constituents give a significant contribution to the evolution of sea surface elevation in the North Adriatic Sea (Book et al., 2009), resulting in a mixed, mainly semidiurnal tidal regime. The tidal wave propagates from the three inlets into the lagoon along the network of tidal channels eventually reaching the tidal flats and marshes.

The lagoon has been subjected to anthropogenic modifications since historical times, dating as far back as 900 BC (Molinaroli et al., 2007). Without human intervention, the lagoon would have gradually silted up by the river sediment deposition. Therefore, starting from the 12th century the main tributaries were diverted directly into the sea (Cavazzoni, 1995; D'Alpaos, 2010; Madricardo and Donnici, 2014). Whereas during the times of the Serenissima (697-1797) the silting process dominated, a strong erosive process took place in the last century and particularly between 1970 and 2000, following the dredging of a large navigation canal from the Malamocco inlet (Fig. I1) to the industrial harbor, the lagoon morphology changed dramatically due to the erosion of salt marshes and to the overall deepening of the tidal channels (Sarretta et al., 2010; Madricardo and Donnici, 2014). The lagoon, particularly in its central area, is gradually assuming the characteristics of a semi-enclosed marine embayment (Carniello et al., 2009; Molinaroli et al., 2009; Sarretta et al., 2010) and a quarter of the lagoon habitats has been lost with a consequent change in the ecological functionality of the environment (Favero, 1991; Elliot and Cutts, 2004).

The recent construction of the MoSE structures (an acronym for *Modulo Sperimentale Elettromeccanico* or Experimental Electromechanical Module from name given to the earliest prototype built to test the functionality of the mobile barriers) at the inlets could substantially affect the lagoon environment by reducing the tidal exchange and increasing the ebb-dominance over tidal flats (Tambroni and Seminara, 2006; Ghezzi et al., 2010; Ferrarin et al., 2015). The mobile barrier project will prevent flooding through the installation of 78 mobile gates, laying at the bottom of the inlet channels (Lido, Malamocco and Chioggia) connecting the Venice Lagoon from the Adriatic Sea. The construction works started in 2003 and it is currently expected to be completed within 2020-2022.

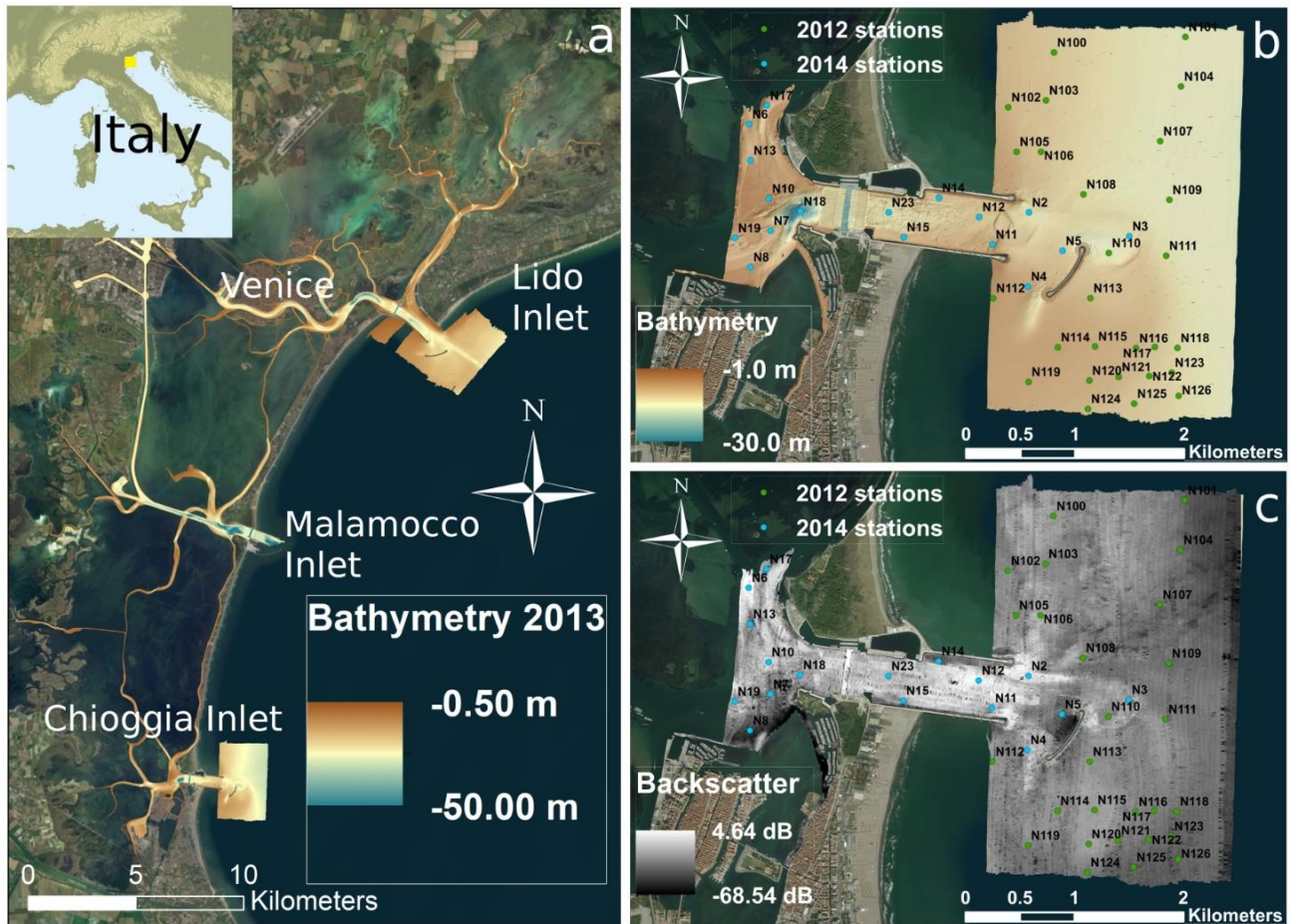


Figure I1: (a) The bathymetry of the tidal channels and inlets of the Venice Lagoon collected during the CNR ISMAR survey in 2013 (Madrcardo et al., 2017); (b) the bathymetry of the Chioggia inlet with the location of the sampling stations for 2012 (green) and 2014 (light blue); (c) the backscatter mosaic extracted from the multibeam data.

The Chioggia inlet

The Chioggia inlet (45°13'54 "N, 12°18'3"E WGS84, geographic coordinates) is the southernmost inlet of the Venice Lagoon and has a tidal prism of $82 \times 10^6 \text{ m}^3$ (Consorzio Venezia Nuova, 1989; Fontolan et al., 2007). The mean water discharge through the inlets varies with tide and current speed reaching a peak value of 0.5 ms^{-1} during tidal phase syzygy (Gačić et al., 2004). Extreme excursion of the water level driven by meteo-marine conditions (storm surges) can cause the current speed to increase up to 2 ms^{-1} .

This inlet has undergone numerous human interventions during historical time. The most evident changes have started in 1912 with the construction of jetties, that were modified again in 1950. The recent works for the construction of MoSE that started in 2003 and are still ongoing reduced the inlet cross-section from 500 to 350 m and the seafloor depth changed significantly due to dredging (Villatoro et al., 2010).

So far, the MoSE project has required: (I) the construction of a 500 m long breakwater on the seaside, southeast of the inlet, (II) the reinforcement of the jetties, (III) the creation of a refuge harbour with a double navigation lock, (IV) the excavation of a 24 m deep and 50 m wide recess for hosting the mobile gates and their concrete housing structures, (V) the stabilization of the seabed near the recess with the deposition of stones and concrete artefacts and (VI) the dredging and deepening of the channels close to the inlet.

3.3. Materials and methods

3.3.1. High resolution MultiBeam EchoSounder Data

The acoustic data in the Chioggia Inlet (survey area of about 10 km²) were collected in October and November 2013 (about 4 weeks of work) by the Institute of Marine Science of National Research Council (ISMAR-CNR) using a Kongsberg EM2040 Dual-Compact MultiBeam Echosounder (MBES) pole-mounted on the CNR research boat Litus, a 10 m long vessel with a draft of 1.5 m. The MBES has 800 beams (400 per swath) and during the survey, the frequency was set to 360 kHz. A Seapath 300 system with the supply of a Fugro HP differential Global Positioning System (DGPS) automatically registered the ship positioning (0.2 m accuracy). For the correction of pitch, roll, heave and yaw movements the Kongsberg motion sensor MRU 5 and a Dual Antenna GPS integrated with the Seapath was used. Sound velocity was continuously measured by a Valeport mini SVS sensor, attached close to the transducers.

CARIS HIPS and SIPS software (v.7 and 9.1) was used for processing MBES data considering sound velocity, tide corrections and manual quality control tools. The bathymetry was created with a raster resolution of 0.5 m using the Swath Angles Weighting option with a Max Footprint size of 9 × 9. The data are referred to the local datum 'Punta Salute 1897', 23.56 cm lower than the national vertical level datum (IGM1942).

The map of the seafloor (backscatter intensity) was created using the software Fledermaus (v7.0) with a resolution of 0.5 m after applying the Angle Varying Gain (AVG) correction to the raw data to remove the angular artifacts of sediment. The bathymetric and backscatter data were then exported as a 32-bit raster files and imported in ArcGis (v10.2) for further analysis (ESRI, 2016).

3.3.1.1. Seafloor features

From the digital elevation model (DEM) obtained from the MBES bathymetric data, we computed in ArcGis the main terrain attributes (Lecours et al., 2017a; Lecours et al., 2017b): slope, broad Bathymetric Position Index (BPI) and Ruggedness. The BPI and ruggedness were calculated with BTM (Wright et al., 2005) with BPI inner and outer radius of 750 and 50 respectively and ruggedness radius of 11. The results are collected in Appendix.

The seafloor features were first manually segmented and then automatically classified using terrain attributes, taking into account the process that generates them (Fig. 12): (i) erosional features (identified by BPI), (ii) depositional features (identified by ruggedness and backscatter), (iii) anthropogenic structures (rip-rap identified by ruggedness and backscatter and dredging areas by BPI) and (iv) biogenic features (identified by ruggedness). Most of the features are recognizable in the DEM, but some morphologies show a characteristic signature also on the backscatter mosaic.

3. Study I: Tidal inlets in the Anthropocene: geomorphology and benthic habitats of the Chioggia inlet, Venice Lagoon (Italy)

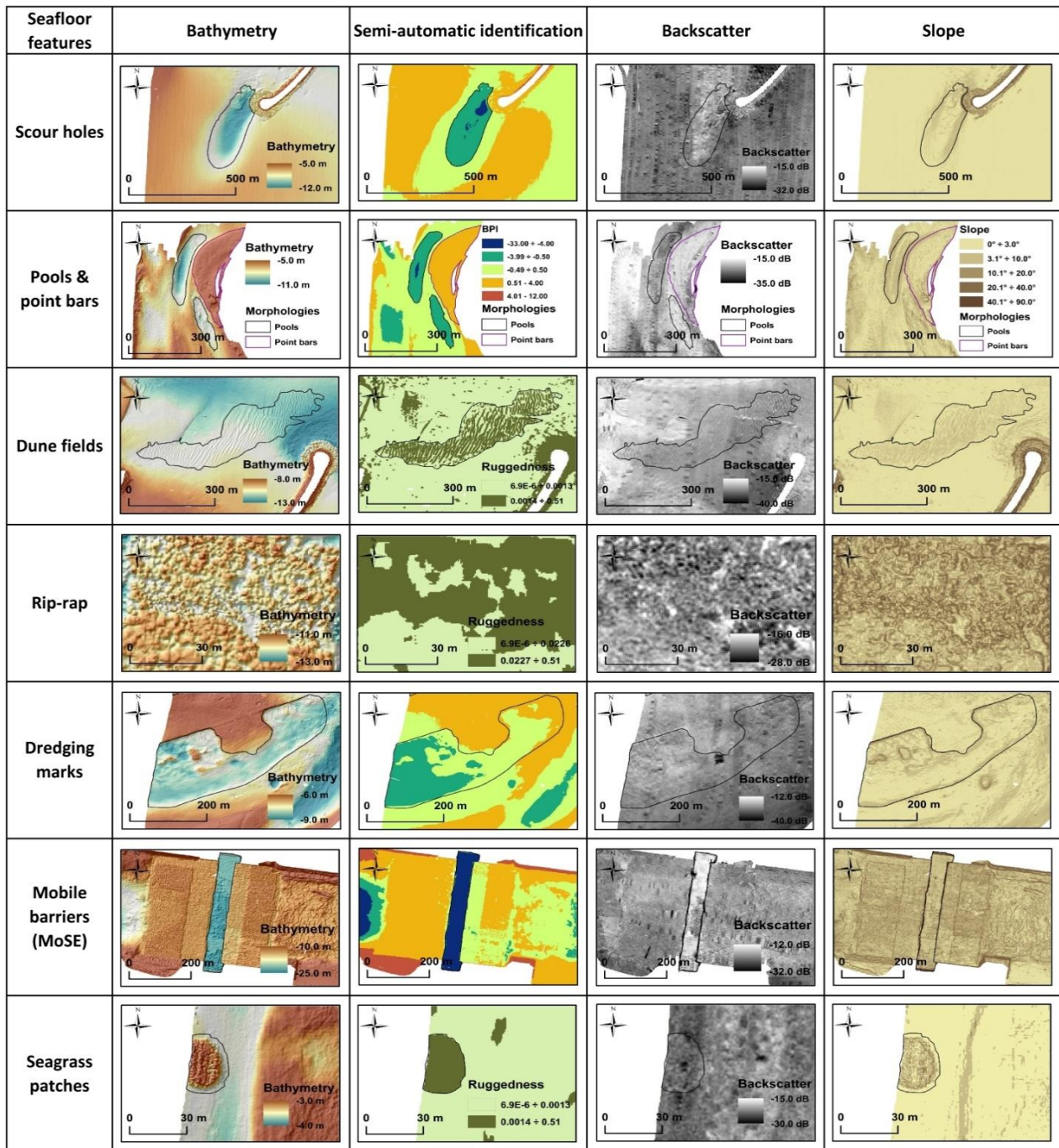


Figure 12: Classified morphologies with their bathymetry (first column with five times vertical exaggeration), with the terrain attribute used for the semi-automatic identification (second column); their backscatter mosaics (third column) and their slope (fourth column).

3.3.1.2. Backscatter classification

Several approaches have been proposed to identify sub-regions with homogeneous surficial composition from the analysis and segmentation of the seafloor backscatter intensity maps (e.g. Brown et al., 2011; Diesing et al., 2014; McGonigle and Collier, 2014; Ierodiaconou et al., 2018). In this study, Jenks' optimization method was used to classify the backscatter data. This method

provided good results in a previous study in the Venice Lagoon (Montereale-Gavazzi et al., 2016). The Jenks' Optimization clustering is an automatic tool implemented in ArcGIS to classify rasters. Given a defined number of classes, the method seeks to reduce the variance within classes and maximize the variance between classes (Jenks, 1967).

3.3.2. Ground-truth data

The main goal of ground-truthing is to characterize the seafloor and validate the maps produced with the MBES acoustic data by means of direct observations. In this study, the ground-truth dataset includes surficial sediment grab samples and underwater images from drop-frame camera.

3.3.2.1. Sediment samples

A total of 44 surficial sediment samples were collected with a Van Veen Grab (5 L) in two different campaigns. The most recent samples were collected in April 2014 (named N2-N23); the locations were selected to include all the characteristic textural patterns identified within the backscatter data. To cover all the study area, we added additional 27 sediment samples collected in March 2012. These latter are located at the seaside, arranged in a regular grid and named from N100 to N126. All samples were classified according to the Folk et al. (1970) method using Gradistat statistical package (Blott and Pye, 2001) after dry sieving (16 mm to 38 μ m).

3.3.2.2. Underwater images (Drop frames)

The underwater images were sampled during a survey carried out on January 2015 at 20 stations by means of a drop-frame camera (3 replicates for each station). The device consisted of an action camera (Go-Pro HERO-3) and underwater lights installed on an aluminum frame, which were easily dropped from the vessel. The underwater images were collected on the same points of a subset of April 2014 sediment samples. Some additional stations were chosen to investigate particular seafloor features (e.g. seagrass patches, rip-rap seabed, etc.).

Representative still images (22.5 x 30 cm) were extracted from each recorded video and characterized in terms of biotic and abiotic features. Epimegabenthos (both living specimens and empty shells) were identified and counted. A total of 60 images were analyzed.

3.4. Results

3.4.1. Bathymetry and seafloor features classification

The measured bathymetry ranges from -30 m to -1 m (Fig. I3). The shallower areas (depth less than 2 m) are located inside the lagoon, near the harbor of Chioggia and the mudflats located in south-west part of the survey area. The deepest areas are within a large scour hole (with maximum depth of 30 m) located at the western entrance of the inlet channel (see also Ferrarin et al., 2018). The inlet channel depths vary from -14 m to -9 m. The south-east part of the inlet channel is shallower and characterized by the presence of a sand deposit.

The seabed of the study area is predominantly flat or gently sloping: generally, the slope has a constant value of 1° , increasing up to 20° on the lee side of the largest dunes. Only scour holes and coastal defense structures show larger gradients up to 30° and 80° , respectively (slope map in Appendix). By the combined analysis of the MBES and ground-truth data, seabed features were classified in: erosional, depositional and biogenic (Fig. I3).

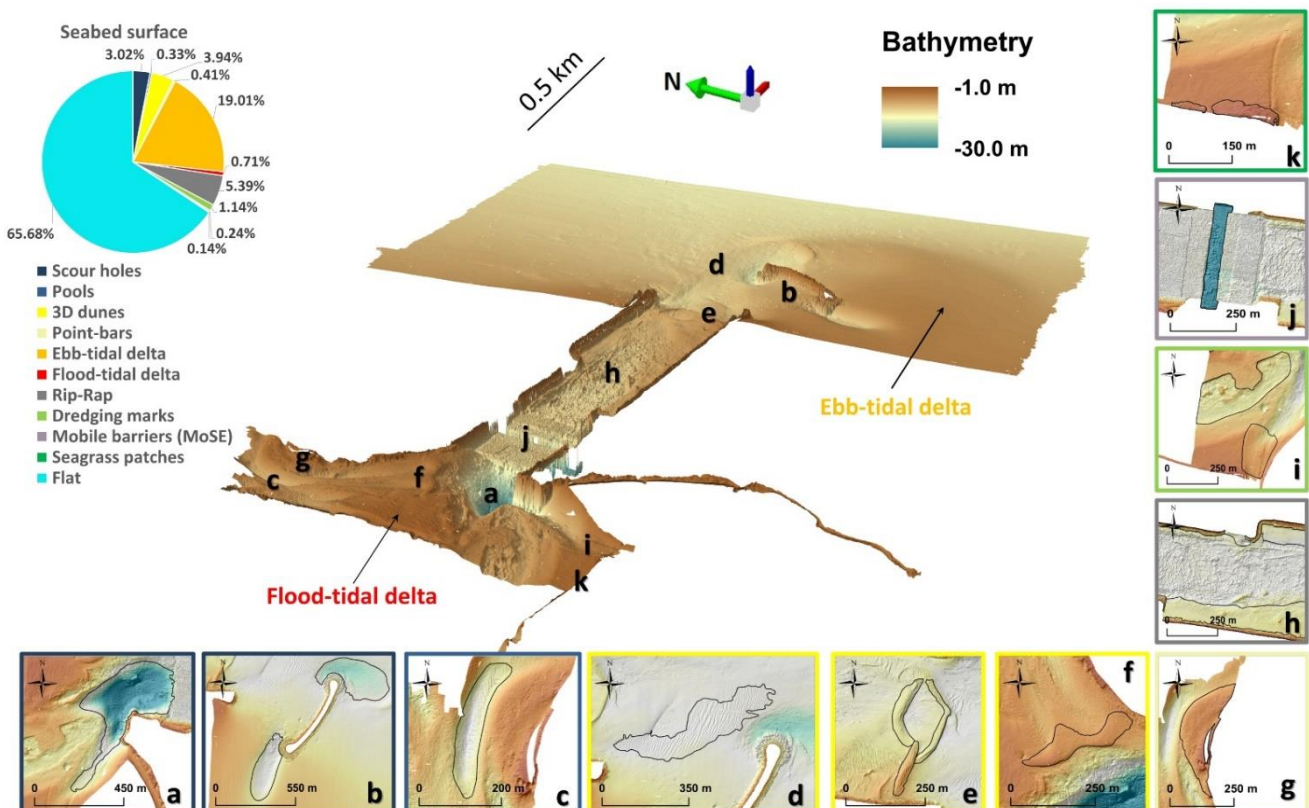


Figure I3: Three-dimensional representation of the Chioggia inlet morphology with the identified seafloor features: (a) and (b) scour holes at hard structures; (c) tidal channel pool; (d) dune field; (e) and (f) large dunes; (g) tidal channel point bar; (h) rip-rap; (i) dredging marks; (j) MoSE trench; (k) seagrass patches. The pie chart in the upper left corner represents the percentage areas occupied by each feature class with respect of the total surveyed area.

3.4.1.1. Erosional features

Scour holes are localized erosional features produced over a sediment surface in a turbulent current (Ferrarin et al., 2018; Madricardo and Rizzetto, 2018). Four scour holes have been identified, covering a total area of 294,371 m² (the 3.02 % of the study area) (Figs. I3a and I3b).

The deepest scour is located inside the lagoon basin, near the inlet entrance and Chioggia harbor (Figs. I3a and I4a). As shown in Balletti et al. (2006), the scour already existed in the historical map of the Venice Lagoon of 1809-1811 by Augusto Dénaix (Magrini, 1934) and in the maps of 1927, 1970 and 2002 (MAV-CVN, 2004). Its current shape is highly irregular, with a maximum relative depth of 20 m and a surface of 119,084 m². The maximum depth is about -30 m, with a slope ranging between 10° and 30° (slope map in Appendix). This scour hole borders the stone-revetment area at the west side of the mobile barrier system (MoSE). The scour is indeed abruptly interrupted by the presence of Mose armored seafloor (Fig. I3a upper right). Inside this morphology we collected a poorly sorted *gravelly sand* (sample N18 in Fig. I1) with a D50 of 243 µm, composed in large part of shell fragments and inorganic clasts > 2 mm. The drop-frames show a sandy seafloor entirely covered by *Ophiothrix* sp.

Two additional scour holes occur at the breakwater ends (Figs. I3b and I4b): the scour at the northern end shows an almost ellipsoidal shape with the 500 m long main axis directed roughly parallel to the tidal inlet channel axis. The slopes at the scour sides range between 5° and 15° (slope map in Appendix). The scour has a surface of 83,022 m², a maximum depth of 3 m relative to the adjacent seafloor, and is characterised by *slightly gravelly muddy sand* (sample N110, Fig. I1b) with a small D50 (67.30 µm).

The scour hole at the southern breakwater tip covers a smaller surface (53,387 m²) and has an oval elongated shape half kilometre long. This scour hole is roughly north-south oriented and has a relative depth of 4 m. The slope profile is quite irregular, with several steps, likely connected to collapse slumping processes due to steep and unstable sides or to changes in lithology of the units eroded below the seafloor. The slope ranges between 5° and 20° (slope map in Appendix).

These two scours formed after the construction of the breakwater that started in 2003, as it can be seen in Villatoro (2010). As the breakwater was built on a regular surface over the ebb-tidal delta, removing the bathymetry associated with these two scour holes and interpolating the remaining surface, we can estimate about 430,000 m³ of sediments have been eroded in about 8 years.

A fourth scour hole (Fig. I4c) was identified at the seaside end of the inlet channel at the end of the northern jetty with an irregular area of 38,900 m² and a relative depth of 2 m. It is almost parallel to scour 2 (Fig. I4b). In the middle of this feature, we collected the coarsest grab sample (sample N2, Fig. I1b): the sediment is a very poorly sorted *sandy gravel* with large D50 (2876 μm). The drop-frames show a sandy seafloor abundant covered by shells and small pebbles. No living organisms were present.

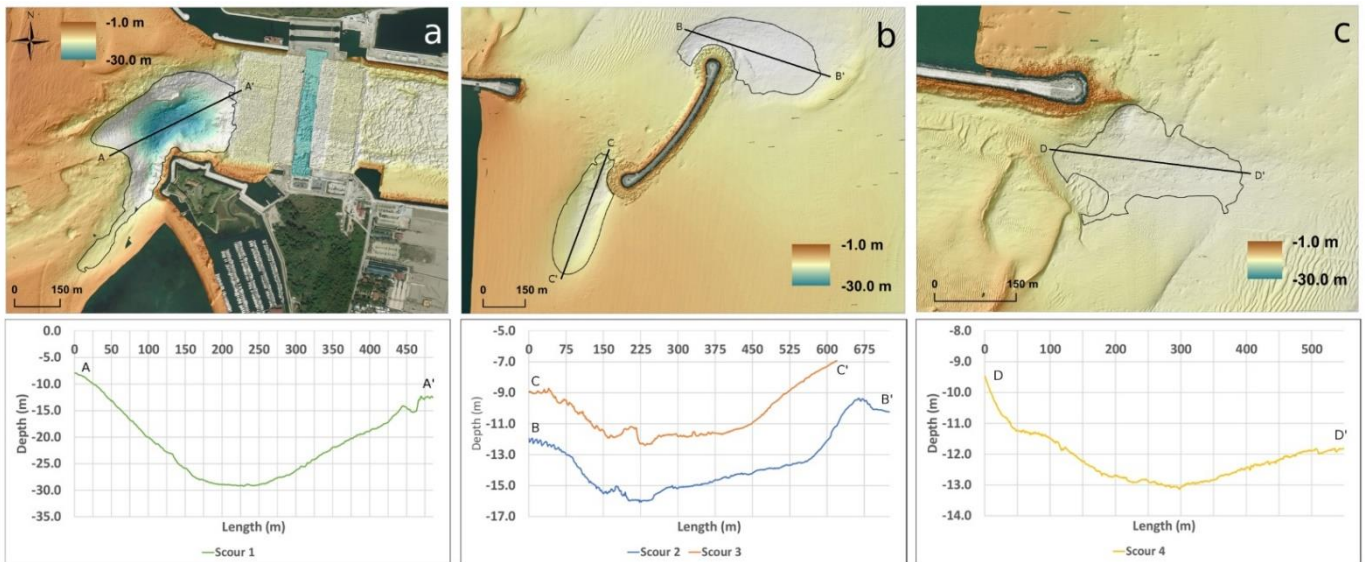


Figure I4: Scour holes and their profiles: (a) the deepest scour hole on lagoon side; (b) the scour holes at breakwater tips; (c) the smallest scour hole near the northern jetty.

Pools are distinct depressions in meandering and straight channels and very common also in fluvial environments (pool-riffle sequence). Their origin is strictly connected to hydrodynamic processes (Keller and Melhorn, 1978): inside a channel, near the curve, the current erodes the longest channel side, deepening the seabed. The pools are similar to scour holes, though more ellipsoidal with lower relative depth (Fig. I3c). Pools are often in pairs with point bars. We identified 3 pools inside the lagoon tidal channels in the survey area. These pools have the longest axis ranging between 100 and 400 m, the minor axis of about 10 to 60 meters, and a relative maximum depth ranges between 2 and 3 m. They occupy a total surface of 31,745 m². Inside the northernmost pool, at a depth of 9 m, we collected a moderately well sorted *slightly gravelly sand* (sample N17, Fig. I1b), and the underwater images show a bare sandy seafloor with vagile fauna such as Paguroidea, *Nassarius nitidus* and a specimen of *Asterina gibbosa*.

3.4.1.2. Depositional Features

Dunes occupy about 4 % of the study area (383,943 m²) and have crests transversally oriented with respect to the main direction of the current (Ashley, 1990). We found distinctive groups of small size dunes (dune fields) and very large, typically isolated, dunes with wave length λ ranging from 2 m to 100 m and height h from 0.02 m to 2 m, respectively (Fig. I5). By interpolating all the values of λ and h , we found the relationship $\lambda = 0.79 * h - 1.13$, very similar to the Flemming equation (Flemming, 2000). All bedforms, regardless of the size, appear oriented seaward, reflecting the direction of the ebb tide (Fig. I5). The largest dunes ($h = 2.5$ m, $\lambda = 110$ m) are located at the inlet entrance close to the southern jetty (seaside) at a depth of 10 m where these bedforms occupy about half of the navigation channel (Figs. I3e and I5b). These dunes are out of phase (Fig. I5b) with the most external large dune having a positive convex linguoid shape and the internal dune show a negative convexity lunate shape. The third large dune to the south of the inlet channel has a straight shape with an angle of 20° with the main channel direction. All the large dunes are considerably asymmetric, clearly oriented toward the sea (from west to east); on the stoss side the slope is about 1.2°, whereas it is 20° on the lee side. Furthermore, over the stoss side, some smaller dunes are superimposed ($h = 20$ cm, $\lambda = 4$ m) on the largest ones (Fig. I5b).

At a ground truth station over the southernmost straight large dune (sample N11, Fig. I1b), we collected *slightly gravelly sand* ($D_{50} = 54$ μm). The drop-frame showed a homogenous sandy seafloor, with small superimposed ripples and a scattered occurrence of loose shells.

Two additional very large dunes inside the lagoon form a double U-shaped feature to the north of the biggest scour hole, close to inlet entrance at a depth of 6 m (Figs. I3f and I5c). Their wavelength is 100 m and their height is 2 m. These dunes are also asymmetric, indicating a seaward migration (southeast), with a stoss side slope of 1.2° and a lee side slope of 22°. Small dunes ($h = 10$ cm, $\lambda = 3$ m) are superimposed on the stoss side. Close to these dunes, a grab sample of the sediment (sample N10, Fig. I1b) was collected and analyzed resulting a very poorly sorted *sandy gravel* ($D_{50} = 653$ μm). The drop-frames reveal a sandy seafloor uniformly covered by shells fragments. The backscatter classification suggests that all the large dunes are covered by the same sediment found in the sample.

3. Study I: Tidal inlets in the Anthropocene: geomorphology and benthic habitats of the Chioggia inlet, Venice Lagoon (Italy)

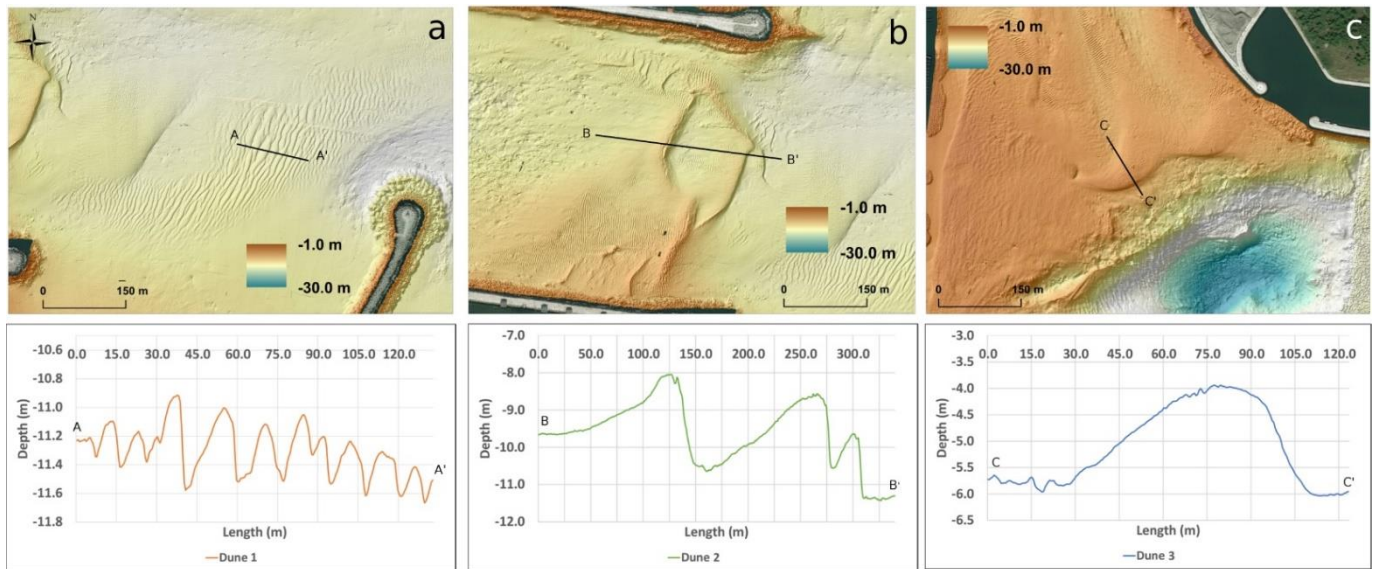


Figure 15: Dune fields and their profiles: (a) dune field on the seaside; (b) large dunes near the eastern inlet entrance (seaside); (c) large dunes near the western inlet entrance (lagoon side).

Point bars are depositional features that form inside channel bends below the slip-off slope (Hickin, 1974). One point-bar in the northern part of the study area inside the lagoon has a surface of 40,046 m², is adjacent to a pool (Fig. I3g). This point bar, characterized by a bowed shape, has a relief of about 3 m on the channel floor with the main axis of 500 m and a width of 130 m. The depths in the point bar area range between 2.5 m to 5 m, making this area one of the shallowest in the study site.

Ebb and flood tidal deltas are two typical physical elements of tidal inlets with distinctive sedimentological and morphological properties. These features are concentrations of sand and mud and reflect the dynamics of ebb and flood currents. These currents are amplified when passing through the inlet and attenuated where flow spreads at both inlet termini. Commonly, the deposited sediments form broad shoals or deltas (Hayes and Fitzgerald, 2013). The ebb-tidal delta genetically related to the Chioggia inlet occupies about 1.85 km² (19 % of the study area) and is located at south of the southernmost jetty at a depth of about 7 m or greater (Fig. I3; see Appendix), with a maximum relative height of 3 m with respect to the neighboring area. However, the ebb-tidal delta was eroded in correspondence of the scour holes created by the tidal jet flowing around the breakwater. Several grab samples were collected over the ebb-tidal delta: all the samples are sands with a small fraction of gravels, with a D50 ranging between 115 μ m to 159 μ m. The mean grain size in correspondence of these feature increases moving from west to east and from north to south. The drop-frames show a medium sand seafloor with some shell fragments with no living organism recorded.

The flood-tidal delta covers a surface of 69,018 m² (0.71 %), is less prominent and its extent was not fully covered by the survey (Fig. I3). The portion of the flood-tidal delta comprised in the survey area is located in the middle of the lagoonal sector at a depth of 3 m and it appears like a plain triangular with the basis in the north south direction and one of the vertices towards east shoal. An extensive dredging area interrupts the flood-tidal delta abruptly (Fig. I3i). Few small dunes ($h = 0.2$ m, $\lambda = 10$ m) are superimposed on the flood-tidal delta.

3.4.1.3. Anthropogenic features

Rip-rap revetments are artificial rock accumulations used to armor shorelines (Pister, 2009). The use of these hard structures is increasing in the world to manage and protect the subaqueous portion of beaches from erosion enhanced by global sea level rise. Rip-rap revetments become a particular habitat for marine species and could alter the sediment dynamics of surrounding areas (Bulleri and Chapman, 2010; Dafforn et al., 2015; Perkins et al., 2015; Aguilera et al., 2017). In the survey area, rip-raps seafloors were mapped around the breakwater and near the jetties. The rock armoring was placed on the seafloor to protect the MoSE trench from erosion by tidal currents and bottom sediment transport and are expected to delay the siltation of the trench hosting the mobile barrier. These features have an irregular profile composed of closely-spaced reliefs and depressions of the bottom (Fig. I3h) and occupy a total surface of 525,937 m² (5.39 % of the total survey area). The dimension of the boulders composing the rip-rap is on average about 2-2.5 m.

One sediment sample collected in the inlet channel (sample N23, Fig. I1b), documents poorly sorted *sandy mud* with abundant shells. The underwater images show concrete boulders alternated with partially consolidated muddy patches; abundant presence of algae fragments, encrusting organisms and *Ophiothrix* sp. One specimen of the crab *Pachygrapsus marmoratus* was also observed.

Dredging marks can be defined by the sharp vertical profiles and the presence of incision due to the re-profiling machinery, mostly grab and backhoe dredgers. In the study area, these features occupy a surface of 111,483 m² (1.14 % of the total survey area). The marks are clearly visible only in very shallow waters. The relative depth of the excavations is variable, but generally is within 2-2.5 m (Fig. I3i).

Mobile barriers (MoSE) represents the trench for the mobile barriers. Their allocation started only in 2015 and should be completed by the end of 2019; the trench is easily identifiable by its regular

rectangular shape (Fig. I3j). It has longitudinal and transversal dimensions of 430 m and 55 m, respectively. It covers a surface of 23,190 m² (0.24 %) and shows a mean vertical profile of 10 m. At the bottom of the trench the seafloor appears strongly cemented.

3.4.1.4. Biogenic features

Seagrass patches have speckled round/ellipsoidal shapes, slightly in relief (Fig. I3k). These natural features are located along the south-west tip of the lagoon, at a depth of 2-2.5 m and occupy a restricted surface area of 13,168 m² (about the 0.14 % of the study area) The drop-frames show a muddy substratum partially covered by seagrass meadows. The dominant species in this area is *Cymodocea nodosa* (Ucria) Asch. The shape and extent of the meadows over the Venice Lagoon have changed over the past decades, however it is quite stable over a short period of time (Curiel et al., 2014). The *Cymodocea nodosa* is a sub-tropical species and during winter it loses most of the foliage. After December, only rhizomes and some leaves can be observed (Rismondo et al., 1997). The acoustic data in the Chioggia Inlet were collected in October and November, within the species vegetative period. Therefore, the observed patches represent the full extent of the meadows.

3.4.2. Ground truth samples analysis

3.4.2.1. Sediment grain size

We analyzed a total of 44 samples, subdivided between open sea, lagoon and the inlet channel (Appendix). The range of median diameters is broad and change from 60.3 µm to 2.9 mm. Most of the sediment is classified as sand; however, in few samples, mud or gravel of biogenic origin prevail. In detail, *slightly gravelly sand* is the predominant size class. Gravels were also found (with 3 *sandy gravel* samples). Only 2 samples were in the mud class (*slightly gravelly sandy mud*). On the seaside, there is a high percentage of sand and also abundant mud. Inside the inlet there is less sand and more gravel. Inside the lagoon, mud increases toward the shallow water salt marshes, whereas gravelly samples occur inside dredged channels.

Few samples are dominated by the coarse fraction (> 2 mm). This coarse fraction consists of bioclasts, mostly shell fragments, especially belonging to bivalve or gastropod mollusks. Other organic material, like wood fragments, is present in low quantities, except for N5 sample (see Fig. I1 for the sample location). Non-bioclastic grains are not abundant, except for sample N18.

Sorting of the sediment samples is strongly site dependent within the study area. All seaside sediments are well-sorted or moderately well-sorted, except for sample N100 which is poorly-sorted. On the contrary, inside the lagoon and along the inlet channel the sediments show a high degree of variability, with the sorting index varying between very poorly-sorted to well-sorted. The least sorted samples consisted of sediments with a lower content of sand: where mud or gravel is abundant the grain size variability is larger; indeed, the very poorly-sorted samples (N2, N6, N10 and N12 in Fig. I1) are sandy gravels or gravelly sands. Sorting correlates with increasing sand content.

3.4.2.2. Seafloor images

Several benthic taxa, characterizing the various habitats, both alive specimens (mainly epimegabenthos) and empty shells, were recognized from underwater images (Appendix). Although some species occur in large abundance, the number of observed taxa remains relatively low, summing to a total of 37. The seabed lacks of macrophyte cover, with the exception of some seagrass patches (*Cymodocea nodosa* (Ucria), Asch), easily recognizable also from MBES data in the western fringe of the lagoon, and red/brown algae colonizing the central inlet rip-rap.

In 11 out of 19 stations, we observed living organisms, most commonly the crab *Carcinus aestuarii*, the gastropod *Nassarius nitidus*, Actiniaria and Paguroidea, mostly on sandy/muddy sediments and over seagrass meadows. The stations with coarse sediment and shell fragments presented a low number of living organisms. In the deepest stations, samples N18 and N23 (Fig. I1), characterized by boulders or pebbles, aggregates of the brittle star *Ophiothrix* sp. covered the seabed.

Empty shell remains belonging to the thanatocoenosis were identified in 14 out of 19 stations, mostly Bivalvia, and in particular Veneridae, Mytilidae, Pectinidae and Ostreidae. Among gastropods, we mostly observed *Nassarius nitidus* and *Bittium* sp.

3.4.3. Backscatter classification

The recorded backscatter ranges from -68.54 dB to 4.64 dB (Fig. I6); some outliers (visibly associated with artifacts) are probably connected to errors during registration or conversion. The backscatter data are characterized by a Gaussian distribution, with a mean of -24.20 dB and a mode of -25.85 dB. The associated standard deviation is 3.22.

Using the Jenks' optimization method, we have obtained 4 backscatter classes (Fig. 16): very low intensity: < -28.07 dB (SGMS_MS_SGSM); medium-low intensity: $-28.07 \div -24.63$ dB (S); medium-high intensity: $-24.63 \div -20.90$ dB (SGS); very high intensity: > -20.90 dB (SG_GS).

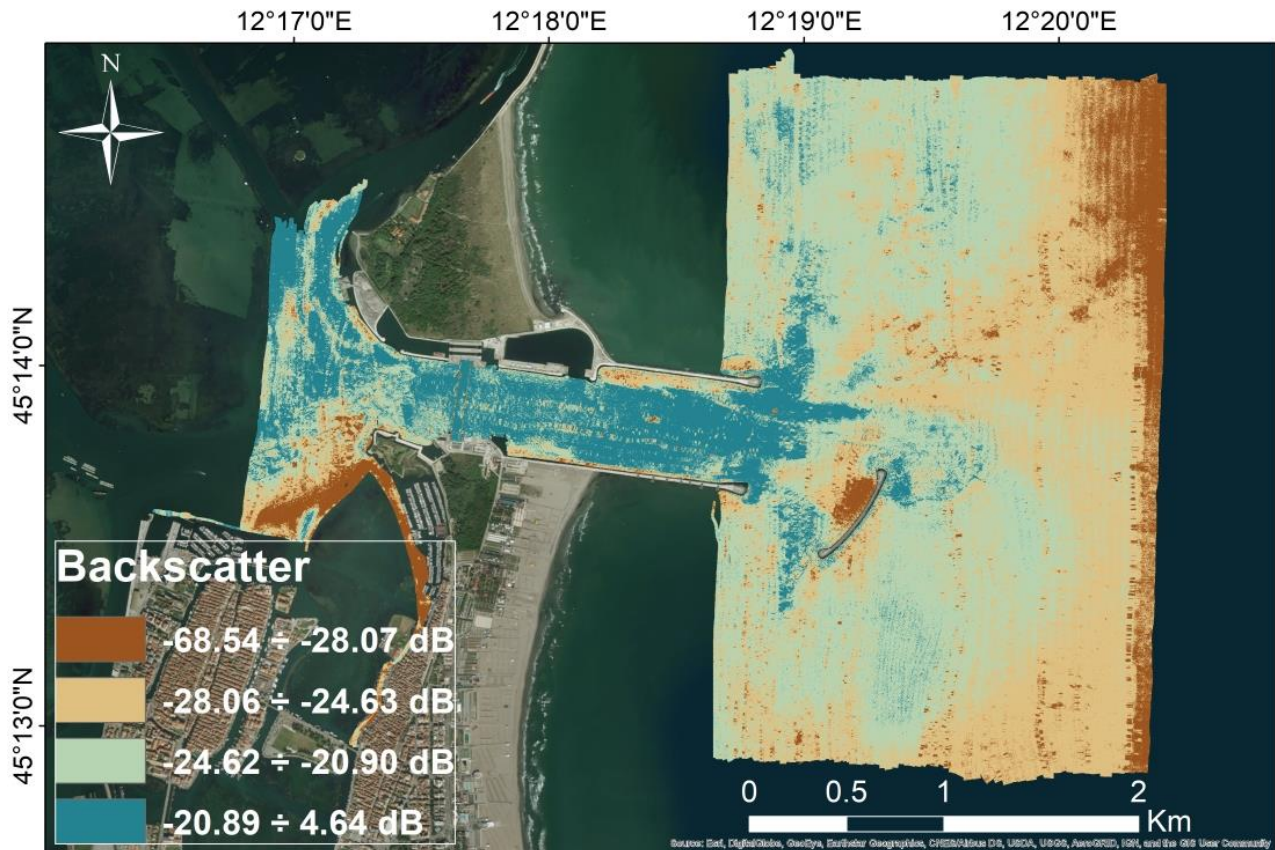


Figure 16: Backscatter classified in four sediment classes with the Jenks' algorithm: Slightly Gravelly Muddy Sand_Muddy Sand_Slightly Gravelly Sandy Mud (SGMS_MS_SGSM) (brown), Sand (S) (beige), Slightly Gravelly Sand (SGS) (light green), Sandy Gravel_Gravelly Sand (SG_GS) (dark green), corresponding to very low backscatter intensity: < -28.07 dB; medium-low backscatter intensity: $-28.07/-24.63$ dB; medium-high backscatter intensity: $-24.63/-20.90$ dB; very high backscatter intensity: > -20.90 dB, respectively.

3.4.4. Backscatter classification accuracy

Many measures exist to verify the accuracy of a classification process. One of the most popular is deriving the confusion matrix and counting the percentage of correctly allocated cases (Foody, 2002). This technique, created for land using research, provides the assessment of the accuracy of a map using two different points of view: user's and producer's accuracy that measures the reliability of the classification (i.e. the probability that a pixel on a map actually represents that

category on the ground) and how well a certain area is classified, respectively (Story and Congalton, 1986). Furthermore, an overall accuracy can be derived from these tables.

The unsupervised Jenks' classification shows an overall accuracy of 75 %, identifying correctly 33 stations on 44 totals (Tab. I1). The used method achieved reasonable accurate predictions of coarser sediments (SG_GS and SGS classes). However, Jenks' did not reach a sufficient accuracy for the classes S and SGMS_SM_SGSM: in particular, the presence of class S is overestimated with respect to reality. We can only speculate that the false stations are probably located in unclear backscatter patches, where there is coexistence of classes. The low accuracy could also be related to the low number of collected grab samples of this seafloor type.

Table I1: Confusion matrix for the backscatter classification in the study area.

		Ground-truth samples				Total classified	Producer accuracy (%)	User accuracy (%)
		SG_GS	SGS	S	SGSMS_MS_SGSM			
Classified samples	SG_GS	5	0	0	1	6	100	83
	SGS	0	22	0	1	23	81	96
	S	0	5	2	4	11	100	18
	SGSMS_MS_SGSM	0	0	0	4	4	40	100
Total ground-truth samples		5	27	2	10	44		
Overall Accuracy (%) = 75								

3.4.5. Benthic habitat classification

Habitat classes are related to the sediment composition, which influences the backscatter signal. The habitat classes, *Coarse shell detritus*, *Sand with sparse shell detritus*, *Bare sand* and *Muddy sediment* at the seaside were defined using the backscatter classification supported by the sediment samples data and the classified seafloor images (Figs. I7 and I8). Each benthic habitat is characterized by specific biotic features specified in the description of Fig. I7.

However, the information from the backscatter intensity alone can sometimes not be enough to differentiate all target habitats (see e.g. De Falco et al., 2010; Lucieer et al., 2013). The habitat classes *Artificial rock bed* and *Seagrass meadows* were isolated also using morpho-bathymetric attributes, like bathymetry itself and ruggedness (Fig. I2) and the *Artificial rock bed* presented indeed very high ruggedness values and a distinctive backscatter pattern characterized by chaotic patches, whereas *Seagrass meadows* were visible in the bathymetry and showed medium to high ruggedness values confined in circle/oval shapes.

The class *Lagoon mudflat* was defined using both the classification of the backscatter and of the morphological classification: the lagoon area with lowest values of backscatter, as well as the tidal point bar and flood-tidal delta were grouped into this habitat class.

3. Study I: Tidal inlets in the Anthropocene: geomorphology and benthic habitats of the Chioggia inlet, Venice Lagoon (Italy)




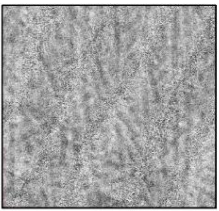
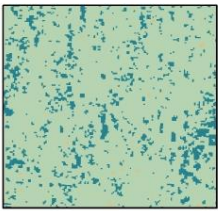

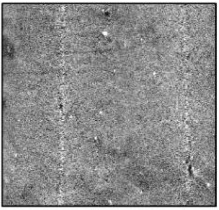
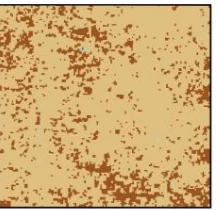
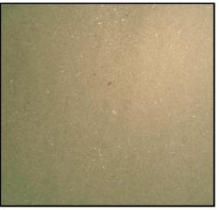

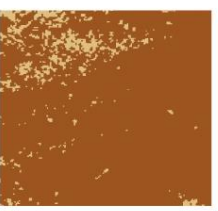

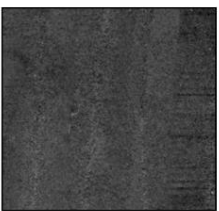
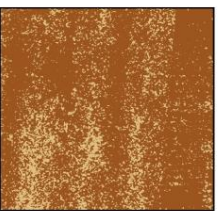
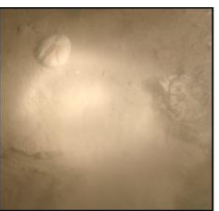
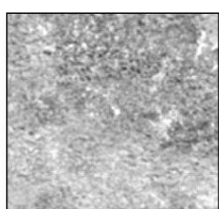
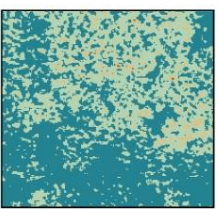

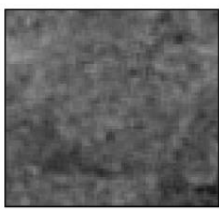


Class	BS range (dB)	Original BS	Classified BS	Drop-frame	Description
1 - Coarse shell detritus	> -20.90				Seafloor completely covered by coarse shell detritus, D50 typical of gravels, poor sorting, scarce vegetation cover. Observed biota includes both infauna and encrusting epifauna (such as Serpulidae and Actiniaria). Occasionally dense Ophiothrix beds are observed.
2 - Sand with sparse shell detritus	-24.63 ÷ -20.90				Coarse sand seafloors with sparse shell detritus and moderate sorting, vegetation absent. Infauna and vagile epifauna (such as <i>Carcinus aestuarii</i> and <i>Nassarius nitidus</i>) prevail.
3 - Bare sand	-28.07 ÷ -24.63				Well sorted sand seafloors, absence of coarse fragments and vegetation, D50 typical of medium sands. Epifauna rarely observed.
4 - Lagoon mudflat	< -28.07				Very well sorted fine muddy, poor presence of shells. Typical mudflat sediment. Significant vegetation cover (mainly <i>Ulva</i> sp.). Observed taxa include vagile epifauna (e.g. <i>Carcinus aestuarii</i> and <i>Nassarius nitidus</i>).
5 - Muddy sediment	< -28.07				Very well sorted fine sediment, absence of coarse fragments. Significant vegetation cover (mainly <i>Ulva</i> sp.). Observed taxa include both infauna (e.g. <i>Echinocardium cordatum</i> and Veneridae) and vagile epifauna (e.g. <i>Carcinus aestuarii</i>).
6 - Artificial rock bed	Variable				Riprap seafloor characterized by rocky substrata with small mud patches. Presence of macroalgae, encrusting and vagile epifauna (e.g. <i>Pachygrapsus marmoratus</i>). Occasionally dense Ophiothrix beds are observed.
7- Seagrass meadow	Variable				Well sorted fine sediment covered by seagrass (<i>Cymodocea nodosa</i>). Diverse infauna and epifauna assemblages.

Figure 17: Schematic description of the habitat classes with their backscatter signal, classified backscatter and corresponding seafloor image.

3. Study I: Tidal inlets in the Anthropocene: geomorphology and benthic habitats of the Chioggia inlet, Venice Lagoon (Italy)

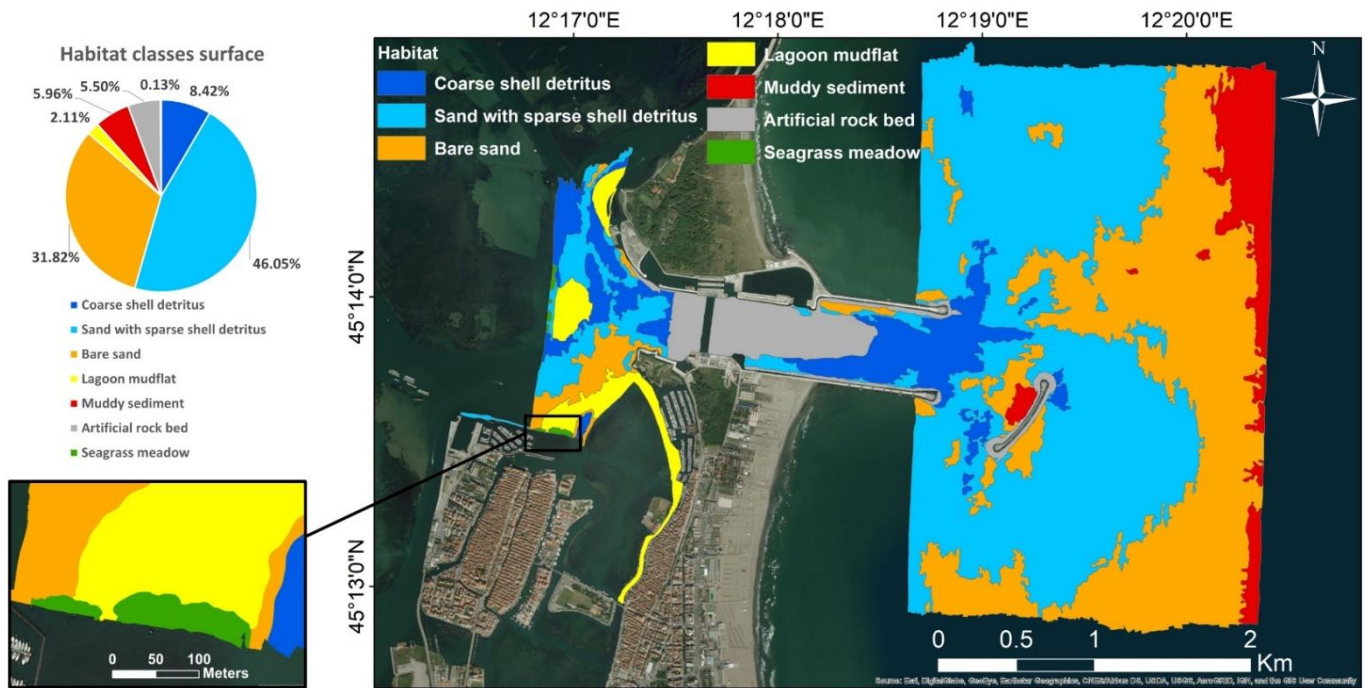


Figure 18: Benthic habitats in the Chioggia inlet, where the dark blue class represents Coarse shell detritus, the light blue Sand with sparse shell detritus, the yellow Bare sand, the red Muddy sediment, the grey Artificial rock bed and the green Seagrass meadow, respectively. The pie chart shows the relative surface occupied by each benthic habitat class with respect to the total study area.

3.4.5.1. Class 1 – Coarse shell detritus

The main feature of this habitat is the thick layer of biogenic detritus composed of coarse shell fragments which covers completely the seafloor, masking the underlying sediment (see drop-frame image in Fig. 17). The shells can have a different degree of cementation and variable fauna colonization. The associated textural group is usually sandy gravel, with very high D50 and very poor sorting. Mud content is typically missing. Coarse shell detritus is very variable in terms of species composition: it includes mostly bivalves such as *Chamelea gallina*, *Venerupis aurea*, *Mytilus galloprovincialis*, Ostreidae indet. and Pectinidae indet., but also gastropods, sea urchins and decapod remains. Occasionally, the brittle star *Ophiothrix* sp. is very abundant and covers completely the seafloor. Observed living organisms include some bivalves and hermit crabs (Paguroidea indet.). Moreover, the coarse and partly cemented detritus behaves as a hard substratum allowing the colonization by epibionts such as Actiniaria indet. and Serpulidae indet. Sometimes macroalgae (*Ulva* sp.) and seagrass fragments are observed.

This class occupies 821,693 m², i.e. about the 8.42 % of the study area (Fig. 18), and is placed especially along the inlet channel and in the northern part of the lagoon, whereas in the open sea it

is less represented. This class is frequently located near rip-rap and as well it is sometimes difficult to distinguish it from the class *Artificial rock bed*. This substratum often fills concave morphologies (i.e. scour holes and pools). It is not completely clear if these bioclastic debris are transported by the currents from the surrounding area or if they are a deep ancient sediment subsequently exposed by current erosion. This kind of seafloor cover is usually related to high backscatter value due to the strong reflectivity of shells (Stanic et al., 1988; Yu et al., 2015).

3.4.5.2. Class 2 – Sand with sparse shell detritus

This is the most abundant habitat in the survey area with a surface area of 4,495,740 m² (\approx 46.05 %) and it is distributed almost everywhere, with the exception of channel (in light blue in Fig. 18). The slightly gravelly sand group dominates the substrate type of this class. High percentages of bioclastic detritus (mostly mollusc shell fragments) are often present (see drop-frame image in Fig. 17). Mud content is low. The sorting is usually moderate. The most common cast shells remains include *Bittium* sp., *Chamelea gallina*, *Solenoida* indet. and *Mytilus galloprovincialis*. Live individuals of *Asterina gibbosa*, *Carcinus aestuarii* and *Nassarius nitidus* have been observed. This class is often found in correspondence to dune fields, scour holes and pools. This substratum has medium to high values of backscatter, depending on the shell density.

3.4.5.3. Class 3 – Bare sand

This is the second largest habitat class in the study area with 3,105,818 m² (\approx 31.82 %) and it is located almost exclusively on the seaside (in orange in Fig. 18). The associated sediment is consistently sand, with very low percentages of other size fractions. The underwater images show a bare homogeneous seabed, with very well sorted sands usually arranged in small ripples (few centimeters of height). There is a paucity of observed epifauna and vegetation cover. Biogenic detritus is typically missing. This habitat is usually not connected to any large bedform and the backscatter signature is medium to low.

3.4.5.4. Class 4 – Lagoon mudflat

This class includes all the mudflats inside the lagoon basin (e.g. Sarretta et al., 2010) and occupies 206,002 m² (\approx 2.11 % of the study area). The typical depths associated to this habitat are shallower

than 4 m (in yellow in Fig. I8). The backscatter signature is typically low, but patches with medium-high backscatter reflect at places the presence of shell deposits or dredging marks. This habitat characterizes also the tidal point bars and the flood-tidal delta. The collected samples are very well sorted muddy sediments, with poor presence of shells. These muds are very dense and with a plastic consistency. Observed taxa include lagoon vagile epifauna (e.g. *Carcinus aestuarii* and *Nassarius nitidus*). This substratum presents sparse macroalgae (mainly *Ulva* sp.) and a benthic diatom film is frequently observed.

3.4.5.5. Class 5 – Muddy sediment

The *Muddy sediment* habitat occupies 582,265 m² (\approx 5.96 % of the survey area). It is distributed mainly on the marine side of the study area, parallel to the coastline and starting at a depth of about 14 m (in red in Fig. I8). This habitat belongs to the terrigenous muddy sediments found in front of the Venetian coasts (Albani, 1988). The substrate in this class is mostly well-sorted muddy sands or sandy muds, with low D50. The percentage of shells fragments is often very low. A benthic diatom film is frequent. This class has a high number of observed species, including in some cases macrophytes. Noticeably, *Ulva* sp. is found on the marine side, either free floating or attached to the thanatocoenosis. Observed zoobenthic taxa include both infauna (e.g. *Echinocardium cordatum* and Veneridae) and vagile epifauna (e.g. *Carcinus aestuarii*). This is the class with the lowest backscatter intensity, clearly indicative of fine sediments. No bedforms are associated with these seafloors.

3.4.5.6. Class 6 – Artificial rock bed

This habitat class occupies a surface of 537,045 m² (\approx 5.50 % of the study area) and corresponds with the seafloor covered with rip-rap. It is distributed along the jetties, the breakwater and in the middle part of the inlet channel (in grey in Fig. I8). This class often coincides with the borders of the surveyed area, due to safety constraints to the survey boat navigation. The underwater images show an irregular seabed with numerous boulders (tetrapods) alternated with muddy sediment patches. A thick layer of bioconcretion, mostly oysters and tube-building worms belonging to Serpulidae, covers the hard surfaces. Macroalgae such as *Ulva* sp. are also present. *Ophiothrix* sp. are present in high number, sometimes covering the entire available surface. Poorly sorted sandy mud, with the

presence of several encrusted shells, has been collected from the small patches between the boulders. The backscatter values associated with this habitat are not uniform, due to the alternate presence of rocks (strong backscatter) and muddy patches (low backscatter). Probably the abundant biological coverage is also affecting the backscatter signature (De Falco et al., 2010; McGonigle and Collier, 2014). This habitat has high values of ruggedness that was used to isolate this class.

3.4.5.7. Class 7 – Seagrass meadow

This habitat class, the smallest in the survey area occupying only 13,152 m² (\approx 0.13 %), represents the seabed with seagrass cover. It is located inside the lagoon, at depths shallower than 3 m, near the Chioggia harbor (in green in Fig. 18). The species is *Cymodocea nodosa* (Ucria) Ascherson, which, together with *Zostera marina* L. and *Nanozostera noltii* Hornemann, make up most of the seagrass prairies over the Venice lagoon (Curiel et al., 2014). Seagrass meadows are a valuable habitat, providing several ecological functions, such as primary production, oxygenation, nutrient absorption, sediment stabilization and protection against erosion. These habitats are shelter and feeding ground for a rich and complex community.

The collected images show a well sorted fine sediment seafloor with some seagrass leaves, some shell fragments and macroalgae, such as *Ulva* sp. Since the ground-truth images were collected during winter, the observed canopy of *Cymodocea nodosa* meadows was reduced. The recorded benthic community, both vagile and sessile, is often abundant. Also in this case, ruggedness has been used to identify this habitat.

3.4.6. Anthropogenic objects

The analysis of high resolution bathymetry (0.2 m) allowed the visual identification of punctual anthropogenic objects placed voluntarily or not on the sea bottom. We mapped a total of 541 objects, grouped into 7 different categories (Fig. 19). The most common described objects are *Rip-rap debris* and *Bricola* (wood piles used to delimit the navigation channels) (in yellow and grey in Fig. 19, respectively). Most of the objects were found inside the lagoon and along the inlet channel and close to the breakwater, whereas the deeper sea area showed less objects. *Tire* (in blue in Fig. 19), commonly used as fenders by boats, and *Bricola* elements were localized exclusively inside the lagoon, whereas in the deeper sea area *Rip-rap debris* prevailed. We found three wrecks (in purple

in Fig. 19) inside the lagoon and in the inlet channel. The bathymetry highlighted the presence of a few cables and poles (in red and light blue in Fig. 19) on the seafloor.

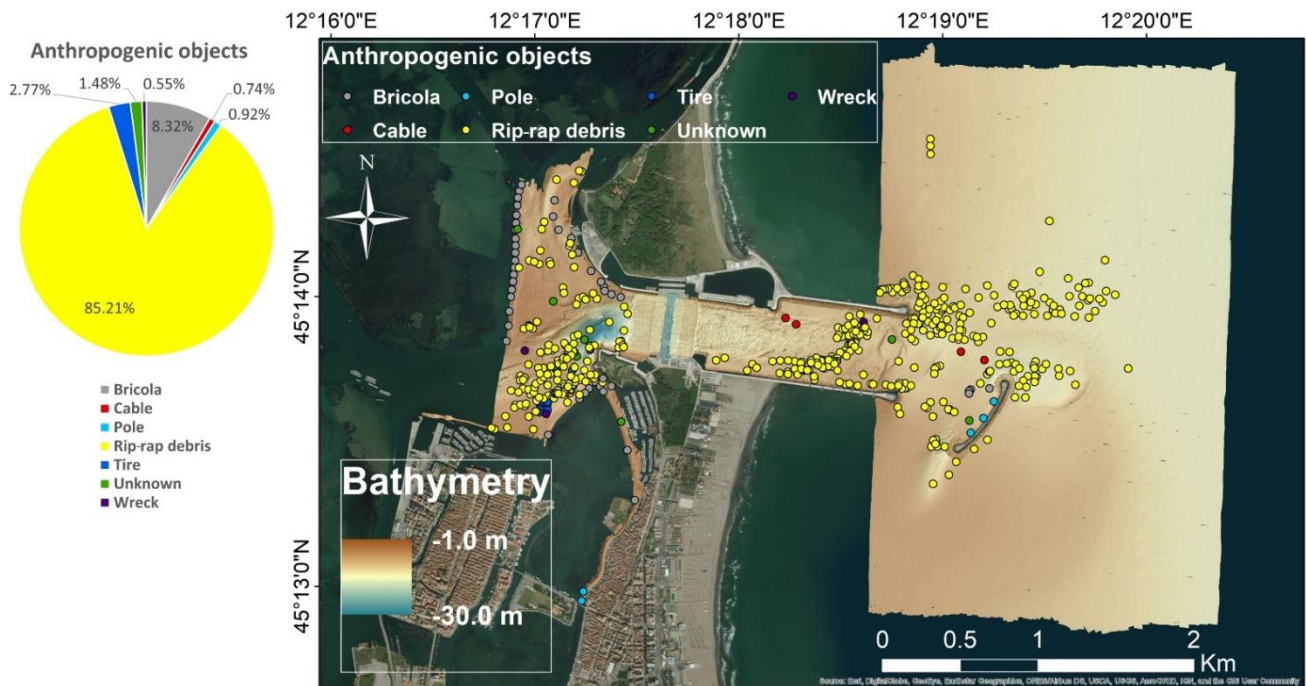


Figure 19: Anthropogenic objects identified in the study area. The pie chart in the upper right corner represents the percentage number of each object type with respect to the total number of mapped objects.

3.5. Discussion

3.5.1. Tidal inlet seafloor features and sediment distribution

The construction of the seaside breakwater, built between 2003 and 2006, most likely significantly changed the hydrodynamic configuration of the flow as predicted by Ghezzi et al. (2010). The changes are schematically summarized in Fig 10.

The water flux splits into two jets: the main one parallel to the inlet channel exit with direction west-east and a secondary one that heads south. The narrowing of the inlet section to provide space for auxiliary MoSE infrastructures, i.e. navigation locks and refuge harbours on the northern jetty and technological buildings at the start of the southern jetty, increased the flow velocity (Ferrarin et al., 2015 and references therein) (Fig. 110). As a direct consequence, a general coarsening of the sediment distribution seems to have occurred inside the inlet channel (Figs. 18 and 110). By comparing our classified BS maps with the results described by Villatoro (2010), we found a belt of

shelly sediments exiting the inlet channel that was not present in 2008 (Figs. I8 and I10). Similar coarse shell detritus patches were already observed in the North Venice Lagoon by Montereale-Gavazzi et al. (2016). Close to the Chioggia inlet channel, the only regions with a finer sediment are located in the southern part of the study area on the lagoon side and in the area protected by the breakwater at the inlet front (yellow and red classes in Fig. I8). Over the residual ebb-tidal delta, we find predominantly the class *Sand with sparse shell detritus* (light blue in Fig. I8) whereas sandy and fine sediments are dominant in the seaward side of the study area (orange and red classes in Fig. I8).

The three scours shown in Fig. I3a and Fig. I3b have different sediment distributions (Fig. I8): coarser sediment at the scour's northern side (classes *Coarse shell detritus* and *Sand with sparse shell detritus*) and finer at the scour's southern side (*Bare sand*). Within the scours at the breakwater's tips (Fig. I3b) the backscatter signal highlights the presence of mainly *Sand with sparse shell detritus* (Fig. I5).

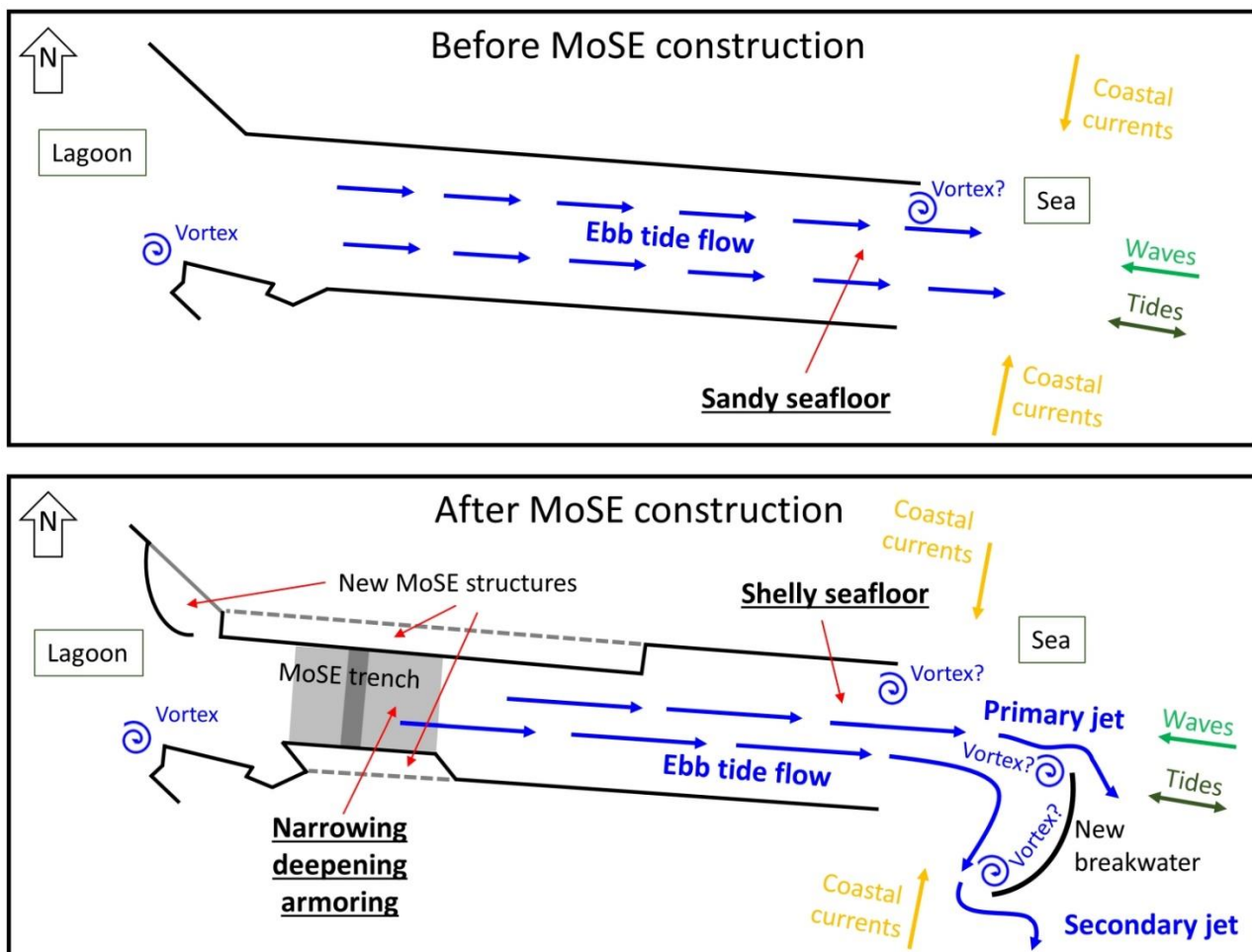


Figure I10: Schematic summary of the dominant processes in the Chioggia inlet before (top) and after (down) the construction of the MoSE hard structures.

The presence of the gravel fraction, i.e. shell detritus, could be related to a) the deposition of shells transported by the currents from the area surrounding the scours, or b) the erosion of a deep ancient fine sediment rich in organic detritus buried by the ebb-tidal delta, leaving the coarser and heavier shells at the bottom of the scours and forming a sort of armoured bed.

The internal lagoon scour is considerably older than the scour holes at the breakwater and its presence is documented already in the historical military hydro-topographic map of Denax of 1810 ca. (Magrini 1933). The sediment distribution is likely related to the action of the currents which is stronger in its northern part, whereas its southern part is closer to an area of deposition, rich in muddy sediment.

It is likely that, these depressions eroded the deep silty clayey sediments at the base of the ebb-tidal delta (sample N110). This material could also belong to the prodelta Holocene sediment facies deposited in a marine-lagoon environment with abundant fresh water inputs coming from a paleo-river Brenta (Zecchin et al., 2008). During marine transgression events, the river delta moved several times. Zecchin et al. (2008) found this sediment at a depth of 15-20 m in the core L1-CNR collected in the area now occupied by the breakwater.

Scour holes around breakwaters have been observed globally (e.g. in Japan - Sato et al., 1968, Katayama et al., 1974; in The Netherlands - Roelvink et al., 1999; in the U.S. - Lillycrop and Hughes, 1993). Processes leading to the formation of scour holes around hard coastal structures have been extensively studied mainly on the basis of tank experiments (Sumer and Fredsøe, 1997; Fredsøe and Sumer, 1997; Sumer et al., 2001; Noormets et al., 2006). Fredsøe and Sumer (1997) investigated in a tank experiment the scouring at the round head of a rubble-mound breakwater (similar to our case) using regular waves. They found that the major mechanism responsible for the scouring was the formation of lee-wake vortices in each half period of the waves. The scouring process, governed by the Keulegan-Carpenter number defined in eq. 6 of Sumer and Fredsøe (1997):

$$KC = 1 + \left(\frac{L}{1.75B}\right)^2,$$

where B is the base width of the breakwater head and L is the width of the protection layer on the seafloor (Fig. 15a). Larger values of KC imply the forming of larger scour holes. In our case with B = 60 m and L = 40 m, we obtained KC = 1.15. This value of KC corresponds to a separated flow regime with no formation of a horse-shoe-vortex in front of the breakwater. In this flow regime, a lee-wave vortex forms close to the structure (Sumer and Fredsøe, 1997). The depth of the scour holes was likely substantially enhanced by the presence of co-directional currents that contribute to the wave

action. In this setting, large-scale vortices generated at the breakwater tip could increase the transport capacity of the flow (Fig. I10).

Sediment from most of the dune fields fall inside the classes *Coarse shell detritus* and *Sand with sparse shell detritus*. Looking at the classified backscatter, however, it is possible to distinguish a repetitive pattern of sediment distribution with the class SG_GS in the troughs and the class SGS over the crests (Fig. I11). This sediment pattern is related to the larger energy that is necessary to remove the coarser sediment from the troughs (Fig. I11). Feldens et al. (2015) found higher side-scan sonar backscatter intensities between dunes in the dune fields close to the Fehmarn Island in the south-western Baltic Sea in water depths between 12 m and 23 m. In deeper waters between 60 m and 110 m, on the outer Murcia continental shelf (western Mediterranean Sea), Durán et al. (2017) found that the backscatter imagery of a dune field extending from Cape Cope to the Aguilas submarine canyon displayed higher intensity values on the crests and lower intensity values on the troughs. The contrasting sediment patterns could be related to the bi-directional nature of the tidal flows in the case of the Chioggia inlet and to the flow reversal within the Fehmarn Belt in the Baltic Sea or possibly to the combined action of the waves and currents. A similar anti-correlation between bathymetry and backscatter values is found also for a sand wave field in the Cook Strait in New Zealand (Lamarche et al., 2011).

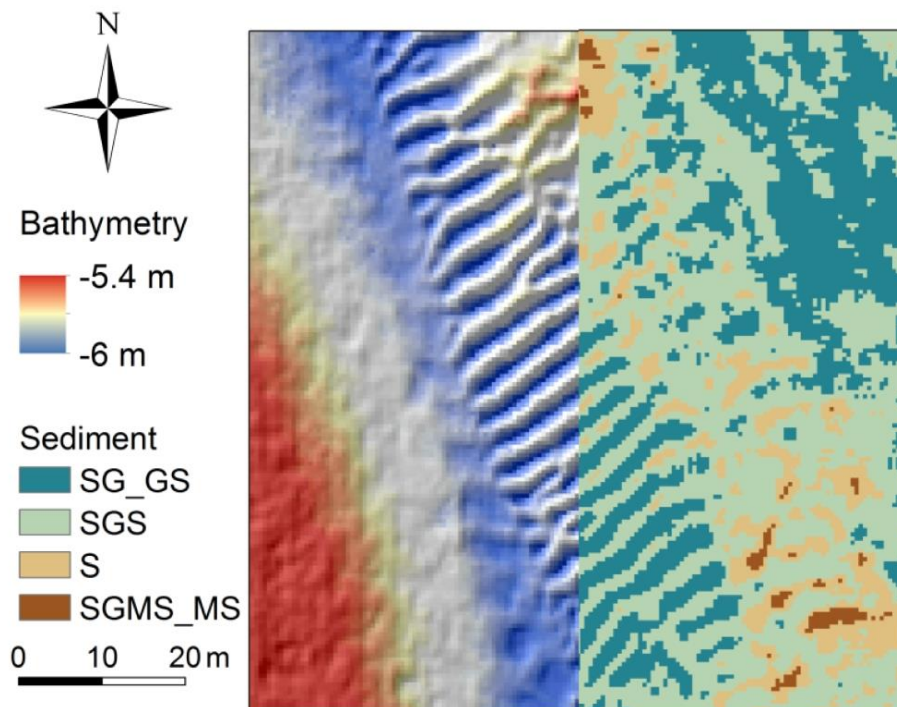


Figure I11: Bathymetry and sediment distribution of a dune field in the Chioggia inlet with Sandy Gravel_Gravelly Sand (SG_GS) in the troughs and Slightly Gravelly Sand (SGS) over the crests.

The relationship between the wavelength and height of the identified dunes is consistent with the empirical relationship found by Flemming (1988). In our case $\lambda = 0.79 * h - 1.13$, where λ is the dune wavelength and h the dune height with the correlation coefficient $R^2 = 0.84$.

Amos et al. (2010) showed that the sand flux through the inlets is dominated by bed-load transport. The strong asymmetry towards the sea of all dunes found in the study area is related to the direction of the residual currents (e.g. Fraccascia et al., 2016) and it suggests a net seaward bed-load transport and a predominant influence of the ebb tide current. This is in agreement with the results of Ferrarin et al. (2015) who found in the last 70 years an increased amplitude of the major tidal components and a shift of the Venice Lagoon tidal asymmetry towards ebb dominance. Particularly, over the last few years, they observed an enhanced ebb dominance over the whole lagoon to be related to the recent reduction of the inlets cross-sectional area.

3.5.2. The anthropogenic impact on tidal inlet benthic habitats

The human influence on the coast is stronger than in other regions of the Earth given that more than 40 % of the world population lives in coastal neighborhoods (Small and Nicholls, 2003; Ouillon, 2018). It is indeed recognized that human activities can be a morphogenetic process (Marriner et al., 2012; Kołodyńska-Gawrysiak and Poesen, 2017; Poesen, 2018) and can influence the main characteristics of an estuarine environment such as the tidal prism (Kerner, 2007; Winterwerp et al., 2013), the turbidity (Rapaglia et al., 2011; Winterwerp et al., 2013; Rodrigues et al., 2017), the sediment budget (Syvitski et al., 2005; Wang et al., 2007; Sarretta et al., 2010; Zhu et al., 2016), the erosion rate (De Roo and Troch, 2015; Zaggia et al., 2017) and the morphodynamics itself (Jeuken and Wang, 2010; Monge-Ganuzas et al., 2013).

The Chioggia tidal inlet represents an example where human-induced morphological processes have radically changed the seafloor over time. By comparing the bathymetric data collected in 2013 and the previous complete bathymetry of the lagoon collected in 2002 (MAV-CVN, 2004), we observed three main processes ongoing in the Chioggia inlet (Figs. I10 and I12): a) the main inlet channel experienced severe to extreme erosion likely due to the increased flow (Fig. I12), and in some parts of the inlet channel the deepening was due to the dredging and the seafloor armouring associated with the MoSE constructions (Figs. I2, I3i, I3j, I10 and I12); b) a strong deposition occurred in correspondence to the flood-tidal delta (Figs. I3 and I12), the large dunes (Figs. I3e, I3f and I12) and

the large internal scour hole (Figs. I3a and I12); c) large scour holes formed around the breakwater tips that were not present before the breakwater construction as documented by Villatoro (2010). In addition, deposition of fine sediments is occurring inside the area protected by the breakwater (Figs. I6 and 8).

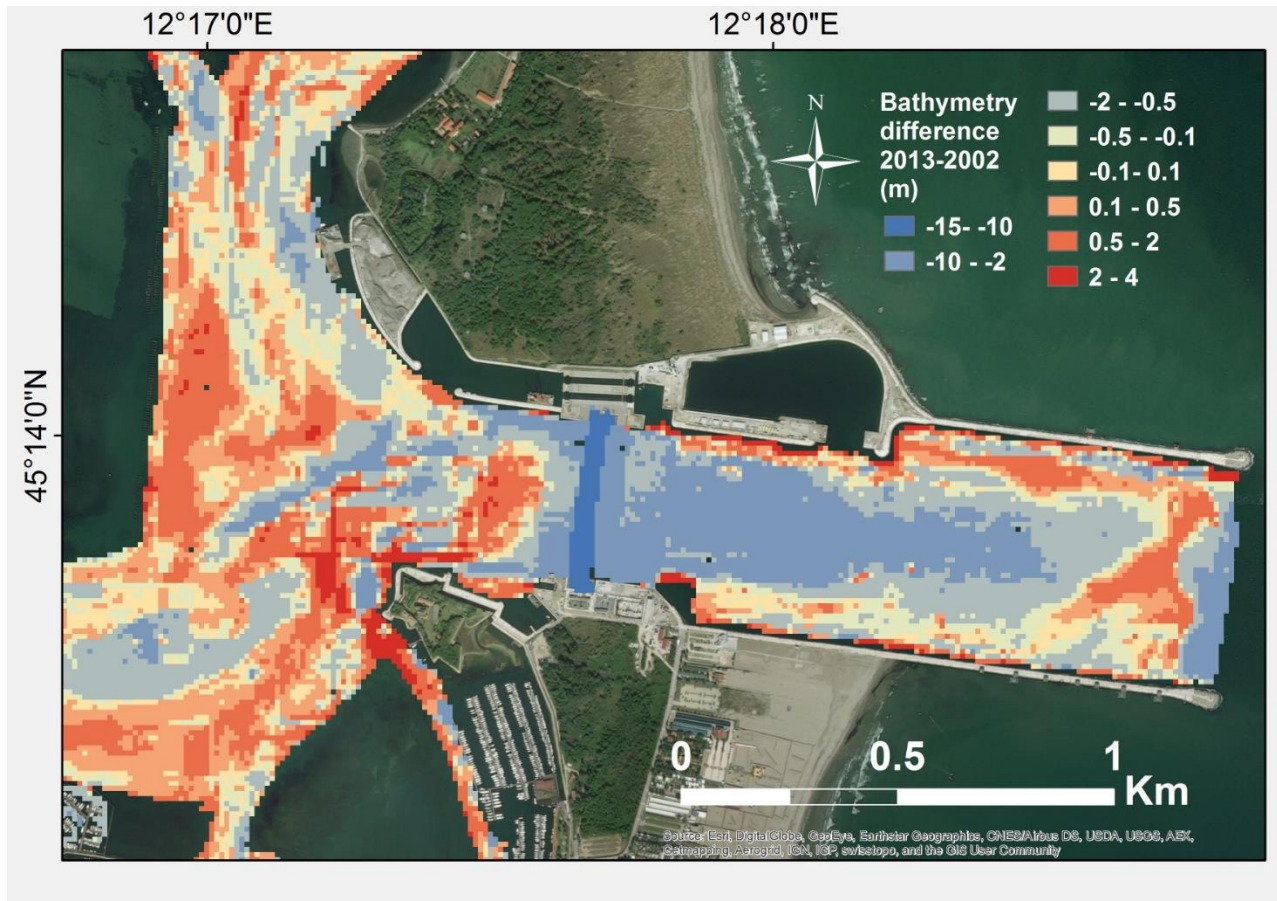


Figure I12: Bathymetric difference between the 2013 and 2002 dataset.

As observed by Sarretta et al. (2010), a generalised erosive process affected the central basin of the Venice Lagoon, with consequent loss of sediment by deposition into the channel network and/or seaward dispersion through the inlets. The southern sub-basin of the lagoon drained by the Chioggia inlet is less affected by this process compared to the Malamocco area (Sarretta et al., 2010). Yet, it is possible that part of the sediment eroded from the lagoon floor is transported to the Chioggia inlet, partly depositing on the flood-tidal delta, on the large dunes and in the internal hard structure scour hole and partly transported outside the inlet into the ebb-tidal delta region.

Within the tidal-channel inlet, the erosive process already observed by comparing the historical maps of 1927 and 1970 by Villatoro (2010) is still active (Fig. I12). The resizing of the inlet channel and the dredging operations within the MOSE project are very likely responsible for the deepening of the channel and a general increase of the current velocities inside the channel inlet, as already

predicted by the modelling study of Ghezzi et al. (2010). Villatoro et al. (2010) found a deposition trend in the inlet approaching the southern jetty (from -10 m in 1927 to -4 m in 2006). The 2013 measures however show a renewed erosive trend in that area.

By comparing our data with the sediment distribution of 2006 by Villatoro et al. (2010), we observe that the grain size of the inlet seafloor has increased with dense shell detritus deposits often dominating.

The ebb-tidal delta started to form after the end of the jetties construction, continuing its deposition process for half a century (Brancolini et al., 2006; Fontolan et al., 2007). After the construction of the breakwater (2003-2006), the erosive process started in just a few years forming large scours at the two breakwater tips. These scour holes could even endanger the stability of the breakwater itself by undercutting its base. In addition, the load of the new structures that will support the MoSE has increased the subsidence rate, showing a deepening up to 40 mm/year in some emerged sectors of the inlet (Tosi et al., 2013).

The benthic habitat classes are characterized by specific seafloor composition and morpho-bathymetric attributes, strongly dependent upon hydrodynamics and morphodynamics. These are major ecological factors for the highly dynamic lagoon inlets determining suspended sediment transport and deposition, oxygenation, saprobity, etc., which overall influence benthic communities recruitment, structure and functioning. Hydrodynamic alteration can indeed strongly modify benthic habitats and communities and their natural succession (e.g. Ashley and Grizzle, 1988; Blanchet et al., 2005; Pranovi et al., 2008; Tagliapietra et al., 2012).

Most of the described habitats, as well as their general spatial succession from the lagoon seawards, are well documented for the mudflats of the Venice Lagoon and the coastal area. The tidal channels and inlet habitats instead are still almost unexplored and their benthic assemblages were described extensively only by a survey carried out in 1930-1932 (Vatova, 1940; Vatova, 1949). In this survey, the Chioggia inlet was not described in detail. Later studies and monitoring efforts on the benthic assemblages focused mostly on the mudflats, with the exception of a few studies of limited spatial extent (e.g. Occhipinti-Ambrogi and Gola, 2001).

The map shown in Fig. 18 represents the first extensive full coverage map of tidal inlet benthic habitats in the Venice Lagoon. In particular, we observed a man-made habitat, here named *Artificial rock bed* (in grey in Fig. 18). This hard substratum habitat class, that occupies about 5.5 % of the study area and is found in correspondence to the jetties and rip-rap, hosts a diversified and structurally complex biological community, in marked contrast with the adjacent habitats. In fact,

nearly all the hard substrata in the west coast of the northern Adriatic Sea are artificial. The recent works at the inlets have greatly expanded this habitat, in particular by filling a 400 meters long section of the channel seabed continuously from side to side.

Several studies have been carried out globally on artificial reef habitats, which are a consequence of increasing human coastal urbanization and coastal protection from sea level rise and should be considered a main driver of change in coastal environments (e.g. Chapman, 2003; Bulleri and Chapman, 2004; Pister, 2009; Bulleri and Chapman, 2010; Perkins et al., 2015). However, this trend does not necessarily represent a negative impact on the ecosystem. Artificial hard substrata over an otherwise soft-sedimentary seabed increase habitat heterogeneity, therefore enhancing biodiversity (Turner, 1989; Williams, 1964). They increment the spatial complexity and the surface available for colonization of benthic communities (Svane and Petersen, 2001) and play as refugia, feeding grounds and nursery areas for fish populations (Brickhill et al., 2005; Clynick et al., 2007). Their ecological function, however, may differ consistently from natural rocky habitats (e.g. Ferrario et al., 2016) as well as from the pre-existing sandy bottom (Bulleri and Chapman, 2010). Although the artificial rock bed, recently deployed on the inlet seabed, is not particularly extended compared to the other habitats, impacts from habitat fragmentation and loss of connectivity cannot be excluded. Moreover, artificial substrata may promote the settlement of non-indigenous species in comparison to a soft-sedimentary environment (Wasson et al., 2005; Glasby et al., 2007). This issue deserves particular attention given that the Venice Lagoon is a hotspot for non-indigenous species within the Mediterranean Sea (Occhipinti-Ambrogi et al., 2011). More ecological research is needed to verify the ecological role of this habitat for the whole system and to understand its evolution.

Dredging is also responsible for significant ecological impacts (e.g. Van Raalte, 2006; Monge-Ganuzas et al., 2013; Van Maren et al., 2015). In many cases, this activity increased environmental deterioration, by changing the pattern of hydrodynamics, augmenting salinity stratification and resuspending muddy sediments, pollutants and nutrients (Newell et al., 1998; Teatini et al., 2017). In this study, we identified 111,483 m² of dredging surfaces (about the 1.14 % of the study area), located exclusively in the shallow lagoon basin. Dredging may have important consequences for the ecosystem functionality due to direct hydrodynamics and morphology alterations (Cozzoli et al., 2017). Dredging can modify the natural development of the lagoon geomorphology (Healy et al., 1996): for example, as previously mentioned the west margin of the flood-tidal delta is sharply cut by the presence of a dredged canal. This physical element that should develop an important and structured shape (Hayes and Fitzgerald, 2013) has been seriously resized to just 69,018 m².

Furthermore, the presence of dredging channels near mudflat and salt marshes, can limit the spreading of seagrass meadows, strongly dependent on the depth gradient (Paulo et al., 2016).

The anthropogenic submerged litter and abandoned fishing gear are an emerging issue for the society and for marine sciences: however, most of the available researches are based on photo/video surveys (e.g. Schlining et al., 2013; Pham et al., 2014) or on samples collected by seabed trawling (Kammann et al., 2017; Grøsvik et al., 2018; Maes et al., 2018; Madricardo et al., 2019) being mainly focused on plastic/glass rubbles. This study also confirms that MBES surveys can be a useful aid in mapping the density distribution of macro-litter and wrecks in shallow coastal areas.

3.6. Conclusions

Through the combined analysis of MBES and ground truth data, we constructed high resolution maps of the seafloor morphology, sediment distribution and habitats of the highly human modified Venice Lagoon tidal inlets.

We found 10 distinctive erosive, depositional morphological features, 4 sediment classes ranging from muds to sandy gravel and 7 benthic habitats among which *Sand with bioclasts* (46 %) and *Bare sand* (32 %) were dominant.

Then, we assessed the direct and indirect modifications induced within the tidal inlet by a new grey infrastructure, the MoSE system, still under construction to protect the historical city of Venice and the other lagoon islands from floods. Specifically:

- 1) We documented that a general coarsening of the sediment distribution has occurred inside the inlet channel likely due to the increased flow velocity induced by the narrowing of the inlet.
- 2) All dunes mapped in the tidal inlet are markedly asymmetric and seaward oriented, showing a net ebb-dominated bedload transport.
- 3) The mechanism of flow separation induced by the construction of the breakwater results in rapid erosion around the structure of 430,000 m³ of sediment in 8 years, threatening the stability of the structure.

- 4) The armoring of the tidal inlet channel seafloor with the rip-rap revetment placed near the mobile barrier lodgments introduced a new habitat, called *Artificial rock bed*, exploited by hard substrata benthic associations.

The proliferation of a variety of built grey infrastructures (breakwaters, seawalls, jetties and pilings, mobile barriers, etc.) and anthropogenic activities in the near shore estuarine and marine waters calls for a comprehensive assessment of their impact on the seafloor to support a knowledge-based management of the coastal environment. The multidisciplinary approach described in this work can be applied to study the consequences of the substantial transformation of coastal landscapes that is taking place in response to urbanization and sea level rise and consequent engineering intervention on the coastal systems.

Acknowledgments

The authors would like to acknowledge all the rest of the ISMAR Team (Federica Foglini, Marco Bajo, Debora Bellafiore, Elisabetta Campiani, Valentina Grande, Lukasz Janowski, Erica Keppel, Elisa Leidi, Francesco Maicu, Vittorio Maselli, Alessandra Mercorella, Claudio Pellegrini, Mariacristina Prampolini, Alessandro Remia, Federica Rizzetto, Marzia Rovere) that contributed to collect and process the MBES data of the Venice Lagoon in 2013 (available from <http://dx.doi.org/10.1594/IEDA/323605>). The authors are grateful to the crew of the CNR research vessel Litus for their skillful help during the survey and to Loris Dametto for his technical help on the ground truth sampling. The authors would like to thank Christian Ferrarin for providing the tidal corrections for the MBES data and William Mc Kiver for reading and commenting the manuscript. Finally, Stefano Fogarin is very grateful to Prof. Giancarlo Rampazzo of the University of Ca' Foscari for his help during his MSc thesis, when part of this work was carried out. This work was supported by the National Flagship Project RITMARE, funded by MIUR, the Italian Ministry of Education, University and Research.

Maps throughout this paper were created using ArcGIS® software by Esri. ArcGIS® and ArcMap™ are the intellectual property of Esri and are used herein under license. Copyright © Esri. All rights reserved. For more information about Esri® software, please visit www.esri.com.

The authors would like to thank the editor and the anonymous reviewers for their valuable suggestions that helped to substantially improve the manuscript.

3.7. References

- Aguilera MA. 2017. Artificial defenses in coastal marine ecosystems in Chile: Opportunities for spatial planning to mitigate habitat loss and alteration of the marine community structure. *Ecological Engineering*.
- Albani AD, Favero VM, Barbero RS. 1998. Distribution of sediment and benthic foraminifera in the Gulf of Venice, Italy. *Estuarine, Coastal and Shelf Science* 46(2): 251-265.
- Amos CL, Villatoro MM, Helsby R, Thompson CEL, Zaggia L, Umgiesser G, Venturini V, Are D, Sutherland TF, Mazzoldi A, Rizzetto F. 2010. The measurement of sand transport in two inlets of Venice lagoon, Italy. *Estuarine, Coastal and Shelf Science* 87(2): 225-236.
- Ashley GM. 1990. Classification of large-scale subaqueous bedforms: a new look at an old problem. *Journal of Sedimentary Petrology* 60: 160-172.
- Ashley GM, Grizzle RE. 1988. Interactions between hydrodynamics, benthos and sedimentation in a tide dominated coastal lagoon. *Marine Geology* 82: 61-81.
- Balletti C. 2006. Digital elaborations for cartographic reconstruction: the territorial transformations of Venice harbours in historical maps. *e-Perimetron* 1(4): 274-286.
- Bird ECF. 1994. Physical setting and geomorphology of coastal lagoons. In Kjerfve, B. (ed.), *Coastal Lagoon Processes*.
- Bird ECF. 2008. *Coastal geomorphology: an introduction*. John Wiley & Sons.
- Blanchet H, de Montaudouin X, Chardy P, Bachelet G. 2005. Structuring factors and recent changes in subtidal macrozoobenthic communities of a coastal lagoon, Arcachon Bay (France). *Estuarine, Coastal and Shelf Science*, 64: 561-576.
- Blott SJ, Pye K. 2001. GRADISTAT: a grain size distribution and statistics package for the analysis of unconsolidated sediments. *Earth surface processes and Landforms* 26(11): 1237-1248.
- Book JW, Perkins H, Wimbush M. 2009. North Adriatic tides: observations, variational data assimilation modeling, and linear tide dynamics. *Geofizika* 26: 115–143.
- Brancolini G, Tosi L, Baradello L, Bratus A, Donda F, Rizzetto F, Zecchin M. 2006. Preliminary results of the high resolution seismic surveys in the Venice Lagoon. *Scientific Research and Safeguarding of Venice, 2004-2006*.
- Brickhill MJ, Lee SY, Connolly RM. 2005. Fishes associated with artificial reefs: attributing changes to attraction or production using novel approaches. *Journal of Fish Biology*, 67: 53-71.
- Brown CJ, Smith SJ, Lawton P, Anderson JT. 2011. Benthic habitat mapping: A review of progress towards improved understanding of the spatial ecology of the seafloor using acoustic techniques. *Estuarine, Coastal and Shelf Science*, 92(3), pp.502-520.

3. Study I: Tidal inlets in the Anthropocene: geomorphology and benthic habitats of the Chioggia inlet, Venice Lagoon (Italy)

- Brown AG, Tooth S, Bullard JE, Thomas DS, Chiverrell RC, Plater AJ, Murton J, Thorndycraft VR, Tarolli P, Rose J, Wainwright J, Downs P, Aalto R. 2017. The geomorphology of the Anthropocene: emergence, status and implications. *Earth Surface Processes and Landforms* 42(1): 71-90.
- Bulleri F, Chapman MG. 2004. Intertidal assemblages on artificial and natural habitats in marinas on the north-west coast of Italy. *Marine Biology* 145(2): 381-391.
- Bulleri F, Chapman MG. 2010. The introduction of coastal infrastructure as a driver of change in marine environments. *Journal of Applied Ecology* 47(1): 26-35.
- Carniello L, Defina A, D'Alpaos L. 2009. Morphological evolution of the Venice lagoon: Evidence from the past and trend for the future. *Journal of Geophysical Research: Earth Surface*, 114: 1-10.
- Cavazzoni S. 1995. La laguna: origine ed evoluzione. *La laguna di Venezia*, Verona; 41-75.
- Chapman MG. 2003. Paucity of mobile species on constructed seawalls: effects of urbanization on biodiversity. *Marine Ecology Progress Series* 264: 21-29.
- Cima F, Ballarin L. 2013. A proposed integrated bioindex for the macrofouling biocoenosis of hard substrata in the lagoon of Venice. *Estuarine, Coastal and Shelf Science* 130: 190-201.
- Clynick BG, Chapman MG, Underwood AJ. 2007. Effects of epibiota on assemblages of fish associated with urban structures. *Marine Ecology Progress Series*, 332: 201-210.
- Consorzio Venezia Nuova. 1989. Progetto preliminare di massima delle opere alle bocche, Volume 2, Descrizione dell'ecosistema, Parte II. Ministero dei Lavori Pubblici, Magistrato alle Acque di Venezia.
- Costanza R, Darge R, Degroot R, Farber S, Grasso M, Hannon B, Limburg K, Naeem S, Oneill RV, Paruelo J, Raskin RG, Sutton P, Vandenbelt M. 1997. The value of the worlds ecosystem services and natural capital. *Nature* 387: 253-260.
- Cozzoli F, Smolders S, Eelkema M, Ysebaert T, Escaravage V, Temmerman S, Meire P, Herman PMJ, Bouma TJ. 2017. A modeling approach to assess coastal management effects on benthic habitat quality: A case study on coastal defense and navigability. *Estuarine, Coastal and Shelf Science* 184: 67-82.
- Curiel D, Checchin E, Miotti C, Pierini A, Rismondo A. 2014. Praterie a fanerogame marine della laguna di Venezia-aggiornamento cartografico al 2010 e confronto storico. *Lav. Society. Venezia. Science. Nature* 39: 55-66.
- Dafforn KA, Glasby TM, Airoldi L, Rivero NK, Mayer-Pinto M, Johnston EL. 2015. Marine urbanization: an ecological framework for designing multifunctional artificial structures. *Frontiers in Ecology and the Environment* 13(2): 82-90.
- D'Alpaos L. 2010. L'evoluzione morfologica della laguna di Venezia attraverso la lettura di alcune mappe storiche e delle sue mappe idrografiche. *Comune di Venezia, Istituzione Centro Previsioni e Segnalazioni Maree Europrint srl, Quinto di Treviso* 2010, 110.

3. Study I: Tidal inlets in the Anthropocene: geomorphology and benthic habitats of the Chioggia inlet, Venice Lagoon (Italy)

- De Falco G, Tonielli R, Di Martino G, Innangi S, Simeone S, Parnum IM. 2010. Relationships between multibeam backscatter, sediment grain size and *Posidonia oceanica* seagrass distribution. *Continental Shelf Research* 30(18): 1941-1950
- De Haas T, Pierik HJ, Van der Spek AJF, Cohen KM, Van Maanen B, Kleinbans MG., 2018. Holocene evolution of tidal systems in The Netherlands: Effects of rivers, coastal boundary conditions, eco-engineering species, inherited relief and human interference. *Earth-Science Reviews*.
- De Roo S, Troch P. 2015. Evaluation of the Effectiveness of a Living Shoreline in a Confined, Non-Tidal Waterway Subject to Heavy Shipping Traffic. *River research and applications* 31(8): 1028-1039.
- Diesing M, Green SL, Stephens D, Lark RM, Stewart HA, Dove D. 2014. Mapping seabed sediments: comparison of manual, geostatistical, object-based image analysis and machine learning approaches. *Continental Shelf Research*, 84: 107-119.
- Durán R, Guillén J, Rivera J, Muñoz A, Lobo FJ, Fernández-Salas LM, Acosta J. 2017. Subaqueous Dunes Over Sand Ridges on the Murcia Outer Shelf. In *Atlas of bedforms in the Western Mediterranean*: 187-192)
- Elliott M, Cutts ND. 2004. Marine habitats: loss and gain, mitigation and compensation. *Marine Pollution Bulletin* 49 (9–10): 671-674.
- ESRI, 2016. ArcGis Desktop: Release 10.2. Environmental System Research Institute.
- De Swart HE, Zimmerman JTF. 2009. Morphodynamics of tidal inlet systems. *Annual review of fluid mechanics*, 41, pp.203-229.
- Favero V. 1991. Evoluzione morfologica e trasformazioni ambientali dalla conterminazione lagunare al nostro secolo. In *Conterminazione lagunare: storia, ingegneria, politica e diritto nella laguna di Venezia*. Proceedings of the Conference Convegno di studio nel bicentenario della conterminazione lagunare; 14-16.
- Feldens P, Diesing M, Schwarzer K, Heinrich C, Schlenz B. 2015. Occurrence of flow parallel and flow transverse bedforms in Fehmarn Belt (SW Baltic Sea) related to the local palaeomorphology. *Geomorphology* 231: 53-62.
- Ferrarin C, Tomasin A, Bajo M, Petrizzo A, Umgiesser G. 2015. Tidal changes in a heavily modified coastal wetland. *Continental Shelf Research* 101: 22-33.
- Ferrarin C, Madricardo F, Rizzetto F, Mc Kiver W, Bellafiore D, Umgiesser G, Kruss, A, Zaggia, L, Foglini, F, Ceregato, A, Sarretta, A, Trincardi, F. 2018. Geomorphology of scour holes at tidal channel confluences. *Journal of Geophysical Research: Earth Surface*.
- Ferrario F, Iveša L, Jaklin A, Perkol-Finkel S, Airoidi L, 2016. The overlooked role of biotic factors in controlling the ecological performance of artificial marine habitats. *Journal of Applied Ecology* 53 (1): 16-24.
- Finney SC, Edwards LE. 2016. The “Anthropocene” epoch: Scientific decision or political statement. *gsa Today* 26(3): 3-4.

3. Study I: Tidal inlets in the Anthropocene: geomorphology and benthic habitats of the Chioggia inlet, Venice Lagoon (Italy)

- Flemming BW. 2000. The role of grain size, water depth and flow velocity as scaling factors controlling the size of subaqueous dunes. In *Marine sandwave dynamics, international workshop*; 23-24.
- Folk RL, Ward WC. 1957. Brazos River bar: a study in the significance of grain size parameters. *Journal of Sedimentary Research* 27(1).
- Folk RL, Andrews PB, Lewis D. 1970. Detrital sedimentary rock classification and nomenclature for use in New Zealand. *New Zealand journal of geology and geophysics*, 13(4), 937-968.
- Fontolan G, Pillon S, Quadri FD, Bezzi A. 2007. Sediment storage at tidal inlets in northern Adriatic lagoons: Ebb-tidal delta morphodynamics, conservation and sand use strategies. *Estuarine, Coastal and Shelf Science* 75(1-2): 261-277.
- Foody GM. 2002. Status of land cover classification accuracy assessment. *Remote sensing of environment* 80(1): 185-201.
- Fraccascia S, Winter C, Ernsten VB, Hebbeln D. 2016. Residual currents and bedform migration in a natural tidal inlet (Knudedyb, Danish Wadden Sea). *Geomorphology* 271: 74-83.
- Fredsøe J, Sumer BM. 1997. Scour at the round head of a rubble-mound breakwater. *Coast. Eng.* 29(3-4), 231-262.
- Fruergaard M, Møller I, Johannessen PN, Nielsen LH, Andersen TJ, Nielsen L, Andersen TJ, Nielsen L, Sander L, Pejrup M. 2015. Stratigraphy, evolution, and controls of a Holocene transgressive–regressive barrier island under changing sea level: Danish North Sea coast. *Journal of Sedimentary Research*, 85(7): 820-844.
- Gačić M, Mosquera IM, Kovačević V, Mazzoldi A, Cardin V, Arena F, Gelsi G. 2004. Temporal variations of water flow between the Venetian lagoon and the open sea. *Journal of Marine systems* 51(1-4): 33-47.
- Gatto P, Carbognin L. 1981. The Lagoon of Venice: natural environmental trend and man-induced modification/La Lagune de Venise: l'évolution naturelle et les modifications humaines. *Hydrological Sciences Journal* 26(4): 379-391.
- Ghezzi M, Guerzoni S, Cucco A, Umgiesser G. 2010. Changes in Venice Lagoon dynamics due to construction of mobile barriers. *Coastal Engineering* 57(7): 694-708.
- Glasby TM, Connell SD, Holloway MG, Hewitt CL. 2007. Nonindigenous biota on artificial structures: Could habitat creation facilitate biological invasions? *Marine Biology* 151: 887-895.
- Gönenç IE, Wolflin JP. 2005, *Coastal Lagoons: Ecosystem Processes and Modeling for Sustainable Use and Development* 500, CRC Press, Boca Raton, Fla.
- Grøsvik BE, Prokhorova T, Eriksen E, Krivosheya P, Horneland PA, Prozorkevich D. 2018. Assessment of Marine Litter in the Barents Sea, a Part of the Joint Norwegian–Russian Ecosystem Survey. *Frontiers in Marine Science* 5: 72.
- Hamilton C. 2016. The Anthropocene as rupture. *The Anthropocene Review* 3(2): 93-106.
- Hayes MO, FitzGerald DM. 2013. Origin, evolution, and classification of tidal inlets. *Journal of Coastal Research* 69(1): 14-33.

3. Study I: Tidal inlets in the Anthropocene: geomorphology and benthic habitats of the Chioggia inlet, Venice Lagoon (Italy)

Healy T, Mathew J, de Lange W, Black K. 1996. Adjustments toward equilibrium of a large flood-tidal delta after a major dredging program, Tauranga Harbour, New Zealand. *Coastal Engineering* 1996: 3284-3294.

Hickin EJ. 1974. The development of meanders in natural river-channels. *American journal of science* 274(4): 414-442.

Hijma MP, Cohen KM, Roebroeks W, Westerhoff WE, Busschers FS. 2012. Pleistocene Rhine–Thames landscapes: geological background for hominin occupation of the southern North Sea region. *Journal of Quaternary Science*, 27(1), pp.17-39.

Ierodiaconou D, Schimel A C, Kennedy D, Monk J, Gaylard G, Young M, Diesin M, Rattray A, 2018. Combining pixel and object based image analysis of ultra-high resolution multibeam bathymetry and backscatter for habitat mapping in shallow marine waters. *Marine Geophysical Research*, pp.1-18.

Jenks GF. 1967. The Data Model Concept in Statistical Mapping, *International Yearbook of Cartography* 7: 186–190

Jeuken MCJL, Wang ZB. 2010. Impact of dredging and dumping on the stability of ebb–flood channel systems. *Coastal Engineering* 57(6): 553-566.

Kammann U, Aust MO, Bahl H, Lang T. 2017. Marine litter at the seafloor—Abundance and composition in the North Sea and the Baltic Sea. *Marine pollution bulletin* 127: 774-780.

Katayama T, Irie I, Kawakami T. 1974. Performance of offshore breakwaters of the Niigata coast. *Coastal Engin. Japan*, 17, 129-139.

Keller EA, Melhorn WN. 1978. Rhythmic spacing and origin of pools and riffles. *Geological Society of America Bulletin*, 89(5): 723-730.

Kerner M. 2007. Effects of deepening the Elbe Estuary on sediment regime and water quality. *Estuarine, coastal and shelf science* 75(4): 492-500.

Kjerfve B, Magill KE. 1989. Geographic and hydrodynamic characteristics of shallow coastal lagoons. *Marine geology*, 88(3-4): 187-199.

Kjerfve B. 1994. *Coastal lagoon processes*. Elsevier, Amsterdam, The Netherlands. Amsterdam: Elsevier: 9–39

Kołodzyńska-Gawrysiak R, Poesen J. 2017. Closed depressions in the European loess belt—Natural or anthropogenic origin? *Geomorphology* 288: 111-128.

Lamarche G, Lurton X, Verdier AL, Augustin JM. 2011. Quantitative characterisation of seafloor substrate and bedforms using advanced processing of multibeam backscatter—Application to Cook Strait, New Zealand. *Continental Shelf Research* 31(2): S93-S109.

Lecours V, Devillers R, Simms AE, Lucieer VL, Brown CJ. 2017. Towards a framework for terrain attribute selection in environmental studies. *Environmental Modelling & Software* 89: 19-30.

3. Study I: Tidal inlets in the Anthropocene: geomorphology and benthic habitats of the Chioggia inlet, Venice Lagoon (Italy)

Lecours V, Devillers R, Lucieer VL, Brown CJ. 2017. Artefacts in marine digital terrain models: a multiscale analysis of their impact on the derivation of terrain attributes. *IEEE Transactions on Geoscience and Remote Sensing* 55(9): 5391-5406.

Lillycrop WJ, Hughes SA. 1993. Scour hole problems experienced by the Corps of Engineers. Data presentation and summary. Miscellaneous papers. CERC-93-2, US Army Engineer Waterways Experiment Station, Coastal Engineering Research Center, Vicksburg, MS.

Lucieer V, Hill NA, Barrett NS, Nichol S. 2013. Do marine substrates 'look' and 'sound' the same? Supervised classification of multibeam acoustic data using autonomous underwater vehicle images. *Estuarine, Coastal and Shelf Science* 117: 94-106.

Luisetti T, Turner RK, Jickells T, Andrews J, Elliott M, Schaafsma M, Beaumont N, Malcolm S, Burdon D, Adams C, Watts W. 2014. Coastal Zone Ecosystem Services: from science to values and decision making; a case study. *Science of the Total Environment* 493: 682-693.

Madricardo F, Donnici S. 2014. Mapping past and recent landscape modifications in the Lagoon of Venice through geophysical surveys and historical maps. *Anthropocene* 6: 86-96.

Madricardo F, Fogliani F, Kruss A, Ferrarin C, Pizzeghello NM, Murri C, Rossi M, Bajo M, Bellafiore D, Campiani E, Fogarin S, Grande V, Janowski L, Keppel E, Leidi E, Lorenzetti G, Maicu F, Maselli V, Mercorella A, Montereale Gavazzi G, Minuzzo T, Pellegrini C, Petrizzo A, Prampolini M, Remia A, Rizzetto F, Rovere M, Sarretta A, Sigovini M, Sinapi L, Umgiesser G, Trincardi F. 2017. High resolution multibeam and hydrodynamic datasets of tidal channels and inlets of the Venice Lagoon. *Scientific data* 4, 170121.

Madricardo F, Rizzetto F. 2018. Shallow Coastal Landforms. In *Submarine Geomorphology*: 161-183.

Madricardo F, Fogliani F, Campiani C, Grande V, Catenacci E, Petrizzo A, Kruss A, Toso C, and Fabio Trincardi F. (2019). Assessing the human footprint on the sea-floor of coastal systems: the case of the Venice Lagoon, Italy, *Scientific Reports*.

Maes T, Barry J, Leslie HA, Vethaak AD, Nicolaius EEM, Law RJ, Lyons BP, Martinez R, Harley B, Thain JE. 2018. Below the surface: Twenty-five years of seafloor litter monitoring in coastal seas of North West Europe (1992–2017). *Science of the Total Environment* 630: 790-798.

Magistrato alle Acque di Venezia. 1997. Interventi alle bocche lagunari per la regolazione dei flussi di marea - Studio di impatto ambientale del progetto di massima, Allegato 6, Tema 5, 163.

Magrini G. 1933. La Laguna di Venezia, in *La Laguna di Venezia*, Monografia coordinata da G. Magrini, Delegazione Italiana della Commissione per l'esplorazione scientifica del Mediterraneo, Atlante II, C. Ferrari, Venezia 1933.

Magrini G. 1934. Carta topografica idrografica militare della laguna di Venezia rilevata dal capitano Augusto Dénaix negli anni 1809-10-11, Atlante Primo, Stamperia Ferrari, Venezia 1934.

3. Study I: Tidal inlets in the Anthropocene: geomorphology and benthic habitats of the Chioggia inlet, Venice Lagoon (Italy)

Marriner N, Flaux C, Morhange C, Kaniewski D. 2012. Nile Delta's sinking past: Quantifiable links with Holocene compaction and climate-driven changes in sediment supply? *Geology* 40(12): 1083-1086.

MAV-CVN. 2004. Attività di aggiornamento del piano degli interventi per il recupero morfologico in applicazione della delibera del Consiglio dei Ministri del 15 Marzo 2001. Studi di base, linee guida e proposte di intervento del piano morfologico. Magistrato alle Acque di Venezia, Consorzio Venezia Nuova, Venice, Italy, Technical Report.

Mayer L, Jakobsson M, Allen G, Dorschel B, Falconer R, Ferrini V, Lamarche G, Snaith H, Weatherall P. 2018. The Nippon Foundation—GEBCO Seabed 2030 Project: The quest to see the world's oceans completely mapped by 2030. *Geosciences* 8(2):63.

McGonigle C, Collier JS. 2014. Interlinking backscatter, grain size and benthic community structure. *Estuarine, Coastal and Shelf Science* 147: 123-136.

Miselis JL, Lorenzo-Trueba J. 2017. Natural and Human-Induced Variability in Barrier-Island Response to Sea Level Rise. *Geophysical Research Letters*, 44(23).

Molinarioli E, Guerzoni S, Sarretta A, Cucco A, Umgiesser G. 2007. Links between hydrology and sedimentology in the Lagoon of Venice, Italy. *Journal of Marine Systems* 68(3-4): 303-317.

Molinarioli E, Guerzoni S, Sarretta A, Masiol M, Pistolato M. 2009. Thirty-year changes (1970 to 2000) in bathymetry and sediment texture recorded in the Lagoon of Venice sub-basins, Italy. *Marine Geology* 258(1-4): 115-125.

Monge-Ganuzas M, Cearreta A, Evans G. 2013. Morphodynamic consequences of dredging and dumping activities along the lower Oka estuary (Urdaibai Biosphere Reserve, southeastern Bay of Biscay, Spain). *Ocean & coastal management* 77: 40-49.

Montereale-Gavazzi G, Madricardo F, Janowski L, Kruss A, Blondel P, Sigovini M, Fogliani F. 2016. Evaluation of seabed mapping methods for fine-scale classification of extremely shallow benthic habitats—application to the Venice Lagoon, Italy. *Estuarine, Coastal and Shelf Science* 170: 45-60.

Moore LJ, Murray AB. 2018. Geometric constraints on long-term barrier migration: from simple to surprising. In *Barrier Dynamics and Response to Changing Climate*: 211-241. Springer, Cham.

Newell R, Seiderer LJ, Hitchcock DR. 1998. The impact of dredging works in coastal waters: a review of the sensitivity to disturbance and subsequent recovery of biological resources on the sea bed. *Oceanography and Marine Biology: An Annual Review* 36: 127-178.

Noormets R, Ernstsens VB, Bartholomä A, Flemming BW, Hebbeln D, 2006. Implications of bedform dimensions for the prediction of local scour in tidal inlets: a case study from the southern North Sea. *Geo-Marine Letters*, 26(3):165-176.

Occhipinti-Ambrogi A, Gola G. 2001. Macrozoobenthos di fondo incoerente in Laguna di Venezia: contributo alla conoscenza del bacino di Malamocco. *Biol. Mar. Mediterr.*, 8 (1): 393-402.

3. Study I: Tidal inlets in the Anthropocene: geomorphology and benthic habitats of the Chioggia inlet, Venice Lagoon (Italy)

Occhipinti-Ambrogi A, Marchini A, Cantone G, Castelli A, Chimenz C, Cormaci M, Froggia C, Furnari G, Gambi MC, Giaccone G, Giangrande A, Gravili C, Mastrototaro F, Mazziotti C, Orsi-Relini L, Piraino S. 2011. Alien species along the Italian coasts: an overview. *Biological Invasions*, 13(1): 215-237.

Oertel GF. 1985. The barrier island system. *Marine Geology* 63: 1-18.

Oost AP, Hoekstra P, Wiersma A, Flemming B, Lammerts EJ, Pejrup M, Hofstede J, Van der Valk B, Kiden P, Bartholdy J, Van der Berg MW, Vos PC, de Vries S, Wang ZB. 2012. Barrier island management: Lessons from the past and directions for the future. *Ocean & coastal management* 68: 18-38.

Ouillon S. 2018. Why and How Do We Study Sediment Transport? Focus on Coastal Zones and Ongoing Methods. *Water* 10(4):390.

Paulo D, Manent P, Barrio JM, Alvares Serrao E, Alberto F. 2016. Recruit survival of *Cymodocea nodosa* along a depth gradient. *CAHIERS DE BIOLOGIE MARINE* 57(2): 137-144.

Perkins MJ, Ng TP, Dudgeon D, Bonebrake TC, Leung K M. 2015. Conserving intertidal habitats: what is the potential of ecological engineering to mitigate impacts of coastal structures? *Estuarine, Coastal and Shelf Science* 167: 504-515.

Pham CK, Ramirez-Llodra E, Alt CH, Amaro T, Bergmann M, Canals M, Company JB, Davies J, Duineveld G, Galgani F, Howell KL, Huvenne VA, Isidro E, Jones DOB, Lastras G, Morato T, Gomes-Pereira JN, Purser A, Stewart H, Tojeira I, Tubau X, Van Rooij D, Tyler PA. 2014. Marine litter distribution and density in European seas, from the shelves to deep basins. *PLoS one* 9(4), e95839.

Pister B. 2009. Urban marine ecology in southern California: the ability of riprap structures to serve as rocky intertidal habitat. *Marine Biology* 156(5): 861-873.

Poesen J. 2018. Soil erosion in the Anthropocene: Research needs. *Earth Surface Processes and Landforms* 43(1): 64-84.

Powell EJ, Tyrrell MC, Milliken A, Tirpak JM, Staudinger MD. 2018. A review of coastal management approaches to support the integration of ecological and human community planning for climate change. *Journal of Coastal Conservation*, pp.1-18.

Pranovi F, Da Ponte F, Torricelli P. 2008. Historical changes in the structure and functioning of the benthic community in the lagoon of Venice. *Estuarine, Coastal and Shelf Science*, 76(4): 753-764.

Rapaglia J, Zaggia L, Ricklefs K, Gelinis M, Bokuniewicz H. 2011. Characteristics of ships' depression waves and associated sediment resuspension in Venice Lagoon, Italy. *Journal of Marine Systems* 85(1-2): 45-56.

Reddy NA, Vikas M, Rao S, Seelam JK. 2015. Classification of tidal inlets along the central east coast of India. *Procedia Engineering* 116: 922-931.

Renaud FG, Syvitski JP, Sebesvari Z, Werners SE, Kremer H, Kuenzer C, Ramesh R, Jeuken A, Friedrich J. 2013. Tipping from the Holocene to the Anthropocene: How threatened are major world deltas?. *Current Opinion in Environmental Sustainability*, 5(6): 644-654.

3. Study I: Tidal inlets in the Anthropocene: geomorphology and benthic habitats of the Chioggia inlet, Venice Lagoon (Italy)

- Rismondo A, Curiel D, Marzocchi M, Scattolin M. 1997. Seasonal pattern of *Cymodocea nodosa* biomass and production in the lagoon of Venice. *Aquatic Botany*, 58(1), 55-64.
- Rodrigues V, Estrany J, Ranzini M, de Cicco V, Martín-Benito JMT, Hedø J, Lucas-Borja ME. 2017. Effects of land use and seasonality on stream water quality in a small tropical catchment: The headwater of Córrego Água Limpa, São Paulo (Brazil). *Science of The Total Environment*: 1553-1561.
- Sarretta A, Pillon S, Molinaroli E, Guerzoni S, Fontolan G. 2010. Sediment budget in the Lagoon of Venice, Italy. *Continental Shelf Research* 30(8): 934-949.
- Roelvink D, Boutmy A, Stam JM. 1999. A simple method to predict long-term morphological changes. In *Coastal Engineering 1998*: 3224-3237.
- Sato S, Tanaka N, Irie I. 1968. Study on scouring at the foot of coastal structures. *Proceedings of 11th Coastal Engineering Conference, American Society of Civil Engineers*: 579-598.
- Schlining K, Von Thun S, Kuhn L, Schlining B, Lundsten L, Stout NJ, Chaney L, Connor J. 2013. Debris in the deep: Using a 22-year video annotation database to survey marine litter in Monterey Canyon, central California, USA. *Deep Sea Research Part I: Oceanographic Research Papers*, 79: 96-105.
- Small C, Nicholls RJ. 2003. A global analysis of human settlement in coastal zones. *Journal of coastal research*: 584-599.
- Smith D, Harrison S, Firth C, Jordan J. 2011. The Early Holocene sea level rise. *Quaternary Science Review* 30 (15): 1846–1860.
- Stanic S, Briggs KB, Fleischer P, Ray RI, Sawyer WB. 1988. Shallow-water high-frequency bottom scattering off Panama City, Florida. *The Journal of the Acoustical Society of America* 83(6): 2134-2144.
- Stanley DJ, Warne AG. 1994. Worldwide initiation of Holocene marine deltas by deceleration of sea-level rise. *Science*, 265(5169), pp.228-231.
- Story M, Congalton RG. 1986. Accuracy Assessment: A User's Perspective. *Photogrammetric Engineering and Remote Sensing* 52: 397-399.
- Stutz ML, Pilkey OH. 2011. Open-Ocean Barrier Islands: Global Influence of Climatic, Oceanographic, and Depositional Settings. *Journal of Coastal Research* 27(2): 207–222.
- Sumer BM, Fredsøe J. 1997. Scour at the head of a vertical-wall breakwater. *Coastal Engineering* 29(3-4), 201-230.
- Sumer BM, Whitehouse RJS, Tørum A. 2001. Scour around coastal structures: a summary of recent research. *Coastal Engineering*. 44(2), 153– 190.
- Svane I, Petersen JK. 2001. On the Problems of Epibioses, Fouling and Artificial Reefs, a Review. *Marine Ecology*, 22 (3): 169-188.
- Syvitski JP, Vörösmarty CJ, Kettner AJ, Green P. 2005. Impact of humans on the flux of terrestrial sediment to the global coastal ocean. *Science* 308(5720): 376-380.

3. Study I: Tidal inlets in the Anthropocene: geomorphology and benthic habitats of the Chioggia inlet, Venice Lagoon (Italy)

- Tagliapietra D, Sigovini M, Magni P. 2012. Saprobity: a unified view of benthic succession models for coastal lagoons. *Hydrobiologia*, 686: 15-28.
- Tambroni N, Seminara G. 2006. Are inlets responsible for the morphological degradation of Venice Lagoon. *Journal of Geophysical Research: Earth Surface* 111.
- Tarolli P. 2014. High-resolution topography for understanding Earth surface processes: Opportunities and challenges. *Geomorphology* 216: 295-312.
- Teatini P, Isotton G, Nardean S, Ferronato M, Mazzia A, Da Lio C, Zaggia L, Bellafiore D, Zecchin M, Baradello L, Cellone F, Corami F, Gambaro A, Libralato G, Morabito E, Volpi Ghirardini A, Broglia R, Zaghi S, Tosi L. 2017. Hydrogeological effects of dredging navigable canals through lagoon shallows. A case study in Venice. *Hydrology and Earth System Sciences* 21(11), 5627.
- Temmerman S, Meire P, Bouma TJ, Herman PM, Ysebaert T, De Vriend HJ (2013). Ecosystem-based coastal defence in the face of global change. *Nature* 504(7478): 79.
- Tosi L, Teatini P, Carbognin L, Frankenfield J. 2007. A new project to monitor land subsidence in the northern Venice coastland (Italy). *Environmental Geology*, 52(5): 889-898.
- Tosi L, Teatini P, Strozzi T. 2013. Natural versus anthropogenic subsidence of Venice. *Scientific reports*, 3, 2710.
- Trincardi F, Barbanti A, Bastianini M, Benetazzo A, Cavaleri L, Chiggiato J, Papa A, Pomaro A, Sclavo M, Tosi L, Umgiesser G. 2016. The 1966 flooding of Venice: what time taught us for the future. *Oceanography* 29(4): 178-186.
- Turner MG, 1989. Landscape ecology - the effect of pattern on process. *Annual Review of Ecology and Systematics* 20: 171-197.
- Van Maren DS, Van Kessel T, Cronin K, Sittoni L. 2015. The impact of channel deepening and dredging on estuarine sediment concentration. *Continental Shelf Research* 95: 1-14.
- Van Raalte GH. 2006. Dredging techniques: adaptations to reduce environmental impact. *Dredging in Coastal Waters*. Taylor and Francis, London, 1-40.
- Vatova A. 1940. Le zoocenosi della Laguna veneta. *Thalassia*, 3(10): 1-28.
- Vatova A. 1949. La fauna bentonica dell'Alto e medio Adriatico. *Nova Thalassia I.* (3): 110.
- Villatoro MM. 2010. Sand transport in Chioggia Inlet, Venice Lagoon and resulting morphodynamic evolution (Doctoral dissertation, University of Southampton).
- Villatoro MM, Amos CL, Umgiesser G, Ferrarin C, Zaggia L, Thompson CE, Are D. 2010. Sand transport measurements in Chioggia inlet, Venice lagoon: Theory versus observations. *Continental Shelf Research* 30(8): 1000-1018.
- Wang ZY, Li Y, He Y. 2007. Sediment budget of the Yangtze River. *Water Resources Research*, 43(4).

3. Study I: Tidal inlets in the Anthropocene: geomorphology and benthic habitats of the Chioggia inlet, Venice Lagoon (Italy)

Wasson K, Fenn K, Pearse JS, 2005. Habitat differences in marine invasions of central California. *Biological Invasions* (2005) 7: 935–948.

Williams CB. 1964. *Patterns in the Balance of Nature*. Academic Press, London.

Williams SJ. 2013. Sea-level rise implications for coastal regions. *Journal of Coastal Research* 63(1): 184-196.

Winterwerp JC, Wang ZB, van Braeckel A, van Holland G, Kösters F. 2013. Man-induced regime shifts in small estuaries—II: a comparison of rivers. *Ocean Dynamics* 63(11-12): 1293-1306.

Woodroffe CD, Webster JM. 2014. Coral reefs and sea-level change. *Marine Geology* 352: 248-267.

Wright D, Lundblad E, Larkin E, Rinehart R, Murphy J, Cary-Kothera L, Draganov K. 2005. *ArcGIS Benthic Terrain Modeler (BTM)*, v. 3.0. Environmental Systems Research Institute, NOAA Coastal Services Center, Massachusetts Office of Coastal Zone Management.

Yu J, Henrys SA, Brown C, Marsh I, Duffy G. 2015. A combined boundary integral and Lambert's Law method for modelling multibeam backscatter data from the seafloor. *Continental Shelf Research* 103: 60-69.

Zaggia L, Lorenzetti G, Manfé G, Scarpa GM, Molinaroli E, Parnell KE, Rapaglia P, Gionta M, Soomere T. 2017. Fast shoreline erosion induced by ship wakes in a coastal lagoon: Field evidence and remote sensing analysis. *PloS one* 12(10): e0187210.

Zecchin M, Baradello L, Brancolini G, Donda F, Rizzetto F, Tosi L. 2008. Sequence stratigraphy based on high-resolution seismic profiles in the late Pleistocene and Holocene deposits of the Venice area. *Marine Geology* 253(3-4): 185-198.

Zecchin M, Brancolini G, Tosi L, Rizzetto F, Caffau M, Baradello L. 2009. Anatomy of the Holocene succession of the southern Venice lagoon revealed by very high-resolution seismic data. *Continental Shelf Research*, 29(10): 1343-1359.

Zecchin M, Tosi L, Caffau M, Baradello L, Donnici S. 2014. Sequence stratigraphic significance of tidal channel systems in a shallow lagoon (Venice, Italy). *The Holocene*, 24(6): 646-658.

Zhu G, Xie Z, Xu X, Ma Z, Wu Y. 2016. The landscape change and theory of orderly reclamation sea based on coastal management in rapid industrialization area in Bohai Bay, China. *Ocean and Coastal Management* (133): 128-137.

3. Study I: Tidal inlets in the Anthropocene: geomorphology and benthic habitats of the Chioggia inlet, Venice Lagoon (Italy)

Table IA2: Brief description of the drop-frames collected from the ground-truth stations.

Stations	Ripples	Matrix dimension	Sorting	General description	Thanatozoenosis	Living biota	Shells coverage %	Shells density	Average shells size	Macrophytobenthos typology	Macrophytobenthos coverage	Notes
N02	NA	NA	NA	Coarse shell fragments	<i>Abra</i> sp., <i>Acanthocardia tuberculata</i> , <i>Cerithium</i> sp., <i>Chamelea gallina</i> , <i>Mytilus galloprovincialis</i> , <i>Nassarius nitidus</i> , <i>Ostreidae</i> indet., <i>Pectinidae</i> sp., <i>Scapharca</i> sp., <i>Serpulidae</i> indet., <i>Spisula subtruncata</i> , <i>Tellina</i> sp., <i>Veneridae</i> indet., <i>Venerupis aurea</i>		95	Very high	2 cm	Seagrass fragments		
N03	NA	<_1_mm	WS	Medium sand			2	Very low	0.5 cm			
N04	NA	<_1_mm	MS	Medium sand	<i>Bittium</i> sp., <i>Chamelea gallina</i> , <i>Spisula</i> sp., <i>Nassarius nitidus</i> , <i>Solenioidea</i> indet., <i>Veneridae</i> indet.	<i>Actiniaria</i> indet.	4	Very low	1.5 cm	Seagrass fragments		
N05	NA	<<_1_mm	WS	Fine sand			0	Very low	NA	Seagrass fragments		
N06	NA	NA	NA	Coarse shell fragments	<i>Cardiidae</i> indet., <i>Cerithium</i> sp., <i>Gibbula</i> sp., <i>Mytilidae</i> indet., <i>Nassarius nitidus</i> , <i>Ostreidae</i> indet., <i>Pectinidae</i> sp., <i>Ruditapes</i> sp., <i>Scapharca</i> sp., <i>Serpulidae</i> indet., <i>Veneridae</i> indet., <i>Venerupis aurea</i>	<i>Actiniaria</i> indet., <i>Pectinidae</i> sp.	100	Very high	2.5 cm	Seagrass patch-type 1	5	
N07	12-20 cm	<_1_mm	WS	Medium sand		<i>Nassarius nitidus</i>	1	Very low	0.5 cm	Seagrass fragments		
N08	NA	<<_1_mm	WS	Fine sand / silt		<i>Nassarius</i> indet.	0	Very low	NA			
N10	NA	<_1_mm	PS	Coarse sand + coarse shell fragments	<i>Chamelea gallina</i> , <i>Cyclope neritea</i> , <i>Ruditapes</i> sp., <i>Serpulidae</i> indet., <i>Venerupis aurea</i>	<i>Bivalvia</i> indet. (siphons)	95	Very high	1.5 cm			near to <i>Ostreidae</i> indet. thanatozoenosis
N11	12-40 cm	1_mm	PS	Coarse sand	<i>Abra</i> sp., <i>Bittium</i> sp., <i>Loripes lacteus</i> , <i>Mytilus galloprovincialis</i> , <i>Scaphopoda</i> indet., <i>Serpulidae</i> indet., <i>Spisula subtruncata</i> , <i>Tellina</i> sp., <i>Veneridae</i> indet.		65	Medium	0.5 cm			
N12	NA	<_1_mm	WS	Medium sand + coarse shell fragments	<i>Acanthocardia tuberculata</i> , <i>Calliostoma</i> sp., <i>Chamelea gallina</i> , <i>Cyclope neritea</i> , <i>Loripes lacteus</i> , <i>Mytilidae</i> indet., <i>Pectinidae</i> sp., <i>Serpulidae</i> indet., <i>Spisula</i> sp., <i>Tellina</i> sp., <i>Veneridae</i> indet., <i>Venerupis aurea</i>	<i>Paguroidea</i> indet.	20	Low	1.5 cm			
N13	20-30 cm	<_1_mm	MS	Medium sand + coarse shell fragments	<i>Bittium</i> sp., <i>Chamelea gallina</i> , <i>Glycymeris violascens</i> , <i>Mytilus galloprovincialis</i> , <i>Scapharca</i> sp., <i>Scaphopoda</i> indet., <i>Serpulidae</i> indet., <i>Solenioidea</i> indet., <i>Veneridae</i> indet., <i>Venerupis aurea</i>		18	Low	1.5 cm			
N14	NA	<<_1_mm	WS	Fine sand		<i>Carcinus aestuani</i> , <i>Nassarius nitidus</i>	1	Very low	1 cm	Seagrass fragments		<i>Ophiotrix</i> sp. observed nearby
N15	20-30 cm	<_1_mm	WS	Medium sand	<i>Mytilidae</i> indet., <i>Solenioidea</i> indet., <i>Veneridae</i> indet.		2	Very low	1 cm			
N17	6-10 cm	1_mm	MS	Medium sand	<i>Bittium</i> sp., <i>Veneridae</i> indet.	<i>Asterina gibbosa</i> , <i>Carcinus aestuani</i> , <i>Paguroidea</i> indet.	1	Very low	0.5 cm	Seagrass fragments		
N18	NA	<_1_mm	WS	Medium sand + gravel	<i>Serpulidae</i> indet., <i>Veneridae</i> indet.	<i>Actiniaria</i> indet., <i>Ophiotrix</i> sp.	7	Very low	0.5 cm	Seagrass fragments		<i>Ophiotrix</i> sp. bed (50% coverage)
N19	NA	<<_1_mm	WS	Partially consolidated fine sand / silt	<i>Veneridae</i> indet.		1	Very low	0.5 cm	Seagrass fragments		
N23	NA	<<_1_mm	WS	Partially consolidated fine sand / silt + rocks	<i>Ostreidae</i> indet., <i>Serpulidae</i> indet.	<i>Pachygrapsus marmoratus</i> , <i>Ophiotrix</i> sp.	0	Very low	NA	Seagrass fragments		Rocks, presence of <i>Ophiotrix</i> sp.
N24	NA	<_1_mm	WS	Medium sand	<i>Veneridae</i> indet.	<i>Carcinus aestuani</i> , <i>Nassarius nitidus</i> , <i>Paguroidea</i> indet., <i>Tunicata</i> indet. (col.)	1	Very low	0.5 cm	Seagrass patch-type 2	48	
N25	NA	<<_1_mm	WS	Fine sand / silt	<i>Veneridae</i> indet.		1	Very low	1 cm	Seagrass patch-type 3	60	

3. Study I: Tidal inlets in the Anthropocene: geomorphology and benthic habitats of the Chioggia inlet, Venice Lagoon (Italy)

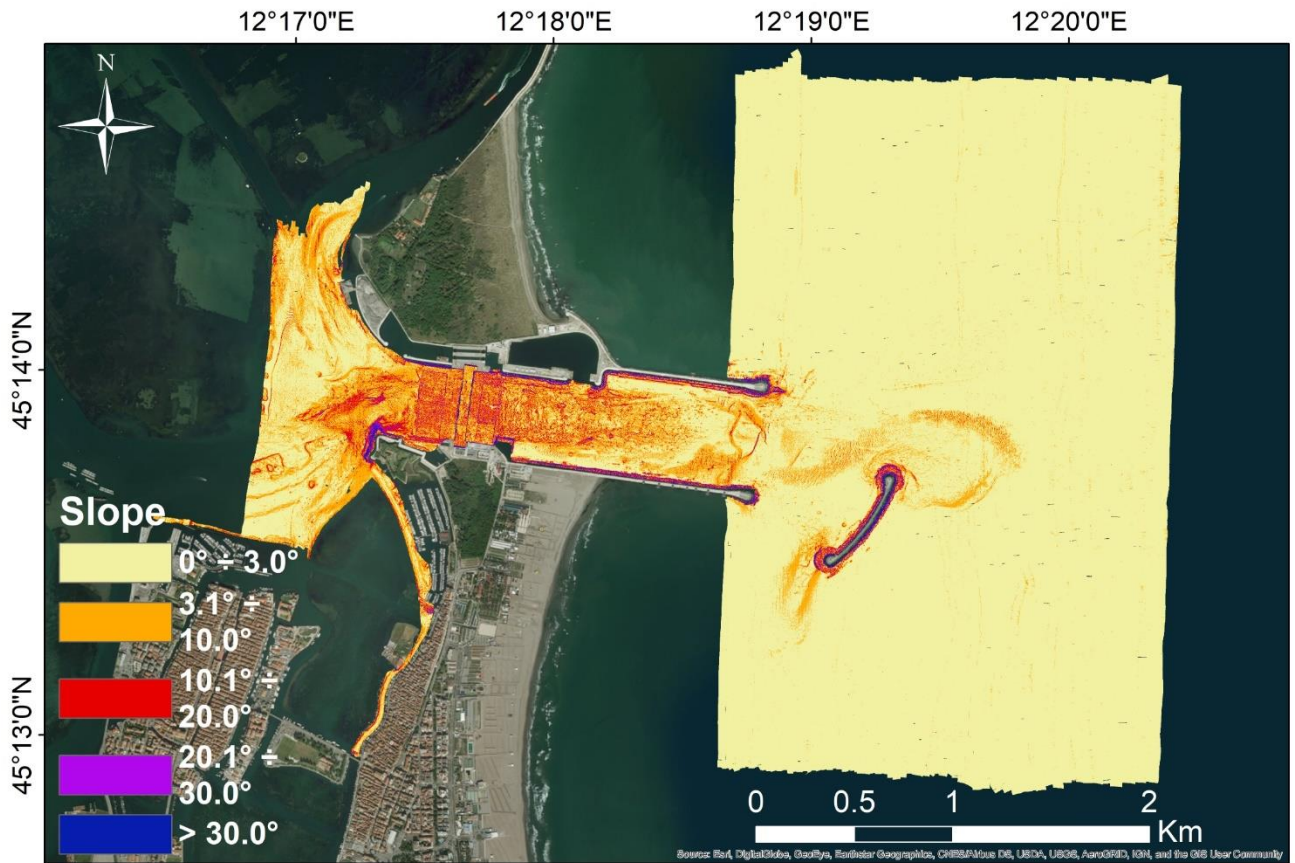


Figure IA1: Slope map of the study area.

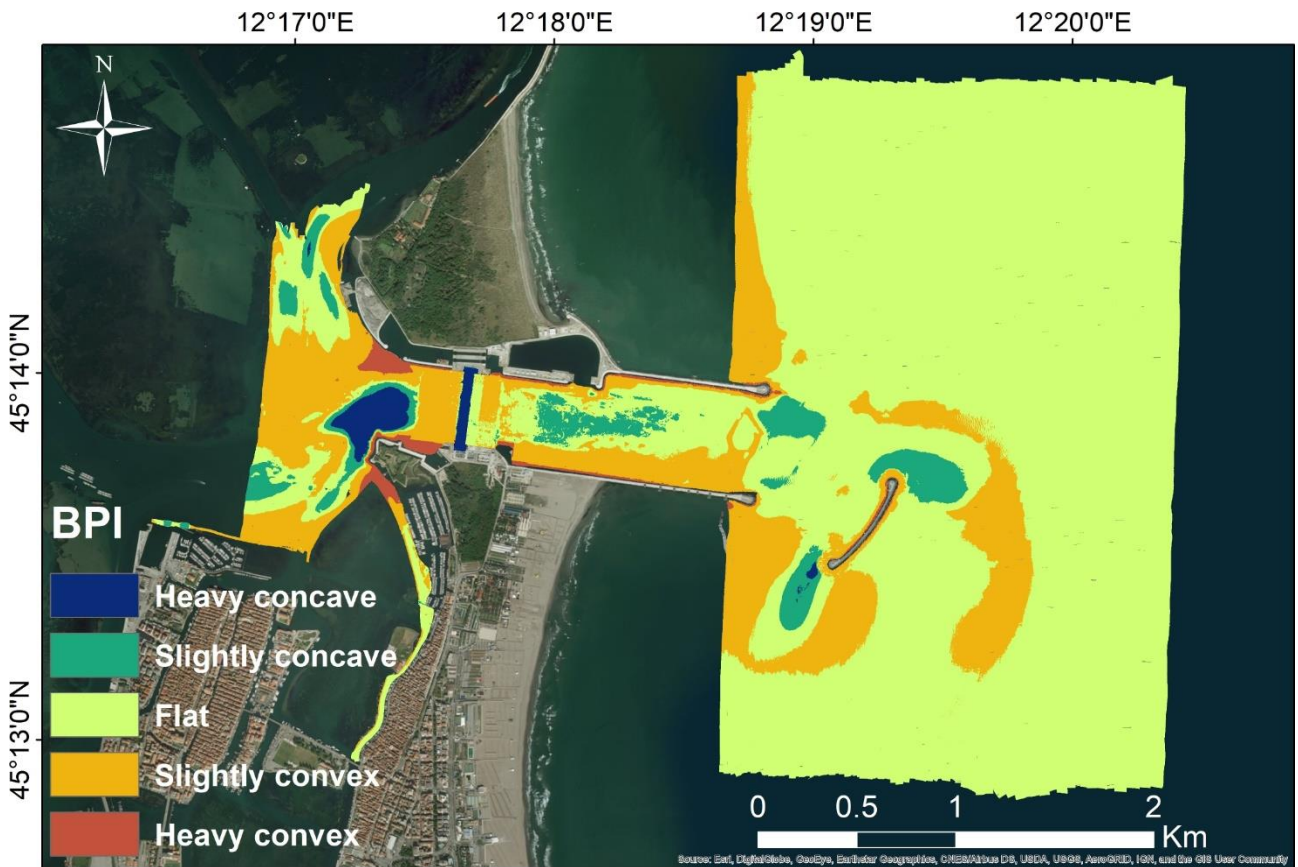


Figure IA2: Broad Bathymetric Position Index (BPI) map of the study area obtained from Benthic Terrain Modeller tool.

3. Study I: Tidal inlets in the Anthropocene: geomorphology and benthic habitats of the Chioggia inlet, Venice Lagoon (Italy)

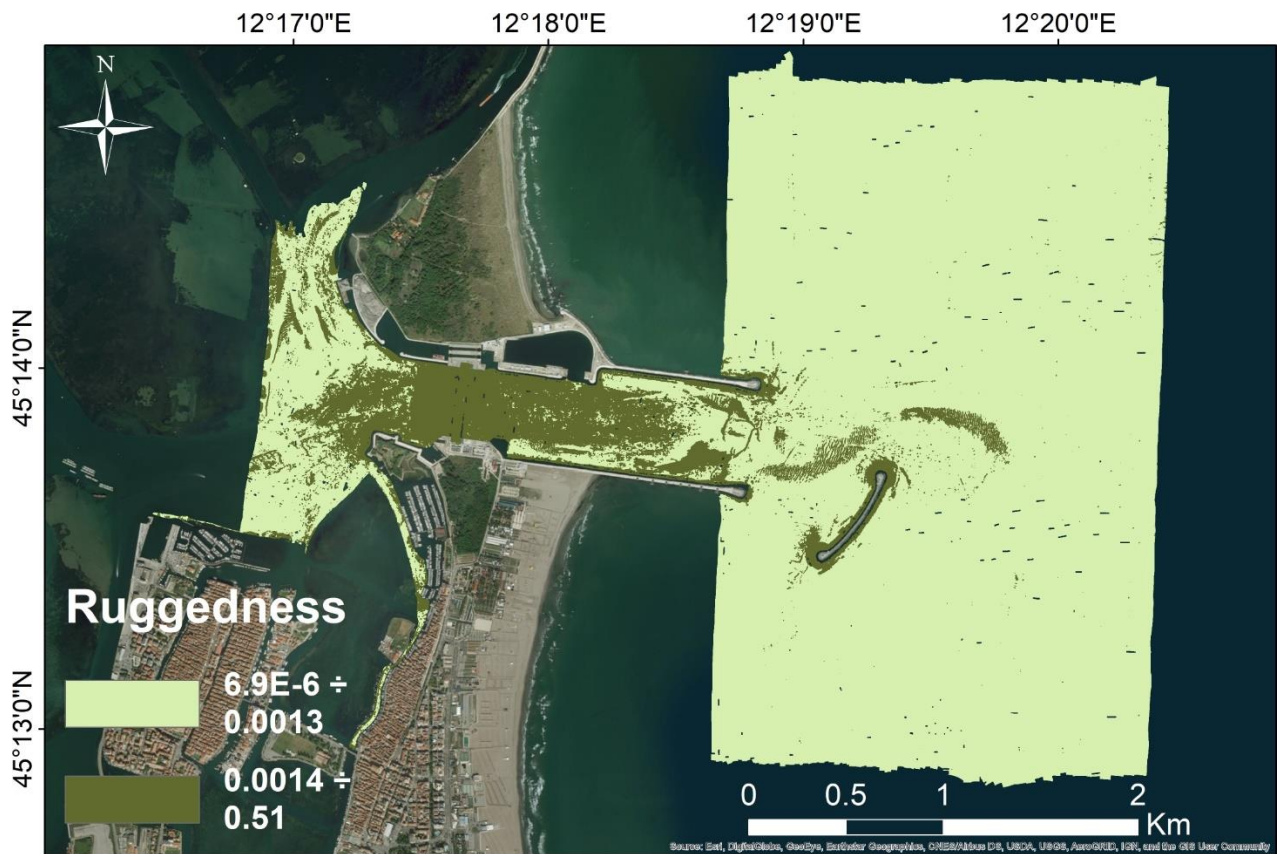


Figure IA3: Ruggedness map of the study area.

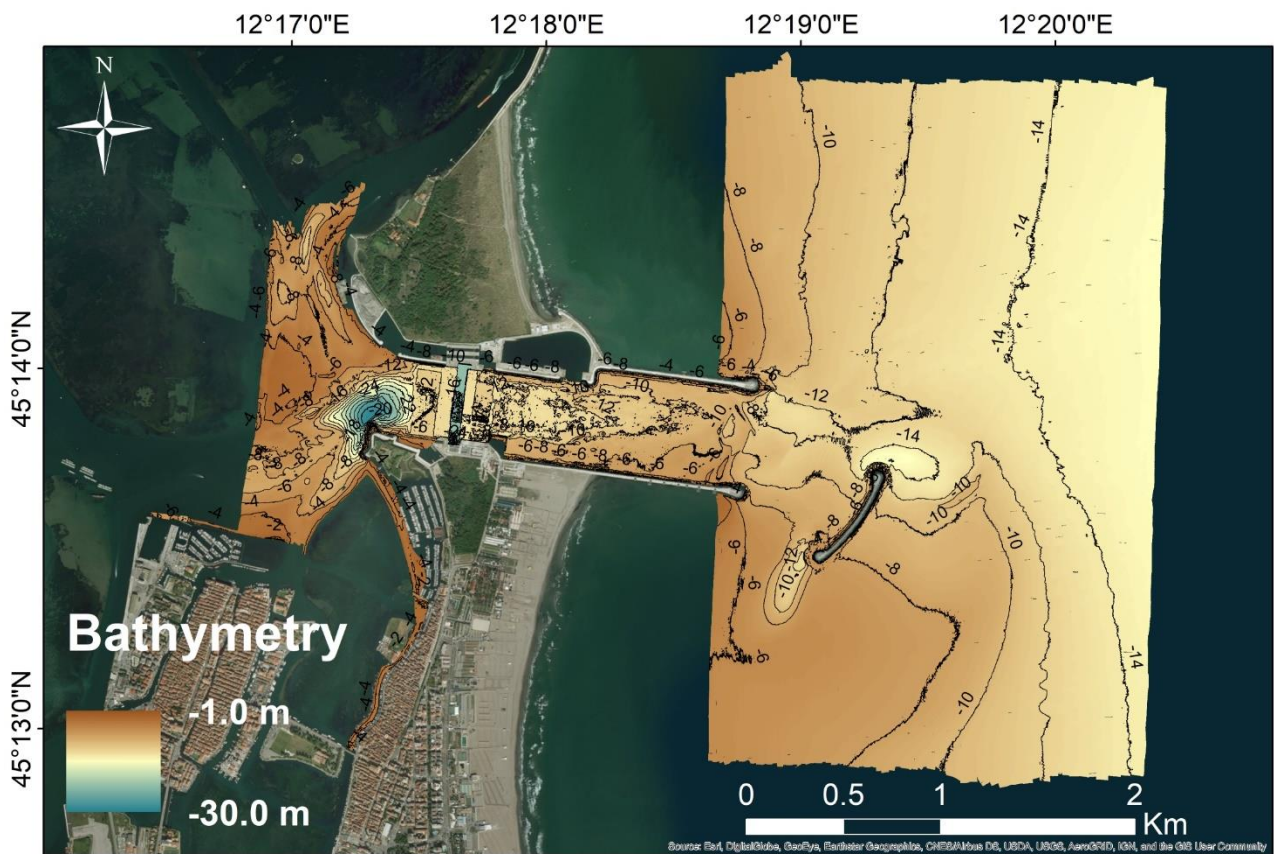


Figure IA4: Bathymetry map of the study area with the isobaths.

4. Study II: Bathymetric and backscatter data of seafloor change of the Chioggia inlet (Venice Lagoon) as a result of human intervention

Stefano Fogarin^{1,2}, Emanuela Molinaroli¹, Fantina Madricardo², Marco Sigovini² and Fabio Trincardi²

¹ Department of Environmental Sciences, Informatics and Statistics (DAIS), Università Ca' Foscari Venezia, Campus Scientifico, Via Torino 155, Mestre, VE, Italy

² Istituto di Scienze Marine-Consiglio Nazionale delle Ricerche, Arsenale - Tesa 104, Castello 2737/F, 30122 Venezia, Italy

Abstract

To characterize the seafloor morpho-bathymetry and substrate composition, seabed mapping and especially multibeam echosounding are increasingly used. It has also been observed that repeated surveys over time can highlight the changes of the seabed, in geomorphological and sedimentological terms. This can help to recognize the active coastal processes and to describe the response of the environment after localized human pressures, such as the construction of hard structures.

Thanks to multiple high-resolution multibeam datasets, we studied the seafloor evolution of a strong impacted tidal inlet, Chioggia inlet in Venice Lagoon (Italy). Adopting state-of-the-art benthic habitat mapping procedures, we described two main important seabed morphologies, i.e. scour holes and dunes, and their short-term changes (time span of 5 years) after the artificial modify of inlet configuration. The used methods allowed also identifying the sediment composition of the seabed and quantifying temporal trends of change of the main substrate classes. The results indicate that after the construction of the hard structure the hydrodynamic of the inlet completely changed, promoting a major water current and bottom shear stress. This reflects in an increased seabed erosion, formation of large scour holes and speeded displacement/shrinking of dune fields.

The methodologies presented in this paper are repeatable and can be used to study the consequences of the transformation of coastal landscapes in response of sea level rise and consequent engineering intervention.

Keywords: Tidal inlet, MultiBeam Echosounder, tidal dynamics, seafloor change detection, Venice Lagoon

4.1. Introduction

Coastal lagoons occupy about the 13 % of the coastlines in the world (Bird, 1994; Kjerfve, 1994). These regions are important for several biogeochemical processes (Sousa et al., 2013) and are an essential part of the ecological heritage (Costanza et al., 1997; Luisetti et al., 2014). These shallow water bodies host different unique ecosystems, such as wetlands, saltmarshes, seagrass meadows, mangroves and tidal plains (Basset et al., 2013; Newton et al., 2018). For the high productivity of these habitats, the lagoons have been historically exploited, hosting intensive agriculture and industry, harbour activities, high population and hard infrastructures (Gönenç and Wolflin, 2005). The changes in these environments may occur as a result of natural driven, e.g. meteo-marine or hydrodynamic conditions (van Denderen et al. 2015), but can be also induced by anthropogenic pressure (Steffen et al., 2011; Lewis and Maslin, 2015). Indeed, the high anthropization increase the exposure of coastal lagoon to potential impacts: pollution, habitat losing, invasion of alien species, sea level rise and overexploitation are the main cause of degradation (MA - Millennium Ecosystem Assessment, 2005).

Nowadays lagoons and tidal inlets are increasingly influenced by human intervention and activities. However, the long-term response of the environment to anthropogenic pressures is still poorly understood. Oftentimes, these impacts reflects on the morpho-bathymetry and the substrate composition of the seafloor; our ability to monitor and quantify these changes, such as the identification of the drivers that induce the modification, is crucial to understand the spatio-temporal behavior of the marine seafloors and the ecosystems (Montereale-Gavazzi et al., 2018). Understanding the temporal dynamics of the seafloors is indeed a key component to their effective management. Moreover, the impact of the human pressure on the coastal zones, especially in

relation of hard structure construction, assumes a crucial role in view of the global mean sea level rise and coastal wetland vulnerability. This is also very important to tutelage the ecosystem services, as indicates by the European Marine Strategy Framework Directive (MSFD – EC 2008-56-EC) that consider the seafloor health an indicator of the “Good Environment Status”. For these purposes, the seafloor mapping, especially using the MultiBeam EchoSounder (MBES), is progressively carried out.

Very few studies that described temporal morphological dynamics of the seafloor are available in the literature. However, these studies are based mainly on optical sensors or ground-truth sampling methods that are logistically limited, both for limited analyzable areas and cost constraints. In this work we quantify the seafloor changes using acoustic methods. We describe and compare between years the sediment distribution and the most important seafloor features, i.e. scour holes, dunes and MoSE area, located in the common area of the three surveys. The aim of this research is to investigate the short-term effects of the construction of hard structures in a strongly impacted tidal inlet, Chioggia Inlet, in Venice Lagoon. The three inlets of Venice Lagoon (Lido-Treporti, Malamocco and Chioggia) are interested by the construction of MoSE project that should defend the historical center of Venice by high water. The project implies the construction of several hard structures and the alteration of the seabed. We will use a set of three repeated MBES surveys, carried out in a period of five years (from 2011 to 2016), to assess the inlet evolution through a monitoring of the seabed sedimentary dynamics.

4.2. Study area

The Venice Lagoon, located at the northern tip of the Adriatic Sea, is the largest of the Mediterranean Sea, with a surface area of 550 km² and it is classified as a “restricted” lagoon (Kjerfve, 1994). It has a mean depth of 1.2 m and only the 5 % of its extent is deeper than 5 m (Molinarioli et al., 2009). The main navigation channels are up to 20 m deep. In response to recurrent historical human modifications, the lagoon today exchanges water and sediments with the Adriatic Sea through three inlets: Lido, Malamocco and Chioggia, from north to south (Ghetti, 1974).

The Venice Lagoon is a microtidal environment where tides and winds are the main factors that influence the water circulation (D’Alpaos et al., 2013). Seven tidal constituents, four semidiurnal (M2, S2, N2 and K2) and three diurnal (K1, O1 and P1) influence significantly the sea surface

elevation in the North Adriatic Sea (Book et al., 2009). While propagating from the inlets to the lagoon, the tidal wave is deformed, either damped or amplified, and it reaches the tidal flats through the network of channels (Rinaldo et al., 2001).

Today, the recent construction of MoSE structures (an acronym for *Modulo Sperimentale Elettromeccanico* or Experimental Electromechanical Module) could alter the lagoon environment by modifying the tidal exchange, increasing the ebb-dominance over tidal flats and influencing the seafloor morpho-bathymetry (Tambroni and Seminara, 2006; Ghezzi et al., 2010, Ferrarin et al. 2015; Fogarin et al., 2019).

The Chioggia inlet (45°13'54 "N, 12°18'3"E WGS84, geographic coordinates) is the southernmost inlet that connects the Venice Lagoon with the north Adriatic Sea (Fig. II1). It has a tidal prism of $82 \times 10^6 \text{ m}^3$ (Consorzio Venezia Nuova, 1989; Fontolan et al., 2007) and the tidal wave precedes those in Lido and Malamocco of about one hour (Gačić et al., 2004; Villatoro et al., 2010). The tidal range is 1 m and the current speed varies with weather conditions reaching about 0.5 ms^{-1} during syzygy (Gačić et al., 2004). However, during strong meteo-marine events (storm surges), the current speed can reach about 2 ms^{-1} .

The inlet has been used as access to the harbour of Chioggia since Roman times and consequently has been subject to numerous anthropogenic interventions. The most evident of these have started in 1912 and finished in 1930 with the construction of concrete jetties. Continuously modification of these structures continues until 1950 (Rinaldo et al., 2001). In the last 16 years, the inlet configuration is completely changed, due to the construction of the MoSE project. The MoSE interventions at the Chioggia inlet are chronologically reported in Tab. II1.

4. Study II: Bathymetric and backscatter data of seafloor change of the Chioggia inlet (Venice Lagoon) as a result of human intervention

Table II1: chronologically intervention at the Chioggia inlet.

Year	Intervention
2003	The construction of the breakwater outside the inlet begins.
2004	Remediation from the possible presence of war device and archaeological investigation. The construction of the refuge harbor and the navigation basin begins. The jetties in correspondence of the navigation basin were modified.
2006	The construction of the refuge harbor continues. The construction of the two navigation locks and the "shoulders" that will connect the refuge harbor with the mobile barriers begins. The reinforcement of the seafloor with boulders and stones where the mobile gates are going to be positioned begins. Two test areas to experience the seafloor reinforcement technologies were realized. The construction of the breakwater is completed.
2007	The construction of the two navigation locks and the "shoulders" continues. The works for the seafloor protection are almost completed.
2008	The refuge harbor is completed and the navigation basin is almost finished. The modification of the jetties is completed and the construction of the north shoulder is almost finished. The excavation of the MoSE trench begins. The area with the prefabrication for MoSE functioning planned within the refuge harbor is being prepared.
2010	The navigation basin has been waterproofed and drained by water. The aim is using this area to build the concrete caissons. The south shoulder is almost completed. The seafloor protection and the excavation of the trench is almost completed.
2013	On the south shoulder the construction of the prefabrication is almost finished. The seafloor protection is completed.
2014	The works to create the support buildings for the MoSE functioning is still ongoing. The caissons have been sunk inside the trench. The navigation basin has been refilled by water.
2017	From 19 September 2017 to 31 January 2019 the procedures to install the 18 mobile gates took place.
2019	All the mobile gates are positioned.

4.3. Material and Methods

4.3.1. Data acquisition

The MBES data have been acquired in a time span of six years, from 2011 to 2016, with a total of three sets of data: A (2011), B (2013) and C (2016). The dataset A was acquired by the Italian

4. Study II: Bathymetric and backscatter data of seafloor change of the Chioggia inlet (Venice Lagoon) as a result of human intervention

Hydrographic Institute (IIM) of the Italian Navy during two campaigns of nautical chart updating. The first campaign took place from 16th May to 30th July 2011, while the second one from 1st August to 3rd September 2011. The dataset B was acquired by the Italian Research Council (CNR-ISMAR) from October to November 2013. The dataset C was acquired by the IIM during May 2016. All the technical characteristics of each survey are reported in Tab. II2. Although the three surveys cover different extents, the central inlet area is common to the three campaigns. Furthermore, despite some differences in acquisition and accuracy of position systems, the three surveys are suitable for a quantitative estimation of the seafloor changes. The processing of the bathymetric data is the same for the three datasets: the software Caris Hydrographic and Side Scan Information Processing System (SIS) were used to consider sound velocity variability, tides and the quality of the acquiring data. The backscatter data is processed using Fledermaus Geocoder Toolbox (FMGT).

Table II2: survey technical setup.

	Dataset A (2011) - First and second survey	Dataset B (2013)	Dataset C (2016)
Investigator	I.I.M.	CNR - ISMAR	I.I.M.
MBES	Kongsberg Simrad EM3002	Kongsberg EM2040 Dual-Compact	Kongsberg EM2040 Dual-Compact
Vessel	7-m long	10-m long	7-m long
Frequency	300 kHz	360 kHz	360 kHz
Acquisition software	SIS	SIS	SIS
Positioning system	Kongsberg Seatex Seapath 300 with Fugro Seastar 3200/LR OMNISTAR correction	Kongsberg Seatex Seapath 300 (DGPS) supplied by a Fugro HP DGPS	Kongsberg Seatex Seapath 300 (DGPS) supplied by a Fugro HP DGPS
Motion sensor	Kongsberg Seatex MRU 5	Kongsberg Seatex MRU 5	Kongsberg Seatex MRU 5
Sound velocity data collection	Valeport mini SVS sensor and an Idronaut Ocean Seven 316 multiparameter probe	Valeport mini SVS sensor and AML oceanographic Smart-X sound velocity profiler	Valeport mini SVS sensor and an Idronaut Ocean Seven 316 multiparameter probe
Tide correction reference	ISPRA gauges	SHYFEM model (Umgiesser et al., 2004; Umgiesser et al., 2006)	ISPRA gauges
Ground-truth survey	Not available	Surficial sediment samples and underwater videos	Surficial sediment samples and underwater videos

After the processing, the bathymetric and backscatter data were exported as a 32-bit raster files and imported in ArcGis v10.2 (ESRI, 2016). Using the bathymetric data, we created three Digital Elevation Models (DEMs) with a raster resolution of 0.5 m. The data are referred to the local datum 'Punta Salute 1897' (ZMPS), 23.56 cm lower than the national vertical level datum (IGM1942). As

well, with the backscatter data we create three different seafloor reflectivity maps with 0.5 m of resolution.

4.3.2. Ground-truth analysis

4.3.2.2. Surficial sediment samples

A ground-truth sampling including 46 sediment samples was carried out in 2013 (17 samples) and 2016 (29 samples). The sediments were collected with a Van Veen Grab (5L). The location of the sampling stations was selected in 2013 in correspondence of the main backscatter patches and in 2016 in correspondence of the main morphologies identified from the MBES imagery processed during the surveys. All the sediment samples were treated following procedure from Loring and Rantala (1992) and were analysed with a dry sieving (fractions ≥ 1 mm) and laser measurement with granulometer MasterSizer 3000 (fractions < 1 mm). The outputs from both analyses were merged and the main grain-size parameters were calculated, according to Folk et al. (1970) classification, using Gradistat statistical package (Blott and Pye, 2001). Finally, the results were processed by the EntropyMax software (Woolfe and Michibayashi 1995; Stewart et al., 2009; Molinaroli et al., 2014) to identify the textural groups (Tab. IIA1).

4.3.2.2. Underwater videos (Drop frames)

A ground-truth video recording was carried out in winter of 2013 and 2016, simultaneously of the grab sampling. The underwater videos were collected using a drop-frame camera (3 replicates for each station). The device consisted of an action camera (Go-Pro HERO-3) and underwater lights installed on an aluminum rectangular frame. The videos were collected in correspondence of grab samples stations and some additional videos were recorded to investigate particular seafloor features (e.g. seagrass patches, rip-rap seabed, etc.).

From each underwater video, representative still images (drop-frames) were extracted and characterized in terms of biotic and abiotic features. Epimegabenthos (both living specimens and empty shells) were identified and counted. A total of 144 images (60 from 2013 dataset and 84 from 2016 dataset) were analyzed (Tab. IIA2).

4.3.3. Backscatter classification

The objective of backscatter (BS) classification is obtaining homogeneous sub-regions of surficial composition (e.g. Brown et al., 2011; Diesing et al., 2014; McGonigle and Collier, 2014; Ierodionou et al., 2018). Several solutions have been proposed in the literature and the choice of the number of classes is still debated. In this study we decide to use Jenk's optimization method to classify the backscatter. This unsupervised method, easily implemented in ArcGis, seeks automatically to reduce the variance within classes and maximize the variance between classes (Jenks, 1967) and had shown good results in previous application in Venice Lagoon (Montereale Gavazzi, 2016; Fogarin et al., 2019). Furthermore, the benefit of this method is that the clusterization is based on frequency distribution and not on the absolute values of backscatter. Despite not having samples collection from the 2011 dataset, we have nevertheless decided to classify the 2011 backscatter considering that the sediment classes recognized on 2013 and 2016 are probably the same during the 2011 survey. We set the Jenks' classification using the values within the common area of the three surveys (about 3.34 km², roughly correspond to the central inlet channel) to have a comparable range values distribution. Backscatter signature and EntropyMax analysis were used to identify the classes. Respect Fogarin et al. (2019) where four classes have been observed, the backscatter and ground-truth data collected in 2016 do not include the S class, because this substratum is present almost exclusively outside the surveyed area. Considering this information, for the backscatter change analysis we merged together the middle classes SGS and S (within 2011 and 2013 datasets), that are considerably similar.

The results of seafloor classification were assessed for accuracy using contingency confusion matrices (Story and Congalton, 1986; Congalton and Green, 2002; Foody, 2002; Rattray et al., 2013). With this technique, it is possible to estimate the reliability of the classification, using the producer's accuracy (indicating how well training set pixels were classified) and the user's accuracy (indicating the probability that a classified pixel represents that class in reality). Furthermore, an overall accuracy can be derived from these tables.

4.3.4. Change assessment

In order to understand the evolution of the morpho-bathymetry of the tidal inlet in the years, we compared the common DEMs area of each survey. We assume that the bathymetric residuals (BR) outside the error interval (set to 0.3 m) are in erosion or deposition, depending on the sign of the

difference. The regions with bathymetric difference inside the error interval can be considered stable.

To understand the change of the seafloor sediment composition in the time span, we created the transition matrices “from-to” for each identified class (Pontius et al., 2004, Braimoh, 2006; Rattray et al., 2013; Montereale-Gavazzi et al., 2018). The evolution of the seafloor is summarized in terms of gain, loss, swap and net change following the methodology of Pontius et al. (2004) and Rattray et al. (2013). Gain and loss to persistence ratios (G_p and L_p) show the behavior of a determined seabed class between years (Braimoh, 2006): values higher than 1 suggest a tendency to gain or to lose rather than persist of a seafloor type from other classes, whereas values close to 0 indicate an absent change. Net change to persistence ratios (N_p), calculates also as $N_p = G_p - L_p$, measures the general trend of a seabed class, indicating the direction of tendency with positive or negative values (Rattray et al., 2013).

4.3.5. Seafloor features analysis

Starting from the DEM obtained from the MBES bathymetric data, we processed in ArcGis the main terrain attributes: slope, broad Bathymetric Position Index (BPI) and Ruggedness (Lecours et al., 2017a; Lecours et al., 2017b). The BPI layer were calculated using BTM package (Wright et al., 2005) with inner and outer radius of 50 and 750 respectively while ruggedness was elaborated with radius of 11. These layers are useful to semi-automatic classify the main morphological features and describe the seafloor’s variability determined by hydrodynamic condition and sediment budgets. All the seafloor morphologies identified in the study area, such as the method to recognized them, are described in detail in Fogarin et al., 2019. The comparison of areas and the vertical profiles between features have been obtained with Arcgis. The tool Minimum Bounding Geometry (Toso et al., 2019) was used to extract length and direction of the main axes of the morphologies.

4.4. Results

4.4.1 Bathymetric DEMs

The measured bathymetry ranges from -30.0 m to -0.8 m (Fig. II1). The shallower sectors (depth less than 2 m) are located inside the lagoon, close to the mudflats and the harbor of Chioggia. The deepest points are within a large scour hole (with maximum depth of -30 m) located at the western entrance of the inlet channel (see also Ferrarin et al., 2018 and Fogarin et al., 2019). The central inlet changes significantly during the three survey due to human activity and sediment mobilization. Excluding the MoSE trench, the depth of this channel ranges between -14 m to -9 m; generally, the southern portion of the channel is shallower than the northern. The MoSE trench instead vary between a minimum of -25 m in 2013 to a maximum of -18 m in 2016. This strong variation in bathymetric values is due to the dredging of the sector and the sequent positioning of the barriers housing (caissons). In appendix (Tab. IIA3) are reported the parameters of each bathymetric dataset collected.

The slope of the study area is generally flat or gently sloping with values around 1° , increasing to 30° in correspondence of larger dunes; only scour holes or coastal defense structures present larger gradients of slope, up to 35° and 80° respectively.

4. Study II: Bathymetric and backscatter data of seafloor change of the Chioggia inlet (Venice Lagoon) as a result of human intervention

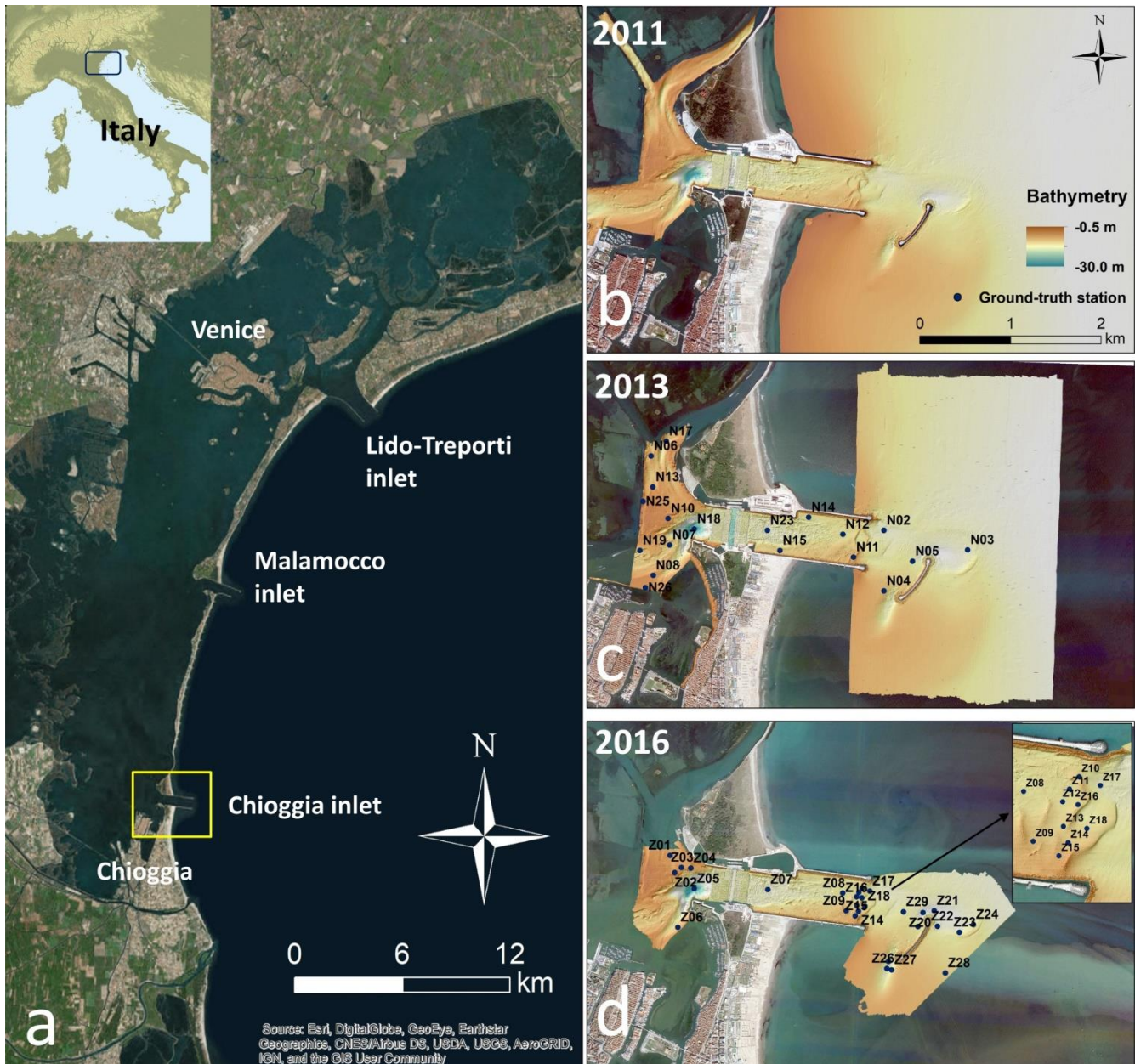


Figure II.1: (a) the Venice Lagoon and the location of the study area (Chioggia inlet); (b,c,d) the morpho-bathymetric models of Chioggia inlet (DEMs) obtained from 2011, 2013 and 2016 surveys and the position of the ground-truth stations (blue dots).

4.4.2. Bathymetric change assessment and volume differences

The results of bathymetric change assessment are reported in Fig. II.2. In blue are the areas under severe erosion ($BR < -2.0$ m), in light blue the areas in slight erosion ($-2.0 \text{ m} \leq BR \leq -0.3$ m), in green the areas stable ($-0.3 \text{ m} < BR < 0.3$ m), in yellow the areas in slight deposition ($0.3 \text{ m} \leq BR \leq 2.0$ m) and in red the areas in severe deposition ($BR > 2.0$ m). During the first two years (2011-2013) we observed a severe erosion, while the sectors in deposition or severe deposition can be overlooked.

In particular, the erosion occurred along the inlet channel and around breakwater's edges in correspondence of scour holes. Small dredged channels are described in the lower part of the lagoon basin. The alternate colors observable on the seaside inlet entrance, indicate a shift of the dunes towards the sea (east direction).

In the second time interval (2013-2016) we observed a less erosion and a significant deposition. The erosion is along the inlet channel and close to breakwater's scour holes. The deposition instead occurs near MoSE rip-rap, where some rocks were sunk to reinforce the seafloor, and around inlet's jetties. The two sectors in severe erosion in the middle inlet are connected to dredging activities. The large displacement of the dunes is still visible.

4. Study II: Bathymetric and backscatter data of seafloor change of the Chioggia inlet (Venice Lagoon) as a result of human intervention

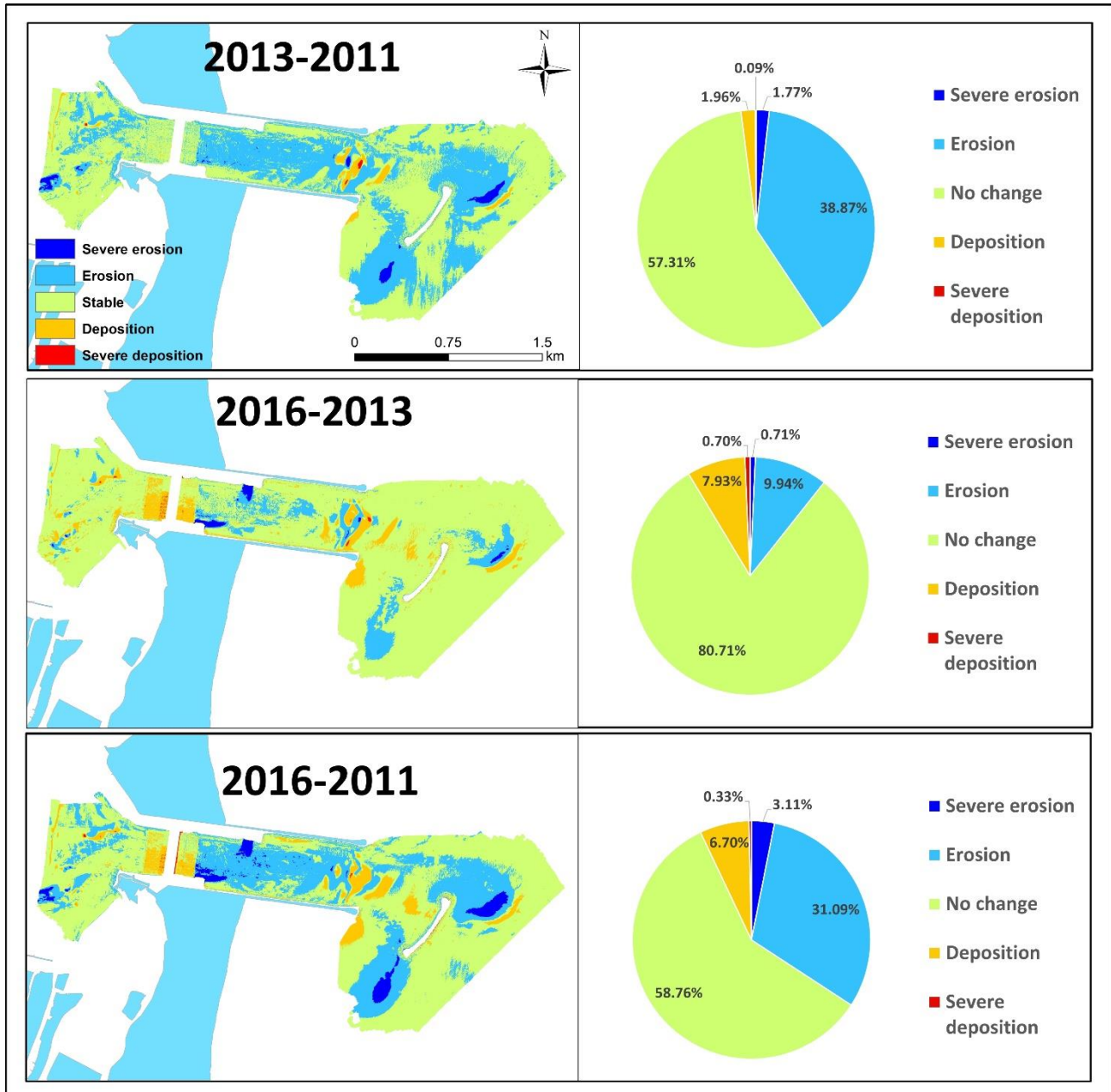


Figure I12: bathymetric change assessment for each time interval. Dark blue: severe erosion ($BR < -2.0$ m), light blue: slight erosion ($-2.0 \text{ m} \leq BR \leq -0.3$ m), green: stable ($-0.3 \text{ m} < BR < 0.3$ m), orange: slight deposition ($0.3 \text{ m} \leq BR \leq 2.0$ m), red: severe deposition ($BR > 2.0$ m). The pie charts on the right represent the surface of the sectors subject to severe erosion, erosion, no change, deposition and severe deposition respect to the total common surface area for each time interval. The area of MoSE trench has been removed.

The volume differences of the common area (excluding the MoSE trench surface) in each time interval are the following: erosion of $-1,164,274 \text{ m}^3$ between 2011-2013 and deposition of $+49,470 \text{ m}^3$ between 2013-2016. These different trends can be summarized in a general volume erosion of more than 1 million of cubic meters in the entire period 2011-2016. In Tab. IIA6 is reported the volume difference calculation for each time interval.

4.4.3. Ground-truth analyses

4.4.3.1. Grain size

We analyzed a total of 46 sediment samples (2013-2016), subdivided between open sea, lagoon and inlet channel. All the textural information of the collected samples is reported in Tab. IIA1. The sediments grain-size range between sandy gravel to slightly gravelly mud (according to Folk et al., 1970). The sand is generally the predominant grain-size, but gravel and mud are often present. The coarse fraction (> 2 mm) consists of bioclastic grains, mostly shells fragments, especially bivalve or gastropod mollusks.

In the 2013 dataset, most of the samples are sand. In detail, slightly gravelly sand is the predominant grain-size. Only 3 gravels and 2 muds were collected. In particular, the three coarser sediments have been found near the inlet channel's extremities (samples N02, N10 and N12 in Fig. II1c), whereas the finer ones have been found inside the lagoon basin (sample N08 in Fig. II1c) and close to the inlet channel rip-rap (sample N23 in Fig. II1c). The median diameter (D50) of the samples ranges from 2887 μm to 19 μm . The sediments are unimodal and bimodal and the sorting ranges between moderately well sorted to very poor sorted.

In the 2016 dataset, the samples are slightly different. The sandy sediments still prevail, but muddy and especially gravelly sediments were often present. Such as in the 2013, the coarser sediments are located near the inlet channel's extremities (samples Z17 and Z01 in Fig. II1d), whereas the finer ones are in a deposition area in the concave side of the breakwater (sample Z20 in Fig. II1d) and close to the inlet channel rip-rap (sample Z07 in Fig. II1d). Inside the two scour holes at breakwater tips, the sediments are more heterogeneous with a mixture of gravelly and muddy sediments. The D50 of the samples ranges from 9420 μm to 15 μm . The sediments are unimodal and bimodal and only in few cases three modes were observed. The sorting is poorly sorted or very poorly sorted, only two samples are moderately sorted (sample Z15 in Fig. II1d) and extremely poorly sorted (sample Z26 in Fig. II1d).

The EntropyMax analysis, applied separately to 2013 and 2016 grain size datasets, identified 3 groups (Fig. IIA4) each year.

1. Group 1 "Sand with shell fragments": coarse sediments composed by shell detritus in a sandy matrix. These sediments are poorly sorted and present generally a primary mode on fine/medium gravel (8/16 mm) and a secondary mode on medium sand (250 μm).

2. Group 2 “Coarse to fine-grained sand”: sandy sediments with low presence of gravel and mud. In general, these sediments are moderately sorted and have a main mode on medium sand (250/354 μm). Secondary modes have been observed in the finer sand grain-sizes (2016 samples).
3. Group 3 “Poorly sorted sandy mud”: very poorly sorted fine sediments, composed by a mixture of sand and mud. Several times, these sediments have three modes which the primary one is placed on very fine sand (88 μm in the 2013 samples) or coarse silt (22 μm in the 2016 samples) and the secondary ones are in the finer grain-sizes.

4.4.3.2. Drop-frames

Several benthic taxa, characterizing the various seafloors, both alive specimens (mainly epimegabenthos) and empty shells, were recognized from the 144 underwater images (Tab. IIA2). We observed a number of taxa relatively low, but some species occur in large abundance. In general, the seabed lacks macrophyte cover, except for some seagrass patches (*Cymodocea nodosa* (Ucria), Asch) located in the western margin of the study area, and red/green algae colonizing the central inlet rip-rap and the bottom of breakwater’s scour holes.

Despite the two surveys being conducted in a different period of the year, the videos collected about the same organisms in 2013 and 2016. In 11 out of 19 stations of 2013, we observed living organisms, most commonly the crab *Carcinus aestuarii*, the gastropod *Nassarius nitidus*, Actiniaria and Paguroidea, typically on sandy/muddy sediments and over seagrass meadows. In 2016 differently, we observed living species in 9 out of 29 stations, mostly Paguroidea. The stations with coarse sediment and shell fragments presented a low number of living species. In few images, N18, N23 and Z07 (Fig. II1c, 1d), characterized by boulders or pebbles, aggregates of the brittle star *Ophiothrix* sp. covered partially the seafloor.

Shells debris resulting from thanatocoenosis were identified in 14 out of 19 and in 26 out of 29 stations in 2013 and 2016 surveys, respectively. The shells belong mostly to Bivalvia, and in particular Veneridae, Mytilidae, Pectinidae and Ostreidae. Among gastropods, we mostly observed *Nassarius nitidus* and *Bittium* sp.

4.4.4. Backscatter mosaics and classification

The distribution of 2011 and 2013 datasets are similar to a Gaussian, whereas the Bs of 2016 shows a bimodal distribution. Some outliers (visibly associated with artifacts) are present in each survey, probably due to errors during registration or conversion. In the Tab. IIA3 are reported the parameters of each Bs dataset.

Using the Jenks’ optimization method and taking into account the results of EntropyMax analysis and the drop-frames information, we classified the BS. The classes are the following (Figs. II3 and II4): Sandy gravel_Gravelly sand (SG_GS) in dark green, Slightly gravelly sand (SGS) in light green, Sand (S) in pink and Slightly gravelly muddy sand_Muddy sand_Slightly gravelly sandy mud (SGMS_MS_SGSM) in red. As already stated, the classes SGS and S are described together (Fig. II3) to make the classification comparable between datasets.

2011 BS range (dB)	2013 BS range (dB)	2016 BS range (dB)	Original BS	Classified BS	Description	Sediment cluster
> -27.36	> -20.11	> -21.52			Sandy seafloors with abundant coarse shell detritus coverage. The sediments are very poorly sorted and present a main mode on gravel size and a secondary mode on sand size. The mud is very low.	<p>Sand with shell fragments</p>
-34.24 ÷ -27.36	-27.82 ÷ -20.11	-29.51 ÷ -21.52			Sandy seafloors with low presence of shells and muds. The sediments are moderately sorted and have a single sandy mode.	<p>Coarse to fine-grained sand</p>
< -34.24	< -27.82	< -29.51			Seafloors composed by a mixture of sand and mud. The sediments present two or three modes on fine sand / silt size.	<p>Poorly sorted sandy mud</p>

Figure II3: schematic description of each substrata class. The class SGS and S are described together keeping the color of SGS class.

4. Study II: Bathymetric and backscatter data of seafloor change of the Chioggia inlet (Venice Lagoon) as a result of human intervention

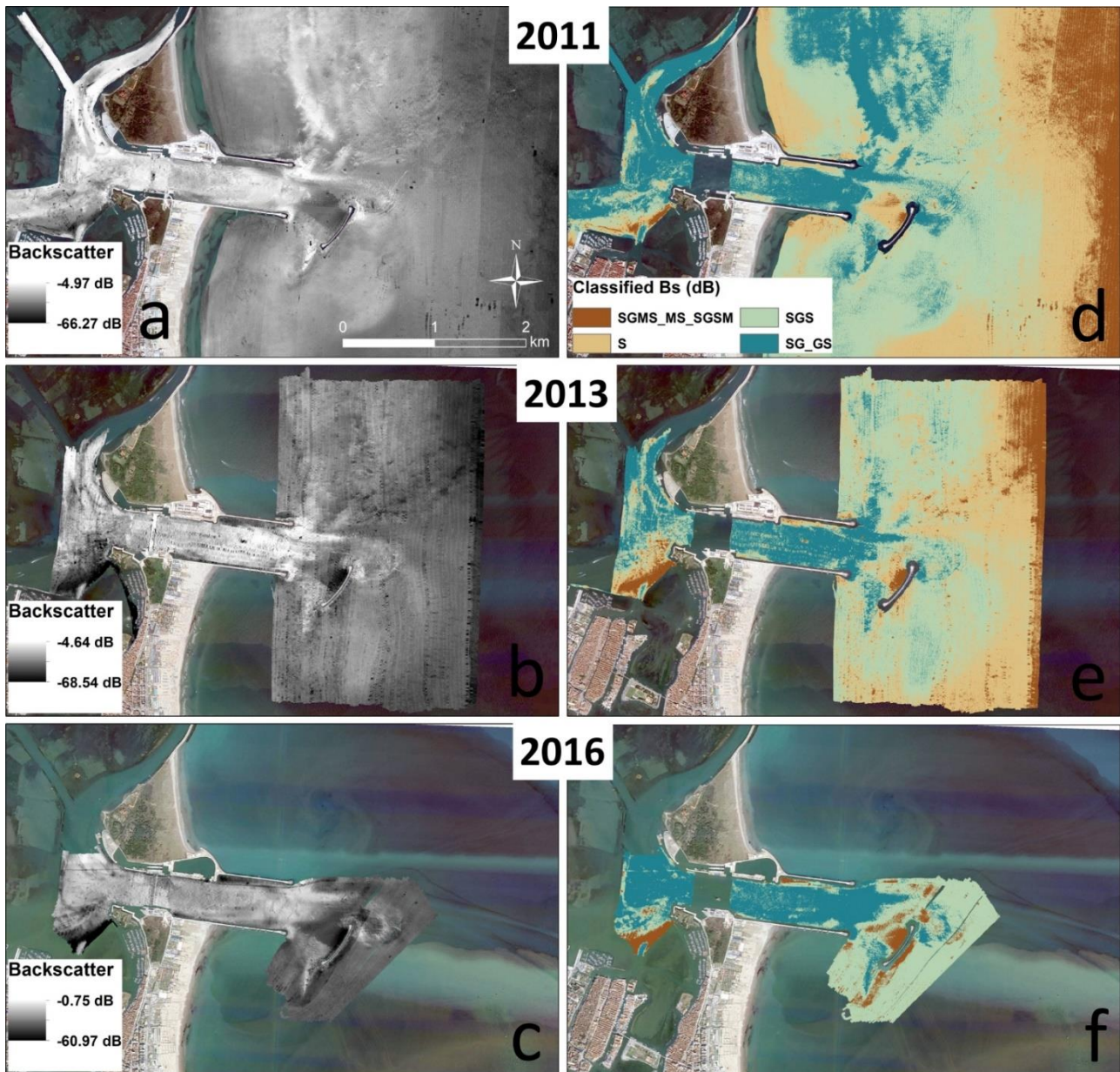


Figure II4: (a, b and c) backscatter signature of the Chioggia inlet seafloor in the years 2011, 2013 and 2016, respectively. (d, e and f) classified backscatter of the Chioggia inlet seafloor in the years 2011, 2013 and 2016, respectively. After the classification the classes SGS and S are merged into a single one (2011 and 2013).

The pattern of the classes in the three surveys is quite similar. The class SGS+S is the most widespread in the study area (clearly visible in 2011 and 2013) especially in the southern part of the lagoon basins. The class SG_GS is located especially in the inlet channel and in the northern-central part of the lagoon. Small patches of SG_GS are also found around breakwater's tips and above the northern jetties on seaside (2011). The SGMS_MS_SGSM, the less diffused class, is located inside the lagoon in correspondence of the shallow seafloors (mudflats), in the concave side of the breakwater (in 2016 also in the convex side) and in the open sea (2011-2013).

4. Study II: Bathymetric and backscatter data of seafloor change of the Chioggia inlet (Venice Lagoon) as a result of human intervention

Considering only the common area of each survey and without including the sectors with rip-rap (e.g. MoSE, jetties, breakwater, etc.), we derived the seafloor sediment composition during the three times (Fig. II5).



Figure II5: pie charts of each backscatter class of each survey respect to the total common area.

The unsupervised Jenks' classification shows an overall accuracy of 82 % in the dataset of 2013, identifying correctly 14 stations on 17 totals (Tab. II3). Differently, in 2016 the correctly identified stations are 20 on 28 with an overall accuracy of 69 % (Tab. II3). The used method reaches a better accuracy in 2013 because the sediment sampling stations are better distributed in the study area covering clearly the different backscatter patches. Conversely, in 2016 the samples are grouped in some sectors of the inlet (i.e. in correspondence of the main morphologies) where often coexists different classes: this could justify the lower overall accuracy found. Besides, the different accuracy values could be related to the general low number of collected sediment samples.

Table II3: confusion matrices for the backscatter classification of 2013 and 2016 surveys.

2013		Ground-truth samples			Total classified samples	Producer accuracy (%)	User accuracy (%)
		SG_GS	SGS+S	SGMS_MS_SGSM			
Classified samples	SG_GS	4	0	1	5	100	80
	SGS+S	0	8	2	10	100	80
	SGMS_MS_SGSM	0	0	2	2	40	100
Total ground-truth samples		4	8	5	17		
Overall Accuracy (%) = 82							
2016		Ground-truth samples			Total classified samples	Producer accuracy (%)	User accuracy (%)
		SG_GS	SGS+S	SGMS_MS_SGSM			
Classified samples	SG_GS	10	6	0	16	83	63
	SGS+S	2	5	4	11	45	45
	SGMS_MS_SGSM	0	0	2	2	33	100
Total ground-truth samples		12	11	6	29		
Overall Accuracy (%) = 69							

4.4.5. Backscatter change assessment

A general pattern of persistence is evident with more than 60 % of the common area remaining stable during the three surveys, mainly driven by the SGS+S class (Tab. II4, Fig. II6). In particular, the major changes appear from 2011 to 2013, whereas between 2013-2016 the changes are minor (Tab. II4, Fig. II6). More than a third of the study area was classified as SGS+S in 2011 (about the 36 %) and remain quite unchanged during times. Conversely, the class SGMS_MS_SGSM is the most mutable during the years (Tab. II4, Fig. II6).

Seafloor changes are described in terms of gain, loss, swap (change in location) and net change (Pontius et al., 2004) in Tab II5. In both time intervals, the class with the major gain is SGS+S, especially during 2011-2013, while the class SGMS_MS_SGSM registers always a low gain level (Tab. II5). From 2011 to 2013 only the class SGS+S shows a positive net gain (real increase), whereas SG_GS and SGMS_MS_SGSM show a negative net change (real decrease). Conversely, between 2013 and 2016 both SGS+S and SGMS_MS_SGSM show a decrease whereas SG_GS registers a strong increase. From 2011 to 2013 only the class SGS+S shows a tendency to increase, whereas SGMS_MS_SGSM suggesting a decreasing trend. SG_GS seems stable. All these values are however quite close to 0, indicating that the real net changes in classes between 2011 and 2013 is negligible. During 2013-2016 only the class SG_GS shows a small tendency to increase, whereas SGS+S and SGMS_MS_SGSM tend to decrease. In particular, the high value close to -1 of the class SGMS_MS_SGSM indicate a real strong loss in extension of this class. Differently the negative tendency of class SGS+S is negligible.

Table II4: change transition matrix (% of study area). The main diagonal (italicized) represents persistence (no change) of classes between years while other values represent 'from-to' changes between categories.

		2013			tot 2011
		<i>SG_GS</i>	<i>SGS+S</i>	<i>SGMS_MS_SGSM</i>	
2011	<i>SG_GS</i>	20.8	9.7	1.2	31.7
	<i>SGS+S</i>	9.2	37.4	6.6	53.2
	<i>SGMS_MS_SGSM</i>	1.1	8.1	5.9	15.1
tot 2013		31.1	55.2	13.7	100.0
		2016			tot 2013
		<i>SG_GS</i>	<i>SGS+S</i>	<i>SGMS_MS_SGSM</i>	
2013	<i>SG_GS</i>	25.2	5.8	0.4	31.3
	<i>SGS+S</i>	11.5	39.3	4.2	55.0
	<i>SGMS_MS_SGSM</i>	1.5	7.3	4.9	13.7
tot 2016		38.2	52.3	9.5	100.0
		2016			tot 2011
		<i>SG_GS</i>	<i>SGS+S</i>	<i>SGMS_MS_SGSM</i>	
2011	<i>SG_GS</i>	25.2	6.3	0.5	32.0
	<i>SGS+S</i>	11.3	37.9	3.8	53.0
	<i>SGMS_MS_SGSM</i>	1.7	8.2	5.2	15.1
tot 2016		38.2	52.4	9.5	100.0

4. Study II: Bathymetric and backscatter data of seafloor change of the Chioggia inlet (Venice Lagoon) as a result of human intervention

Table II5: Changes in classifications expressed as percentage of the common study area (3.34 km²). Gains and losses between years are attributed to swapping (location) change and net (quantity) change. gp = gain/persistence, lp = loss/persistence, np = net change/persistence.

	2011	2013	Gain	Loss	Tot change	Persistence	Net change	Swap (location)	gp	lp	np
SG_GS	33.7	32.5	10.2	10.9	21.2	20.8	-0.7	20.5	0.5	0.5	0.0
SGS+S	51.3	53.8	17.8	15.8	33.5	37.4	2.0	31.5	0.5	0.4	0.1
SGMS_MS_SGSM	15.0	13.7	7.8	9.1	16.9	5.9	-1.4	15.5	1.3	1.5	-0.2
Tot	100.0	100.0	35.8	35.8	71.6	64.2	4.0	67.5			

	2013	2016	Gain	Loss	Tot change	Persistence	Net change	Swap (location)	gp	lp	np
SG_GS	32.5	39.4	13.0	6.1	19.1	25.2	6.8	12.3	0.5	0.2	0.3
SGS+S	53.8	51.2	13.1	15.7	28.8	39.3	-2.6	26.1	0.3	0.4	-0.1
SGMS_MS_SGSM	13.7	9.4	4.5	8.7	13.3	4.9	-4.2	17.5	0.9	1.8	-0.9
Tot	100.0	100.0	30.6	30.6	61.1	69.4	13.7	55.9			

	2011	2016	Gain	Loss	Tot change	Persistence	Net change	Swap (location)	gp	lp	np
SG_GS	33.7	39.4	13.0	6.7	19.7	25.2	6.2	13.5	0.5	0.3	0.2
SGS+S	51.3	51.2	14.5	15.1	29.5	37.9	-0.6	30.2	0.4	0.4	0.0
SGMS_MS_SGSM	15.0	9.4	4.3	9.9	14.1	5.2	-5.6	8.5	0.8	1.9	-1.1
Tot	100.0	100.0	31.7	31.7	63.4	68.3	12.4	52.2			

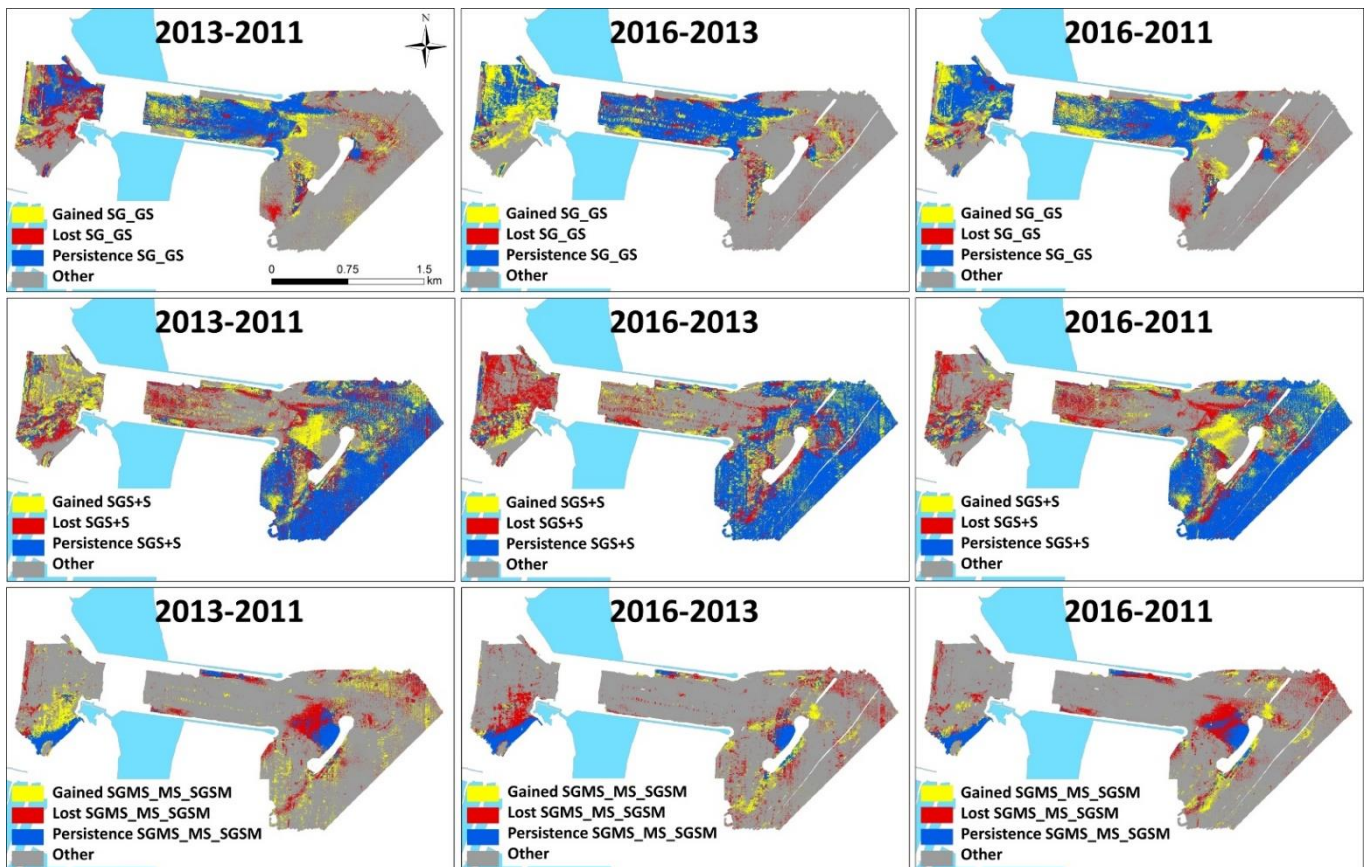


Figure II6: Gains, losses and persistence in the common area between the years 2011-2013 (first column), 2013-2016 (second column) and 2011-2016 (third column) for the classes SG_GS (first row), SGS+S (second row) and SGMS_MS_SGSM (third row). Persistence (blue) indicates no change in class attributions, gains (yellow) and losses (red) indicate where classes have changed in distribution. The grey indicates other classes changes (not modelled).

4.4.6. Seafloor features analysis

The location and the shapes of the features analyzed in the time span in this study are reported in Fig. II7.

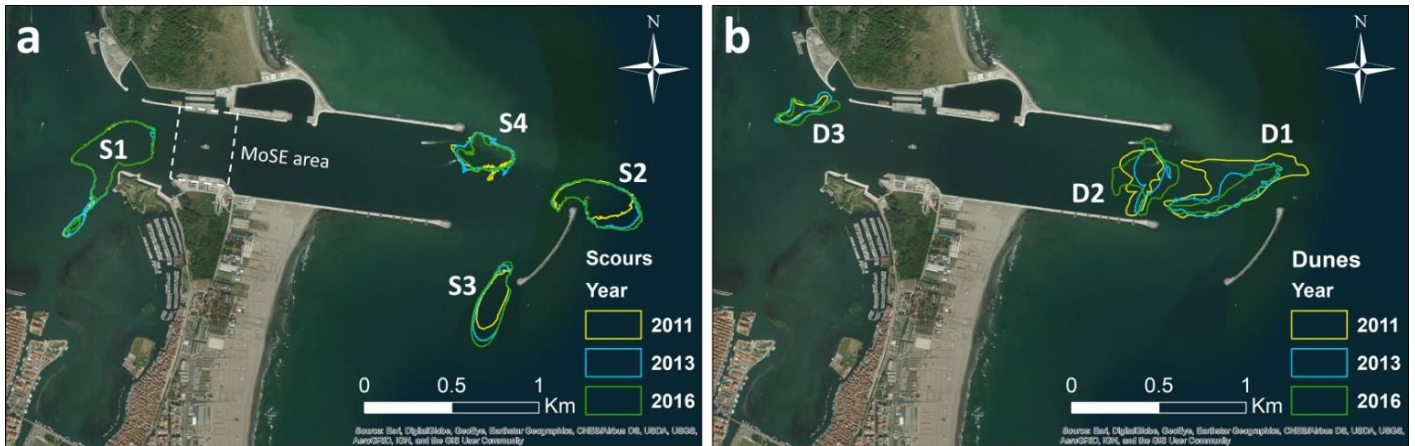


Figure II7: (a) shapes and position of the analyzed scour holes during the 2011, 2013 and 2016 surveys and mobile barriers location (MoSE); (b) shapes and position of the analyzed dunes/dune fields during the 2011, 2013 and 2016 surveys. The decrease in dune fields areal extension evidences the net sediment transport toward the sea.

4.4.6.1. Scour holes

Using the automatic BPI tool (see Fogarin et al., 2019 for detail), we extract the area of each scour hole from each DEM. Scour holes are defined as localized erosional features produced over a sediment surface in a turbulent current (Ferrarin et al., 2018; Madricardo and Rizzetto, 2018). In the study area four scour holes have been identified (Fig. II7). In figure II8 are reported shapes and profiles of the scour holes in the times.

Scour hole S1

The largest and deepest scour hole is located inside the lagoon basin, close to the western inlet entrance (Fig. II7a). As shown in Balletti et al. (2006), this morphology is already identifiable in the historical map of 1809-1811 by Augusto Dénaix (Magrini, 1934) and in the maps of 1927, 1970 and 2002 created by Magistrato alle Acque (MAV-CVN, 2004). The surface area covered by this irregular scour hole is about 111,690 m² in 2011, 112,408 m² in 2013 and 88,037 m² in 2016 (Tab. IIA5). The shape, such as the vertical profiles of this morphology are significantly stable during the three surveys (Fig. II8a). The two main axes measure about 780 m and 320 m, and the maximum relative depth is 20 m. The deepest point reaches -30 m. The vertical section is quite homogeneous, but shows some steps towards south-east direction. The average slope ranges between 10° and 35°,

reaching about 80° near anthropogenic foundation of coastline. Calculating the volume differences of this morphology during the years (Tab. IIA5), we obtained about -9,516 m³ between 2011-2013 and about 10,537 m³ between 2013-2016, meaning that after a small erosion occurred in the first period, this scour hole tends to silt up.

The backscatter signature associated to this scour holes (Fig. II4) is quite different during the three surveys and shown a coexistence of classes: the sediment seafloor of the central part appears mostly coarse in 2011 (class SG_GS), becoming finer in 2013 (class SGS+S) and returning coarser in 2016 (BS class SG_GS). Conversely, the bottom of the south-west appendix is always covered by fine sediments (class SGMS_MS_SGSM).

Scour hole S2

The second largest scour hole is located at the northern end of the breakwater (Fig. II7a). It has an almost ellipsoidal shape roughly parallel to the tidal inlet channel axis. This morphology is very active during the times and increases its surface and deep very quickly (Fig. II8b). The surface area is about 62,499 m² in 2011, 81,672 m² in 2013 and 105,112 m² in 2016 (Tab. IIA5) meaning that in five years its surface is almost doubled. The main axis measures 430 m in 2011, 500 m in 2013 and 530 m in 2016, while the secondary axis is more constant measuring 230 m in 2011 and 250 m in 2013 and 2016. In particular, the direction of development of the morphology is along the main axis towards south-east (according to the ebb-tide flow direction). Accordingly, the maximum depth is also increasing in times, reaching about -16 m in 2016 (starting from -15 m in 2011). The vertical profiles (relative depth of 2 m in 2011 and 3 m in 2013/2016), show that the deepest points are in the central-west part of the morphology with slopes ranging from 5° to 15°. Calculating the volume differences during the times, we estimate an erosion of about 61,516 m³ in the period 2011-2013 and about 21,585 m³ in the period 2013-2016 (Tab. IIA5).

The backscatter signature associated to this scour holes is very inhomogeneous (Fig. II4). During the 2011 the seafloor was mainly sandy (class SGS+S), with a small patch of coarse materials (class SG_GS) located near the breakwater end. A small zone of fine sediment (class SGMS_MS_SGSM) is also present in the eastern portion of the scour hole. During the 2013 the seafloor become entirely sandy (class SGS+S), but the patch of SG_GS is preserved. Finally, during the 2016, the seafloor remains predominantly sandy (class SGS+S), the SG_GS patch is moved towards south and a small

zone of SGMS_MS_SGSM occurs in the deepest part of the scour hole. During this last survey, a thin belt of coarse sediments (class SG_GS) borders the eastern part of the features.

Scour hole S3

Another scour hole is located at the southern breakwater tip (Fig 7a). It has an oval shape roughly oriented from north to south (Fig. II8c). This scour hole is similar to scour holes S2 suggesting the same origin. As scour hole S2, this morphology increases very quickly its dimension and nearly doubled its area. Starting from a surface of 35,485 m² (main axis 400 m long) in 2011, it becomes 52,596 m² (main axis 480 m long) in 2013 and it reaches 61,659 m² (main axis 520 m long) in 2016 (Tab. IIA5). The width is more stable during the years: 125 m in 2011, 150 m in 2013 and 165 m in 2016. The direction of development of the morphology is along the main axis towards the south. The maximum depth also increases (-11.5 m in 2011, -12 m in 2013 and -12.5 m in 2016). The vertical profiles (relative depth of 3 m in 2011, 3.5 m in 2013 and 4 m in 2016), identified the deepest point in the norther part of the morphology with slopes ranging from 5° to 20°. The profiles measured are quite irregular, with several sharp steps, likely connected to slumping processes due to steep and unstable sides or to changes in lithology of the units eroded below the seafloor. Calculating the volume differences during the times, we estimate an erosion of about 58,829 m³ in the period 2011-2013 and about 23,796 m³ in the period 2013-2016 (Tab. IIA5).

The backscatter signatures of this morphology registered in 2011, 2013 and 2016 are very similar (Fig. II4). They display a coarse sediment seafloor (class SG_GS) in the middle and deepest part of the scour hole, while the margins are mostly sandy (class SGS+S). A fine sediment belt (class SGMS_MS_SGSM) always occurs in the south-east (clearly visible in the 2016 survey).

Scour hole S4

The smallest scour hole is located at the seaside end of the northern jetty (Fig. II7a). It has an irregular shape and it is roughly parallel to scour hole S2 (Fig. II8d). The surface area covered by this morphology is 46,287 m² in 2011, 49,312 m² and 38,027 m² in 2016 (Tab. IIA5). The main axes are moderately static during the years, measuring about 330 m and 210 m. Also the depth is pretty stable, measuring about -13 m. The vertical profile (relative depth of about 2 m) show a homogeneous slope with values around 5°. Calculating the volume differences of this morphology

4. Study II: Bathymetric and backscatter data of seafloor change of the Chioggia inlet (Venice Lagoon) as a result of human intervention

during the two time intervals (Tab. IIA5), we obtained about $-12,420 \text{ m}^3$ between 2011-2013 and about 30 m^3 between 2013-2016, meaning that after a small erosion occurred in the first period, this scour hole volume is now quite stable (small deposition).

The backscatter in correspondence of this morphology does not change so much during the times (Fig. II4). Starting from the 2011 where the seafloor of this scour hole was half SG_{GS} and SG_S+S, the seafloor becomes coarser during the years, up to becomes completely SG_{GS} in 2016.

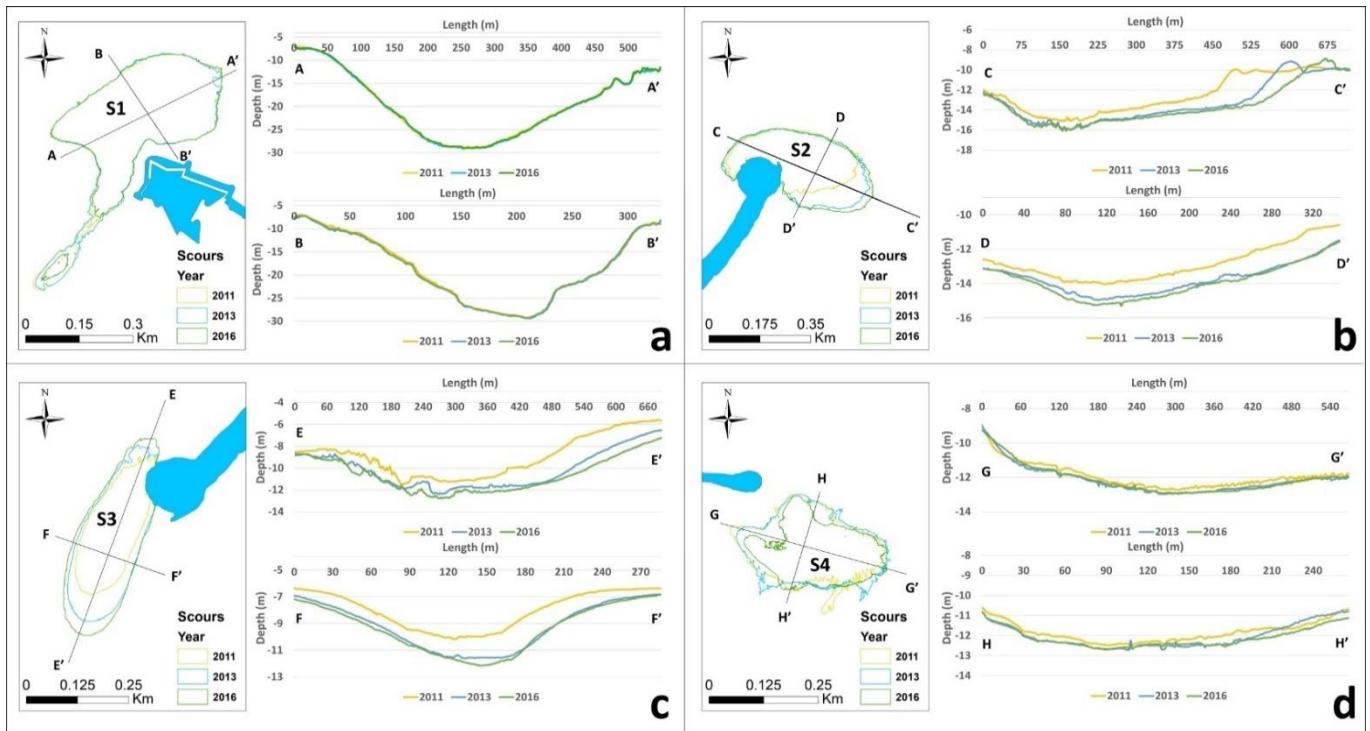


Figure II8: shapes of each analyzed scour holes and their vertical profiles during the three surveys.

4.4.6.2. Dunes and dune fields

Dunes are depositional morphologies which crests are transversally oriented with respect to the main direction of the current (Ashley, 1990). We found distinctive groups of small size dunes (dune fields) and very large, typically isolated, dunes with wavelength λ ranging from 2 m to 100 m and height h from 0.02 m to 2 m, respectively. All dunes, regardless of the size, seem oriented towards the sea, reflecting the direction of the ebb tide. Using the layer ruggedness (see Fogarin et al., 2019 for detail), we semi-automatic delineate and extract the area of each dune from each DEM. Hereafter we describe the evolution over time of the three dune fields identified in Fogarin et al. (2019).

Dune field D1

The dune field D1 is located at the seaside entrance of the inlet channel, close to the northern breakwater tip (Fig. II7b). It develops from south-west to north-east forming an irregular arcuate shape (Fig. II9a and 9d) at a depth of about -11 m. Some measures of vertical profiles, realized where the individual dunes are most developed, shown that the dimensions of these ones change significantly. The entirely surface covered by the dune field was 140,588 m² in 2011, 71,541 m² in 2013 and 14,316 m² in 2016 (Tab. IIA5), meaning that in about five years the extension of this field was reduced to a tenth with respect to the initial size. Accordingly, also the sediment volume associated was subject to a constant erosion, i.e. -26,974 m³ between 2011-2013 and -6,744 m³ between 2013-2016 (Tab. IIA5).

During the 2011 survey, the individual dunes were very regular, slightly oriented seaward (from west to east) and they measured about 25 cm in height and about 8 m in wavelength. The slopes of the stoss and lee side range from 4° to 5° and from 6° to 9°, respectively. During the 2013, the number of dunes inside the field is reduced but the dimensions increase. The maximum height and wavelength measured 50 cm and 17 m, respectively. The orientation was clearly towards the sea. The stoss slopes vary between 2° and 6°, while the lee slopes between 15° and 25°. During the 2016, all the dunes are almost disappeared. A rippled seafloor is still recognizable, but the height of the individual bedforms is strongly resized ($h \approx 15$ cm, $\lambda \approx 30$ m and slope $< 2.5^\circ$).

The backscatter signature associated to this morphology is different from 2011 to 2013, but remains quite similar between 2013-2016 (Fig. II4). During the 2011, the dune field is mostly composed of SGS+S class on the northern part and mostly by SGMS_MS_SGSM class on the southern part. During the 2013, the SGMS_MS_SGSM seafloors are smaller (still present on the eastern part). In particular, in both 2011 and 2013 surveys, a pattern of alternating BS values are recognizable in some parts of the dune field: on the crests the BS is lower (class SGMS_MS_SGSM) indicating a fine sediments seafloors, while on the troughs the BS is higher (class SGS+S) indicating a coarser grain size seafloors. During the 2016, the dune field area is almost completely composed by SGS+S.

Dune field D2

A clearly visible dune field is present at the eastern entrance of the inlet channel, about in correspondence of the jetties ends (Fig. II7b). This morphology is composed by the largest dunes identifiable in the study area (a and b in Fig. II9e). This field occupies 52,511 m² in 2011, 37,293 m² in 2013 and 46,898 m² in 2016 (Tab. IIA5). Calculating the sediment volume differences of the entire

fields, we obtained an erosion of $-13,503 \text{ m}^3$ between 2011-2013 and a deposition of $9,275 \text{ m}^3$ between 2013-2016 (Tab. IIA5). Overall, seen the low values, we can assert that the volume of the dune field is quite stable. What is really changeable in the times is the morphology and the position of the individual dunes composing the field. From the DEMs, it is indeed clear the shift of the individual dunes towards the sea, measurable in about 100 m in both time intervals.

In the 2011, the recognizable dunes were 7 (Fig. II9e). Most of them have the concave side toward the sea and are classifiable as very large barchan dunes (a, b and c in Figs. II9b and II9e). The largest measures about 3 m of height and about 120 m of wavelength (b in Fig. II9e). All the dunes are slightly orientated seaward, with the stoss slope of $5^\circ/10^\circ$ and the lee slope of $15^\circ/20^\circ$. Over the stoss side, some smaller dunes are superimposed ($h \approx 20 \text{ cm}$ and $\lambda \approx 4 \text{ m}$). In the 2013, the number of the individual dunes becomes 4 (Fig. II9e), because some of them merged each other. These dunes are out of phase with the most external large dune having a positive convex linguoid shape and the internal dune show a negative convexity lunate shape (a and b in Fig. II9e). The largest dune measures about 2.5 m of height and about 110 m of wavelength (b in Fig. II9e). In particular, these dunes develop a clear orientation toward the sea, with the stoss and the lee slope ranging from 3° to 5° and from 20° to 30° , respectively. The heights and the asymmetries generally become smaller at the edges of the dunes fields where they pass outward into rippled sand flats. Over the stoss side, smaller superimposed dunes are still present ($h \approx 20 \text{ cm}$ and $\lambda \approx 4 \text{ m}$). In the 2016, the number of dunes is increased to 6 (Fig. II9e). Some new dunes were formed on the west side, while on the east some dunes merged each other (e.g. de in Fig. II9e). These dunes are more detached respect of the other years. The largest dunes measure 2/2.5 m of height and reach about 130 m of wavelength (a and bc in Fig. II9e). The dunes are still oriented seaward, with the stoss slope of $3^\circ/5^\circ$ and the lee slope of $20^\circ/30^\circ$.

The backscatter signatures associated of this bedform are the same in the three surveys (Fig. II4). The seafloor is indeed completely composed by coarse sediments (class SG_GS). Only in the southern part of the field, close to the southern jetty, an area of SGS+S is present. Several sediment samples were collected in 2016 in the middle part of the field, with the aim of investigating the textural differences between lee and stoss sides of the dunes. However, no significant differences were found.

Dunes D3

Two very large connected dunes are identifiable in the north of the internal scour hole, close to the western entrance of the inlet channel (Fig. II7b). These morphologies are oriented from north-west to south-east (Figs. II9c and II9f). The dunes are asymmetric toward sea, indicating a net seaward migration and, by comparing the different datasets, this asymmetry increased over time. The total surface area covered by the two dunes is 19,815 m² in 2011, 22,359 m² in 2013 and 46,898 m² in 2016 (Tab. IIA5). The calculation of the sediment volume results in erosion of -13,503 m³ between 2011-2013 and a deposition of 9,275 m³ between 2013-2016 (Tab. IIA5). Focusing on the shift of the crests, we measured a seaward movement of about 12 m in the first interval period and 40 m in the second one.

In the first survey, the dunes had a height of about 1.8 m and a wavelength of 70 m. They were slightly asymmetric with the maximum stoss slope of 6° and the maximum lee slope of 12°. A small circular depression (relative depth of about 3 m) was present on the eastern side of the dunes. In the 2013 the values of height and wavelength were about 2 m and 100 m, respectively. The dunes were more oriented toward sea, with the stoss slope of 3° and the lee slope of 20°. Finally, in the 2016, the dunes measure 2.5 m of height and 115 m of wavelength. They were strongly asymmetric, with the stoss slope of 2° and the lee slope of 24°. Over the stoss side, some small dunes appeared ($h \approx 20$ cm and $\lambda \approx 6$ m).

The associated backscatter signatures are very similar in the three surveys (Fig. II4): the two dunes seem clearly composed by coarse sediments (class SG_GS). Only in the 2013 some patches of lower Bs (class SGS+S) appear in the northern sector (stoss slope) of the dunes.

4. Study II: Bathymetric and backscatter data of seafloor change of the Chioggia inlet (Venice Lagoon) as a result of human intervention

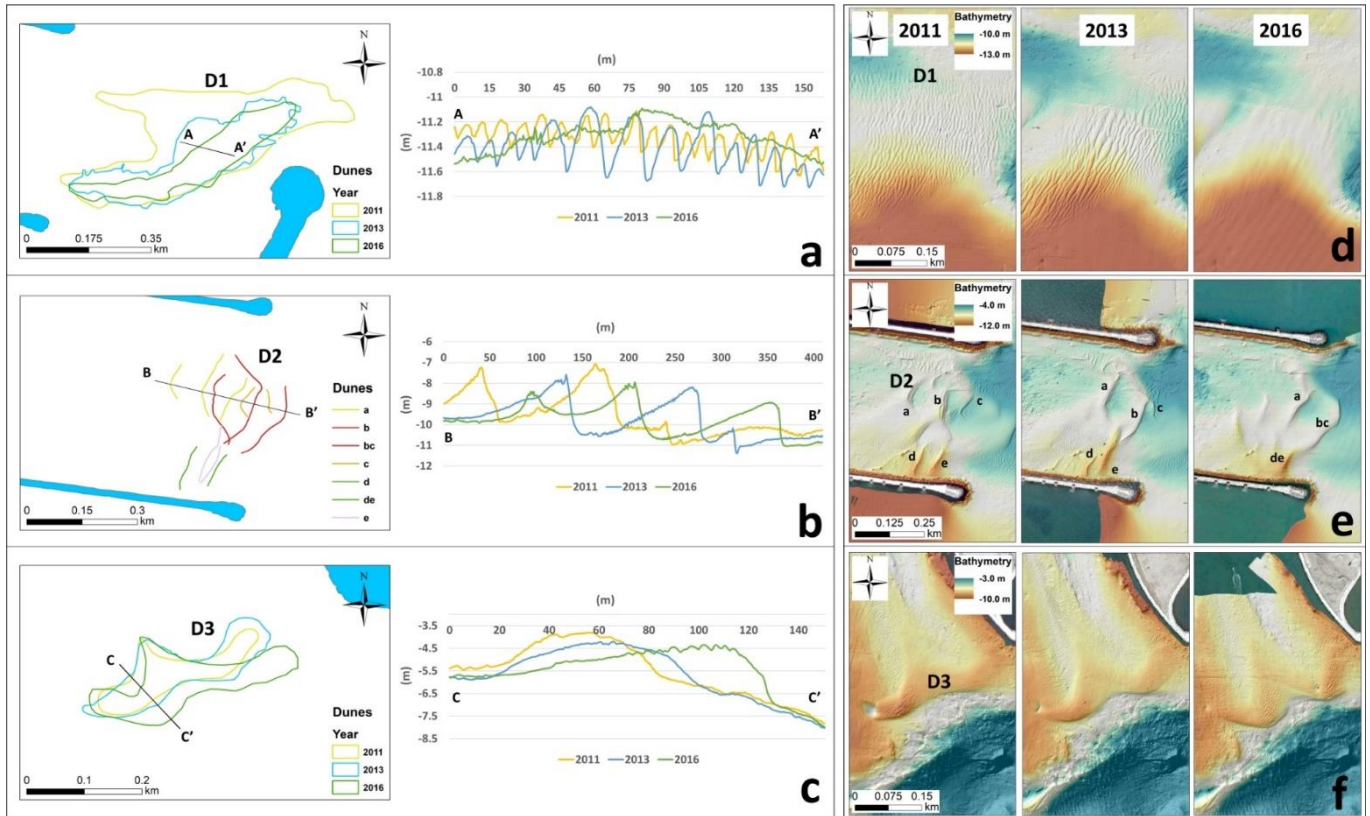


Figure II9: shapes of each analyzed dunes / dune fields and their vertical profiles during the three surveys.

4.4.6.3. MoSE area

In the western part of the tidal inlet, the MoSE allocation site is easily identifiable by the regularity of the shapes (Figs. II1, II7). Analyzing the seafloor, three different MoSE elements are recognizable, in a total surface area of about 160,000 m². The most evident is a thin rectangular trench, measuring 415 x 50 m, located transversal respect the inlet channel (Fig. II10). This element will host the mobile barriers. At the lateral side of the trench, two armored seafloors (the eastern measures 360 x 150 m, the western 360 x 200 m) composed by boulders and concrete are identifiable. These features, classifiable as rip-rap, appear very similar to the jetties' foundation and their goal is to protect the trench and the mobile gates from the bottom sediment transport. Part of the rip-rap, with a lower boulder density, continues to the east until it disappears under bottom sediments. In the east indeed, the net boundary of this feature is difficultly recognizable.

4. Study II: Bathymetric and backscatter data of seafloor change of the Chioggia inlet (Venice Lagoon) as a result of human intervention

Some differences are observable on the MoSE construction progresses. During 2011, the trench had an average depth of -16 m. The begin of the dredging processes is clearly conceivable by the different levels of the seafloor inside the trench (a depth of -22 m is recognizable on the north). The two lateral rip-raps are already present, but some steps inside the features suggest that these sectors were not finished yet. In the 2013, the dredging of the trench is almost ended: the corresponding seafloors, although not homogeneous, are levelled to about -24 m. The later rip-raps are not changed from the first survey. Finally, during the 2016, the MoSE area seems to be completed and ready to host the mobile gates. The profiles of the caissons are easy visible, with the lateral raised banks and the flat bottom. Looking the profile, it is also possible to recognize the several hinges that are necessary to connect the mobile gates. Moreover, the lateral rip-raps are nearly finished and levelled to -16 m (a small step is still present on the north-west).

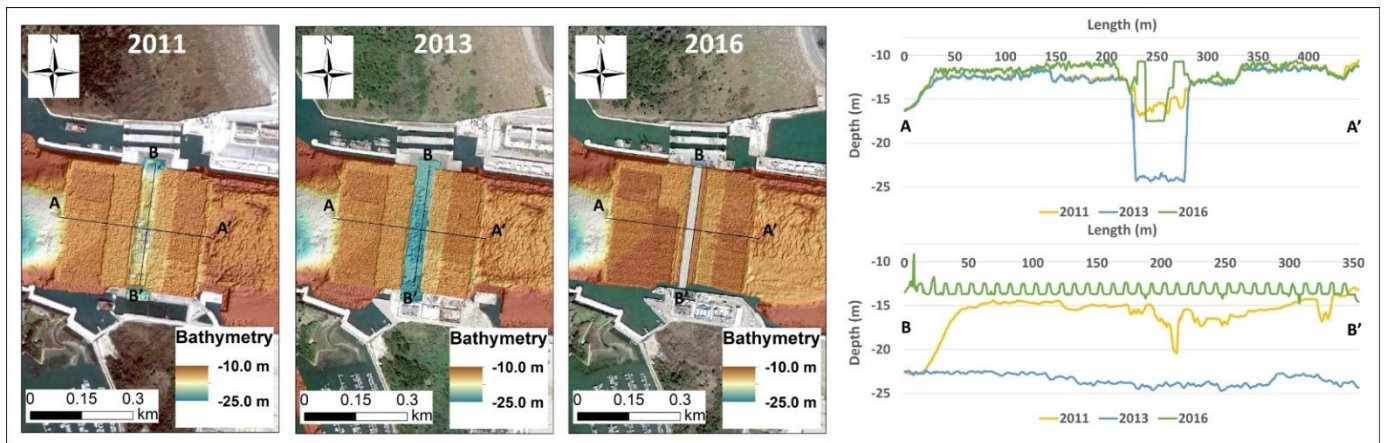


Figure II10: morpho-bathymetry of the MoSE area in the 2011, 2013 and 2016 and vertical profiles. The regular undulation visible in 2016 profile (B-B') is given by the 36 hinges, i.e. the connections between the 6 concrete caissons and the 18 mobile barriers.

4.5. Discussion

Although the use of MBES is becoming more widespread for the studying, planning and managing of the coastal areas, the researches that analyzed seafloor evolution based on repeated MBES survey data are sporadic. The published papers generally focus either on changes of backscatter distribution (e.g. Montereale-Gavazzi et al., 2019; Janowski et al., in press), of substrata composition (e.g. Rattray et al., 2013; Montereale-Gavazzi et al., 2018) or on bedform dynamics (e.g. Ernsten et al., 2005; Smith et al., 2007; Li et al., 2014; Todd et al., 2014; Fraccascia et al., 2016;

Homrani et al., 2019). In this study, instead, we analyzed the changes of the seafloor taking into account both the morpho-bathymetry and the substrata typology.

The study area is an “anthropogenic inlet”, delimited by long jetties, occasionally dredged in some areas, and in recent times altered by the construction of the MoSE project. For these reasons, the inlet lost its natural characteristics and behaviors (Fogarin et al., 2019). Despite the remote sensing analysis (e.g. satellite images) in which the inlet seems to be stable instead, the seafloor changes significantly over time.

As already observed in Fogarin et al. (2019), the construction of the breakwater in defense of the mobile barriers and the cross-section shrinkage had strongly altered the inlet dynamics. The change in the configuration increased the current speed in the inlet channel, as suggested by the modelling simulations of Ghezzi et al. (2010), with a consequent increase in the bottom shear stress and sediment resuspension, reallocation and possible transport outside the inlet. The comparison of the sediment distribution over time obtained by the MBES data analyses and the literature review confirms this hypothesis since in the inlet channel, the mainly sandy sediment is replaced by mainly gravelly sediment (shell detritus). These results support the conceptual model of the processes that followed the MoSE construction reported in Fogarin et al. (2019).

By comparing the bathymetric surveys of 2011 and 2013, we confirmed a general erosive trend with a net volume loss of more than $1.1 \times 10^6 \text{ m}^3$ (Fig. II2 and Tab IIA6). This great erosion is easily recognizable along the inlet channel and in correspondence of the two scour holes at breakwater tips. Conversely, in the period 2013-2016, the erosion decreases and a slight deposition occurs (about $+ 50.000 \text{ m}^3$). This deposition is concentrated in correspondence of the large dunes in the eastern inlet entrance and near the rip-rap at MoSE trench lateral sides. An identical result is found in correspondence of the Lido inlet (Toso et al., 2019), the northern connection between the Venice Lagoon and the Adriatic Sea (see Fig. II1 for Lido inlet location). The different behavior in the two time span (2011-2013 and 2013-2016) could be related to the fact that after a first phase of adjustment, the system starts to gain a new equilibrium that is partially reached after 2013. However, as observed by Toso et al. (2019), this difference in the two periods could also be due to the meteorological conditions that induced an increase of the tidal prism as a consequence of big storms on November 2012 and February 2013.

As already mentioned in (Fogarin et al., 2019) the construction of the breakwater outside the inlet induced a change in the hydrodynamics with the consequent formation of two scour holes (S2 and

4. Study II: Bathymetric and backscatter data of seafloor change of the Chioggia inlet (Venice Lagoon) as a result of human intervention

S3) at breakwater tips eroding the ebb-tidal delta (Fig. II11). These morphologies were not present before the breakwater was established (Magistrato alle Acque 2002; Villatoro, 2010). As the hard structure was built on a regular surface over the ebb-tidal delta, removing the bathymetric depression associated with these two scour holes and interpolating the remaining surface, we can estimate about 476,000 m³ of sediments have been eroded after the construction of the breakwater (completed in 2006). An identical scouring with the formation of two scour holes over the ebb-tidal delta is observed at Lido inlet (Toso et al., 2019) indicating that similar processes are acting. The deepening and expansion of the two scour holes occurred mostly in the period 2011-2013. In the samples Z19, Z20, Z21 and Z27 (Fig. II1) collected in the middle of the scours S2 and S3 at a depth of about 15 m and 10 m, respectively, we found a consolidated mud and an over-consolidated layer visible also in the drop-frames Z20, Z21, Z25 and Z27. These sediments could belong to the Pleistocene limit, also known locally with the name of “caranto”, that Zecchin et al. (2008) set in this area at about the same depth, i.e. -15 m. The presence of caranto could also be responsible for the slowing down of the erosive process. This hypothesis however must be confirmed after further sampling and sediment analyses.

The lagoonal scour holes S1 was not influenced by the construction of the MoSE, indeed its shape and depth did not substantially change in the last 20 years (Fig. II11). The limited changes of scour holes S4 are probably connected to the movement of bottom shelly sediments (Fig. II11). It is possible that these two morphologies had already reached them equilibrium.

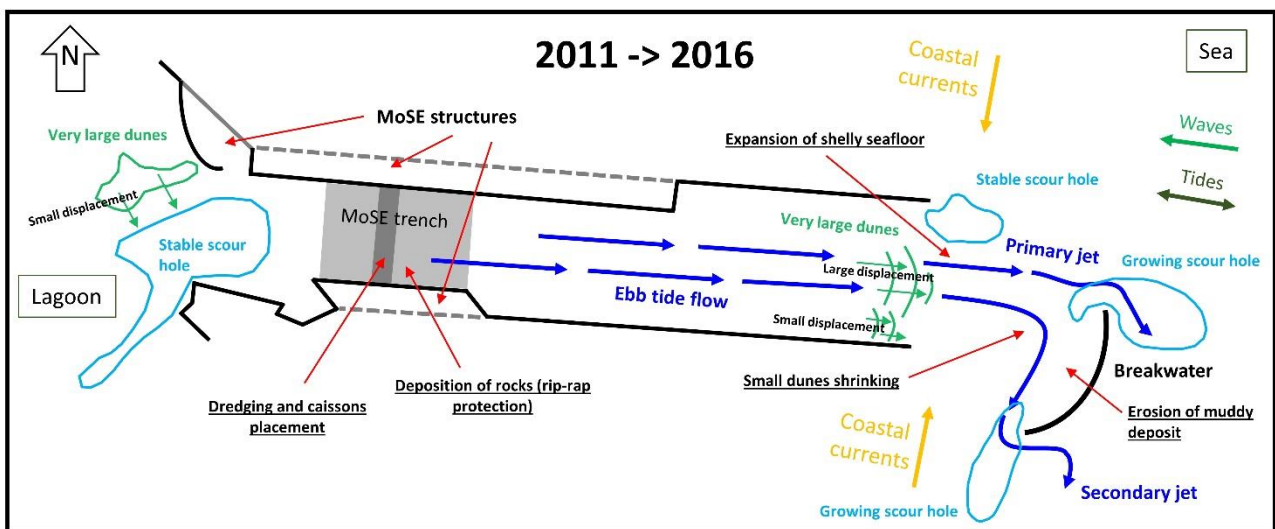


Figure II11: schematic summary of the seabed evolution and dominant processes during ebb tide phase in the Chioggia inlet between the 2011 and 2016.

Several studies applied morphometric semi-automated techniques to describe dunes parameters, such as height, wavelength, slope, orientation, etc. (Duffy, 2012; Cazenave, et al., 2013), or to evaluate their migration in time (Duffy et al., 2005; Duffy et al., 2012; Salvatierra et al., 2015, Fraccascia et al., 2016). In some cases, geomorphometric analyses of the dunes is crucial to prevent hazards related to human activities (e.g. navigation, construction of pipelines, etc.).

The distribution of bedforms in the seafloor is determined by the spatial pattern of tidal currents and substrate types (Todd et al., 2014). It is also well established that the morphology of submarine dunes is determined by current strength and sediment transport that are driven by tides, waves and winds (Allen, 1980). The migration of bedforms is a major sediment transport process (Allen et al., 1982). All the bedforms that we mapped appear oriented seaward. In agreement with Dalrymple and Rhodes (1995), most estuarine dunes, regardless of size, are generally asymmetric, with a gentler stoss side and a steeper lee side. The exact shape and profile of the dunes depend on several factors, including flows strength, sediment transport rate, presence of superimposed dunes, etc.

In the Chioggia inlet we classified the dunes by measuring their average proprieties from the MBES bathymetry as described in Fogarin et al. (2019). Hereafter we discuss the evolution over time of the three dune fields identified in that study (see Fig. II9).

The D1 dunes are clearly visible and show a very regular pattern in 2011 (Fig. II9a). In 2013 the number of dunes decrease, but their wavelength and height increase. Finally, in 2016 the dunes almost disappeared and only few ripples are still recognizable. This change could be the result of erosion of sediments from the top of the dunes, then deposited in the troughs. Taking into account that the texture of the sediments of the seafloor remains pretty unchanged in time (Figs. II4 and II6), the evolution of these dunes can be mainly explained by the changes in the hydrodynamic configuration. An increase of the current velocities could indeed be responsible of the partial disappearing of the dunes. As already stated, the construction of the breakwater and the increase of the fluxes in the eastern inlet extremity, has triggered a general erosion of the seabed that required some years to level the dunes (Fig. II11). The same behavior was found in Toso et al. (2019) in the Lido inlet.

The largest dunes are located at both of inlet entrances (b and c in Fig. II9). These dunes are strongly asymmetric with a clear orientation towards the sea. According to Dalrymple and Rhodes (1995), Hennings et al. (2000) and Cuadrado et al. (2003), large and very large dunes are generally asymmetric in the direction of net bottom sediment transport. The strong asymmetry may be

sufficient to infer a net seaward sediment transport, but we plan to ascertain this with repetitive bathymetric surveys.

By comparing the different bathymetric surveys, the D2 dunes at the inlet entrance have the largest migration rate (Fig. II2 and II9). In detail, the largest migration rate values belong to the dunes in the middle of the inlet channel (a and b in Fig. II9e, Fig. II11), whereas the peripheral dunes register lower movements (d and e in Fig. II9e, Fig. II11). Taking into account the time span of each survey (2.3 years the first interval and 2.5 years the second interval), we obtain an average migration rate of these dunes is of about 44 m year^{-1} (0.12 m day^{-1}) in 2011-2013 and 40 m year^{-1} (0.11 m day^{-1}) in 2013-2016. This result confirms that there was a net seaward bottom sediment transport over the years (Amos et al., 2010; Villatoro et al., 2010; Ferrarin et al., 2010) that slightly slowed down in the second time period.

These values are similar to those found by Duffy and Hughes-Clarke (2005) in the high anthropized Bay of Fundy (New Brunswick, Canada) where they measured a migration rate of $36/54 \text{ m year}^{-1}$ for dunes with smaller dimension (height of 30 cm and wavelength of 20 m). The bottom current velocity that the authors measured in the area is 1.1 m sec^{-1} (7.33 mm day^{-1}), a value comparable with the Chioggia inlet current velocity. Conversely, Fraccascia et al. (2016) measured a considerably lower migration rate in a natural tidal inlet of Wadden Sea (Denmark) characterized with a peak current velocity of 1.39 m sec^{-1} (9.27 mm day^{-1}). They indeed estimated a migration rate of 3 m year^{-1} (8.22 mm day^{-1}) for dunes with 155 m and 2.3 of wavelength and height, respectively. However, the Wadden Sea tidal channel is completely natural, without jetties and with the possibility to expand through lateral shoals in cases of high tides or storm events. Differently, the hard armored set up of Chioggia inlet imposed an increase of tidal prism during flooding events that could have possibly augmented the bedload sediment transport along the inlet channel. Indeed, these high migration rate values have not been registered in correspondence of dunes inside the lagoon, where the water has the possibility to expand.

The different migration rates found within the D2 dune field can be related to the different sediment texture: the dunes in the middle and north part (a, b and c in Fig. II9e) of the inlet channel are completely covered by shelly substrata in the three years, whereas in the southern part (d and e in Fig. II9e) the bare sand is dominant (Fig. II4). This sediment distribution is a marker of different hydrodynamic conditions: in the middle/northern part of the channel the currents are the highest causing a major bedload sediment transport (Defendi et al., 2010).

Considering the backscatter associated to these bedforms and the sediment samples collected nearby, we do not observe significant change in sediment substrata in the years (Figs. II4 and II6). For this reason, the changes in the dunes can be attributed only to the hydrodynamic conditions and not to the different sediment supply. Moreover, the fact that new dunes (Fig. II9e) were formed at the western side of the channel suggest that a continuously bottom sediment transport take place in the inlet.

A significant large dune displacement took place at the western inlet entrance (D3 in Fig. II9). These dunes migrate 10 m between 2011-2013 (about 4.3 m year^{-1} or $11.78 \text{ mm day}^{-1}$) and 40 m between 2013-2016 (about 16 m year^{-1} or $43.84 \text{ mm day}^{-1}$) showing that the bottom sediment transport inside the lagoon is less than in the inlet channel. However, the migration rate increases significantly over time.

The direction of the displacement is south-east, according to the ebb tide (Fig. II11). Since the large scour hole S1 is in the trajectory of the migration, part of the sediments eroded the dunes could have settled into the scour, contributing in the silting up of this morphology.

In view of the backscatter classification and the substrata distribution over the surveys, we can make three main observation (Fig. II11). (i) The class SG_GS increased their extension, covering large sectors which are previously occupied by the SGS+S class particularly along the inlet channel. The increased current fluxes introduced by the MoSE structures are indeed be responsible of the continuously coarsening of the seabed sediments along the inlet channel as already pointed out in Fogarin et al. (2019). (ii) The finest class SGMS_MS_SGSM decreased considerably their extension because replaced by the SGS+S class. This reduction is very strong in the concave side of the breakwater where a muddy deposit is rapidly resized between the 2011-2013. This change is produced by the previously described process and can be observed also in the Lido Inlet (Toso et al., 2019). (iii) Toward the seaside the bottom is stable and remains mainly SGS+S over the times, excluding in correspondence of the scour holes at breakwater tips.

4.6. Conclusions

We successfully developed and applied an interdisciplinary methodology to study the evolution of a shallow water seabed throughout multiple MBES and ground-truth surveys. We have been able to quantify the short-term erosion of the scour holes and to identify the displacement or shrinking of the dunes.

In particular we observed:

- The scour holes at breakwater tips largely increased their dimension from the 2006 (end of the breakwater construction); however, in the last period their erosion is slowing down, probably hampered by the exposure of a compacted layer (caranto) on the bottom of the features. Considering both scour holes, we estimate about 476,000 m³ of sediments have been eroded in about 10 years.
- A large part of the dune fields, especially the smaller ones, disappeared from 2013 survey. This is probably due to the increased water current introduced by inlet cross-section restriction.
- The large dunes observed at the entrances of the inlet channel shown an important displacement toward the sea (about 100 m in both periods), in agreement with the ebb tide domination. In detail the dune fields D2 at eastern side move with high velocities, similar with dunes on the open-sea environment of New Brunswick coasts. Also the internal dunes D3 registered a slight displacement seaward.
- The changes on sediment texture are mainly concentrated along the inlet channel: in this sector of the study area we observed a general coarsening of the seabed, whereas near the breakwater the muddy deposit is rapidly resized.

This study shows how combining repetitive MBES surveys with ground-truth data is useful to investigate the seafloor properties and their evolution over the times, especially in response of engineering intervention to coping the sea level rise.

Acknowledgments

The authors would like to acknowledge all the rest of the ISMAR Team that contributed to collect and process the MBES data of the Venice Lagoon in 2013 and 2016. The authors would like to thank

also the IIM of the Italian Navy for contributing in this project and providing of the 2011 dataset acquisition. The authors are grateful to the crew of the CNR research vessel Litus for their skillful help during the survey and to Loris Dametto for his technical help on the ground truth sampling. The authors would like to thank Christian Ferrarin for providing the tidal corrections for the MBES data. This work was supported by the National Flagship Project RITMARE, funded by MIUR, the Italian Ministry of Education, University and Research.

Maps throughout this paper were created using ArcGIS® software by Esri. ArcGIS® and ArcMap™ are the intellectual property of Esri and are used herein under license. Copyright © Esri. All rights reserved. For more information about Esri® software, please visit www.esri.com.

4.7. References

- Allen, J. R. L. (1980). Sand waves: a model of origin and internal structure. *Sedimentary Geology*, 26(4), 281-328.
- Allen, J. R. L. (1982). Mud drapes in sand-wave deposits: a physical model with application to the Folkestone Beds (early Cretaceous, southeast England). *Philosophical Transactions of the Royal Society of London. Series A, Mathematical and Physical Sciences*, 306(1493), 291-345.
- Amos, C. L., Villatoro, M., Helsby, R., Thompson, C. E. L., Zaggia, L., Umgiesser, G., ... & Rizzetto, F. (2010). The measurement of sand transport in two inlets of Venice lagoon, Italy. *Estuarine, Coastal and Shelf Science*, 87(2), 225-236.
- Ashley, G. M. (1990). Classification of large-scale subaqueous bedforms; a new look at an old problem. *Journal of Sedimentary Research*, 60(1), 160-172.
- Balletti, C. (2006). Digital elaborations for cartographic reconstruction: the territorial transformations of Venice harbours in historical maps. *e-Perimetron*, 1(4), 274-286.
- Basset, A., Elliott, M., West, R. J., & Wilson, J. G. (2013). Estuarine and lagoon biodiversity and their natural goods and services.
- Bird, E. C. F. (1994). Physical setting and geomorphology of coastal lagoons. In *Coastal Lagoon Processes*, Kjerfve B (ed). Elsevier: Amsterdam; 9–30.
- Blott, S. J., & Pye, K. (2001). GRADISTAT: a grain size distribution and statistics package for the analysis of unconsolidated sediments. *Earth surface processes and Landforms*, 26(11), 1237-1248.
- Book, J. W., Perkins, H., & Wimbush, M. (2009). North Adriatic tides: observations, variational data assimilation modeling, and linear tide dynamics. *Geofizika*, 26(2), 115-143.

4. Study II: Bathymetric and backscatter data of seafloor change of the Chioggia inlet (Venice Lagoon) as a result of human intervention

- Braimoh, A. K. (2004). Seasonal migration and land-use change in Ghana. *Land degradation & development*, 15(1), 37-47.
- Brown, C. J., Smith, S. J., Lawton, P., & Anderson, J. T. (2011). Benthic habitat mapping: A review of progress towards improved understanding of the spatial ecology of the seafloor using acoustic techniques. *Estuarine, Coastal and Shelf Science*, 92(3), 502-520.
- Cazenave, P. W., Dix, J. K., Lambkin, D. O., & McNeill, L. C. (2013). A method for semi-automated objective quantification of linear bedforms from multi-scale digital elevation models. *Earth Surface Processes and Landforms*, 38(3), 221-236.
- Congalton, R. G., & Green, K. (2002). *Assessing the accuracy of remotely sensed data: principles and practices*. CRC press.
- Costanza, R., d'Arge, R., De Groot, R., Farber, S., Grasso, M., Hannon, B., ... & Raskin, R. G. (1997). The value of the world's ecosystem services and natural capital. *nature*, 387(6630), 253.
- Cuadrado, D. G., Gómez, E. A., & Ginsberg, S. S. (2003). Large transverse bedforms in a mesotidal estuary. *Latin American Journal of Sedimentology and Basin Analysis*, 10(2), 163-172.
- D'Alpaos, A., Carniello, L., & Rinaldo, A. (2013). Statistical mechanics of wind wave-induced erosion in shallow tidal basins: Inferences from the Venice Lagoon. *Geophysical Research Letters*, 40(13), 3402-3407.
- Dalrymple, R. W., & Rhodes, R. N. (1995). Estuarine dunes and bars. In *Developments in sedimentology* (Vol. 53, pp. 359-422). Elsevier.
- Diesing, M., Green, S. L., Stephens, D., Lark, R. M., Stewart, H. A., & Dove, D. (2014). Mapping seabed sediments: Comparison of manual, geostatistical, object-based image analysis and machine learning approaches. *Continental Shelf Research*, 34, 107-119.
- Duffy, G. P., & Hughes-Clarke, J. E. (2005). Application of spatial cross correlation to detection of migration of submarine sand dunes. *Journal of Geophysical Research: Earth Surface*, 110(F4).
- Duffy, G. P. (2012). Patterns of morphometric parameters in a large bedform field: Development and application of a tool for automated bedform morphometry. *Irish Journal of Earth Sciences*, 31-39.
- Duffy, G. P., & Clarke, J. E. H. (2012). Measurement of bedload transport in a coastal sea using repeat swath bathymetry surveys: assessing bedload formulae using sand dune migration. *Sediments, Morphology and Sedimentary Processes on Continental Shelves: Advances in Technologies, Research, and Applications*, 249-271.
- Ernstsen, V. B., Noormets, R., Winter, C., Hebbeln, D., Bartholomä, A., Flemming, B. W., & Bartholdy, J. (2005). Development of subaqueous barchanoid-shaped dunes due to lateral grain size variability in a tidal inlet channel of the Danish Wadden Sea. *Journal of Geophysical Research: Earth Surface*, 110(F4).
- Ferrarin, C., Cucco, A., Umgiesser, G., Bellafiore, D., & Amos, C. L. (2010). Modelling fluxes of water and sediment between Venice Lagoon and the sea. *Continental Shelf Research*, 30(8), 904-914.

4. Study II: Bathymetric and backscatter data of seafloor change of the Chioggia inlet (Venice Lagoon) as a result of human intervention

- Ferrarin, C., Tomasin, A., Bajo, M., Petrizzo, A., & Umgiesser, G. (2015). Tidal changes in a heavily modified coastal wetland. *Continental Shelf Research*, 101, 22-33.
- Ferrarin, C., Madricardo, F., Rizzetto, F., Kiver, W. M., Bellafore, D., Umgiesser, G., ... & Sarretta, A. (2018). Geomorphology of scour holes at tidal channel confluences. *Journal of Geophysical Research: Earth Surface*, 123(6), 1386-1406.
- Fogarin, S., Madricardo, F., Zaggia, L., Sigovini, M., Montereale-Gavazzi, G., Kruss, A., ... & Trincardi, F. (2019). Tidal inlets in the Anthropocene: geomorphology and benthic habitats of the Chioggia inlet, Venice Lagoon (Italy). *Earth Surface Processes and Landforms*, 44(11), 2297-2315.
- Folk, R. L., & Ward, W. C. (1957). Brazos River bar [Texas]; a study in the significance of grain size parameters. *Journal of Sedimentary Research*, 27(1), 3-26.
- Folk RL, Andrews PB, Lewis D. 1970. Detrital sedimentary rock classification and nomenclature for use in New Zealand. *New Zealand journal of geology and geophysics*, 13(4), 937-968.
- Fontolan, G., Pillon, S., Quadri, F. D., & Bezzi, A. (2007). Sediment storage at tidal inlets in northern Adriatic lagoons: Ebb-tidal delta morphodynamics, conservation and sand use strategies. *Estuarine, Coastal and Shelf Science*, 75(1-2), 261-277.
- Foody, G. M. (2002). Status of land cover classification accuracy assessment. *Remote sensing of environment*, 80(1), 185-201.
- Fraccascia, S., Winter, C., Ernsten, V. B., & Hebbeln, D. (2016). Residual currents and bedform migration in a natural tidal inlet (Knudedyb, Danish Wadden Sea). *Geomorphology*, 271, 74-83.
- Gačić, M., Mosquera, I. M., Kovačević, V., Mazzoldi, A., Cardin, V., Arena, F., & Gelsi, G. (2004). Temporal variations of water flow between the Venetian lagoon and the open sea. *Journal of Marine Systems*, 51(1-4), 33-47.
- Ghetti, A. (1974). I problemi idraulici della Laguna di Venezia. Istituto di idraulica dell'Università di Padova.
- Ghezzi, M., Guerzoni, S., Cucco, A., & Umgiesser, G. (2010). Changes in Venice Lagoon dynamics due to construction of mobile barriers. *Coastal Engineering*, 57(7), 694-708.
- Gonenc, I. E., & Wolflin, J. P. (Eds.). (2004). *Coastal lagoons: ecosystem processes and modeling for sustainable use and development*. CRC Press.
- Hennings, I., Lurin, B., Vernemmen, C., & Vanhessche, U. (2000). On the behaviour of tidal current directions due to the presence of submarine sand waves. *Marine Geology*, 169(1-2), 57-68.
- Homrani, S., Le Dantec, N., Floc'h, F., Franzetti, M., Delacourt, C., Sedrati, M., & Winter, C. (2019). Multi time-scale morphological evolution of a shell sand, dune bank in a shallow mesotidal environment. *MARID VI*, 121.

4. Study II: Bathymetric and backscatter data of seafloor change of the Chioggia inlet (Venice Lagoon) as a result of human intervention

Ierodiaconou, D., Schimel, A. C., Kennedy, D., Monk, J., Gaylard, G., Young, M., ... & Rattray, A. (2018). Combining pixel and object based image analysis of ultra-high resolution multibeam bathymetry and backscatter for habitat mapping in shallow marine waters. *Marine Geophysical Research*, 39(1-2), 271-288.

Janowski, L., Tegowski, J. & Nowak, J., 2018. Marine seafloor mapping of multibeam echosounder bathymetry and backscatter data using Object-Based Image Analysis: a case study from the Rewal site, Southern Baltic. *Oceanological and Hydrobiological Studies*. (in press).

Jenks, G. F. (1967). The data model concept in statistical mapping. *International yearbook of cartography*, 7, 186-190.

Kjerfve, B. (1994). Coastal lagoons. In *Elsevier oceanography series* (Vol. 60, pp. 1-8). Elsevier.

Lecours, V., Devillers, R., Lucieer, V. L., & Brown, C. J. (2017). Artefacts in marine digital terrain models: A multiscale analysis of their impact on the derivation of terrain attributes. *IEEE Transactions on Geoscience and Remote Sensing*, 55(9), 5391-5406.

Lecours, V., Devillers, R., Simms, A. E., Lucieer, V. L., & Brown, C. J. (2017). Towards a framework for terrain attribute selection in environmental studies. *Environmental modelling & software*, 89, 19-30.

Lewis, S. L., & Maslin, M. A. (2015). Defining the anthropocene. *Nature*, 519(7542), 171.

Li, M. Z., Shaw, J., Todd, B. J., Kostylev, V. E., & Wu, Y. (2014). Sediment transport and development of banner banks and sandwaves in an extreme tidal system: Upper Bay of Fundy, Canada. *Continental Shelf Research*, 83, 86-107.

Loring, D.H. & Rantala, R.T.T., (1992). Manual for the geochemical analyses of marine sediments and suspended particulate matter. *Earth-science reviews*, 32, 235-283.

Luisetti, T., Turner, R. K., Jickells, T., Andrews, J., Elliott, M., Schaafsma, M., ... & Watts, W. (2014). Coastal zone ecosystem services: from science to values and decision making; a case study. *Science of the Total Environment*, 493, 682-693.

Madricardo, F., Fogliani, F., Kruss, A., Ferrarin, C., Pizzeghello, N. M., Murri, C., ... & Fogarin, S. (2017). High resolution multibeam and hydrodynamic datasets of tidal channels and inlets of the Venice Lagoon. *Scientific data*, 4, 170121.

Madricardo F., Rizzetto F. (2018). Shallow coastal landforms. In *Submarine. Geomorphology*. Springer: Cham; 161–183.

Magrini G. 1934. Carta topografica idrografica militare della laguna di Venezia rilevata dal capitano Augusto Dénaix negli anni 1809-10-

11. Atlante Primo, Stamperia Ferrari: Venice.

MAV-CVN. 2004. Attività di aggiornamento del piano degli interventi per il recupero morfologico in applicazione della delibera del Consiglio dei Ministri del 15 Marzo 2001. Studi di base, linee guida e proposte di intervento del piano morfologico, Technical Report. Magistrato alle Acque di Venezia, Consorzio Venezia Nuova: Venice.

McGonigle, C., & Collier, J. S. (2014). Interlinking backscatter, grain size and benthic community structure. *Estuarine, Coastal and Shelf Science*, 147, 123-136.

4. Study II: Bathymetric and backscatter data of seafloor change of the Chioggia inlet (Venice Lagoon) as a result of human intervention

Ministero dell'Ambiente, Magistrato alle Acque. 1997. Interventi alle bocche lagunari per la regolazione dei flussi di marea – Studio di impatto ambientale del progetto di massima, Vol. 163. Allegato 6, Tema 5. Magistrato alle Acque di Venezia: Venice.

Molinarioli, E., Guerzoni, S., Sarretta, A., Masiol, M., & Pistolato, M. (2009). Thirty-year changes (1970 to 2000) in bathymetry and sediment texture recorded in the Lagoon of Venice sub-basins, Italy. *Marine Geology*, 258(1-4), 115-125.

Molinarioli, E., Sarretta, A., Ferrarin, C., Masiero, E., Specchiulli, A., & Guerzoni, S. (2014). Sediment grain size and hydrodynamics in Mediterranean coastal lagoons: Integrated classification of abiotic parameters. *Journal of earth system science*, 123(5), 1097-1114.

Montereale-Gavazzi, G. M., Madricardo, F., Janowski, L., Kruss, A., Blondel, P., Sigovini, M., & Foglini, F. (2016). Evaluation of seabed mapping methods for fine-scale classification of extremely shallow benthic habitats—Application to the Venice Lagoon, Italy. *Estuarine, Coastal and Shelf Science*, 170, 45-60.

Montereale-Gavazzi, G., Roche, M., Lurton, X., Degrendele, K., Terseleer, N., & Van Lancker, V. (2018). Seafloor change detection using multibeam echosounder backscatter: case study on the Belgian part of the North Sea. *Marine Geophysical Research*, 39(1-2), 229-247.

Montereale-Gavazzi, G., Roche, M., Degrendele, K., Lurton, X., Terseleer, N., Baeye, M., ... & Van Lancker, V. (2019). Insights into the short-term tidal variability of multibeam backscatter from field experiments on different seafloor types. *Geosciences*, 9(1), 34.

Newton, A., Brito, A. C., Icely, J. D., Derolez, V., Clara, I., Angus, S., ... & Béjaoui, B. (2018). Assessing, quantifying and valuing the ecosystem services of coastal lagoons.

Pontius Jr, R. G., Shusas, E., & McEachern, M. (2004). Detecting important categorical land changes while accounting for persistence. *Agriculture, Ecosystems & Environment*, 101(2-3), 251-268.

Rattray, A., Ierodiaconou, D., Monk, J., Versace, V. L., & Laurenson, L. J. B. (2013). Detecting patterns of change in benthic habitats by acoustic remote sensing. *Marine Ecology Progress Series*, 477, 1-13.

Rinaldo, A., Lanzoni, S., & Marani, M. (2001). River and tidal networks. In *River, Coastal and Estuarine Morphodynamics* (pp. 191-211). Springer, Berlin, Heidelberg.

Salvatierra, M. M., Aliotta, S., & Ginsberg, S. S. (2015). Morphology and dynamics of large subtidal dunes in Bahia Blanca estuary, Argentina. *Geomorphology*, 246, 168-177.

Sousa, L. P., Lillebø, A. I., Gooch, G. D., Soares, J. A., & Alves, F. L. (2013). Incorporation of local knowledge in the identification of Ria de Aveiro lagoon ecosystem services (Portugal). *Journal of Coastal Research*, 65(sp1), 1051-1057.

Smith, A. M., Murray, T., Nicholls, K. W., Makinson, K., Aðalgeirsdóttir, G., Behar, A. E., & Vaughan, D. G. (2007). Rapid erosion, drumlin formation, and changing hydrology beneath an Antarctic ice stream. *Geology*, 35(2), 127-130.

4. Study II: Bathymetric and backscatter data of seafloor change of the Chioggia inlet (Venice Lagoon) as a result of human intervention

- Steffen, W., Persson, Å., Deutsch, L., Zalasiewicz, J., Williams, M., Richardson, K., ... & Molina, M. (2011). The Anthropocene: From global change to planetary stewardship. *Ambio*, 40(7), 739.
- Stewart, L. K., Kostylev, V. E., & Orpin, A. R. (2009). Windows-based software for optimising entropy-based groupings of textural data. *Computers & Geosciences*, 35(7), 1552-1556.
- Story, M., & Congalton, R. G. (1986). Accuracy assessment: a user's perspective. *Photogrammetric Engineering and remote sensing*, 52(3), 397-399.
- Tambroni, N., & Seminara, G. (2006). Are inlets responsible for the morphological degradation of Venice Lagoon?. *Journal of Geophysical Research: Earth Surface*, 111(F3).
- Todd, B. J., Shaw, J., Li, M. Z., Kostylev, V. E., & Wu, Y. (2014). Distribution of subtidal sedimentary bedforms in a macrotidal setting: The Bay of Fundy, Atlantic Canada. *Continental Shelf Research*, 34, 64-85.
- Toso, C., Madricardo, F., Molinaroli, E., Fogarin, S., Kruss, A., Petrizzo, A., ... & Trincardi, F. (2019). Tidal inlet seafloor changes induced by recently built hard structures. *PloS one*, 14(10).
- Van Denderen, P. D., Bolam, S. G., Hiddink, J. G., Jennings, S., Kenny, A., Rijnsdorp, A. D., & Van Kooten, T. (2015). Similar effects of bottom trawling and natural disturbance on composition and function of benthic communities across habitats. *Marine Ecology Progress Series*, 541, 31-43.
- Villatoro Lacouture, M. M. (2010). Sand transport in Chioggia Inlet, Venice Lagoon and resulting morphodynamic evolution (Doctoral dissertation, University of Southampton).
- Villatoro, M. M., Amos, C. L., Umgiesser, G., Ferrarin, C., Zaggia, L., Thompson, C. E., & Are, D. (2010). Sand transport measurements in Chioggia inlet, Venice lagoon: Theory versus observations. *Continental Shelf Research*, 30(8), 1000-1018.
- Woolfe, K. J., & Michibayashi, K. (1995). "Basic" entropy grouping of laser-derived grain-size data: an example from the Great Barrier Reef. *Computers & Geosciences*, 21(4), 447-462.
- Wright, D. J., Pendleton, M., Boulware, J., Walbridge, S., Gerlt, B., Eslinger, D., ... & Huntley, E. (2012). ArcGIS Benthic Terrain Modeler (BTM), v. 3.0, Environmental Systems Research Institute, NOAA Coastal Services Center, Massachusetts Office of Coastal Zone Management. Available online at <http://esriurl.com/5754>.
- Zecchin, M., Tosi, L., Caffau, M., Baradello, L., & Donnici, S. (2014). Sequence stratigraphic significance of tidal channel systems in a shallow lagoon (Venice, Italy). *The Holocene*, 24(6), 646-658.

4. Study II: Bathymetric and backscatter data of seafloor change of the Chioggia inlet (Venice Lagoon) as a result of human intervention

4.8. Appendix

Table IIA1: grain size of the sediment samples collected in 2013 and 2016. Sorting is referred to μm unit scale.

	Year	SAMPLE TYPE:	TEXTURAL GROUP:	D ₅₀ (μm):	GRAHICAL SORTING	MODE 1 (μm):	MODE 2 (μm):	MODE 3 (μm):	% GRAVEL:	% SAND:	% MUD:
N02	2013	Bimodal, Very Poorly Sorted	Sandy Gravel	2886.5	5.946	12000.0	302.0		55.1%	41.8%	3.1%
N03	2013	Unimodal, Moderately Sorted	Slightly Gravelly Sand	301.5	1.809	302.0			0.1%	93.7%	6.3%
N04	2013	Unimodal, Poorly Sorted	Slightly Gravelly Sand	173.2	2.095	163.0			0.6%	92.0%	7.4%
N05	2013	Bimodal, Poorly Sorted	Slightly Gravelly Muddy Sand	106.1	3.761	137.0	26.70		0.1%	67.4%	32.5%
N06	2013	Bimodal, Very Poorly Sorted	Muddy Sandy Gravel	451.1	6.635	302.0	6000.0		43.5%	49.3%	7.2%
N07	2013	Unimodal, Moderately Sorted	Slightly Gravelly Sand	281.2	1.839	302.0			1.7%	92.7%	5.7%
N08	2013	Bimodal, Very Poorly Sorted	Slightly Gravelly Sandy Mud	37.78	4.045	106.7	26.70		0.1%	38.1%	61.8%
N10	2013	Bimodal, Very Poorly Sorted	Sandy Gravel	588.5	6.544	302.0	23750.0		44.1%	52.4%	3.6%
N11	2013	Unimodal, Moderately Well Sorted	Slightly Gravelly Sand	503.5	1.604	427.0			1.5%	96.5%	2.0%
N12	2013	Bimodal, Very Poorly Sorted	Gravelly Sand	561.7	4.692	427.0	23750.0		24.1%	73.2%	2.7%
N13	2013	Unimodal, Moderately Well Sorted	Slightly Gravelly Sand	340.9	1.463	302.0			2.0%	95.0%	3.0%
N14	2013	Bimodal, Poorly Sorted	Slightly Gravelly Muddy Sand	87.46	3.920	137.0	26.70		0.1%	60.8%	39.1%
N15	2013	Unimodal, Moderately Sorted	Slightly Gravelly Sand	322.7	1.777	302.0			0.1%	94.5%	5.5%
N17	2013	Unimodal, Poorly Sorted	Slightly Gravelly Sand	262.7	2.057	302.0			1.0%	89.9%	9.0%
N18	2013	Unimodal, Poorly Sorted	Gravelly Muddy Sand	260.7	3.288	302.0			8.0%	81.5%	10.5%
N19	2013	Unimodal, Moderately Sorted	Slightly Gravelly Sand	282.0	1.850	302.0			1.0%	92.7%	6.3%
N23	2013	Unimodal, Very Poorly Sorted	Slightly Gravelly Sandy Mud	18.6	4.417	26.70			4.1%	12.4%	83.5%
Z01	2016	Bimodal, Very Poorly Sorted	Muddy Sandy Gravel	6982.8	7.409	12000.0	302.0		63.8%	30.6%	5.6%
Z02	2016	Bimodal, Very Poorly Sorted	Gravelly Sand	424.5	5.771	427.0	12000.0		27.9%	67.5%	4.6%
Z03	2016	Bimodal, Very Poorly Sorted	Sandy Gravel	646.1	5.093	427.0	12000.0		37.1%	60.6%	2.3%
Z04	2016	Bimodal, Very Poorly Sorted	Gravelly Sand	478.8	4.514	427.0	12000.0		22.0%	73.8%	4.3%
Z05	2016	Unimodal, Very Poorly Sorted	Gravelly Muddy Sand	308.6	7.705	302.0			19.3%	66.7%	14.0%
Z06	2016	Unimodal, Poorly Sorted	Slightly Gravelly Sandy Mud	20.17	3.538	26.70			0.5%	15.7%	83.8%
Z07	2016	Unimodal, Poorly Sorted	Slightly Gravelly Mud	16.99	3.394	26.70			1.3%	9.5%	89.2%
Z08	2016	Unimodal, Poorly Sorted	Gravelly Sand	470.2	2.638	427.0			8.3%	84.7%	7.0%
Z09	2016	Unimodal, Poorly Sorted	Gravelly Sand	435.4	2.182	427.0			5.5%	89.1%	5.5%
Z10	2016	Trimodal, Very Poorly Sorted	Sandy Gravel	2328.2	4.868	603.5	23750.0	3000.0	52.7%	44.8%	2.4%
Z11	2016	Unimodal, Poorly Sorted	Gravelly Sand	531.8	2.042	603.5			9.2%	87.8%	3.0%
Z12	2016	Unimodal, Poorly Sorted	Gravelly Sand	589.9	3.363	603.5			16.7%	78.8%	4.5%
Z13	2016	Trimodal, Very Poorly Sorted	Sandy Gravel	771.3	5.025	603.5	12000.0	3000.0	35.7%	60.9%	3.5%
Z14	2016	Bimodal, Very Poorly Sorted	Gravelly Sand	637.5	4.052	427.0	12000.0		26.5%	70.0%	3.6%
Z15	2016	Unimodal, Moderately Sorted	Slightly Gravelly Sand	472.5	1.709	427.0			3.3%	92.6%	4.1%
Z16	2016	Bimodal, Very Poorly Sorted	Sandy Gravel	3444.5	5.150	23750.0	603.5		54.3%	44.0%	1.7%
Z17	2016	Bimodal, Very Poorly Sorted	Sandy Gravel	9419.8	5.172	12000.0	427.0		71.5%	26.7%	1.7%
Z18	2016	Bimodal, Very Poorly Sorted	Sandy Gravel	994.4	4.704	603.5	23750.0		39.2%	57.7%	3.1%
Z19	2016	Bimodal, Very Poorly Sorted	Slightly Gravelly Sandy Mud	44.50	4.083	137.0	26.70		0.1%	42.4%	57.5%
Z20	2016	Unimodal, Poorly Sorted	Slightly Gravelly Mud	15.43	3.547	18.85			2.9%	7.4%	89.7%
Z21	2016	Unimodal, Poorly Sorted	Slightly Gravelly Sandy Mud	17.73	3.584	18.85			1.5%	12.2%	86.3%
Z22	2016	Bimodal, Very Poorly Sorted	Muddy Sandy Gravel	5476.0	12.872	23750.0	137.0		60.8%	26.6%	12.6%
Z23	2016	Unimodal, Poorly Sorted	Slightly Gravelly Muddy Sand	126.6	2.715	137.0			2.3%	79.3%	18.3%
Z24	2016	Unimodal, Poorly Sorted	Slightly Gravelly Muddy Sand	214.2	2.696	302.0			1.0%	83.7%	15.3%
Z25	2016	Polymodal, Very Poorly Sorted	Gravelly Muddy Sand	228.9	13.491	137.0	302.0	6000.0	25.1%	47.8%	27.1%
Z26	2016	Trimodal, Extremely Poorly Sorted	Muddy Gravel	139.4	20.588	12000.0	106.7	26.70	37.6%	26.0%	36.3%
Z27	2016	Bimodal, Very Poorly Sorted	Slightly Gravelly Sandy Mud	28.85	4.265	26.70	137.0		0.4%	30.4%	69.2%
Z28	2016	Unimodal, Poorly Sorted	Slightly Gravelly Muddy Sand	175.6	2.235	213.5			1.4%	88.7%	9.9%
Z29	2016	Unimodal, Poorly Sorted	Slightly Gravelly Muddy Sand	347.1	2.272	427.0			0.6%	88.0%	11.3%

4. Study II: Bathymetric and backscatter data of seafloor change of the Chioggia inlet (Venice Lagoon) as a result of human intervention

Table IIA3: parameters of the bathymetric and backscatter datasets for each survey.

	2011	2013	2016
Min. value (m)	-29.30	-29.50	-29.53
Max. value (m)	-0.58	-0.95	-1.56
Mean (m)	-11.03	-10.89	-9.64
Primary mode (m)	-17.27	-12.63	-12.75
Standard deviation	4.63	3.31	3.43

	2011	2013	2016
Min. value (dB)	-66.27	-68.54	-60.97
Max. value (dB)	-4.97	-4.64	-0.75
Mean (dB)	-33.89	-24.20	-24.43
Primary mode (dB)	-34.70	-25.85	-26.36
Standard deviation	4.08	3.22	3.42

4. Study II: Bathymetric and backscatter data of seafloor change of the Chioggia inlet (Venice Lagoon) as a result of human intervention

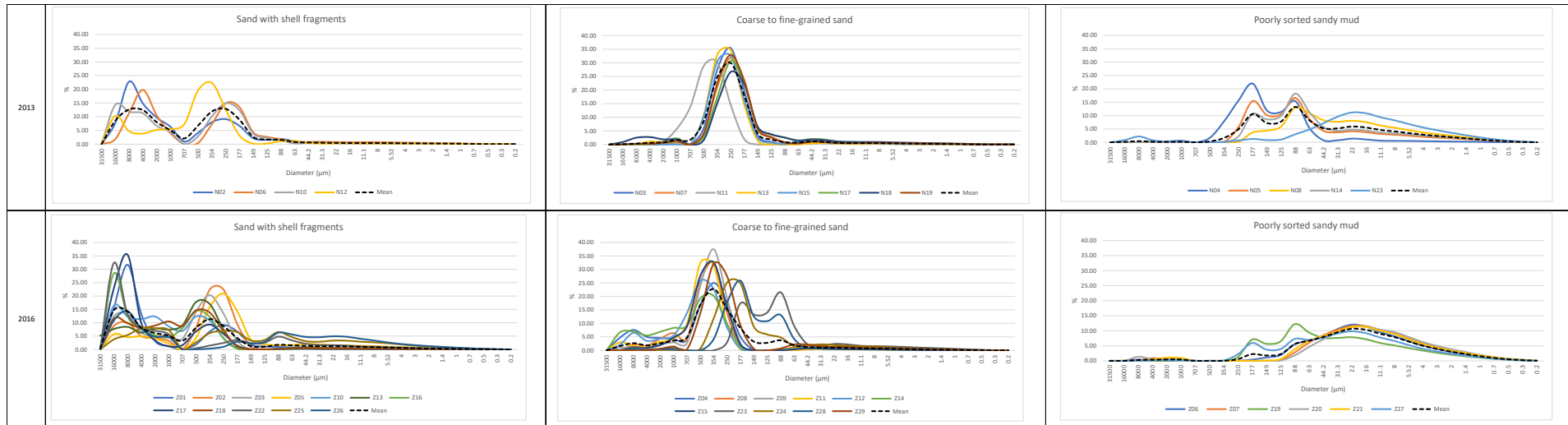


Figure IIA4: textural clusters used for the backscatter classification obtained from EntropyMax analysis.

Table IIA5: extension areas and area differences between surveys for the analyzed scour holes and dunes/dune fields.

	Scour S1		Scour S2		Scour S3		Scour S4		Dunefield D1		Dunefield D2		Dune D3	
	Area (m ²)	Volume difference (m ³)	Area (m ²)	Volume difference (m ³)	Area (m ²)	Volume difference (m ³)	Area (m ²)	Volume difference (m ³)	Area (m ²)	Volume difference (m ³)	Area (m ²)	Volume difference (m ³)	Area (m ²)	Volume difference (m ³)
2011	111689.8		62498.6		35484.7		46287.0		140588.3		52511.4		19815.3	
2013	112408.0		81671.7		52595.5		49312.0		71540.7		37293.0		22358.6	
2016	88036.5		105111.7		61659.1		38027.0		14315.5		76010.0		46897.7	
2013-2011	718.2	-9515.6	19173.1	-61515.7	17110.8	-58829.4	3025.0	-12420.1	-69047.6	-26974.1	-15218.4	-43776.6	2543.4	-13503.4
2016-2013	-24371.5	10536.7	23440.0	-21584.5	9063.6	-23796.1	-11285.0	29.9	-57225.1	-6743.5	38717.0	15204.3	24539.1	9275.4
2016-2011	-23653.3	10211.1	42613.1	-83100.3	26174.4	-82625.5	-8260.0	-12390.2	-126272.8	-33717.6	23498.6	-28572.2	27082.5	-4228.0

Table IIA6: differences in sediment volume between surveys for the entire study area.

	2011-2013	2013-2016	2011-2016
Volume difference (m ³)	-1'164'274.00	49'470.00	-1'114'804.00

5. Study III: Short-term evolution of Po della Pila delta lobe from high-resolution multibeam bathymetry (2013-2016)

Alessandro Bosman¹, Claudia Romagnoli^{2,1}, Fantina Madricardo³, Annamaria Correggiari⁴, Alessandro Remia⁴, Riccardo Zubalich², Stefano Fogarin^{5,3}, Aleksandra Kruss⁴ and Fabio Trincardi⁴

¹CNR - Istituto di Geologia Ambientale e Geoingegneria (IGAG), Area della Ricerca di Roma 1 Via Salaria Km 29,300 - C.P. 10 00016 Monterotondo Stazione, Roma, Italy

²Dip. Scienze Biologiche, Geologiche e Ambientali, Università di Bologna, Piazza di Porta S. Donato 1, Bologna, Italy

³CNR - Istituto di Scienze Marine (ISMAR), Arsenale-Tesa 104, Castello 2737/F, 30122 Venezia, Italy

⁴CNR - Istituto di Scienze Marine (ISMAR), Via P. Gobetti 101, I-40129 Bologna, Italy

⁵Dipartimento di Scienze Ambientali, Informatica e Statistica (DAIS), Università Ca' Foscari Venezia, Campus Scientifico, Via Torino 155, Mestre, VE, Italy

Abstract

Over the last few years (2013-2016) repeated high-resolution multibeam surveys were carried out at the recent-most delta lobe of the Po river (in correspondence to Po della Pila). The collected multibeam bathymetry together with backscatter data, seabed samples and high-resolution seismic profiles provided insights on the short-term morphological and sedimentological evolution of this extremely dynamic submarine portion of the delta. A high variety of geomorphological features and depositional bodies were observed from the mouth bar to the prodelta slope such as, for example, the alongshore and transverse bars (formed under the effect of marine currents), gravitational instability phenomena and collapse depressions (driven by fluid expulsion). Concurrently, the analysis of the seabed reflectivity and sediment samples allowed the identification of two main dominant types of seafloor sediment, corresponding to sandy and muddy seabed and the mapping of their variable distribution in the study area.

The comparison of time-lapsed, high-resolution DEMs showed that the main changes occurred on the northern side of the prodelta slope, where a new lobe-shaped fine-sediment deposit built up to 4.5 m adding roughly a volume of 1.16 Mm³ of new sediments. At the same time in the prodelta slope transverse depositional bars showed a clear migration toward the south of the system and local subsidence phenomena of up to 1.5 m between 7 and 10 m water depth are observed.

Keywords: North Adriatic Sea, Po delta, delta submarine portion, offshore bars, collapse depressions, time-lapse bathymetry

5.1. Introduction

River deltas are highly dynamical and valuable environments and often undergo strong natural changes and human-induced pressures that need careful observation and monitoring. They hold unique ecological and socio-economic values and provide valuable lands for about 500 million of the human population (Woodroffe et al., 2006; Syvitski et al., 2009; Jiang et al., 2017). Delta systems respond quickly to natural and human changes (Orton and Reading, 1993; Blum and Roberts, 2009; Syvitski et al., 2009; Maselli and Trincardi, 2013; Dai et al., 2014) and they are largely exposed to human pressures (Overeem and Brakenridge 2009). Anthropogenic activities have, in fact, contributed to alter river flow, sediment discharges and coastline dynamics (Hood, 2010; Anthony et al., 2014). Urbanization, exploitation of natural resources and intense use of groundwater have induced soil compaction, creating subsidence phenomena and therefore increasing the vulnerability of delta areas to erosion and to the sea level rise. On river delta areas the effects of subsidence can be easily recognized on the subaerial portions through the use of satellite remote sensing (SAR), GPS and/or high-precision levelling surveys. These methods cannot be used to map the submerged portions of the delta areas, with the consequence that currently, little is known about the seabed morphology of delta systems in shallow water apart from the early studies of Coleman and Prior (1978) and Prior et al. (1986) and more recently of Maillet et al. (2006). The recent technological development of multibeam echosounders prove them to be the most effective and reliable system to generate high-resolution DEMs which can be compared over time with the measurements collected on shore (Bosman et al., 2014; Anzidei et al., 2016 and 2017). In this paper, we present

the results of repeated high-resolution multibeam surveys carried out over a period of three years (2013-2016) in the submarine portion of the Po della Pila delta, the most active among the five mouths of the modern Po delta (see inset in Fig. IIIA1 APPENDIX). The Po della Pila had an extremely dynamic short-term morphological evolution, as shown by Correggiari et al. (2005a). The high-resolution mapping of the Po della Pila delta lobe allowed the identification of a variety of geomorphological and erosional-depositional features at different sizes. The comparison among the repeated surveys, integrated by subsurface seismic facies from the sonar Chirp acoustic profiles collected in 2014, highlighted the dynamic evolution of the delta lobe over a 3-years time lapse in the framework of the high-resolution architecture of the most recent prodelta lobe.

The Po delta

The Po river is the longest river of Italy (673 km) with a medium flow of 1540 m³/s and a watershed of 71.000 km². The Po originates in the western Alps, runs from west to east through the entire Po Valley and outflows into the Adriatic Sea splitting into five sub-branches: Po di Maestra, Po della Pila, Po di Tolle, Po di Gnocca and Po di Goro (Fig. IIIA1 in APPENDIX). According to Syvitski et al. (2005), Po della Pila transports 61 % of the freshwater on the delta, while Maestra, Tolle, Gnocca and Goro supply 3 %, 12 %, 16 % and 8 % respectively. The Po delta is the widest delta of the Adriatic Sea, with the largest solid and liquid discharge (Amorosi et al., 2015). Almost 5x10⁶ tons/year of suspended sediment load reaches the Adriatic Sea (Cattaneo et al., 2003, 2007) through the Po delta, most of it being carried by the Po della Pila distributary channel. Furthermore, the estimation of sediment load indicates a supply of Pila 74 %, Maestra 1 %, Tolle 7 %, Gnocca 10 % and Goro 8 % (Nelson, 1970; Syvitski et al., 2005; Tesi et al., 2011; Falcieri et al., 2014; Braga et al., 2017). Historically a growth rate of 47 m/year was reported for the Po della Pila lobe after 1886 when the main branch of the Po river was artificially straightened to protect the delta plain from flooding (Visentini and Borghi, 1938). In historical and recent times, the entire Po delta system underwent extensive human alteration for land use and freshwater management; the lobes and the morphologies have been continuously repositioned by river diversion and changes in sediment supply (Trincardi et al., 2004; Maselli and Trincardi, 2013). Since 1950, in fact, the Po delta has been subjected to a strong degradation and a partial retreat, primarily due to the lack of sediment supply caused by exploitation of inert material from the riverbed and by the channelization of watercourses

(Stefani and Vincenzi, 2005). Recently, based on satellite images of the delta coastline, Ninfo et al. (2018) have inferred a restart of progradation for the northern portion of the Po della Pila mouth.

The hydrodynamic of the Po delta area is influenced by currents, winds and tides and by the river freshwater input. Water circulation in the Adriatic is driven by the general cyclonic circulation of the basin (Artegiani et al., 1997a, b; Boldrin et al., 2005). The dense freshwaters from the Northern Adriatic (North Adriatic Dense Water – NAdDW, Benetazzo et al., 2014) are responsible for sediment redistribution along the eastern Italian coast (Trincardi et al., 2004; Cattaneo et al., 2007; Amorosi et al., 2015). In the Po area, the littoral current thus flows dominantly from the north to the south along the western coast of the Adriatic basin. The dominant winds are the cold Bora wind coming from north-east and the warm Scirocco wind coming from south-east (Orlić et al., 1994).

5.2. Data and methods

During 2013 and 2014, high-resolution multibeam bathymetry (bathymetry and backscatter), Chirp seismic profiles (Table IIIA1 and Fig. IIIA1 in APPENDIX) and 18 grab samples were collected (Fig. III1b, c). In 2016 a further high-resolution multibeam bathymetric survey was carried out, having a complete coverage of the delta area (from 0.5 m to 23 m of water depth) such as the data acquired in 2013, while the bathymetric data collected in 2014 extend from 5 m to 23 m water depth and lack the shallow-water part. Due to this, we could compare bathymetric data in shallow water only for the 2013 and 2016 data set.

5.2.1. Multibeam data acquisition and processing

A first multibeam survey was carried out in June-July 2013 (Fig. III1a and Table IIIA1 in APPENDIX) collecting data between 12 m and 28 m water depth with a Kongsberg EM2040 Dual Compact Multibeam Echosounder System pole-mounted on the vessel *R/V Litus*, a 10-m long boat with 1.5-m draft. The multibeam was set to use the equidistant mode with a frequency of 360 kHz and 800 beams (400 per swath). The positioning system was a Kongsberg Seapath 300 with the correction of a Fugro HP Differential Global Positioning System (horizontal accuracy: 0.2 m). A Kongsberg Seatex IMU (MRU 5) corrected pitch, roll, heave and yaw movements. A Valeport mini SVS sensor mounted

close to the transducers measured continuously the sound velocity for the beam forming. Sound velocity profiles were systematically collected with an AML oceanographic Smart-X sound velocity profiler. Data were logged, displayed and checked in real-time with the Kongsberg SIS software (Seafloor Information System).

During the same period (June-July 2013), a second multibeam survey was carried out in very shallow water between 0.5 m and 12 m water depth using a small, 6-m long boat with 0.4 m draft, equipped with Teledyne Reson SeaBat 7125 SV2 pole-mounted (400 kHz) and Applanix POS MV (Table IIIA1 in APPENDIX). The positioning of the second multibeam survey was carried out in Real Time Kinematic (RTK) by means of a ground control station located near to the harbor. For the 2013 surveys a Valeport tide-gauge appropriately calibrated was installed near the study area to measure and correct sea level changes in response to tidal bi-diurnal excursion. Another dataset was collected in September 2014 (Fig. III1b and Table IIIA1 in APPENDIX) with the Kongsberg EM2040 Dual Compact Multibeam Echosounder System pole-mounted on the vessel R/V Litus as in 2013 (Table IIIA1 in APPENDIX) however, archiving a bathymetric coverage between 5 m and 23 m water depth. The last dataset (Fig. III1c) was acquired in May 2016 with a Kongsberg EM2040 single head system, with the frequency that was set to 300 kHz, hull-mounted in the vessel 1213 belonging to the Italian Hydrographic Office (IHO, Table IIIA1 in APPENDIX) which allowed a bathymetric coverage between 0.5 m and 23 m water depth. The positioning system was a Kongsberg Seapath 330, corrected with a Fugro HP Differential Global Positioning System (horizontal accuracy: 0.2 m). A Kongsberg Seatex Inertial Motion Reference Unit MRU 5 was used to correct pitch, roll, heave and yaw movements. Sound velocity profiles were collected with a Valeport sound velocity profiler. For all the surveys, a local tidal station belonging to the Italian National Network was used to measure and correct sea level changes (<http://www.mareografico.it>).

5. Study III: Short-term evolution of Po della Pila delta lobe from high-resolution multibeam bathymetry (2013-2016)

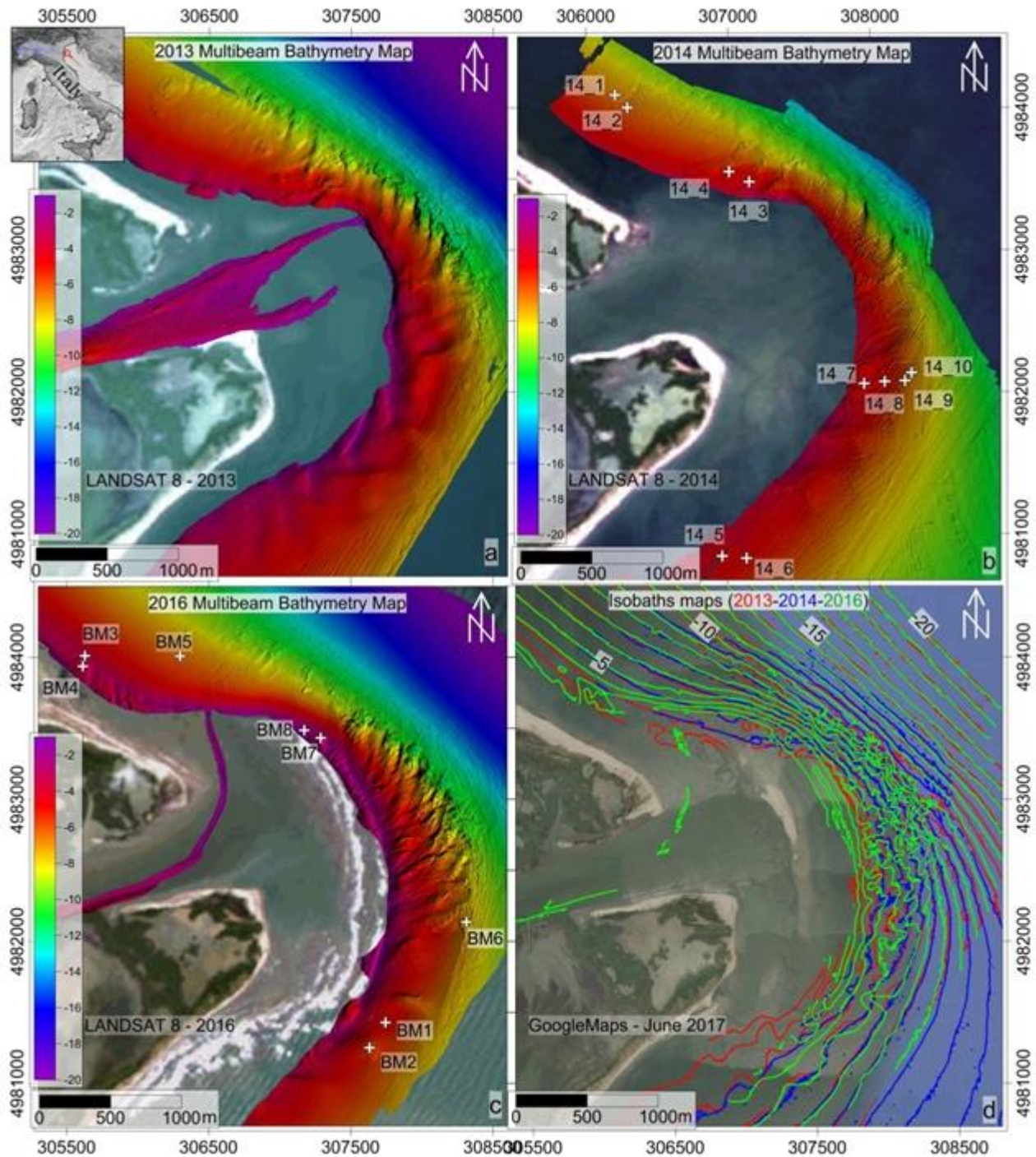


Fig. III.1: High-resolution multibeam bathymetry datasets and grab samples collected between 2013 and shore Po della Pila (a, b, c) and stack of isobaths maps (d). Crosses with labels indicate the samples collected in 2014 (b) and 2016 (c).

All bathymetric multibeam data were processed using *Caris H&S* hydrographic software. Processing workflow consists in: *PosPac* navigation processing, including processing of the Inertial Motion Unit and GNSS data-set, patch test, and the application of statistical and geometrical filters to remove coherent/incoherent noise (Bosman et al., 2015). Particular care was dedicated to the sound velocity correction because river mouths are characterized by complex and rapidly changing

hydrodynamic conditions in the water column (Fig. III2), with stratifications of fresh and salty water. For this reason, each day several vertical sound velocity casts were acquired throughout all the areas at different times. The investigated area is a microtidal environment and particular attention was devoted to the tide corrections to make sure that the three dataset acquired were comparable. The local hydrometric level has been related to the permanent tide station of Bocca di Lido Venezia belonging of National Tide gauge Network (<http://www.mareografico.it>).

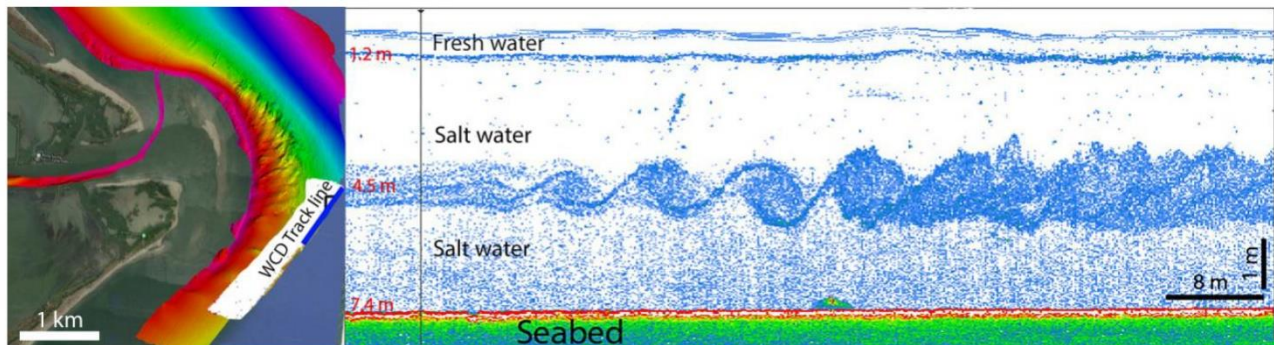


Fig. III2: Backscatter acoustic image (Water Column Data) of the water data recorded by multibeam in the outer side of the river mouth, showing the interaction between water masses with different density: above the fresh water plume coming from the river and, below, two layers of salt water. This is an example of Kelvin-Helmholtz instability (Miles 1959) at the interface between the deepest (salty) and the intermediate water layers, a dynamic that may influence the formation of sea floor bedforms approaching shallower waters.

The soundings were merged and gridded for the generation of DEMs at 0.3-1 m cell size resolution (Fig. III1; Bosman et al., 2015) that were compared to produce the residual maps. The residual maps quantify the change in elevation with positive and negative values associated with seafloor accretion/deposition and erosion/instability, respectively. The volumes associated with surface changes are obtained by integrating the difference in depth over the area of interest through a GIS software dedicated to the calculation of volumes (i.e. *Global Mapper 20.0*). The reliability of residual maps and volumes extrapolated is dependent on the accuracy of the DEMs that, in turn, is related to uncertainties in depth estimation. Several sources of error can affect the accuracy of the vertical and horizontal measurement of the soundings, such as the system used (frequency and footprint size), measurements of transmission speed of acoustic waves in the water (sound velocity casts), offset between the GPS antennas, transducers and inertial motion unit, patch-test to calibrate the alignment of the transducers, accuracy of positioning (PPK, RTK, HP), tidal correction, and finally the sensitivity / capacity of the processing operators. A quantitative estimate of the errors related to the EM2040 DC data are provided in Toso et al. (2019) computed from the calculation of the Total Propagated Uncertainty (TPU) provided by the *Caris H&S* software.

The backscatter intensity (BS) maps (or mosaics), were created using the software Fledermaus (v7.0) by combining each georeferenced survey line and after applying the Angle Varying Gain (AVG) correction to remove the angular artifacts of sediment. The maps were exported as a 32-bit float file with a resolution of 0.5 m per pixel. The BS map represents the seabed acoustic reflectivity and it is widely used to describe the seafloor in terms of its abiotic and biotic components (McGonigle et al., 2009).

5.2.2. Seismic survey

High-resolution seismic profiles were collected in May 2014 during the CP14 cruise, aboard the motor board M/B *San Rocco*. Seismic profiles were obtained using a 2-7 kHz Benthos DSP-662 Chirp III. About 80 km of profiles were collected both at delta front and in the three main distributary channels of Pila (Table IIIA1 in APPENDIX). Positioning was carried out through a Trimble DSM-232 GPS receiver with the EGNOS differential correction (2 m accuracy). Processing and interpretation were performed using *Geo-Suite AllWorks* software package. A filters processing sequence such as automatic gain control, trace equalization and mute of the water column, was used for a better characterization of sub-surface reflectors. For the interpretation, the depth on seismic profiles were converted assuming a constant sound velocity of 1500 m/sec.

5.2.3. Ground-truth data

To validate the BS data, 18 grab samples (Figs. III1b, III1c) were collected with a Van Veen Grab (7L) in 2014 and 2016 (i.e. ground-truth surveys). The locations of the samples were selected to include the most characteristic textural patterns identified during the surveys within the backscatter imagery. The samples were washed and dried following the procedure illustrated by Loring and Rantala (1992) and were analysed with a dry sieving (fractions ≥ 1 mm) and laser measurement with granulometer MasterSizer 3000 (fractions < 1 mm) The outputs from both analyses were merged and the main grain-size parameters were calculated (Table IIIA2 in APPENDIX), according to Folk et al. classification (1970), using Gradistat statistical package (Blott and Pye, 2001). Finally, the *Gradistat* outputs were processed by the *EntropyMax* software (Woolfe and Michibayashi 1995; Stewart et al., 2009; Molinaroli et al., 2014) to identify the dominant textural groups in the study area.

5.2.4. Backscatter intensity classification

Several approaches have been proposed in the literature to classify the BS mosaics and to cluster areas with homogeneous seafloor characteristics (e.g. Brown et al. 2011; McGonigle and Collier, 2014; Ierodiaconou et al. 2018). In this study, the Jenks' optimization algorithm was applied to the BS mosaics. This algorithm was successfully applied to BS mosaics in the Venice Lagoon (Montereale-Gavazzi et al., 2016; Fogarin et al., 2019; Toso et al., 2019). Once the number of BS classes were defined, the algorithm performed the mosaic classification by minimizing the variance within classes and maximizing it among classes, respectively (Jenks, 1967). The BS classes were associated with the textural groups by overlapping the mosaics with the samples (see section 5.3.4).

In this way, it was possible to obtain sediment distribution maps for the different datasets. The calculation of the confusion matrices following Foody (2002) (section 5.3.4) provided an estimate of the classification accuracy of the sediment distribution maps. The creation of the transition matrices (Braumoh 2006; Rattray et al., 2013) from one sediment map to the other, allowed to quantitatively assess the change of the sediment distribution over time through quantitative parameters of change such as persistence, gain and loss.

5.3. Results

5.3.1. Morphological characterization of Po della Pila submarine lobe

The submerged sector of the Po della Pila consist mostly in a prodelta lobe. The lobe is skewed toward the southern direction, with asymmetric shape formed by a narrow and steeper ($\approx 2^\circ$) portion in the north and a wider and more gentle ($\approx 0.4^\circ$) side to the south (Fig. III3A). The high-resolution bathymetry portrays a maze of complex morphological features on the delta front and prodelta slope, including a longshore bar, transversely-distributed smaller bars, collapse depressions (Figs. III3A, III3B) and superficial instability features (Fig. III4).

Longshore bar: in the delta front (1.7-2.7 m water depth), an almost continuous, submerged bar rims the mouth bar (Fig. III3B), with a longitudinal extent of about 4.5 km and 1.2-1.5 m relief from the surrounding seafloor. The submerged bar is detached from the mouth bar by a 2.5-3 m deep long-shore trough (section a-a' in Fig III3B). On the southern sector the bar is at 4 m water depth,

while it is not present in the northern side of the delta upper slope, in proximity of the North channel mouth (Fig. III3A).

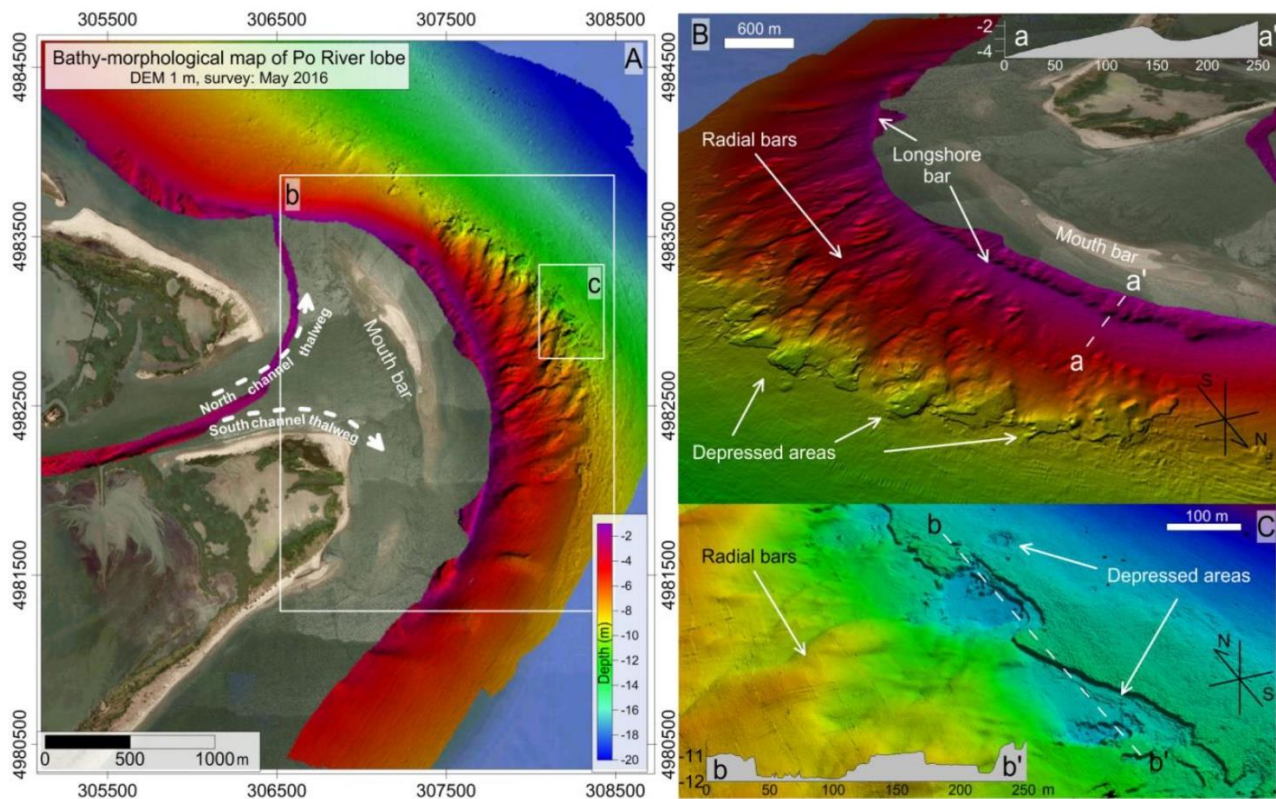


Fig. III3: A) Bathymorphological map of the Po della Pila lobe obtained from the 2016 dataset (DEM resolution 1m, vertical exaggeration 15x); B) Three-dimensional view of the Po della Pila delta front and slope, with main morphological features (see text for details). The bathymetric section a - a' is also reported; C) Example of depressed areas (collapse depressions) located in the prodelta zone and related bathymetric section (b - b').

Transverse bars: transverse bars are large-scale bedforms (with wavelength larger than 70 m) located in the eastern portion of the delta slope, in the lower shoreface, between about -5 and -10 m. They appear as rhythmic features, separated by well-elongated troughs (Figs. III3A, III3B). The transverse bars are oriented transversely to the coastline (from 20° up to 60°N). They are 300-500 m long and about 1 m high and have a crest to crest distance of about 70-100 m. They are only present below 4 m water depth, i.e. below the active level of most low energy sea waves and out of the influence of the longshore bar.

Collapse depressions: several depressed areas (Fig. III3B, C), have been identified in the prodelta slope, having variable shapes and sizes. The larger depressions are observed at the foot of the prodelta slope; they are mostly sub-circular, with a diameter ranging from 50 to 150 m and depths varying from 0.3 m to about 1.5 m. They appear to be the result of multiple collapses, with stepped vertical scars and a flat bottom, where relict blocks can be observed (Fig. III3C). Smaller depressions are instead observed along both the upper and the lower portion of the prodelta slope; they have a width ranging from 5 to 10 m and a few decimeters depth, with generally sub-circular shapes. They are frequently coalescent. The collapse depressions are mainly localized at the foot of the northeastern prodelta slope and of the transverse bars. However, they also occur locally in shallower water, and overlap with superficial gravitational-instability phenomena (Fig. III4). Their morphological characteristics (width, depth and area) and the geological context of the river delta, suggest that these features can be associated to collapse depressions, similar to those found on the Mississippi delta front and on the modern Huanghe (Yellow river) delta (Prior et al., 1986; Prior and Coleman 1982).

Gravity instability features: some slide scars and associated deposits have been identified in the northern sector of the submarine delta, on the prodelta slope (Fig. III4). The scars are located between 3 and 6 m water depth, very close to the coastline, and are widespread on low-gradient (0.5° to 1.5°) seabed. They likely originate even at shallower depth, where there is no multibeam data coverage. Near the coast, the slide scars are 100 to 500 m-wide, but reduce to a few tens of meters showing a "bottleneck" morphology moving deep ward (Fig. III4). Related slide deposits have been identified at the foot of the slide scars on the delta slope. They appear as 150-200 m long and few decimeters thick debris deposits characterized by chaotic facies (debris and small blocks).

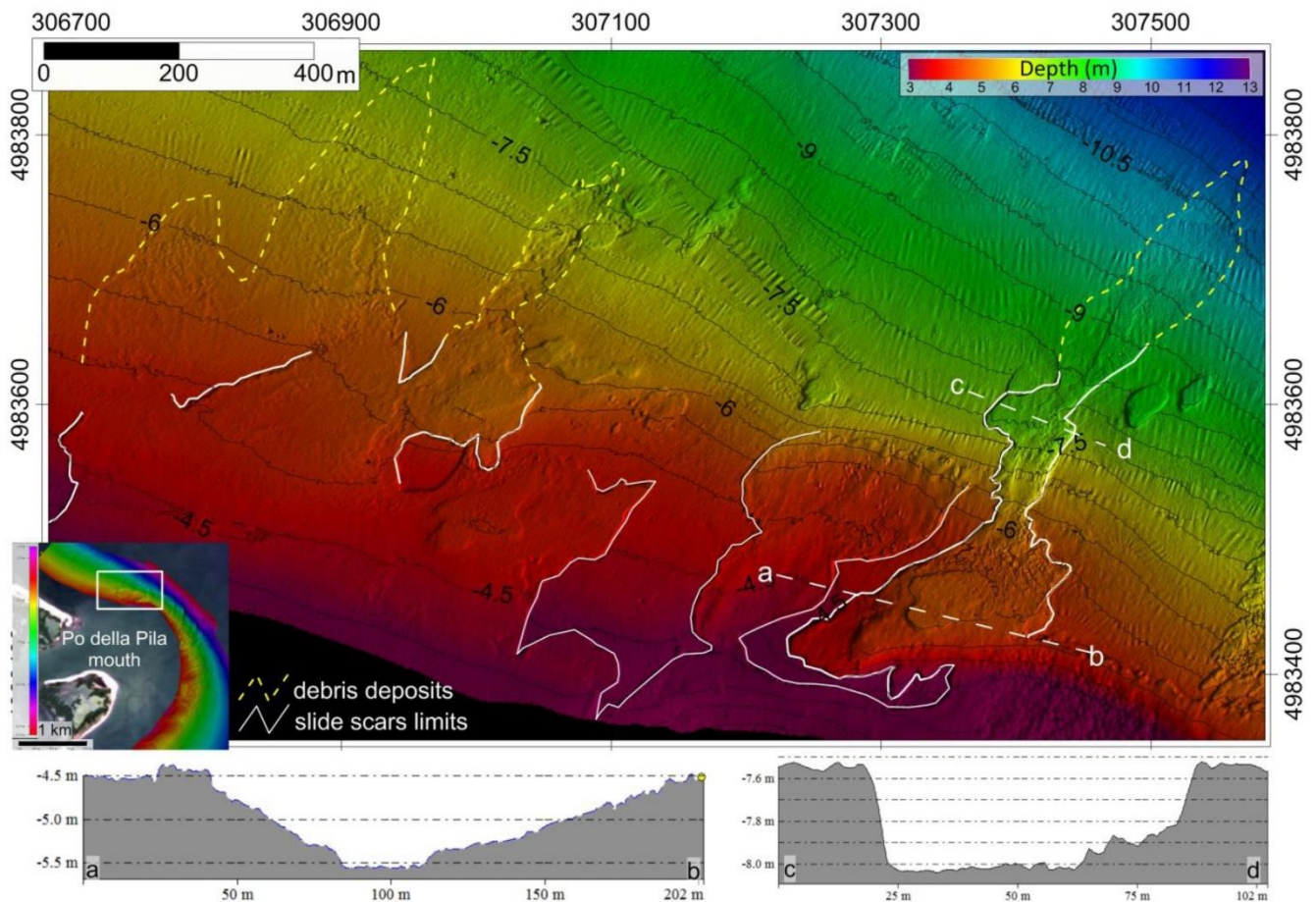


Fig. III4: Surface slides and associated deposits and collapse depressions on the northern sector of the prodelta slope, identified during the multibeam survey of September 2014. The bathymetric sections below (Vert. exagg. 20 x) show the flat morphology at the base of the evacuation zones in shallow water where typically less than one meter of sediment was removed.

5.3.2. Morphological changes over time

The comparison of bathymetric data collected in 2013, 2014 and 2016 (Fig. III5) points out important morphological changes in the seabed (positive and negative bathymetric residuals), attesting to the dynamic evolution of the delta lobe.

5. Study III: Short-term evolution of Po della Pila delta lobe from high-resolution multibeam bathymetry (2013-2016)

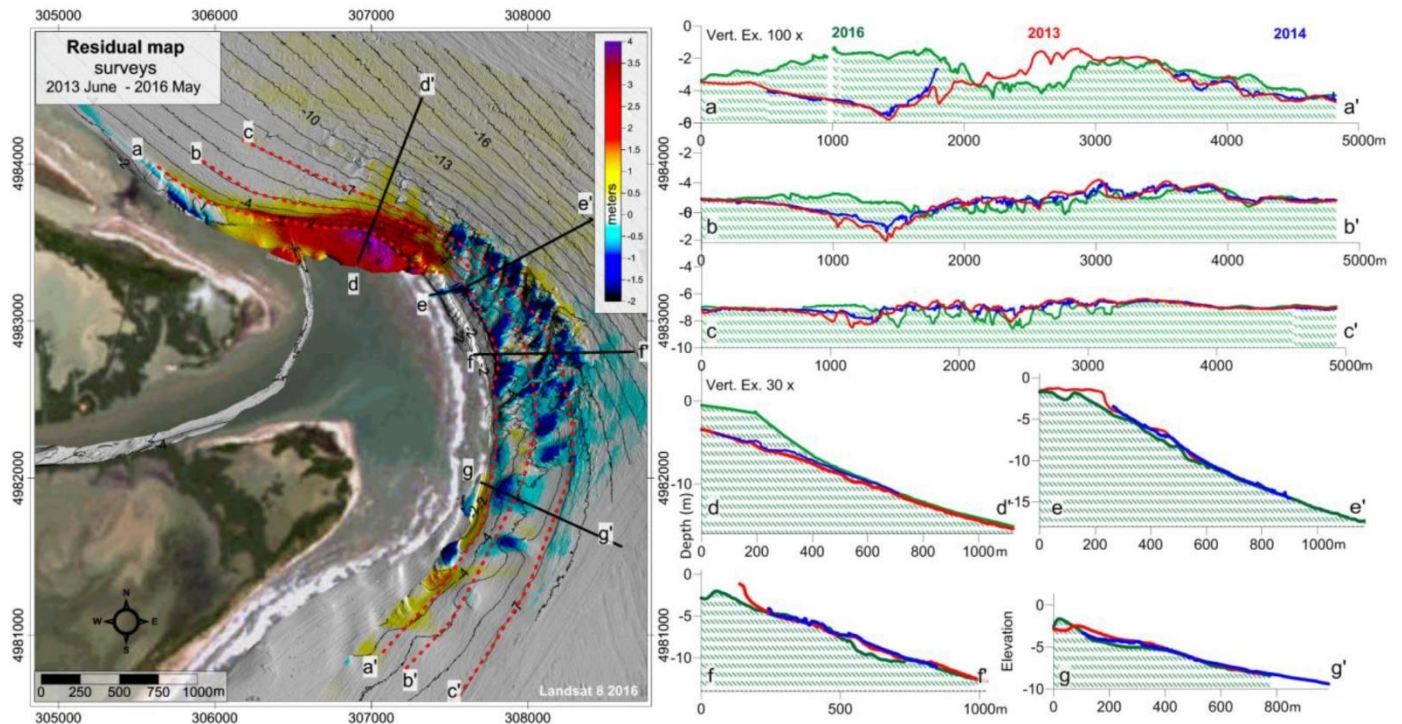


Fig. III5: Cumulative bathymetric residual map of Po della Pila DEM between 2016 and the 2013 datasets highlighting the bathymetric changes occurred in the time frame. On the right, the bathymetric sections extracted from the 2013, 2014 and 2016 datasets are compared. Sections a-a', b-b', c-c', running at different depth parallel to contours in the front and prodelta lobe, show local depth differences in the seabed up to some meters over a 3-year time interval. A general deepening of the seafloor is evident on the eastern side of the prodelta slope (blue tones in residual map and section f-f').

The residual map and related comparative sections among the three datasets (2013, 2014 and 2016; Fig. III5) show areas with different behavior. In the northern area of the Po della Pila lobe, the bathymetric residuals close to the northern channel highlight the presence of a 4 m-thick depositional body elongated in the East-West direction (Fig. III5). This sedimentary body is highly asymmetric and extends over a surface of about 1 km², with a volume (positive residual with respect to the 2013 survey) of about +1.16 Mm³. This volume was calculated taking into account also the seafloor portion that was not investigated in 2016, by reconstructing a synthetic surface up to the 0.5 m depth to compare with the 2013 DEM (Fig. III5, sections a-a' and d-d'), also supported by the Chirp data acquisition on June 2014. The sediment accumulation in this sector of the delta front and slope can be related the river flood event occurred in November 2014 (Fig. III6a).

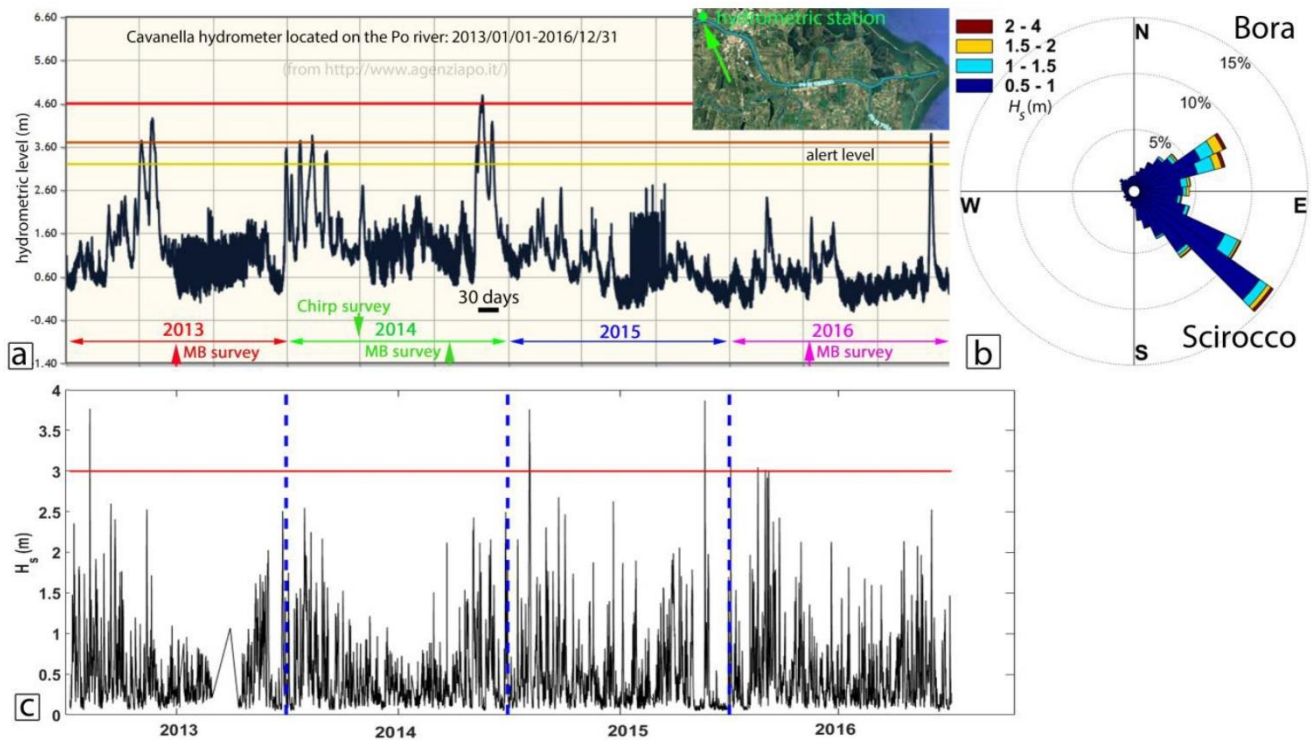


Fig. III6: a) Hydrometric level of Cavanella tide gauge station during the three years of monitoring the Po della Pila (from Interregional Agency for the Po River). The arrows indicate the multibeam and Chirp surveys performed on the Pila delta. The graph shows the exceptional event occurred in November 2014 immediately after the second multibeam survey. b) Circular histogram of the wave directions and significant wave height (H_s) plotted using the directional wave time series recorded from 2013 to 2016 at the “Acqua Alta” oceanographic research tower, located NE of the Po delta (Pomaro et al., 2018). c) Significant wave height (H_s) time series recorded from 2013 to 2016 at the “Acqua Alta” station.

In front of the delta mouth, elongated negative residuals on the delta slope (in blue in Fig. III5) primarily reflect the gradual southward migration of transverse bars in the 3-years time frame. A generalized deepening of the seabed of the order of 0.5 m (pale blue in Fig. 5 and sections a-b, b-c in Fig. III7a) is observed on most of the eastern and south-eastern submarine extension of the delta lobe. The high-resolution DEM and related bathymetric sections extracted from the 2013 and 2016 data (Fig. III7a) show a southward migration of the transverse bars of hundreds of meters at 5-10 m water depth.

Negative values up to -2 m in the residuals 2013-2016 are also locally observed in the delta slope and at the foot of the prodelta slope, where many, often coalescent, collapse depressions occur on the seabed. Here local positive residuals are related to the obliteration of collapse depressions and other morphological lows (Fig. III5). In the southern area of the Po della Pila, the bathymetric residuals highlight the presence of slight positive residuals in the form of depositional bodies 1 m thick, with elongated or sinuous shape (Fig. III5, section a-a’).

5.3.3. Sedimentological characteristics of the submerged delta

5.3.3.1. Sediment grain sizes

The grain size analysis of the 10 seafloor sediment samples collected in 2014 (Fig. III1b) shows the presence of sandy and muddy sediments in variable proportions, with values of the median diameter (D50) ranging from 11.23 to 252.10 μm (see Table IIIA2 in APPENDIX). Two main clusters have been identified: the group sand (Fig. III7b), composed by samples with sand and muddy sand and D50 ranging between ca. 171 and 252 μm and the group mud (Fig. III7b), consisting of sandy mud and mud, with D50 varying between ca 11 and 31 μm .

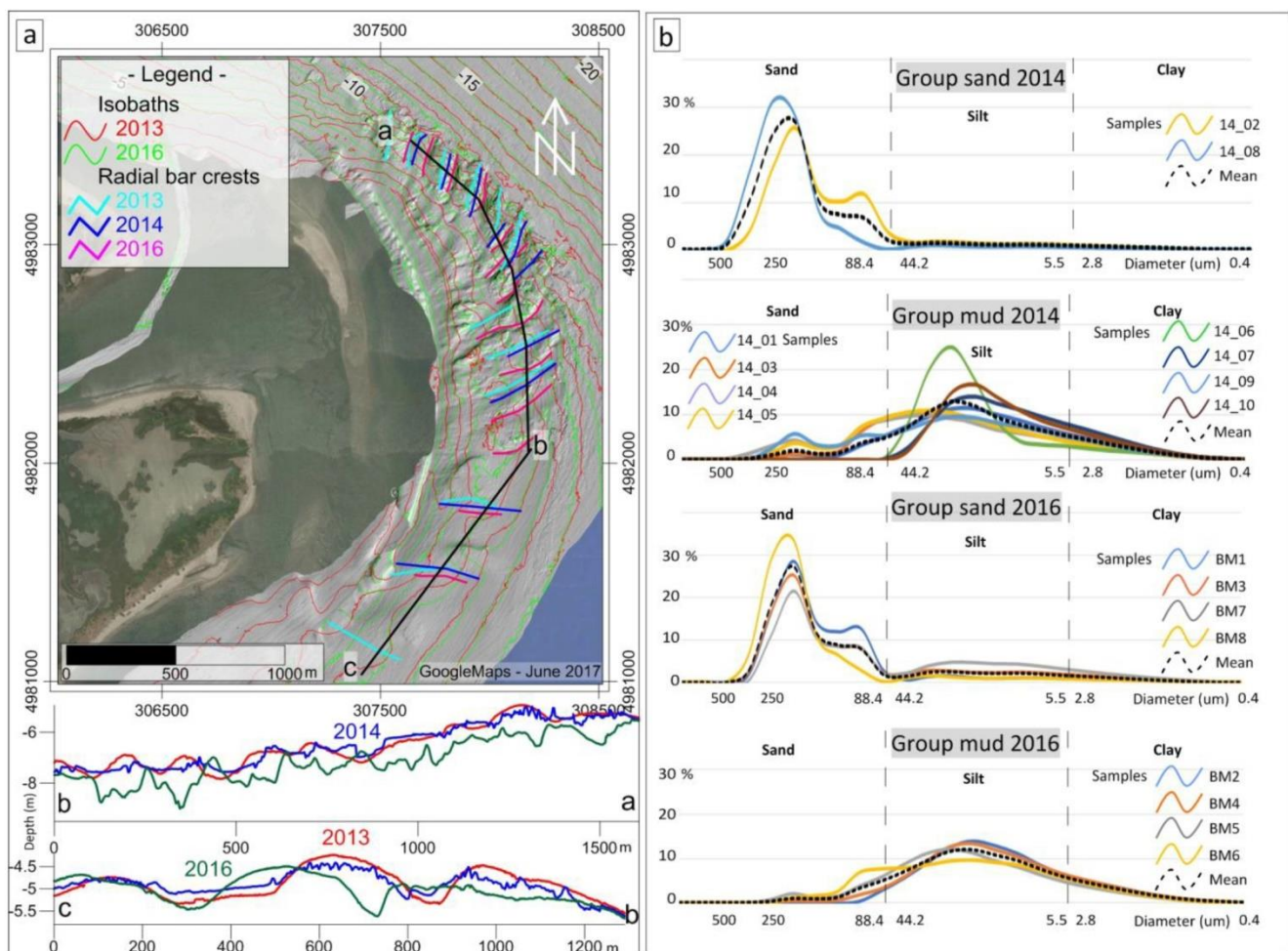


Fig III7: a) Shaded relief map of 2016 bathymetric survey (isobaths of 2013 are indicated for comparison) and position of the main transverse bar crests varied over time. Below, the bathymetric sections a-b and c-d on the prodelta slope and main transverse bar extracted from the 2013, 2014 and 2016 datasets are compared. b) Sediment samples groups clustered by means of the EntropyMax software on the base of D50 grain size for the 2014 and 2016 samples.

The grain size analysis of the 8 superficial sediment samples collected in 2016 (Fig. III1c) highlight the presence of muddy sand, sandy mud and mud (see Table IIIA2 in APPENDIX). The median diameter (D50) of the samples ranges from 13.5 to 216.12 μm . The two main textural groups

identified that are comparable with the clusters found for the 2014 samples, are: group sand, including 4 samples with muddy sand, with a D50 of ca. 130-216 μm and the group mud, including sandy mud and mud, with D50 between ca. 13 and 20 μm .

5.3.3.2. Backscatter classification and sediment distribution changes over time

From the backscatter intensity (BS) maps collected over the years 2013, 2014 and 2016, BS values range from -72 dB to -8 dB, with a general correspondence of high tones (high BS) to coarser materials and of dark tones (low BS) to finer sediments (Figs. III8 a, b, c). In particular, two main acoustic classes were distinguished (Figs III8 d, e, f): BS values range from -72 dB to -31 dB (low BS) and from -31 dB to -8 dB (high BS). These two acoustic classes (with lower and higher BS, dark and light tones, respectively) were associated with the textural group mud (Fig. III8) and sand respectively. This association is possible by comparing the BS datasets for the years 2014 and 2016 with the sediment samples (Figs. III8 e, f). and verifying a general correspondence. This comparison is not possible, instead, for the BS dataset of 2013 since no sediment samples were available for that survey. The overall accuracy of the BS classification is 50 % for 2014 (see the confusion matrix in Table IIIA3 in APPENDIX) and 87.5 % for 2016 (see the confusion matrix in Table IIIA4 in APPENDIX). Finally, the comparison between the acoustic classes and the textural group was not possible for the dataset of 2013 since no sediment samples were available. For this reason, the classification for 2013 was done based only on the BS values.

The sediment distribution changes over time were assessed semi-quantitatively by comparing the classified BS maps for the different years over an overlapping area covered in all three surveys (Fig. III8) and by extracting the corresponding transition matrix from one map to the other. The distribution of the two acoustic BS classes ("Sand/Mud") associated with the respective most-represented textural groups shows significant changes over the 2013-2016 time frame (Fig. III8 and Table IIIA5 in APPENDIX). The BS class "Sand" contributes to the sediment distribution in the area by 40 % in 2013 and by 75 % in 2014, indicating a general coarsening of the superficial seafloor sediment size. In 2016, the class "Sand" was relatively stable with respect to 2014 still occupying 72 % of the area. The class "Mud" is complementary to class "Sand", so it changed from 60 % (2013), to 25 % (2014) and finally to 28 % (2016).

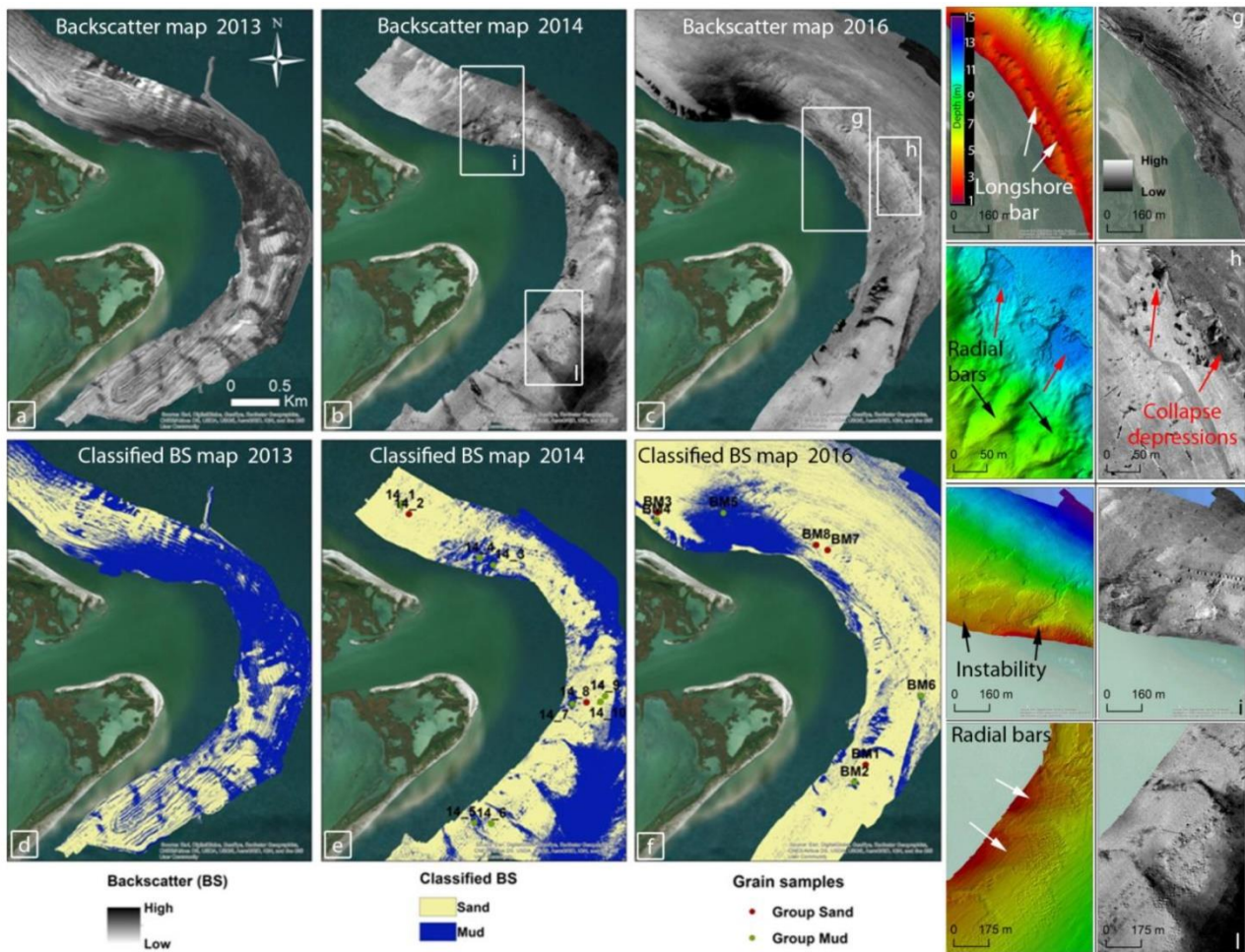


Fig. III8: a), b), c) Multibeam backscatter (BS) intensity maps of the seafloor of Po della Pila lobe collected in 2013, 2014 and 2016 respectively; d), e), f) classified backscatter using Jenks' optimization algorithm of 2013, 2014 and 2016 surveys, respectively; the location of collected sediment samples is reported in e) and f). On the right: comparison between morphologies and backscatter intensity of the main morphological features identified on the prodelta slope.

It appears that in the northern part of the delta, close to the North channel mouth (see Fig. III3 for location), the superficial sediments are mainly sandy in 2013 (partly) and in 2014, while they appear as mostly muddy in 2016. This is the area where the main positive bathymetric residuals are observed in the time frame 2013-2016 and where a sediment accumulation occurred in relation to the river flood event of November 2014 (Figs. III5 and III6). In the central part of the survey area, in front of the delta mouth, the mostly muddy sediment distribution of 2013 appears, instead. Mainly sandy in 2014 and in 2016. In this area, the longshore bar in 2016 has low backscatter indicating that this morphology was superficially covered with the mud sediment (Fig. III8 g and III8f). Also the transverse bars show an enhanced signature in the 2016 backscatter with general high values (Fig. III8 h), suggesting that their crests in this sector were covered with sandy sediments. The collapse depressions (Fig. III8 h) and superficial gravity features (Fig. III8 i) have a characteristic BS signature:

the collapse depression have a very low BS with a patchy pattern, whereas the superficial gravity instability features have low BS patchy signal in the reliefs alternating with a chaotic higher BS pattern in the lows (Fig. III8 i).

The southern part of the study area shows an opposite trend in backscatter distribution between 2013 and 2016, with the crests of the transverse bars (Fig. III8 l) having relatively high backscatter, and the troughs lower backscatter being probably covered by dominantly muddy sediments in 2014 and more sandy sediments in 2016 (Fig. III8 e, f). Elsewhere the BS in the southern area appears relatively stable, with prevalent high values (possibly corresponding to sandy sediments) among the 3 surveys. In summary, the main changes in backscatter highlighted in Fig. III8 and IIIA2 in APPENDIX occur in the northern area (possibly suggesting sand to mud transition in the dominant superficial sediments) and central part (mud to sand transition) of the surveyed area in the three-years time frame. In the southern part, mainly sandy sediments are present on the seabed over the three surveys. A more specific correspondence between BS and morphological features is difficult to verify due to the limited number of available seabed samples.

5.3.5. Seismic facies analysis of the delta front

High-resolution Chirp profiles were collected in spring 2014 after the first multibeam bathymetric survey of 2013 and before the one of 2014. The bathymetric profiles from multibeam data of 2013 (red), 2014 (blue) and 2016 (green) are plotted on the Chirp lines in Fig. III9: they indicate that between 2013 and 2014 there were no substantial differences in the seabed, while the 2016 bathymetry highlights the deposition of new sediment carried by the flood of the end of 2014 (Fig. III6) also evidenced by the residual map (Figs. III5 and III9, map 2).

5. Study III: Short-term evolution of Po della Pila delta lobe from high-resolution multibeam bathymetry (2013-2016)

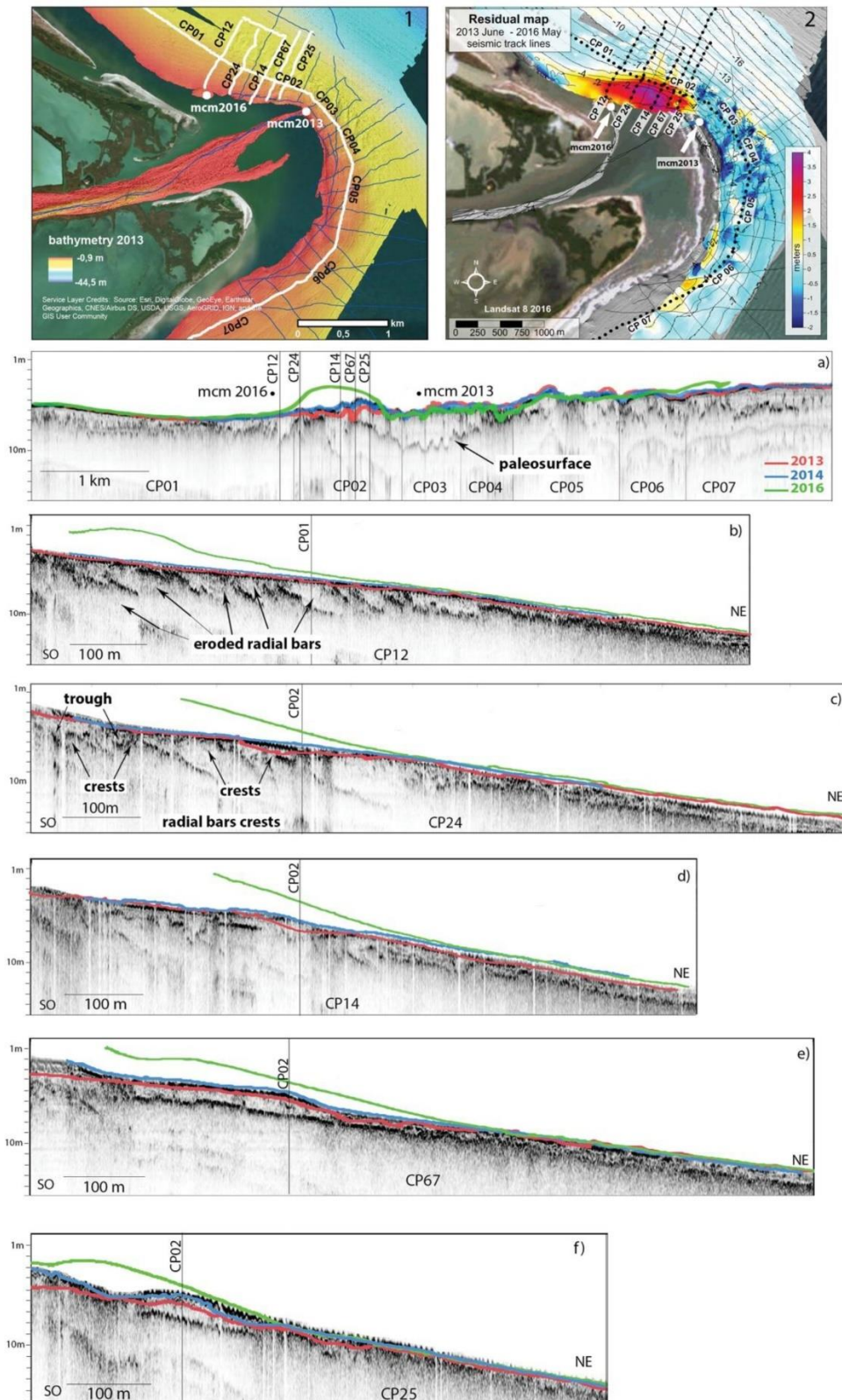


Fig. III-9: Navigation map of seismic profiles a to f, acquired in June 2014 after the bathymetric survey of 2013 and before the 2014 one. In the map 1 the Chirp profiles are located on the 2013 bathymetry, while in map 2 they appear on the cumulative bathymetric residuals 2016-2013. In the first composite longitudinal Chirp profile (a), not at the same horizontal scale as the other (shore normal) profiles, the two positions of the main channels of Po della Pila mouth are identified with "mcm2013" and "mcm2016" (mcm= main channel mouth, see also map 1 for location in plan-view).

The composite Chirp profile (from CP01 to CP07) parallel to the mouth bar of Po della Pila (Fig. III9 a) shows clear evidence of the subsurface deposits architecture before the sedimentation shed by the 2014 flood. In the prodelta environment the deposits present mostly transparent seismic facies, related to sandy sediment in the proximal delta front or homogeneous very fine-grained silty sand in channel-fill deposits (Correggiari et al. 2005a). Another common acoustic facies consists in high amplitude reflections related to a change in acoustic impedance, normally caused by silty/clay sediment or alternating thin layers of fine sand, silty clay or clay (due to flooding events) but also possibly caused by shallow gas trapped under low-permeability layers. In particular, in the central part of the CP 03 profile, a concave paleosurface is shown close to the previous main channel mouth (mcm2013 in Fig. III9 a). Seismic profiles in figure III9 b-f have been acquired in cross-shore direction in the northern portion of the Po della Pila's mouth bar before the deposition of the November 2014 flood event. Seismic profile CP12 (Fig. III9 b) is characterized by a shingled reflector pattern formed by several erosive remnants (transparent acoustic facies) of sand transverse bar system draped by thin muddy layers (high-amplitude reflectors). The location of the subsequent deposit is highlighted by the green morphological profile of the 2016 multibeam bathymetry (more than 3 m of thickness over the 2013 and 2014 seabed). In figure III9 c (profile CP24) some older transverse bars related to a previous depositional phase are also preserved under the seafloor with crests and troughs. In figure III9 d (profile CP14) buried transverse bars are less evident, possibly due to the concurrent delivery of sediment in the alongshore transport. Two subdued morphological steps are evident in the CP 67 Chirp profile (Fig. III9 e) and the most recent deposit (corresponding to green morphological profile) follows a similar shape. An example of sedimentation of a new forming bar in a trough is shown in figure III9f (profile CP 25) where the easternmost portion of the 2014 deposit (green morphological profile at minimum depth of 2-3 m below sea level) lies on the muddy veneer between two preexisting crests.

5.4. Discussion

It has been shown that the delta-prodelta system of Po della Pila is asymmetric and skewed toward the south, reflecting the prevalent (downdrift) sediment dispersal and shore-parallel advection. All the bedforms on the upper prodelta slope also indicate a migration towards the southern sectors,

consistent with a dominant southward sediment transport (Trincardi et al., 2004). Hydrodynamic models of the superficial circulation at the Po delta front (Maicu et al., 2018) show, as well, that the plume of the riverine outflow from Busa Dritta (the main, E-W oriented, distributary channel in the Po della Pila, Fig. IIIA1 in APPENDIX) deviates southward during flood events, confirming a predominant direction of currents toward the south. Hydrodynamic models also indicate that there is an area of relative minimum in the currents just south of the Po della Pila lobe (Maicu et al., 2018). Part of the river plume from the two main tributary channels during floods does not deposit on the prodelta, but it is transported offshore, as shown by the satellite images (Falcieri et al., 2014; Braga et al 2017; Manzo et al 2018). The observed morphology of the mouth bar reflects the interplay between river sediment discharge and the reworking action by storm waves that contribute to sediment resuspension and dispersal (Rodriguez & Metha 2000; Maillet et al., 2006). When wave action is weak the bar slowly grows (Esposito et al 2013). In the Po case, most of the waves come from the NE and SE sectors (caused by Bora and Scirocco winds, respectively, see Fig. III6b reporting the directional wave time series recorded from 2013 to 2016 at the “Acqua Alta” oceanographic research tower and wind regime reported by Falcieri et al., 2014). This suggests that their redistributing effect in shallow-water is more relevant in the central sector of the study area which is exposed to both predominant waves directions.

From the multibeam and Chirp integrated data, we see that the emerged and submerged mouth of the main branch of the Po della Pila consists of composite lobes due to rapid sedimentation during short-lived flood events, typically a few weeks in duration. These deposits, located close to the main channel mouth, are subsequently reorganized to feed transverse bar systems that have been recognized, eroded or preserved, even in the stratigraphic record through seismoacoustic data (fig. III9). Overall, a marked short-term variability at the 3-year time frame is observed in the Po di Pila submarine delta lobe, as evidenced by bathy-morphological, sedimentological and seismic data.

5.4.1. Distribution and variability of submarine morphological features in the 2013-2016 frame

Time lapse high-resolution bathymetric surveys on Po della Pila lobe show substantial geomorphological changes of the seafloor over a time frame of three years. By comparing the 2013 and 2016 data set having a complete overlapping (bathymetric data collected in 2014 lack the shallow-water part), we observe a significant restyling of the observed morphostructures (longshore bar, depressed areas and instability phenomena, etc.), through rapid shifts and alternating phases

of construction/obliteration connected to riverine depositional processes and to coastal drift dynamics. The latter are mainly acting in shallow-water (i.e. < 15 m) where most of the along-shelf distribution of the sediment input occurs (Friedrichs and Scully, 2007).

As for riverine processes, the main positive bathymetric change identified in the 2016 data set with respect to the 2013 and 2014 bathymetry, occurs on the northern side of the prodelta slope (in front of the main present active channel), where a lobe-shaped sedimentary deposit 4 m thick was detected (Fig. III5). This deposit is lying on an erosional surface, below which several eroded transverse bars are visible on Chirp sonar profile (Fig. III9). Its formation is accompanied by a change in seafloor sediment distribution from mostly sandy sediments in 2013 and 2014 to mostly muddy sediment in 2016 (Fig. III8 and Fig. IIIA2 in APPENDIX). This sediment accumulation is related to the river flood event in November 2014 (Fig. III6) that did not produce relevant modifications in the eastern and southern delta front and prodelta slope. The negative bathymetric residuals observed on the central delta slope (in blue in Fig. III5) mostly correspond to the gradual southward migration of elongated, NNE-SSW to E-W oriented transverse bars, and to a gradual shift of the transverse bar crests (Fig. III7). The transverse bars show a significant migration in the range of 50 to over 100 m between 5-10 m water depth (Fig. III7), suggesting the activity of bottom currents along the coast. The occurrence of active bottom currents here is in agreement with the dominant sandy grain size in the seabed.

A recent growth/emersion of mouth bars at the main distributary mouths of Po della Pila was pointed out by Ninfo et al. (2018) through the analysis of 2015-2017 Sentinel-2 satellite images, suggesting a resumed overall delta progradation over this time scale. However, similar evidences are lacking in the submarine part of the delta, where there seems to be no progradation with the exception of the localized sediment accumulation in the northern area, in front of the distributary channel. A generalized lowering in the seabed (values of about 0.5 m in the 2013-2016 time frame) affected, instead, most of the eastern and southern submarine extension of the delta lobe, suggesting that the role of active subsidence may play an important role, not compensated by sediment supply.

Subsidence is well documented for the subaerial Po delta (Fabris et al., 2016; Tosi et al., 2016; Da Lio and Tosi, 2019) with rates up to -15 mm/year. Localized subsidence also occurs in the eastern portion of the delta submarine slope, in correspondence to the observed collapse depressions up to 1 m deep (see next section).

5.4.2. Collapse and gravity instability features

The Po della Pila delta front and prodelta slope revealed widespread sub-circular collapse depressions and superficial slides, with variable size and morphology. Collapse depressions (Fig. III3 C) may record multi-stage collapses, possibly driven by degassing and fluid escape processes (Lu et al., 1991). The classification of the backscatter data indicates that these depressions are characterized by low BS signal and are mostly covered by fine sediment. According to Prior and Coleman (1982) the high organic content of deltaic fine sediments makes the development of methanogenesis processes highly probable and this suggests that the interstitial methane gas may have a strong impact on the morphological development of the Pila lobe's superficial instabilities.

Orange et al. (2005) documented a substantial concentration of biogenic gas in shallow sediment cores from Po della Pila prodelta lobe. Liquefaction processes may also have induced a reorganization of the sediments structure to dissipate overpressures (Prior and Coleman 1979; Prior et al., 1986a, Xu et al., 2009).

As for superficial slides (Fig. III4) their location in very shallow water in the northern sector of the delta, where the highest sedimentary supply occurs, their geometry and that of related deposits, suggest that gravity instability phenomena commonly affect the delta front and prodelta slope. These phenomena are probably caused by storm waves-seabed cyclic interactions, or by localized slope oversteepening, increasing pore pressures in saturated layers. According to Prior and Coleman (1980, 1981 and 1982) these kind of instability features show a pronounced evacuation area, similar to collapse depressions. However, at their downslope margins they have narrow openings through which fine-grained sediment debris moves seaward over the surrounding seabed (bottleneck slides).

This seems to be due to a "spreading failure" mechanism similar to that of subaerial quick clays, involving liquefaction with consequent rapid and substantial reduction in sediment strength. This interpretation is also supported by the BS mosaic (Fig. III8), showing that these features are covered by patches of muddy sediments alternated with a chaotic higher BS pattern, likely corresponding to debris-flow deposits, and by sediment samples collected in these areas, where abundant mud was found.

Finally, seismicity data in a range of about 100 km of the study area (<http://cnt.rm.ingv.it/events>) during the three years of geophysical survey, do not highlight critical conditions. Few and deep

earthquakes of low intensity could be excluded as the trigger of the instability phenomena in shallow water and the cause of the collapse depressions formation.

5.5. Conclusions

The time-lapse comparison of high-resolution multibeam, reflection-seismic and sampling data collected in 2013-2016 allowed the characterization of the morphological structure of the modern Po della Pila prodelta and its short-term evolution. The study documents that:

1. Multiple morpho-sedimentary processes are active in the whole delta complex, with rapidly changing depositional and erosive phenomena. The main sedimentary deposition of riverine origin occurs near the northern channel close to the Pila mouth. Here a total of about 1.16 Mm³ deposited mainly as a consequence of a not-exceptional Po river flood in November 2014. Sediments accumulate on the delta front and alongshore currents rework depositional bodies, with net southward transport and a consequent marked asymmetry of the entire delta front.
2. A general lowering of the delta front seafloor in the eastern and southern sector of the surveyed area occurred during the 3 years of monitoring, with maximum estimated values of 1.5 m found at depths between 7 and 10 m. This deepening is not only related to the well known starvation of the delta due to the human activity and to the accelerated subsidence, but it is probably also due to the presence of sediment with a high water and organic material content. This type of sediment is able to fluidify and/or to consolidate over extremely short time, as suggested by the presence of many collapse and gravity instability features.
3. The occurrence of gravitational instability phenomena mainly on the northern sector of the investigated prodelta shows that this sector is the most dynamic one. The high quantity of deposited sediment over a short time promotes, in fact gravitational instability and sediment transport towards the prodelta lobe.
4. Given the high rates of sediment accumulation and rapid erosion due to storms and currents, this area represents a highly relevant site to study the Anthropocene short-term climate-driven variability of the coastal region including the possible interaction among human-

induced changes in sediment supply, coastal erosion, alongshore sediment transport, local subsidence (both natural and anthropogenic) and submarine slope instability.

Acknowledgments

This work was fully financed by the National Flagship Project RITMARE, funded by MIUR, the Italian Ministry of Education, University and Research. For the 2016 bathymetric survey, the authors are grateful to the Italian Hydrographic Office of the Italian Navy, that was a partner in the project and that gave a crucial technical and logistical support during the survey. The authors would like to thank Prof. Molinaroli of the Ca' Foscari University in Venice and all the staff of the sedimentological laboratory for their help in the grain size analyses.

5.6. References

- Amorosi, A., Bruno, L., Campo, B., Morelli, A., 2015. The value of pocket penetration tests for the high-resolution palaeosol stratigraphy of late Quaternary deposits. *Geological Journal*, 50, 670-682.
- Anthony, E.J., Marriner, N., Morhange, C., 2014. Human influence and the changing geomorphology of Mediterranean deltas and coasts over the last 6000 years: From progradation to destruction phase? *Earth-Science Reviews* 139: 336-361.
- Anzidei, M., Bosman, A., Casalbore, D., Tusa, S., La Rocca, R., 2016. New insights on the subsidence of Lipari island (Aeolian Islands, Southern Italy) from the submerged Roman age pier at Marina Lunga. *Quaternary International* 401 162e173. DOI: 10.1016/j.quaint.2015.07.003.
- Anzidei, M., Bosman, A., Carluccio, R., Casalbore, D., D'Ajello, Caracciolo, F., Esposito, A., Nicolosi, I., Pietrantonio, G., Vecchio, A., Carmisciano, C., Chiappini, M., Chiocci, F., Muccini, F., Sepe, V., 2017. Flooding scenarios due to land subsidence and sea-level rise: a case study for Lipari Island (Italy). *Terra Nova* 29: 44–51. doi: 10.1111/ter.12246.
- Artegiani, A., Bregant, D., Paschini, E., Pinardi, N., Raicich, F., Russo, A., 1997a. The Adriatic Sea general circulation: Part I. Air–sea interactions and water mass structure. *J. Phys. Oceanogr.*, 27 (1997), pp. 1492-1514.
- Artegiani, A., Bregant, D., Paschini, E., Pinardi, N., Raicich, F., Russo, A., 1997b. The Adriatic Sea general circulation: Part II. Baroclinic circulation structure *J. Phys. Oceanogr.*, 27 (1997), pp. 1515- 1532.
- Benetazzo, A., Bergamasco, A., Bonaldo, D., Falcieri, F.M., Sclavo, M., Langone, L., Carniel, S., 2014. Response of the Adriatic Sea to an intense cold air outbreak: dense water dynamics and wave-induced transport. *Progress in Oceanography*, 128, 115-138.

- Blott, S.J. and Pye, K., 2001. GRADISTAT: a grain size distribution and statistics package for the analysis of unconsolidated sediments. *Earth Surface Processes and Landforms Earth Surf. Process. Landforms* 26, 1237–1248 (2001). DOI: 10.1002/esp.261.
- Blum, M.D., Roberts, H.H., 2009. Drowning of the Mississippi Delta due to insufficient sediment supply and global sea-level rise. *Nature Geoscience*, 2: 488.
- Boldrin, A., Langone, L., Miserocchi, S., Turchetto, M. and Acri, F., 2005. Po River plume on the Adriatic continental shelf: dispersion and sedimentation of dissolved and suspended matter during different river discharge rates. *Marine Geology*, 222, pp.135-158.
- Bosman, A., Casalbore, D., Romagnoli, C., Chiocci, F.L., 2014. Formation of an ‘a’ā lava delta: insights from time-lapse multibeam bathymetry and direct observations during the Stromboli 2007 eruption. *Bulletin of Volcanology*, 76: 838. <https://doi.org/10.1007/s00445-014-0838-2>.
- Bosman, A., Casalbore, D., Anzidei, M., Muccini, F., Carmisciano, C., Francesco Latino, C., 2015. The first ultra-high resolution Digital Terrain Model of the shallow-water sector around Lipari Island (Aeolian Islands, Italy). *Annals of Geophysics*. doi:10.4401/ag-6746.
- Braga, F., Zaggia, L., Bellafiore, D., Bresciani, M., Giardino, C., Lorenzetti, G., Maicu, F., Manzo, C., Riminucci, F., Ravaioli, M., Brando, V.E., 2017. Mapping turbidity patterns in the Po river prodelta using multi-temporal Landsat 8 imagery. *Estuarine, Coastal and Shelf Science*, 198, 555- 567.
- Braimoh, A.K., 2006. Random and systematic land-cover transitions in northern Ghana. *Agric Ecosyst Environ* 113: 254–263.
- Brown, C.J., Smith, S.J., Lawton, P. Anderson, J.T., 2011. Benthic habitat mapping: A review of progress towards improved understanding of the spatial ecology of the seafloor using acoustic techniques. *Estuarine, Coastal and Shelf Science*, 92: 502-520.
- Cattaneo, A., Correggiari, A., Langone, L. and Trincardi, F., 2003. The late-Holocene Gargano subaqueous delta, Adriatic shelf: sediment pathways and supply fluctuations. *Marine Geology*, 193(1-2), pp.61-91.
- Cattaneo, A., Trincardi, F., Asioli, A., Correggiari, A., 2007. The Western Adriatic shelf clinoform: energy-limited bottomset. *Continental Shelf Research*. Vol. 27, Issues 3–4, 1 February 2007, Pages 506-525.
- Coleman, J.M., Prior, D.B. 1978. Submarine Landslides in the Mississippi River Delta (No. TR- 263). Louisiana State Univ Baton Rouge Coastal Studies Inst. 10th OTC in Houston, Texas., May 1978, pp. 1067-1074.
- Correggiari, A., Cattaneo, A., Trincardi, F., 2005a. Depositional patterns in the late Holocene Po delta system in Concepts, Models, and Examples (Janok P. Bhattacharya & Liviu Giosan Eds) SEPM Special Publication No. 83 (ISBN 1-56576-113-8.): 365–392.
- Correggiari, A., Cattaneo, A., Trincardi, F., 2005b. The modern Po Delta system: Lobe switching and asymmetric prodelta growth. *Marine Geology*, 222–223: 49–74.

- Da Lio, L., and Tosi, L., 2019. Vulnerability to relative sea-level rise in the Po river delta (Italy), *Estuarine, Coastal and Shelf Science*, Vol. 228, 2019. <https://doi.org/10.1016/j.ecss.2019.106379>.
- Dai, Z., Liu, J.T., Wei, W. Chen, J., 2014. Detection of the Three Gorges Dam influence on the Changjiang (Yangtze River) submerged delta. *Scientific Reports*, 4: 6600.
- Esposito, C. R., Georgiou, I. Y., & Kolker, A.S., 2013. Hydrodynamic and geomorphic controls on mouth bar evolution. *Geophysical Research Letters*, 40(8), 1540-1545.
- Fabris, M., Achilli, V., Fiaschi, S., Floris, M., Menin, A., Monego, M., 2016. Stima della subsidenza recente nell'area del delta del Po da dati GPS e Sentinel-1A. *Federazione Italiana delle Associazioni per le Informazioni Territoriali e Ambientali Asita 2016*. pp. 357-364. ISBN: 978-88-941232-6-5.
- Falcieri, F.M., Benetazzo, A., Sclavo, M., Russo, A., Carniel, S., 2014. Po River plume pattern variability investigated from model data. *Continental Shelf Research* 34: 84–95.
- Fogarin, S., Madricardo, F., Zaggia, L., Sigovini, M., Montereale Gavazzi, G., Kruss, A., Lorenzetti, G., Manfé, G., Petrizzo, A., Molinaroli, E., Trincardi, F., 2019. Tidal inlets in the Anthropocene: geomorphology and benthic habitats of the Chioggia inlet, Venice Lagoon (Italy). *Earth Surface Processes and Landforms*, 44(11), 2297-2315.
- Folk RL, Andrews PB, Lewis D. 1970. Detrital sedimentary rock classification and nomenclature for use in New Zealand. *New Zealand journal of geology and geophysics*, 13(4), 937-968.
- Foody, GM., 2002. Status of land cover classification accuracy assessment. *Remote sensing of environment* 80: 185-201.
- Friedrichs, C.T., & Scully, M.E. 2007. Modeling deposition by wave-supported gravity flows on the Po River prodelta: from seasonal floods to prograding clinoforms. *Continental Shelf* Hood, W.G., 2010. Tidal channel meander formation by depositional rather than erosional processes: examples from the prograding Skagit River Delta (Washington, USA)." *Earth Surface Processes and Landforms: The Journal of the British Geomorphological Research Group* 35: 319- 330.
- Ierodiaconou, D., Schimel, A.C, Kennedy, D., Monk, J., Gaylard, G., Young, M., Diesin, M., Rattray, A., 2018. Combining pixel and object based image analysis of ultra-high resolution multibeam bathymetry and backscatter for habitat mapping in shallow marine waters. *Marine Geophysical Research*:1-18.
- Jenks, G.F., 1967. The Data Model Concept in Statistical Mapping, *International Yearbook of Cartography* 7: 186–190.
- Jiang, C., Pan, S., Chen, S., 2017. Recent morphological changes of the Yellow River (Huanghe) submerged delta: Causes and environmental implications." *Geomorphology* 293: 93-107.
- Loring, D.H., Rantala, R.T.T., 1992. Manual for the geochemical analyses of marine sediments and suspended particulate matter. *Earth-science reviews*, 32, 235-283.
- Lu, N.Z., Suhayda, J.N., Prior, D.B., Bornhold, B.D., Keller, G.H., Wiseman Jr, Wm. J., Wright, L. D., Yang, Z. S., 1991. Sediment Thixotropy and Submarine Mass Movement, Huanghe Delta, China. *Geo-Marine Letters*, 11;9-15.

- Maicu, F., De Pascalis, F., Ferrarin, C., & Umgiesser, G., 2018. Hydrodynamics of the Po River Delta Sea System. *Journal of Geophysical Research: Oceans*, 123(9), 6349-6372.
- Miles, J. W. 1959. On the generation of surface waves by shear flows Part 3. Kelvin-Helmholtz instability. *Journal of Fluid Mechanics*, 6(04), 583. doi:10.1017/s0022112059000842. *Research*, 27(3-4), 322-337.
- Maillet, G.M., Vella, C., Berné, S., Friend, P.L., Amos, C.L., Fleury, T.J., Normand, A., 2006. Morphological changes and sedimentary processes induced by the December 2003 flood event at the present mouth of the Grand Rhône River (southern France). *Marine Geology*, 234: 159-177.
- Manzo, C., Braga, F., Zaggia, L., Brando, V. E., Giardino, C., Bresciani, M., & Bassani, C., 2018. Spatio-temporal analysis of prodelta dynamics by means of new satellite generation: the case of Po river by Landsat-8 data. *International journal of applied earth observation and geoinformation*, 66, 210-225.
- McGonigle, C., Brown, C., Quinn, R., & Grabowski, J., 2009. Evaluation of image-based multibeam sonar backscatter classification for benthic habitat discrimination and mapping at Stanton Banks, UK. *Estuarine, Coastal and Shelf Science*, 81(3), 423-437.
- McGonigle, C., Collier, J.S., 2014. Interlinking backscatter, grain size and benthic community structure. *Estuarine, Coastal and Shelf Science* 147: 123-136.
- Molinarioli, E., Sarretta, A., Ferrarin, C., Masiero, E., Specchiulli, A., Guerzoni, S., 2014. Sediment grain size and hydrodynamics in Mediterranean coastal lagoons: Integrated classification of abiotic parameters. *Journal of earth system science*, 123: 1097-1114.
- Montereale-Gavazzi, G., Madricardo, F., Janowski, L., Kruss, A., Blondel, P., Sigovini, M., Foglini, F., 2016. Evaluation of seabed mapping methods for fine-scale classification of extremely shallow benthic habitats—application to the Venice Lagoon, Italy. *Estuarine, Coastal and Shelf Science* 170 : 45-60.
- Nelson B.W. 1970. Hydrography, sediment dispersal and recent historical development of the Po river delta, Italy J.P. Morgan (Ed.), *Deltaic Sedimentation, Modern and Ancient*, SEPM Special Publication, vol. 15 (1970), pp. 152-184.
- Ninfo, A., Ciavola P., Billi, P., 2018. The Po Delta is restarting progradation: geomorphological evolution based on a 47-years Earth Observation dataset. *Scientific reports* 8: 3457.
- Olariu, C., Bhattacharya, J.P., 2006. Terminal distributary channels and delta front architecture of river-dominated delta systems. *Journal of Sedimentary Research*, 76: 212–233.
- Orange, D., Garcia-Garcia, A., Lorensen, T, Nittrouer, C., Milligan, T., Miserocchi, S., Langone, L., Correggiari, A., Trincardi, F., 2005. Shallow gas and flood deposition on the Po Delta. *Marine Geology* 222–223: 159– 177.
- Orlić, M., Kuzmić, M., Pasarić, Z., 1994. Response of the Adriatic Sea to the bora and sirocco forcing. *Continental Shelf Research*, 14: 91-116.
- Orton, G.J., Reading, H.G., 1993. Variability of deltaic processes in terms of sediment supply, with particular emphasis on grain size. *Sedimentology* 40: 475-512.

- Overeem, I., Brakenridge, R.G., 2009. Dynamics and vulnerability of delta systems. GKSS Research Centre, LOICZ Internat. Project Office, Inst. for Coastal Research.
- Pomaro, A., Cavaleri, L., Papa, A., Lionello, P., 2018. 39 years of directional wave recorded data and relative problems, climatological implications and use. *Scientific data*, 5:180139.
- Prior, D.B., & Coleman, J.M., 1979. Submarine landslides-geometry and nomenclature. *Zeitschrift für Geomorphologie*, 23(4), 415-426.
- Prior, D.B., Coleman, J.M., 1980. Sonograph mosaic of submarine slope instabilities, Mississippi river delta. *Marine Geology*, 36: 227-239.
- Prior, D.B., Coleman, J.M., 1981. Resurveys of active mudslides, Mississippi Delta. *Geo-Marine Letters*, 1: 17–21. doi:10.1007/BF02463296.
- Prior, D.B., Coleman, J.M., 1982. Active slides and flows in underconsolidated marine sediments on the slopes of the Mississippi Delta. In *Marine Slides and other Mass Movements*. DOI: 10.1007/978-1-4613-3362-3.
- Prior, D.B., Yang, Z.S., Bornhold, B.D., Keller, G.H., Lu, N.Z., Wiseman Jr, W.J., Wright, L.D. Zhang, J., 1986a. Active slope failure, sediment collapse, and silt flows on the modern subaqueous Huanghe (Yellow River) delta. *Geo-Marine Letters*, 6:85-95.
- Prior, D.B., Yang, Z.S., Bornhold, B.D., Keller, G.H., Lin, Z.H., Wiseman Jr, W.J., Wright, L.D., Lin, T.C., 1986b. The subaqueous delta of the modern Huanghe (Yellow River). *Geo-Marine Letters*, 6: 67-75.
- Rattray, A., Ierodiaconou, D., Monk, J., Versace, V.L., Laurenson, L.J.B., 2013. Detecting patterns of change in benthic habitats by acoustic remote sensing. *Marine Ecology Progress Series*, 477: 1-13.
- Rodriguez, H. N., & Mehta, A. J., 2000. Longshore transport of fine-grained sediment. *Continental Shelf Research*, 20(12-13), 1419-1432.
- Stefani, M., and Vincenzi, S., 2005. Holocene stratigraphic architecture and depositional evolution of the Po. *Marine geology*, 222–223 (2005), pp. 19-48.
- Stewart, L. K., Kostylev, V.E., Orpin, A.R., 2009. Windows-based software for optimising entropybased groupings of textural data. *Computers & Geosciences*, 35: 1552-1556.
- Syvitski, J.P.M., Kettner, A.J., Correggiari, A. Nelson, B.W., 2005, Distributary channels and their impact on sediment dispersal, *Marine Geology*, 246: 222-230.
- Syvitski, J.P.M., Kettner, A.J., Overeem, I., Hutton, E.W., Hannon, M.T., Brakenridge, G. R., Day, J., Vörösmarty, C., Saito, Y., Giosan, L., Nicholls, R.J., 2009. Sinking deltas due to human activities. *Nature Geoscience*, 2: 681.
- Tesi, T., Miserocchi, S., Goñi, M.A., Turchetto, M., Langone, L., De Lazzari, A., Albertazzi, S., Correggiari, A., 2011. Influence of distributary channels on sediment and organic matter supply in event-dominated coastal margins: the Po prodelta as a study case, *Biogeosciences*, 8: 365-385. <https://doi.org/10.5194/bg-8-365-2011>, 2011.

Tosi, L., Da Lio, C., Strozzi, T., Teatini, P., 2016. Combining L- and X-Band SAR Interferometry to Assess Ground Displacements in Heterogeneous Coastal Environments: The Po River Delta and Venice Lagoon, Italy. *Remote Sens*, 8: 308. doi:10.3390/rs8040308.

Toso, C., Madricardo, F., Molinaroli, E., Fogarin, S., Kruss, A., Petrizzo, A., ... & Trincardi, F. 2019. Tidal inlet seafloor changes induced by recently built hard structures. *PloS one*, 14(10).

Trincardi, F., Cattaneo, A., Correggiari, A., 2004. Mediterranean prodelta systems: natural evolution and human impact investigated by EURODELTA. *Oceanography*, 17: 34-45.

Visentini, M., and Borghi, G., 1938. Le spiagge padane da Porto fossone a Cervia. *Ricerche sulle variazioni delle spiagge italiane*, C.N.R., Roma (1938), pp. 1-68.

Woodroffe, C.D., Nicholls, R.J., Saito, Y., Chen, Z., Goodbred, S.L., 2006. Landscape variability and the response of Asian megadeltas to environmental change. In *Global change and integrated coastal management*: 277-314. Springer, Dordrecht.

Woolfe, K.J., Michibayashi, K., 1995. "Basic" entropy grouping of laser-derived grain-size data: an example from the Great Barrier Reef. *Computers & Geosciences*, 21: 447-462.

Xu, G., Sun, Y., Wang, X., Hu, G., & Song, Y., 2009. Wave-induced shallow slides and their features on the subaqueous Yellow River delta. *Canadian Geotechnical Journal*, 46(12), 1406-1417.

5.7 Appendix

Table IIIA1: Summary of geophysical surveys carried out in the study area and related days, equipment, frequencies, sampling and vertical accuracy.

Surveys R/V	Days	Multibeam	Frequency	Sampling	Tide gauge	Seismic	Range (m)	Vertical accuracy
Litus - 2013	8	EM2040 C	360 kHz	-	On site	-	12-24	0.2 m
Laguna P. - 2013	14	7125	400 kHz	-	On site	-	0.5-12	0.1 m
San Rocco - 2014	4	-	2-7 kHz	-	-	Chirp III	2-24	0.4 m
Litus - 2014	13	EM2040 C	360 kHz	Grab	On site	-	5-23	0.2 m
IHO - 2016	24	EM2040	300 kHz	Grab	On site	-	0.5-23	0.15 m

Table IIIA2: Grain size of the sediment samples collected from 2014 and 2016 ground-truth surveys. Sorting, skewness and kurtosis are referred to μm unit scale

SAMPLE	YEAR	SAMPLE TYPE	TEXTURAL GROUP	ENTROPYMAX	MEAN (μm)	GRAPHICAL SORTING	GRAPHICAL SKEWNESS	GRAPHICAL KURTOSIS	D50 (μm)	GRAVEL	SAND	MUD	CLAY
14_1	2014	Unimodal, Poorly Sorted	Sandy Mud	Group Mud	15.63	3.61	-0.10	1.01	17.04	0	12.8%	87.2%	6.4%
14_2	2014	Unimodal, Poorly Sorted	Muddy Sand	Group Sand	151.58	2.53	-0.45	1.98	171.09	0	85.7%	14.3%	1.3%
14_3	2014	Unimodal, Poorly Sorted	Sandy Mud	Group Mud	19.90	3.83	-0.16	0.89	22.68	0	21.1%	78.9%	5.5%
14_4	2014	Unimodal, Very Poorly Sorted	Sandy Mud	Group Mud	27.26	4.37	-0.14	0.97	30.94	0	30.2%	69.8%	4.8%
14_5	2014	Unimodal, Poorly Sorted	Sandy Mud	Group Mud	26.49	3.83	-0.15	0.99	29.69	0	27.1%	72.9%	4.1%
14_6	2014	Unimodal, Poorly Sorted	Mud	Group Mud	19.07	2.44	-0.44	1.47	23.09	0	0.4%	99.6%	4.9%
14_7	2014	Unimodal, Poorly Sorted	Mud	Group Mud	9.79	2.87	-0.21	0.91	11.23	0	0.2%	99.8%	8.7%
14_8	2014	Unimodal, Moderately Sorted	Sand	Group Sand	247.00	1.98	-0.33	2.12	252.12	0	92.5%	7.5%	0.6%
14_9	2014	Bimodal, Very Poorly Sorted	Sandy Mud	Group Mud	23.11	4.55	-0.01	0.94	22.40	0	25.5%	74.5%	5.4%
14_10	2014	Unimodal, Poorly Sorted	Mud	Group Mud	10.66	2.72	-0.29	0.97	12.67	0	0.0%	100.0%	7.5%
BM1	2016	Unimodal, Poorly Sorted	Muddy Sand	Group Sand	162.14	2.22	-0.39	2.23	171.39	0	89.2%	10.8%	1.2%
BM2	2016	Unimodal, Poorly Sorted	Mud	Group Mud	12.06	2.98	-0.18	1.01	13.50	0	3.4%	96.6%	7.0%
BM3	2016	Unimodal, Poorly Sorted	Muddy Sand	Group Sand	93.77	3.89	-0.65	1.43	163.60	0	75.0%	25.0%	2.5%
BM4	2016	Unimodal, Poorly Sorted	Mud	Group Mud	13.12	3.13	-0.15	1.03	14.56	0	6.4%	93.6%	6.5%
BM5	2016	Unimodal, Poorly Sorted	Sandy Mud	Group Mud	18.91	3.53	-0.11	1.07	20.73	0	15.7%	84.3%	5.1%
BM6	2016	Unimodal, Poorly Sorted	Sandy Mud	Group Mud	18.75	3.86	-0.07	0.91	19.21	0	20.2%	79.8%	5.6%
BM7	2016	Bimodal, Very Poorly Sorted	Muddy Sand	Group Sand	64.32	4.66	-0.64	0.81	129.80	0	61.9%	38.1%	3.3%
BM8	2016	Unimodal, Poorly Sorted	Muddy Sand	Group Sand	209.92	2.10	-0.39	2.55	216.21	0	89.6%	10.4%	1.0%

Table IIIA3: confusion matrix for the backscatter classification of 2014 survey.

		Ground-truth samples		Total classified	Producer accuracy	User accuracy
		Group S	Group M			
Classified samples	Group S	2	5	7	100	29
	Group M	0	3	3	38	100
Total ground-truth samples		2	8	10		
Overall Accuracy (%) = 50						

Table IIIA4: confusion matrix for the backscatter classification of 2016 survey.

		Ground-truth samples		Total classified	Producer accuracy	User accuracy
		Group S	Group M			
Classified samples	Group S	4	1	5	100	80
	Group M	0	3	3	75	100
Total ground-truth samples		4	4	8		
Overall Accuracy (%) = 87.5						

5. Study III: Short-term evolution of Po della Pila delta lobe from high-resolution multibeam bathymetry (2013-2016)

Table IIIA5: Changes in seafloor sediment classifications expressed as percentage of the study area (2.7 km²) overlapping in the three surveys. Gains and losses in sediment classes between years are attributed to swapping change and net change. *gp* = gain/persistence, *lp* = loss/persistence, *np* = net change/persistence.

2013-2014		2013	2014	Gain	Loss	Tot change	Persistence	Net change	Swap location	gp	lp	np
	Sand (%)	40	75	40	5	44.80	35	35.42	9.38	1.15	0.13	1.01
Mud (%)	60	25	5	40	44.80	20	-35.42	9.38	0.23	2.01	-1.77	
Tot	100	100	45	45	89.60	55	70.84	18.76				
2014-2016		2014	2016	Gain	Loss	Tot change	Persistence	Net change	Swap location	gp	lp	np
	Sand (%)	75	72	19	22	41.59	53	-3.26	38.33	0.36	0.42	-0.06
Mud (%)	25	28	22	19	41.59	5	3.26	38.33	4.49	3.83	0.65	
Tot	100	100	42	42	83.18	58	6.52	76.65				
2013-2016		2013	2016	Gain	Loss	Tot change	Persistence	Net change	Swap location	gp	lp	np
	Sand (%)	40	72	46	14	59.79	26	32.18	27.61	1.77	0.53	1.24
Mud (%)	60	28	14	46	59.79	14	-32.18	27.61	0.99	3.28	-2.30	
Tot	100	100	60	60	119.58	40	64.36	55.22				

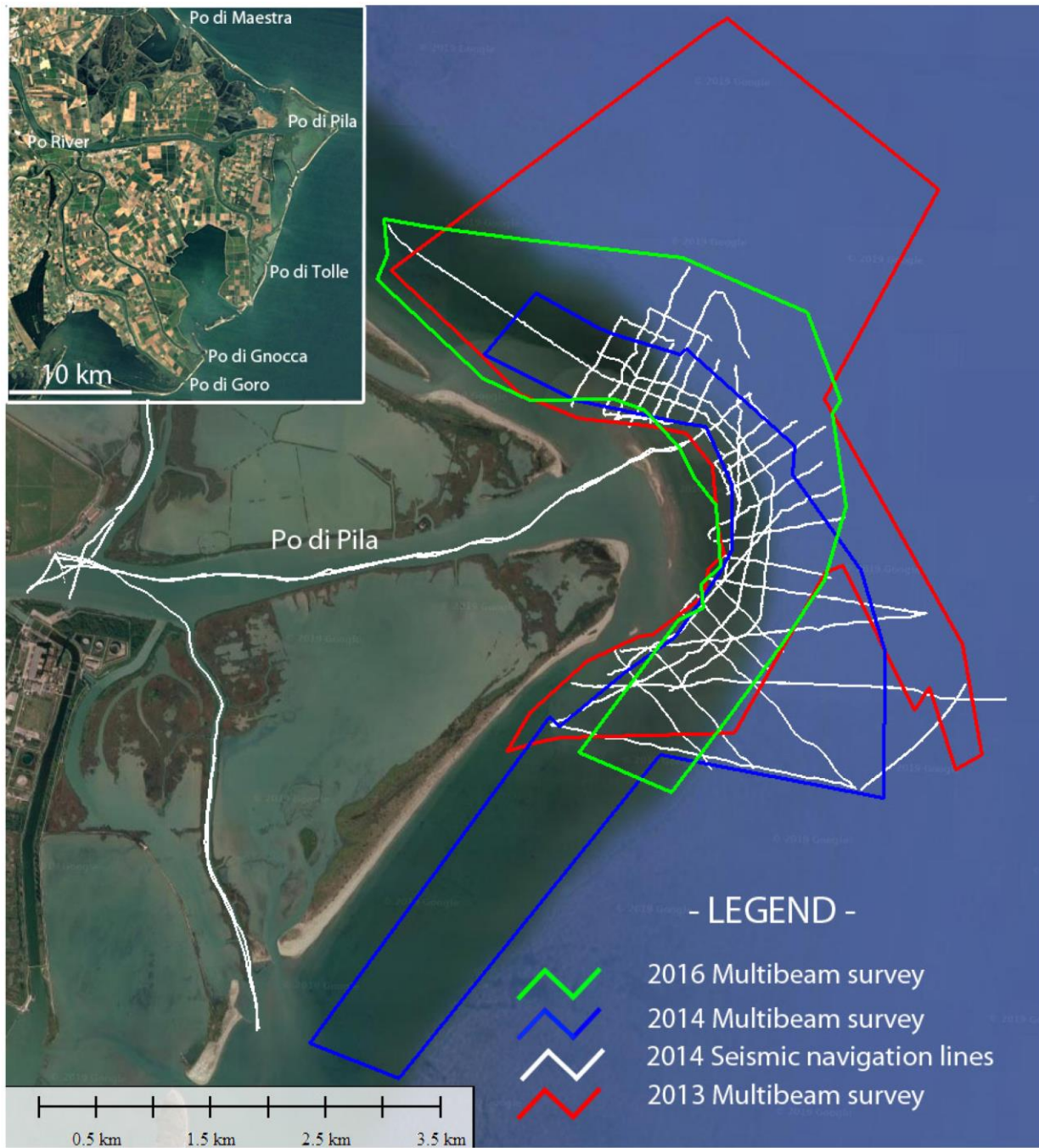


Fig. IIIA1: Coverage of multibeam surveys collected from 2013 to 2016 and location of the seismic lines recorded in 2014. For the location of the seismic profiles used in this work, see figure III9. In the inset, the five mouths of the modern delta are indicated.

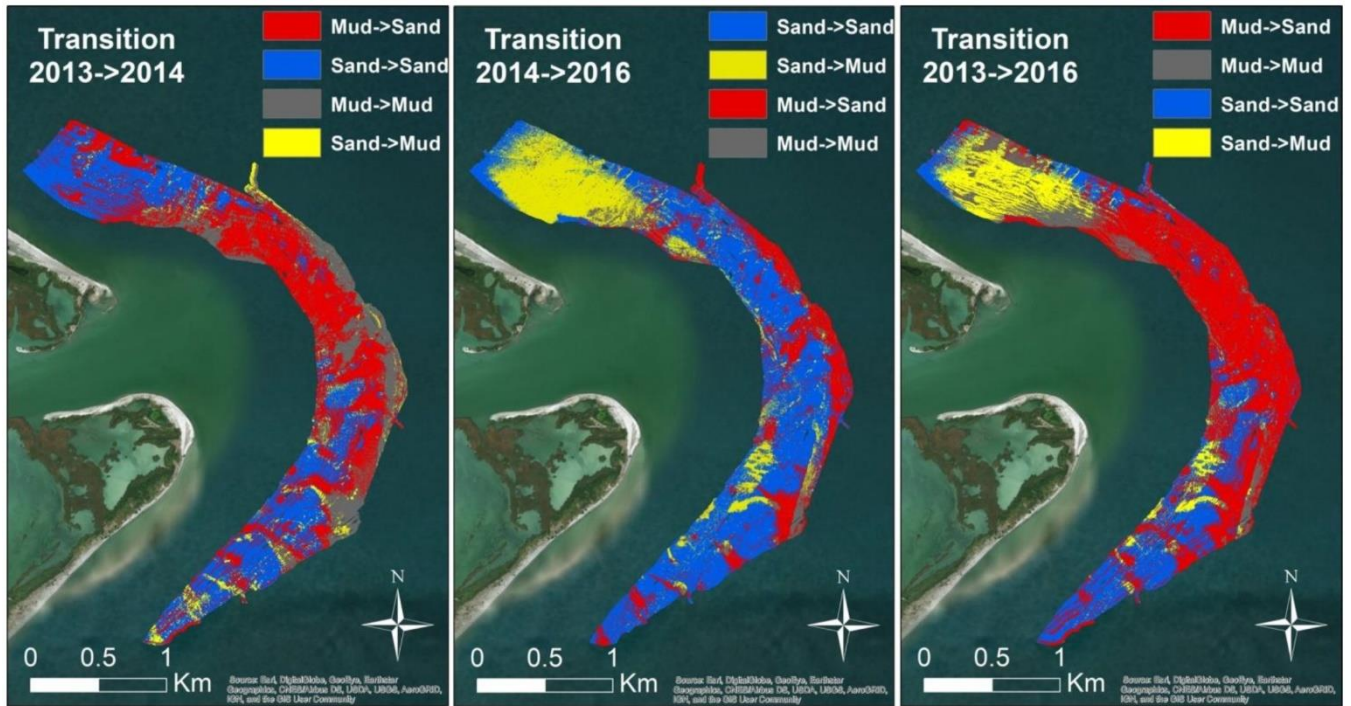


Fig. IIIA2: Evolution of superficial sediment distribution from backscatter classes between 2013- 2014, 2014-2016 and 2013-2016 in the overlapping area of surveys.

6. Discussion and conclusions

Through the combined analysis of the results of repeated MBES surveys and ground-truth data, we presented here a multidisciplinary study of the shallow water seafloors of high dynamic environments of the North Adriatic Sea. Whilst MBES have been used extensively in deep and open-sea waters, their application in shallow waters (< 10 m depth) is only very recent.

Specifically, we collected very high resolution data from two different areas of the North Adriatic Sea: the Chioggia inlet on the Venice Lagoon and Po River prodelta. We carried out the surveys in a comparable period of time (i.e. 2011-2016 Chioggia, 2013-2016 Po delta) but we documented that the evolution of the two areas is very different: while the investigated Po river prodelta area seems to be mainly driven by natural forces, the recent changes in the Chioggia inlet were induced by the human actions.

In Chioggia inlet we observed different consequences of the anthropogenic interventions. Starting from the 900 AD, during the Roman Empire, the Chioggia inlet was repeatedly subject to severe human-intervention to guarantee the channel navigability and the access to the internal harbor (Villatoro et al., 2010). Today, the modifications in the inlet are still ongoing, with the construction of the MoSE project: (i) the reduction of the channel cross-section, (ii) the construction of a breakwater, (iii) the renovation of the two lateral jetties, and (iv) the stabilization of the seabed with rock artifacts (rip-rap). The Chioggia tidal inlet represents indeed an example where human-induced processes have radically changed the seafloor over time.

The presence of the new hard structures in the inlet resulted in a new man-made benthic habitat, here named Artificial rock bed. This hard substratum habitat class, found in correspondence to the artificial structures and rip-rap, hosts a diversified and structurally complex biological community, in marked contrast with the adjacent soft-sedimentary habitats (Glasby et al., 2007). In fact, nearly all the hard substrata in the west coast of the northern Adriatic Sea are artificial. The ecological role of these habitats is not fully understood: despite they increment the spatial complexity and the surface available for colonization of benthic communities (Svane and Petersen, 2001) and play as refugia, feeding grounds and nursery areas for fish populations (Brickhill et al., 2005; Clynick et al., 2007), they can promote the settlement of non-indigenous species (Wasson et al., 2005; Glasby et al., 2007). The presence itself of this habitat remove space for the typical lagoonal biocoenosis (e.g. seagrass meadows) that were already endangered by dredging activities (Pranovi and Giovanardi,

1994), eutrophication (Sfriso and Marcomini, 1996), clams fisheries (Sfriso et al., 2005b; Solidoro et al., 2010), pollutants dispersal (Dalla Valle et al., 2005; Frignani et al., 2005) and climate change (Cossarini et al., 2008; Solidoro et al., 2010). The recent MoSE works at the inlet have greatly extended this habitat, in particular with the construction of the breakwater and by filling a 400 meters long section of the channel seabed from side to side.

Another indirect consequence of the human modification in the inlet is the generation of large scour holes. These erosive depressions can have natural origins (e.g. vortex action in the confluence of tidal channels) or can be linked to the artificial modifications (e.g. placement of poles in the seabed, construction of pointed structures).

Scour holes in correspondence of hard coastal structures were documented in the Venice Lagoon already in the historical military hydro-topographic surveys of Denaix of 1810 ca. (Magrini, 1934). For example, the lagoonal Chioggia scour hole is considerably ancient and its location/shape is well documented in the maps of Denaix and Magistrato alle Acque of 1927, 1970 and 2002 (Magrini, 1934; MAC-CVN, 2004). Analogous large morphologies were observed in similar position in Lido-Treporti and Malamocco inlets (Balletti, 2006).

However, the scour holes can also be very recent: in Chioggia and Lido-Treporti we described their formation after the MoSE works (Madricardo et al., 2017; Toso et al., 2019). The construction of the seaside breakwater in Chioggia inlet, built between 2003 and 2006, produced significant changes in the hydrodynamic configuration of the flow, increasing the scouring, as suggested by Ghezzi et al. (2010). The ebb tide flow now splits into two faster jets: the main one parallel to the navigation channel with direction west-east and a secondary one that heads south. The narrowing of the inlet section by the MoSE infrastructures, (i.e. navigation locks and refuge harbors) increased the flow velocity (Ferrarin et al., 2015). This human alteration triggered two main processes: (i) the general coarsening of the seabed sediments along the inlet channel in response of the increased bottom shear stress, and (ii) the formation of two deep scour holes at breakwater tips. In addition, the load of the new structures that support the MoSE has increased the subsidence rate, showing a deepening up to 40 mm/year in some sectors of the inlet (Tosi et al., 2013).

In this Phd study, we attested how rapidly can be formed a scour hole after the construction of a hard structure in the middle of an inlet entrance. These man-induced concave features, that were not present in Chioggia before breakwater establishment (Villatoro, 2010; Villatoro et al., 2010), grew rapidly from 2006 (end of breakwater construction) and almost doubled their extension between 2011 and 2016. These scour holes could even endanger the stability of the breakwater

itself that will probably require a continuous nourishment at its base. We estimated that after 2006, the overall erosion associated to these two morphologies is equal to about 746,000 m³ of sediments. This erosion however seems to be recently slowed. This could be related to the fact that the scouring reached an ancient compacted muddy layer that could belong to the Pleistocene limit (“caranto”) and that is already described in the area at depths of 15 m (Zecchin et al., 2008). This hypothesis however must be confirmed after further sampling and sediment analyses.

Previously studies found that the major mechanism responsible for the scouring was the formation of lee-wake vortices in each half period of the waves (Sumer and Fredsøe, 1997; Fredsøe and Sumer, 1997; Sumer et al., 2001; Noormets et al., 2006). The depth of the scour holes was likely substantially enhanced by the presence of co-directional currents that contribute to the wave action.

As previously mentioned, the artificial modification of the inlet triggered also a constant increase in the substrata grain-size. Indeed, we mapped a large seabed area with a thick coverage of coarse shells (Sandy gravel_gravelly sand class). The substratum origin is linked to the strong bottom currents: the load carrying capacity is indeed able to remove the smaller particles (i.e. mud and sand), but not the coarser ones (i.e. shells) that remain on the bottom. This process creates a sort of “armored seabed”. This coarse shell sediment class has already been locally described in the Venice Lagoon (Monteale-Gavazzi et al., 2016) and its presence is becoming widespread, as observed also by Stellino (2015) in the Treporti Channel (northern lagoon) and Toso et al. (2019) in the Lido inlet.

Amos et al. (2010) showed that the sediment flux through the Venice inlets is dominated by bed-load transport. By analyzing the dune fields characteristics, we confirmed in this PhD study that a great bed-load transport is acting in the Chioggia inlet. Indeed, the strong asymmetry towards the sea of larger dunes found in the study area is related to the direction of the residual currents (e.g. Fraccascia et al., 2016) and it suggests a net seaward bottom transport. According to Dalrymple and Rhodes (1995), Hennings et al. (2000) and Cuadrado and Gomez (2011), large and very large dunes are generally asymmetric in the direction of net bottom sediment transport. The seaward asymmetry measured in Chioggia reflects the dominance of the ebb tide current. This is in agreement with the results of Ferrarin et al. (2015) who found in the last 70 years an increased amplitude of the major tidal components and a shift of the Venice Lagoon tidal asymmetry towards ebb dominance.

The repeated surveys documented the recent shrinking of the smaller dune fields in the study area. The same reduction of the dune fields was observed by Toso et al. (2019) in the Lido inlet. Moreover, the comparison of the surveys allowed the calculation of the migration rate of the large dunes that between the 2011 and 2013 reached a maximum value of 44 m year^{-1} (0.12 m day^{-1}). This value is much smaller than the one found in other natural tidal inlets: for example, Fraccascia et al. (2016) found a migration rate of 3 m year^{-1} (8.22 mm day^{-1}) for dunes with similar dimension in a tidal inlet in the Wadden Sea (Denmark) characterized by comparable water current. However, this tidal channel is completely natural, without jetties and with the possibility to expand through lateral shoals in cases of high tides or storm events. Differently, the hard armored set up of Chioggia inlet imposed an increase of tidal prism during flooding events that could have increased the bedload sediment transport along the inlet channel. Indeed, these high migration rate values have not been registered in correspondence of large dunes inside the lagoon, where the water has the possibility to expand through the neighbor mudflats. However, the dunes migration in the inlet seems to slow down after the 2013. This different evolution in the two time span (2011-2013 and 2013-2016) could be related to the fact that after a first phase of recalibration, the system starts to gain a new equilibrium that is partially reached after the 2013. However, as observed by Toso et al. (2019), the difference could also be related to the meteorological conditions that induced an increase of the tidal prism as a consequence of big storms on November 2012 and February 2013.

Finally, the anthropogenic pressures in the Chioggia inlet are demonstrated by the presence of numerous objects placed voluntarily or not on the seabed bottom. We mapped a large variety of objects, mainly driven by rip-rap debris and bricola remains. This is the first high-resolution mapping of anthropogenic object in the Chioggia area (see Madricardo et al., 2019 for detail) and it is a forefront study for the evaluation of the human footprints in the coastal regions. Indeed, considering the large attention that is gaining the issue of abandoned litter in the oceans, the mapping and sequent removal of these objects (e.g. marGnet project in the North Adriatic Sea – www.margnet.eu) play an important role in the coastal management.

A different evolution is observed in the Po delta seafloor. The scientific studies on the deltas in the world are generally based on a modeling approach. For examples, several researches focus on the hydrodynamic configuration (e.g. Canestrelli et al., 2010; Fagherazzi et al., 2014; Maicu et al., 2018). In some cases, ecology and geomorphology are merged together to predict the evolution of deltas

and salt marshes (e.g. D'Alpaos et al., 2006; Mariotti and Fagherazzi, 2010; Fagherazzi et al., 2013). Other studies use satellite image analysis for the study of the deltas (e.g. Syvitski et al., 2012; Braga et al., 2018; Bellafiore et al. 2019). However, to our knowledge, high resolution MBES mapping of the subaqueous morphostructures of the Po delta have never been done before. There are only very few similar studies in other deltas, such as the study by Prior and Coleman (1982) who mapped the Mississippi Delta with side-scan sonars and sub-bottom profilers and the more recent studies by Girardclos et al. (2012), Arantegui et al. (2012) and Chaytor et al. (2017).

In the Po prodelta we applied the same approach used in Chioggia inlet and we described the main changes due to natural and anthropogenic forcings. The mapping of the Po prodelta features realized in this PhD is the first ever done, indeed the morpho-bathymetry of this area was partially unexplored before. It is well known that the current delta layout is a result of numerous anthropogenic actions, e.g. modification of the river discharge, sediment flux altering on the catchment, magnification of the subsidence due to methane extraction (Cencini, 1998; Trincardi et al., 2004). Despite the delta area is today quite anthropized with the presence of cities, agriculture and industrial and economical activities (Tosi, 2013), the human footprint in the prodelta seabed is not so evident (except for some trawling furrows in the deeper sectors). The absences of important human signatures can however be explained by the relative recent age of the prodelta (Di Giulio et al., 2017) and its extreme level of dynamism (Trincardi et al., 2004).

The characterization on very high resolution of the modern prodelta seabed on a 3-years time frame (2013-2016) shows substantially a geomorphological change of the seafloor with a complex configuration of the morphostructures, particularly in the shallow waters (i.e. < 15 m) where most of the along-shelf distribution of the sediment input occurs (Friedrichs and Scully, 2007).

At large scale, several morpho-sedimentary processes are affecting the delta, varying quickly the depositional and erosive phenomena. Generally, the Adriatic longshore currents (WACC) influences the seabed features, setting a constant net southward sediment transport and a consequent marked asymmetry of the entire delta front. This marked bedform asymmetry in agreement with Adriatic circulation has been already observed in other parts of Italian Adriatic coastal seafloors (Cattaneo et al., 2003; Bonaldo et al., 2016).

On smaller scale, the recognized morphological features (especially those in shallow water, i.e. in the first 10 m) underwent rapid shifts and alternating phases of construction/obliteration. They reflect the interplay between the river sediment discharge and the reworking action of the sea (e.g.

tides, currents and waves) that contribute to sediment resuspension and dispersal (Maillet et al., 2006; Rodriguez et al., 2000). The most evident example is the deposition of a 4 m thick muddy body in the northern part of the Po lobe close to the northern discharge channel. This elongated and asymmetrical bedform seems to be originated after the strong river flood event of November 2014 and it will be naturally reshaped by waves and currents.

From Chirp data, we see that the submerged mouth consists of composite lobes shaped during rapid flood events. Similar deposition processes of detrital material after short-time flood events (also called flash-flood deposits) were also observed in the Mississippi prodelta (Tye and Coleman, 1989) and in the Fiumara mouth in the western Sicily Strait (Casalbore et al., 2011). These chaotic deposits, located near the main Po distributary channels, are subsequently reworked to feed the radial bar systems, eroded or preserved, even in the stratigraphic record. In the survey period, the mouth bar grew and emerged, as detected by satellite image analysis and as pointed out by Ninfo et al. (2018) who described an overall delta progradation between 2015 and 2017. In front of the river mouth, the patches of deposition/erosion indicate the southward migration of the radial bars, while a generalized deepening of the seafloor (≈ 0.5 m) is described on southernmost and easternmost parts of the delta lobe, suggesting the role of active subsidence, that appears not overwhelmed by sediment supply. This deepening is only marginally due to the well-known accelerated subsidence, but it is also probably linked to the presence of muddy sediments rich of water and organic content. These materials are able to rapidly fluidize and/or consolidate in extremely short time, as attested by the numerous presences of collapse and gravity instability features. According to Prior and Coleman (1982) that observed similar features on the Mississippi delta, the high organic content of muddy sediments makes the development of methanogenesis processes highly plausible and this suggests that the interstitial methane gas may have a strong impact on the morphological development of the Pila lobe's superficial instabilities.

To conclude, in this PhD study I described in detail their seafloor features of two study highly dynamic areas in terms of seabed sediment transport. I assessed quantitatively their evolution over time highlighting the main active processes in the time span of the investigation.

The methodology presented in the thesis turned out to be very effective in both areas. The results obtained from the combined analysis of acoustic data and ground-truth information has proven to be appropriate to study coastal seafloors that conventionally presented research difficulties for shallow water areas, morphological complexity and high turbidity.

As a final remark, this study showed that, also for shallow marine environments, human activities can be a morphogenetic process (Marriner et al., 2012; Kołodyńska-Gawrysiak and Poesen, 2017; Poesen, 2018) that must be taken into account in the management of the coastal areas.

7. References

- Albani, A. D., Favero, V. M., & Barbero, R. S. (1998). Distribution of sediment and benthic foraminifera in the Gulf of Venice, Italy. *Estuarine, Coastal and Shelf Science*, 46(2), 251-265.
- Amorosi, A., & Milli, S. (2001). Late Quaternary depositional architecture of Po and Tevere river deltas (Italy) and worldwide comparison with coeval deltaic successions. *Sedimentary geology*, 144(3-4), 357-375.
- Amorosi, A., Centineo, M. C., Colalongo, M. L., Pasini, G., Sarti, G., & Vaiani, S. C. (2003). Facies architecture and latest Pleistocene–Holocene depositional history of the Po Delta (Comacchio area), Italy. *The Journal of Geology*, 111(1), 39-56.
- Amorosi, A., Maselli, V., & Trincardi, F. (2016). Onshore to offshore anatomy of a late Quaternary source-to-sink system (Po Plain–Adriatic Sea, Italy). *Earth-Science Reviews*, 153, 212-237.
- Amos, C. L., Villatoro, M., Helsby, R., Thompson, C. E. L., Zaggia, L., Umgiesser, G., ... & Rizzetto, F. (2010). The measurement of sand transport in two inlets of Venice lagoon, Italy. *Estuarine, Coastal and Shelf Science*, 87(2), 225-236.
- Antonioli, F., Anzidei, M., Amorosi, A., Presti, V. L., Mastronuzzi, G., Deiana, G., ... & Marsico, A. (2017). Sea-level rise and potential drowning of the Italian coastal plains: Flooding risk scenarios for 2100. *Quaternary Science Reviews*, 158, 29-43.
- Arantegui, A., Corella, J. P., Loizeau, J. L., Anselmetti, F. S., & Girardclos, S. (2012). Environmental and human impact on the sedimentary dynamic in the Rhone Delta subaquatic canyons (France-Switzerland). In *EGU General Assembly Conference Abstracts* (Vol. 14, p. 6293).
- ARPA Emilia-Romagna, 2002. Stato del litorale emiliano-romagnolo all'anno 2002. Quaderni di Arpa, Arpa Linea Editoriale, Italy, p.120
- Artegiani, A., Paschini, E., Russo, A., Bregant, D., Raicich, F., & Pinardi, N. (1997). The Adriatic Sea general circulation. Part I: Air–sea interactions and water mass structure. *Journal of physical oceanography*, 27(8), 1492-1514.
- Balletti C. 2006. Digital elaborations for cartographic reconstruction: the territorial transformations of Venice harbours in historical maps. *e-Perimetron* 1(4): 274–286.
- Barbier, E. B., Hacker, S. D., Kennedy, C., Koch, E. W., Stier, A. C., & Silliman, B. R. (2011). The value of estuarine and coastal ecosystem services. *Ecological monographs*, 81(2), 169-193.
- Battaglia, M., Murray, M. H., Serpelloni, E., & Bürgmann, R. (2004). The Adriatic region: An independent microplate within the Africa-Eurasia collision zone. *Geophysical Research Letters*, 31(9).
- Bellafiore, D., Umgiesser, G., & Cucco, A. (2008). Modeling the water exchanges between the Venice Lagoon and the Adriatic Sea. *Ocean Dynamics*, 58(5-6), 397-413.

- Bellafiore, D., & Umgiesser, G. (2010). Hydrodynamic coastal processes in the North Adriatic investigated with a 3D finite element mode. *Ocean Dynam*, 60, 255273.
- Bellafiore, D., Ferrarin, C., Braga, F., Zaggia, L., Maicu, F., Lorenzetti, G., ... & De Pascalis, F. (2019). Coastal mixing in multiple-mouth deltas: A case study in the Po delta, Italy. *Estuarine, Coastal and Shelf Science*, 106254.
- Blondel, P. (2010). *The handbook of sidescan sonar*. Springer Science & Business Media.
- Bonaldo, D., Benetazzo, A., Bergamasco, A., Campiani, E., Foglini, F., Sclavo, M., ... & Carniel, S. (2016). Interactions among Adriatic continental margin morphology, deep circulation and bedform patterns. *Marine Geology*, 375, 82-98.
- Bonardi, M., Breda, A., Bonsembiante, N., Tosi, L., Rizzetto, F., 2005. Spatial variations of the superficial sediment characteristics of the lagoon of Venice, Italy. *Scientific research and safeguarding of V enice, Research programme*, 131-144.
- Bondesan, M., & Simeoni, U. (1983). *Dinamica e analisi morfologica statistica dei fondali del delta del Po e alle foci dell'Adige e del Brenta*.
- Book, J. W., Perkins, H., & Wimbush, M. (2009). North Adriatic tides: observations, variational data assimilation modeling, and linear tide dynamics. *Geofizika*, 26(2), 115-143.
- Braga, F., Zaggia, L., Bellafiore, D., Bresciani, M., Giardino, C., Lorenzetti, G., ... & Brando, V. E. (2017). Mapping turbidity patterns in the Po river prodelta using multi-temporal Landsat 8 imagery. *Estuarine, Coastal and Shelf Science*, 198, 555-567.
- Brambati, A., Marocco, R., Catani, G., Carobene, L., & Lenardon, G. (1978). Stato delle conoscenze dei litorali dell'Alto Adriatico e criteri di intervento per la loro difesa. *Memorie della Societa Geologica Italiana*, 19, 389-398.
- Brambati, A., Marocco, R., & Fanzutti, G. P. (1983). A new sedimentological and textural map of Northern and Central Adriatic Sea.
- Brickhill, M. J., Lee, S. Y., & Connolly, R. M. (2005). Fishes associated with artificial reefs: attributing changes to attraction or production using novel approaches. *Journal of Fish Biology*, 67, 53-71.
- Brown, C. J., & Blondel, P. (2009). The application of underwater acoustics to seabed habitat mapping.
- Brown, C. J., Smith, S. J., Lawton, P., & Anderson, J. T. (2011). Benthic habitat mapping: A review of progress towards improved understanding of the spatial ecology of the seafloor using acoustic techniques. *Estuarine, Coastal and Shelf Science*, 92(3), 502-520.
- Bruun, P. (1986). Morphological and navigational aspects of tidal inlets on littoral drift shores. *Journal of Coastal Research*, 123-145.
- Bulleri F, Chapman MG. 2004. Intertidal assemblages on artificial and natural habitats in marinas on the north-west coast of Italy. *Marine Biology* 145(2): 381–391.

- Bulleri F, Chapman MG. 2010. The introduction of coastal infrastructure as a driver of change in marine environments. *Journal of Applied Ecology* 47(1): 26–35.
- Canestrelli, A., Fagherazzi, S., Defina, A., & Lanzoni, S. (2010). Tidal hydrodynamics and erosional power in the Fly River delta, Papua New Guinea. *Journal of Geophysical Research: Earth Surface*, 115(F4).
- Cappucci, S., Amos, C. L., Hosoe, T., & Umgiesser, G. (2004). SLIM: a numerical model to evaluate the factors controlling the evolution of intertidal mudflats in Venice Lagoon, Italy. *Journal of Marine Systems*, 51(1-4), 257-280.
- Carbognin, L., Teatini, P., Tosi, L., Strozzi, T., & Tomasin, A. (2011). Present relative sea level rise in the Northern Adriatic coastal area.
- Carniello, L., Defina, A., & D'Alpaos, L. (2009). Morphological evolution of the Venice lagoon: Evidence from the past and trend for the future. *Journal of Geophysical Research: Earth Surface*, 114(F4).
- Carniello, L., Defina, A., & D'Alpaos, L. (2012). Modeling sand-mud transport induced by tidal currents and wind waves in shallow microtidal basins: Application to the Venice Lagoon (Italy). *Estuarine, Coastal and Shelf Science*, 102, 105-115.
- Carniello, L., Silvestri, S., Marani, M., D'Alpaos, A., Volpe, V., & Defina, A. (2014). Sediment dynamics in shallow tidal basins: In situ observations, satellite retrievals, and numerical modeling in the Venice Lagoon. *Journal of Geophysical Research: Earth Surface*, 119(4), 802-815.
- Casalbore, D., Chiocci, F. L., Mugnozsa, G. S., Tommasi, P., & Sposato, A. (2011). Flash-flood hyperpycnal flows generating shallow-water landslides at Fiumara mouths in Western Messina Strait (Italy). *Marine Geophysical Research*, 32(1-2), 257.
- Cattaneo, A., Correggiari, A., Langone, L., & Trincardi, F. (2003). The late-Holocene Gargano subaqueous delta, Adriatic shelf: sediment pathways and supply fluctuations. *Marine Geology*, 193(1-2), 61-91.
- Cattaneo, A., Trincardi, F., Asioli, A., & Correggiari, A. (2007). The Western Adriatic shelf clinoform: energy-limited bottomset. *Continental Shelf Research*, 27(3-4), 506-525.
- Cencini, C. (1998). Physical processes and human activities in the evolution of the Po delta, Italy. *Journal of Coastal Research*, 14(3).
- Chapman, M. G. (2003). Paucity of mobile species on constructed seawalls: effects of urbanization on biodiversity. *Marine Ecology Progress Series*, 264, 21-29.
- Chapman, M. G. (2012). Restoring intertidal boulder-fields as habitat for “specialist” and “generalist” animals. *Restoration Ecology*, 20(2), 277-285.
- Chaytor, J. D., Baldwin, W. E., Danforth, W. W., Bentley, S. J., Miner, M. D., & Damour, M. (2017, December). New High-Resolution Multibeam Mapping and Seismic Reflection Imaging of Mudflows on the Mississippi River Delta Front. In AGU Fall Meeting Abstracts.

- Clynick, B. G., Chapman, M. G., & Underwood, A. J. (2007). Effects of epibiota on assemblages of fish associated with urban structures. *Marine Ecology Progress Series*, 332, 201-210.
- Coll, M., Piroddi, C., Steenbeek, J., Kaschner, K., Lasram, F. B. R., Aguzzi, J., ... & Danovaro, R. (2010). The biodiversity of the Mediterranean Sea: estimates, patterns, and threats. *PloS one*, 5(8), e11842.
- Consorzio Venezia Nuova (1989). Progetto preliminare di massima delle opere alle bocche, Volume 2, Descrizione dell'ecosistema, Parte II. Ministero dei Lavori Pubblici, Magistrato alle Acque di Venezia.
- Correggiari, A., Field, M. E., & Trincardi, F. (1996). Late Quaternary transgressive large dunes on the sediment-starved Adriatic shelf. *Geological Society, London, Special Publications*, 117(1), 155-169.
- Correggiari, A., Cattaneo, A., & Trincardi, F. (2005). The modern Po Delta system: lobe switching and asymmetric prodelta growth. *Marine Geology*, 222, 49-74.
- Correggiari, A., Perini, L., Foglini, F., Remia A., Gallerani A., Campiani E., Luciani P. (2011) Research and exploitation of shelf marine sand deposit for coastal renourishment: geodatabase guidelines from Emilia-Romagna experience. 7th EUREGEO, Bologna Italy June 12-15th 2012.
- Cossarini, G., Libralato, S., Salon, S., Gao, X., Giorgi, F., & Solidoro, C. (2008). Downscaling experiment for the Venice lagoon. II. Effects of changes in precipitation on biogeochemical properties. *Climate Research*, 38(1), 43-59.
- Costanza, R., De Groot, R., Farber, S., Grasso, M., Hannon, B., Limburg, K., ... & Van Den Belt, M. (1998). The value of the world's ecosystem services and natural capital. *Ecological economics*, 25(1), 3-15.
- Cozzi, S., & Giani, M. (2011). River water and nutrient discharges in the Northern Adriatic Sea: current importance and long term changes. *Continental Shelf Research*, 31(18), 1881-1893.
- Crossland, C. J., Baird, D., Ducrotoy, J. P., Lindeboom, H., Buddemeier, R. W., Dennison, W. C., ... & Swaney, D. P. (2005). The coastal zone—a domain of global interactions. In *Coastal fluxes in the Anthropocene* (pp. 1-37). Springer, Berlin, Heidelberg.
- Cuadrado, D. G., Gómez, E. A., & Ginsberg, S. S. (2003). Large transverse bedforms in a mesotidal estuary. *Latin American Journal of Sedimentology and Basin Analysis*, 10(2), 163-172.
- Cucco, A., & Umgiesser, G. (2006). Modeling the Venice Lagoon residence time. *Ecological modelling*, 193(1-2), 34-51.
- Da Lio, C., & Tosi, L. (2019). Vulnerability to relative sea-level rise in the Po river delta (Italy). *Estuarine, Coastal and Shelf Science*, 106379.
- Dalla Valle, M., Marcomini, A., Jones, K. C., & Sweetman, A. J. (2005). Reconstruction of historical trends of PCDD/Fs and PCBs in the Venice Lagoon, Italy. *Environment international*, 31(7), 1047-1052.
- Dalrymple, R. W., & Rhodes, R. N. (1995). Estuarine dunes and bars. In *Developments in sedimentology* (Vol. 53, pp. 359-422). Elsevier.

- De Roo, S., & Troch, P. (2015). Evaluation of the Effectiveness of a Living Shoreline in a Confined, Non-Tidal Waterway Subject to Heavy Shipping Traffic. *River research and applications*, 31(8), 1028-1039.
- De Falco, G., Tonielli, R., Di Martino, G., Innangi, S., Simeone, S., & Parnum, I. M. (2010). Relationships between multibeam backscatter, sediment grain size and *Posidonia oceanica* seagrass distribution. *Continental Shelf Research*, 30(18), 1941-1950.
- Defendi, V., Kovačević, V., Arena, F., & Zaggia, L. (2010). Estimating sediment transport from acoustic measurements in the Venice Lagoon inlets. *Continental shelf research*, 30(8), 883-893.
- Elliott, M., & Cutts, N. D. (2004). Marine habitats: loss and gain, mitigation and compensation. *Marine Pollution Bulletin*, 9(49), 671-674.
- Fagherazzi, S., Fitzgerald, D. M., Fulweiler, R. W., Hughes, Z., Wiberg, P. L., McGlathery, K. J., ... & Johnson, D. S. (2013). Ecogeomorphology of tidal flats.
- Fagherazzi, S., Mariotti, G., Banks, A. T., Morgan, E. J., & Fulweiler, R. W. (2014). The relationships among hydrodynamics, sediment distribution, and chlorophyll in a mesotidal estuary. *Estuarine, Coastal and Shelf Science*, 144, 54-64.
- Ferrari, R., McKinnon, D., He, H., Smith, R., Corke, P., González-Rivero, M., ... & Upcroft, B. (2016). Quantifying multiscale habitat structural complexity: a cost-effective framework for underwater 3D modelling. *Remote Sensing*, 8(2), 113.
- Ferrarin, C., Tomasin, A., Bajo, M., Petrizzo, A., & Umgiesser, G. (2015). Tidal changes in a heavily modified coastal wetland. *Continental Shelf Research*, 101, 22-33.
- Ferrini, V. L., & Flood, R. D. (2006). The effects of fine-scale surface roughness and grain size on 300 kHz multibeam backscatter intensity in sandy marine sedimentary environments. *Marine Geology*, 228(1-4), 153-172.
- Fiaschi, S., Fabris, M., Floris, M., & Achilli, V. (2018). Estimation of land subsidence in deltaic areas through differential SAR interferometry: the Po River Delta case study (Northeast Italy). *International journal of remote sensing*, 39(23), 8724-8745.
- Filatova, T., Voinov, A., & van der Veen, A. (2011). Land market mechanisms for preservation of space for coastal ecosystems: an agent-based analysis. *Environmental Modelling & Software*, 26(2), 179-190.
- Fonseca, L., Mayer, L., Orange, D., & Driscoll, N. (2002). The high-frequency backscattering angular response of gassy sediments: model/data comparison from the Eel River Margin, California. *The Journal of the Acoustical Society of America*, 111(6), 2621-2631.
- Fontolan, G., Pillon, S., Quadri, F. D., & Bezzi, A. (2007). Sediment storage at tidal inlets in northern Adriatic lagoons: Ebb-tidal delta morphodynamics, conservation and sand use strategies. *Estuarine, Coastal and Shelf Science*, 75(1-2), 261-277.
- Fox, J. M., Hill, P. S., Milligan, T. G., & Boldrin, A. (2004). Flocculation and sedimentation on the Po River Delta. *Marine Geology*, 203(1-2), 95-107.

- Fredsøe, J., & Sumer, B. M. (1997). Scour at the round head of a rubble-mound breakwater. *Coastal engineering*, 29(3-4), 231-262.
- Friedrichs, C. T., & Scully, M. E. (2007). Modeling deposition by wave-supported gravity flows on the Po River prodelta: from seasonal floods to prograding clinoforms. *Continental Shelf Research*, 27(3-4), 322-337.
- Frignani, M., Bellucci, L. G., Favotto, M., & Albertazzi, S. (2005). Pollution historical trends as recorded by sediments at selected sites of the Venice Lagoon. *Environment International*, 31(7), 1011-1022.
- Foster-Smith, B., Connor, D. Davies, J. (2007): What is habitat mapping? In: MESH Guide to Habitat Mapping, MESH Project, 2007, JNCC, Peterborough.
- Fraccascia, S., Winter, C., Ernsten, V. B., & Hebbeln, D. (2016). Residual currents and bedform migration in a natural tidal inlet (Knudedyb, Danish Wadden Sea). *Geomorphology*, 271, 74-83.
- Frignani, M., Langone, L., Ravaioli, M., Sorgente, D., Alvisi, F., & Albertazzi, S. (2005). Fine-sediment mass balance in the western Adriatic continental shelf over a century time scale. *Marine Geology*, 222, 113-133.
- Gačić, M., Mosquera, I. M., Kovačević, V., Mazzoldi, A., Cardin, V., Arena, F., & Gelsi, G. (2004). Temporal variations of water flow between the Venetian lagoon and the open sea. *Journal of Marine Systems*, 51(1-4), 33-47.
- Ghezzi, M., Guerzoni, S., Cucco, A., & Umgiesser, G. (2010). Changes in Venice Lagoon dynamics due to construction of mobile barriers. *Coastal Engineering*, 57(7), 694-708.
- Girardclos, S., Hilbe, M., Corella, J. P., Loizeau, J. L., Kremer, K., DelSontro, T., ... & Anselmetti, F. S. (2012). Searching the Rhone delta channel in Lake Geneva since François-Alphonse Forel. *Arch Sci*, 65, 103-118.
- Glasby, T. M., Connell, S. D., Holloway, M. G., & Hewitt, C. L. (2007). Nonindigenous biota on artificial structures: could habitat creation facilitate biological invasions?. *Marine biology*, 151(3), 887-895.
- Gugliuzzo, E. (2018). The "Serenissima" at hazard: the Historical Phenomenon of Acqua Alta in Venice. *Humanities*, 6(2), 33-45.
- Hayes, M. O. (1980). General morphology and sediment patterns in tidal inlets. *Sedimentary geology*, 26(1-3), 139-156.
- Hennings, I., Lurin, B., Vernemmen, C., & Vanhessche, U. (2000). On the behaviour of tidal current directions due to the presence of submarine sand waves. *Marine Geology*, 169(1-2), 57-68.
- Holmes, K. W., Van Niel, K. P., Radford, B., Kendrick, G. A., & Grove, S. L. (2008). Modelling distribution of marine benthos from hydroacoustics and underwater video. *Continental Shelf Research*, 28(14), 1800-1810.
- Homrani, S., Le Dantec, N., Floc'h, F., Franzetti, M., Delacourt, C., Sedrati, M., & Winter, C. (2019). Multi time-scale morphological evolution of a shell sand, dune bank in a shallow mesotidal environment. *MARID VI*, 121.
- Hughes Clarke, J., Brucker, S., Muggah, J., Hamilton, T., Cartwright, D., Church, I., & Kuus, P. (2012). Temporal progression and spatial extent of mass wasting events on the Squamish prodelta slope. In *Landslides and engineered slopes: Protecting society through improved understanding* (pp. 1091-1096). Taylor and Francis Group London.

- IMAGE. (2006) Dipartimento di ingegneria idraulica, marittima, ambientale e geotecnica – Università di Padova, 2006. Valutazioni preliminari degli effetti idrodinamici dovuti all'incremento delle resistenze localizzate alle bocche di porto della Laguna di Venezia. Comune di Venezia, 1-62.
- Jeuken, M. C. J. L., & Wang, Z. B. (2010). Impact of dredging and dumping on the stability of ebb–flood channel systems. *Coastal Engineering*, 57(6), 553-566.
- Jong, C. d., Lachapelle, G., Skone, S., & Elema, I. (2010). *Hydrography*. Delft: DUP Blue Print.
- Katayama, T., Irie, I., & Kawakami, T. (1974). Performance of Offshore Breakwaters of the Niigata Coast. *Coastal Engineering in Japan*, 17(1), 129-139.
- Kerner M. 2007. Effects of deepening the Elbe Estuary on sediment regime and water quality. *Estuarine, Coastal and Shelf Science* 75(4): 492–500.
- Kjerfve, B. (1994). Coastal lagoons. In Elsevier oceanography series (Vol. 60, pp. 1-8). Elsevier.
- Knights, A. M., Koss, R. S., & Robinson, L. A. (2013). Identifying common pressure pathways from a complex network of human activities to support ecosystem-based management. *Ecological Applications*, 23(4), 755-765.
- Kołodzyńska-Gawrysiak R, Poesen J. 2017. Closed depressions in the European loess belt – natural or anthropogenic origin? *Geomorphology* 288: 111–128.
- Kostylev, V. E., Todd, B. J., Fader, G. B., Courtney, R. C., Cameron, G. D., & Pickrill, R. A. (2001). Benthic habitat mapping on the Scotian Shelf based on multibeam bathymetry, surficial geology and sea floor photographs. *Marine Ecology Progress Series*, 219, 121-137.
- Le Bas, T. P., & Huvenne, V. A. I. (2009). Acquisition and processing of backscatter data for habitat mapping—comparison of multibeam and sidescan systems. *Applied Acoustics*, 70(10), 1248-1257.
- Lecours, V., Dolan, M. F., Micallef, A., & Lucieer, V. L. (2016). A review of marine geomorphometry, the quantitative study of the seafloor. *Hydrology and Earth System Sciences*, 20(8), 3207.
- Lillycrop, W. J., & Hughes, S. A. (1993). Scour hole problems experienced by the Corps of Engineers; Data presentation and summary (No. CERC-93-2). COASTAL ENGINEERING RESEARCH CENTER VICKSBURG MS.
- Lucieer, V., Hill, N. A., Barrett, N. S., & Nichol, S. (2013). Do marine substrates 'look' and 'sound' the same? Supervised classification of multibeam acoustic data using autonomous underwater vehicle images. *Estuarine, Coastal and Shelf Science*, 117, 94-106.
- Lurton, X. (2003). Theoretical modelling of acoustical measurement accuracy for swath bathymetric sonars. *The International hydrographic review*, 4(2).
- Lurton, X., & Augustin, J. M. (2010). A measurement quality factor for swath bathymetry sounders. *IEEE Journal of Oceanic Engineering*, 35(4), 852-862.

- Lütjens, M. C. (2018). Immersive Virtual Reality Visualisation of the Arctic Clyde Inlet on Baffin Island (Canada) by Combining Bathymetric and Terrestrial Terrain Data (Doctoral dissertation, HafenCity).
- Madricardo, F., Foglini, F., Kruss, A., Ferrarin, C., Pizzeghello, N. M., Murri, C., ... & Fogarin, S. (2017). High resolution multibeam and hydrodynamic datasets of tidal channels and inlets of the Venice Lagoon. *Scientific data*, 4, 170121.
- Madricardo, F., Foglini, F., Campiani, E., Grande, V., Catenacci, E., Petrizzo, A., ... & Trincardi, F. (2019). Assessing the human footprint on the sea-floor of coastal systems: the case of the Venice Lagoon, Italy. *Scientific reports*, 9(1), 6615.
- Magrini G. 1934. Carta topografica idrografica militare della laguna di Venezia rilevata dal capitano Augusto Dénaix negli anni 1809-10-11. Atlante Primo, Stamperia Ferrari: Venice.
- Maicu, F., De Pascalis, F., Ferrarin, C., & Umgiesser, G. (2018). Hydrodynamics of the Po River-Delta-Sea System. *Journal of Geophysical Research: Oceans*, 123(9), 6349-6372.
- Maillet, G. M., Vella, C., Berné, S., Friend, P. L., Amos, C. L., Fleury, T. J., & Normand, A. (2006). Morphological changes and sedimentary processes induced by the December 2003 flood event at the present mouth of the Grand Rhône River (southern France). *Marine Geology*, 234(1-4), 159-177.
- Malačić, V., Viezzoli, D., & Cushman-Roisin, B. (2000). Tidal dynamics in the northern Adriatic Sea. *Journal of Geophysical Research: Oceans*, 105(C11), 26265-26280.
- Mariotti, G., & Fagherazzi, S. (2010). A numerical model for the coupled long-term evolution of salt marshes and tidal flats. *Journal of Geophysical Research: Earth Surface*, 115(F1).
- Maselli, V., & Trincardi, F. (2013). Man made deltas. *Scientific Reports*, 3, 1926.
- Marini, M., Grilli, F., Guarnieri, A., Jones, B. H., Klajic, Z., Pinaridi, N., & Sanxhaku, M. (2010). Is the southeastern Adriatic Sea coastal strip an eutrophic area?. *Estuarine, Coastal and Shelf Science*, 88(3), 395-406.
- Marriner, N., Flaux, C., Morhange, C., & Kaniewski, D. (2012). Nile Delta's sinking past: Quantifiable links with Holocene compaction and climate-driven changes in sediment supply?. *Geology*, 40(12), 1083-1086.
- Marsico, A., Lisco, S., Lo Presti, V., Antonioli, F., Amorosi, A., Anzidei, M., ... & Moretti, M. (2017). Flooding scenario for four Italian coastal plains using three relative sea level rise models. *Journal of Maps*, 13(2), 961-967.
- Mascioli, F., Bremm, G., Bruckert, P., Tants, R., Dirks, H., & Wurpts, A. (2017). The contribution of geomorphometry to the seabed characterization of tidal inlets (Wadden Sea, Germany). *Zeitschrift für Geomorphologie, Supplementary Issues*, 61(2), 179-197.
- MAV-CVN. 2004. Attività di aggiornamento del piano degli interventi per il recupero morfologico in applicazione della delibera del Consiglio dei Ministri del 15 Marzo 2001. Studi di base, linee guida e proposte di intervento del piano morfologico, Technical Report. Magistrato alle Acque di Venezia, Consorzio Venezia Nuova: Venice.
- McGonigle, C., & Collier, J. S. (2014). Interlinking backscatter, grain size and benthic community structure. *Estuarine, Coastal and Shelf Science*, 147, 123-136.

- MESH, 2008. MESH Guide to Habitat Mapping: a synopsis. Jon Davies & Sarah Young, Mapping European Seabed Habitats.
- Molinarioli, E., Guerzoni, S., Sarretta, A., Cucco, A., & Umgiesser, G. (2007). Links between hydrology and sedimentology in the Lagoon of Venice, Italy. *Journal of Marine Systems*, 68(3-4), 303-317.
- Monge-Ganuzas, M., Cearreta, A., & Evans, G. (2013). Morphodynamic consequences of dredging and dumping activities along the lower Oka estuary (Urdaibai Biosphere Reserve, southeastern Bay of Biscay, Spain). *Ocean & coastal management*, 77, 40-49.
- Montereale-Gavazzi, G. M., Madricardo, F., Janowski, L., Kruss, A., Blondel, P., Sigovini, M., & Foglini, F. (2016). Evaluation of seabed mapping methods for fine-scale classification of extremely shallow benthic habitats—Application to the Venice Lagoon, Italy. *Estuarine, Coastal and Shelf Science*, 170, 45-60.
- Montereale-Gavazzi, G., Roche, M., Lurton, X., Degrendele, K., Terseleer, N., & Van Lancker, V. (2018). Seafloor change detection using multibeam echosounder backscatter: case study on the Belgian part of the North Sea. *Marine Geophysical Research*, 39(1-2), 229-247.
- Neves, B. M., Du Preez, C., & Edinger, E. (2014). Mapping coral and sponge habitats on a shelf-depth environment using multibeam sonar and ROV video observations: Learmonth Bank, northern British Columbia, Canada. *Deep Sea Research Part II: Topical Studies in Oceanography*, 99, 169-183.
- Ninno, A., Ciavola, P., & Billi, P. (2018). The Po Delta is restarting progradation: geomorphological evolution based on a 47-years Earth Observation dataset. *Scientific reports*, 8(1), 3457.
- NOAA., 2014. How Much of the Ocean Have We Explored? <http://oceanservice.noaa.gov/facts/exploration.html>.
- Noormets, R., Ernsten, V. B., Bartholomä, A., Flemming, B. W., & Hebbeln, D. (2006). Implications of bedform dimensions for the prediction of local scour in tidal inlets: a case study from the southern North Sea. *Geo-Marine Letters*, 26(3), 165-176.
- Orlić, M., Kuzmić, M., & Pasarić, Z. (1994). Response of the Adriatic Sea to the bora and sirocco forcing. *Continental Shelf Research*, 14(1), 91-116.
- Perkins, M. J., Ng, T. P., Dudgeon, D., Bonebrake, T. C., & Leung, K. M. (2015). Conserving intertidal habitats: what is the potential of ecological engineering to mitigate impacts of coastal structures?. *Estuarine, Coastal and Shelf Science*, 167, 504-515.
- Pister, B. (2009). Urban marine ecology in southern California: the ability of riprap structures to serve as rocky intertidal habitat. *Marine Biology*, 156(5), 861-873.
- Poesen J. 2018. Soil erosion in the Anthropocene: research needs. *EarthSurface Processes and Landforms* 43(1): 64–84.
- Pousa, J., Tosi, L., Kruse, E., Guaraglia, D., Bonardi, M., Mazzoldi, A., ... & Schnack, E. (2007). Coastal processes and environmental hazards: the Buenos Aires (Argentina) and Venetian (Italy) littorals. *Environmental Geology*, 51(8), 1307-1316.

- Pranovi, F., Giovanardi, O. (1994). The impact of hydraulic dredging for short-necked clams, *Tapes* spp., on an infaunal community in the lagoon of Venice. *Sci. mar*, 58(4), 345-353.
- Preti, M. (2000) Eustatismo, subsidenza e linee di intervento per la difesa del territorio costiero in Emilia-Romagna. In: *Maree cambiamenti globali*, ICRAM, ARPA_ Ingegneria Ambientale, Bologna, IT, 2000, pp 167-179
- Pribičević, B., Đapo, A., Kordić, B., & Pijanović, N. (2016). Mapping of underwater habitats based on the analysis of backscatter intensity of the return acoustic signal. *Annual... of the Croatian Academy of Engineering*, 1, 79-96.
- Prior, D. B., & Coleman, J. M. (1982). Active slides and flows in underconsolidated marine sediments on the slopes of the Mississippi Delta. In *Marine slides and other mass movements* (pp. 21-49). Springer, Boston, MA.
- Rapaglia, J., Zaggia, L., Ricklefs, K., Gelinis, M., & Bokuniewicz, H. (2011). Characteristics of ships' depression waves and associated sediment resuspension in Venice Lagoon, Italy. *Journal of Marine Systems*, 85(1-2), 45-56.
- Rattray, A., Ierodiaconou, D., Monk, J., Versace, V. L., & Laurenson, L. J. B. (2013). Detecting patterns of change in benthic habitats by acoustic remote sensing. *Marine Ecology Progress Series*, 477, 1-13.
- Rodrigues, V., Estrany, J., Ranzini, M., de Cicco, V., Martín-Benito, J. M. T., Hedø, J., & Lucas-Borja, M. E. (2018). Effects of land use and seasonality on stream water quality in a small tropical catchment: the headwater of Córrego Água Limpa, São Paulo (Brazil). *Science of the total environment*, 622, 1553-1561.
- Rodríguez, J. F., García, M. H., Bombardelli, F. A., Guzmán, J. M., Rhoads, B. L., & Herricks, E. (2000). Naturalization of urban streams using in-channel structures. In *Building Partnerships* (pp. 1-10).
- Roelvink, D., Boutmy, A., & Stam, J. M. (1999). A simple method to predict long-term morphological changes. In *Coastal Engineering 1998* (pp. 3224-3237).
- Sarretta, A., Pillon, S., Molinaroli, E., Guerzoni, S., & Fontolan, G. (2010). Sediment budget in the Lagoon of Venice, Italy. *Continental Shelf Research*, 30(8), 934-949.
- Simeoni, U., Fontolan, G., Tessari, U., & Corbau, C. (2007). Domains of spit evolution in the Goro area, Po Delta, Italy. *Geomorphology*, 86(3-4), 332-348.
- Simonini, R., Ansaloni, I., Pagliai, A. B., Cavallini, F., Iotti, M., Mauri, M., ... & Prevedelli, D. (2005). The effects of sand extraction on the macrobenthos of a relict sands area (northern Adriatic Sea): results 12 months post-extraction. *Marine Pollution Bulletin*, 50(7), 768-777.
- Sfriso, A., & Marcomini, A. (1996). Decline of *Ulva* growth in the lagoon of Venice. *Bioresource technology*, 58(3), 299-307.
- Sfriso, A., Facca, C., Marcomini, A. (2005a). Sedimentation rates and erosion processes in the lagoon of Venice. *Environment International*, 31(7), 983-992.
- Sfriso, A., Facca, C., Marcomini, A. (2005b) Conseguenze ambientali legate alla pesca e all'allevamento della vongola *Tapes philippinarum* (Adams & Reeve, 1850) nella laguna di Venezia. 65-73 In: V. Boatto, M. Pellizzato (Eds.).

- Smith, D. (1984). The hydrology and geomorphology of tidal basins. In Chapter on the closure of tidal basins. Delft University Press Netherlands.
- Solidoro, C., Bandelj, V., Bernardi, F. A., Camatti, E., Ciavatta, S., Cossarini, G., ... & Pastres, R. (2010). Response of Venice Lagoon ecosystem to natural and anthropogenic pressures over the last 50 years. *Coastal Lagoons: Systems of Natural and Anthropogenic Change*, CRC press, Taylor and Francis, 483-511.
- Stefani, M., & Vincenzi, S. (2005). The interplay of eustasy, climate and human activity in the late Quaternary depositional evolution and sedimentary architecture of the Po Delta system. *Marine Geology*, 222, 19-48.
- Stellino, S. 2015. Mappatura degli habitat e degli oggetti antropici della laguna di Venezia. MSc thesis, University of Bologna, Italy.
- Sumer BM, Fredsøe J. 1997. Scour at the head of a vertical-wall breakwater. *Coastal Engineering* 29(3-4): 201-230.
- Sumer, B. M., Whitehouse, R. J., & Tørum, A. (2001). Scour around coastal structures: a summary of recent research. *Coastal Engineering*, 44(2), 153-190.
- Sutherland, T. F., Galloway, J., Loschiavo, R., Levings, C. D., & Hare, R. (2007). Calibration techniques and sampling resolution requirements for groundtruthing multibeam acoustic backscatter (EM3000) and QTC VIEW™ classification technology. *Estuarine, Coastal and Shelf Science*, 75(4), 447-458.
- Svane, I. B., & Petersen, J. K. (2001). On the problems of epibioses, fouling and artificial reefs, a review. *Marine Ecology*, 22(3), 169-188.
- Syvitski, J. P., Kettner, A. J., Correggiari, A., & Nelson, B. W. (2005). Distributary channels and their impact on sediment dispersal. *Marine Geology*, 222, 75-94.
- Syvitski, J. P., Overeem, I., Brakenridge, G. R., & Hannon, M. (2012). Floods, floodplains, delta plains—a satellite imaging approach. *Sedimentary Geology*, 267, 1-14.
- Temmerman, S., Meire, P., Bouma, T. J., Herman, P. M., Ysebaert, T., & De Vriend, H. J. (2013). Ecosystem-based coastal defence in the face of global change. *Nature*, 504(7478), 79.
- Tesi, T., Miserocchi, S., Acri, F., Langone, L., Boldrin, A., Hatten, J. A., & Albertazzi, S. (2013). Flood-driven transport of sediment, particulate organic matter, and nutrients from the Po River watershed to the Mediterranean Sea. *Journal of hydrology*, 498, 144-152.
- Torresan, S., Critto, A., Rizzi, J., & Marcomini, A. (2012). Assessment of coastal vulnerability to climate change hazards at the regional scale: the case study of the North Adriatic Sea. *Natural Hazards and Earth System Sciences*, 12(7), 2347-2368.
- Tosi, L., Teatini, P., & Strozzi, T. (2013). Natural versus anthropogenic subsidence of Venice. *Scientific reports*, 3, 2710.

- Tosi, L., Da Lio, C., Strozzi, T., & Teatini, P. (2016). Combining L-and X-band SAR interferometry to assess ground displacements in heterogeneous coastal environments: the Po River Delta and Venice Lagoon, Italy. *Remote Sensing*, 8(4), 308.
- Toso, C., Madricardo, F., Molinaroli, E., Fogarin, S., Kruss, A., Petrizzo, A., ... & Trincardi, F. (2019). Tidal inlet seafloor changes induced by recently built hard structures. *PloS one*, 14(10).
- Trincardi, F., Cattaneo, A., & Correggiari, A. (2004). Mediterranean prodelta systems: natural evolution and human impact investigated by Eurodelta. *Oceanography*, 17(4), 34-45.
- Tye, R. S., & Coleman, J. M. (1989). Depositional processes and stratigraphy of fluviially dominated lacustrine deltas; Mississippi delta plain. *Journal of Sedimentary Research*, 59(6), 973-996.
- Urgeles, R., Locat, J., Schmitt, T., & Clarke, J. E. H. (2002). The July 1996 flood deposit in the Saguenay Fjord, Quebec, Canada: implications for sources of spatial and temporal backscatter variations. *Marine Geology*, 184(1-2), 41-60.
- Vandelli, V., 2013. Analisi morfo-sedimentologica dell'area di piattaforma continentale antistante la costa nord-orientale dell'isola di Malta tramite l'utilizzo di dati Multibeam Echosounder. MSc Thesis.
- Van Rijn, L. C. (2005). Estuarine and coastal sedimentation problems. *International Journal of Sediment Research*, 20(1), 39-51.
- Villatoro Lacouture, M. M. (2010). Sand transport in Chioggia Inlet, Venice Lagoon and resulting morphodynamic evolution (Doctoral dissertation, University of Southampton).
- Villatoro, M. M., Amos, C. L., Umgiesser, G., Ferrarin, C., Zaggia, L., Thompson, C. E., & Are, D. (2010). Sand transport measurements in Chioggia inlet, Venice lagoon: Theory versus observations. *Continental Shelf Research*, 30(8), 1000-1018.
- Visentini, M., & Borghi, G. (1938). Le spiagge padane da Portofossone a Cervia. In *Ricerche sulle variazioni delle spiagge italiane* (pp. 1-68). CNR Roma.
- Wang, Z. Y., Li, Y., & He, Y. (2007). Sediment budget of the Yangtze River. *Water Resources Research*, 43(4).
- Wasson, K., Fenn, K., & Pearse, J. S. (2005). Habitat differences in marine invasions of central California. *Biological invasions*, 7(6), 935-948.
- Weber, J., Vrabec, M., Pavlovčič-Prešeren, P., Dixon, T., Jiang, Y., & Stopar, B. (2010). GPS-derived motion of the Adriatic microplate from Istria Peninsula and Po Plain sites, and geodynamic implications. *Tectonophysics*, 483(3-4), 214-222.
- Winterwerp, J. C., Wang, Z. B., Van Braeckel, A., Van Holland, G., & Kösters, F. (2013). Man-induced regime shifts in small estuaries—II: a comparison of rivers. *Ocean Dynamics*, 63(11-12), 1293-1306.
- Zaggia, L., Lorenzetti, G., Manfé, G., Scarpa, G. M., Molinaroli, E., Parnell, K. E., ... & Soomere, T. (2017). Fast shoreline erosion induced by ship wakes in a coastal lagoon: Field evidence and remote sensing analysis. *PloS one*, 12(10), e0187210.

- Zecchin, M., Baradello, L., Brancolini, G., Donda, F., Rizzetto, F., & Tosi, L. (2008). Sequence stratigraphy based on high-resolution seismic profiles in the late Pleistocene and Holocene deposits of the Venice area. *Marine Geology*, 253(3-4), 185-198.
- Zecchin, M., Donda, F., & Forlin, E. (2017). Genesis of the northern Adriatic Sea (northern Italy) since early pliocene. *Marine and Petroleum Geology*, 79, 108-130.
- Zhu, G., Xie, Z., Xu, X., Ma, Z., & Wu, Y. (2016). The landscape change and theory of orderly reclamation sea based on coastal management in rapid industrialization area in Bohai Bay, China. *Ocean & Coastal Management*, 100(133), 128-137.
- Zunica, M., 1971. *Le spiagge del Veneto*. Consiglio Nazionale delle Ricerche, Centro di studio per la geografia fisica, 10-129.

A. Appendix

A.1. Declaration of contributions

Study I: **Tidal inlets in the Anthropocene: geomorphology and benthic habitats of the Chioggia inlet, Venice Lagoon (Italy).**

Predominant work; Contributions: writing the manuscript (85 %), maps creation (90 %), analysis of the MBES data (75 %), analysis of the ground-truth data (80 %), commenting the manuscript (5 %).

Status: published; Paper type: full research paper, peer reviewed; Journal: Earth Surface Processes and Landforms (ESPL).

Study II: **Bathymetric and backscatter data of seafloor change of the Chioggia inlet (Venice Lagoon) as a result of human intervention.**

Predominant work; Contributions: writing the manuscript (90 %), maps creation (100 %), analysis of the MBES data (100 %), analysis of the ground-truth data (90 %), commenting the manuscript (5 %).

Status: ready to be submitted; Paper type: full research paper.

Study III: **Short-term evolution of Po della Pila delta lobe from high-resolution multibeam bathymetry (2013-2016).**

Secondary work; Contributions: writing the manuscript (25 %), maps creation (20 %), analysis of the MBES data (30 %), analysis of the ground-truth data (100 %), commenting the manuscript (10 %).

Status: submitted; Paper type: full research paper, peer reviewed; Journal: Estuarine, Coastal and Shelf Sciences (ECSS).

A.2. List of publications (not included in this thesis)

- Madricardo, Fantina; Foglini, Federica; Kruss, Aleksandra; Ferrarin, Christian; Pizzeghello, Nicola Marco; Murri, Chiara; Rossi, Monica; Bajo, Marco; Bellafiore, Debora; Campiani, Elisabetta; **Fogarin, Stefano**; Grande, Valentina; Janowski, Lukasz; Keppel, Erica; Leidi, Elisa; Lorenzetti, Giuliano; Maicu, Francesco; Maselli, Vittorio; Mercorella, Alessandra; Montereale Gavazzi, Giacomo; Minuzzo, Tiziano; Pellegrini, Claudio; Petrizzo, Antonio; Prampolini, Mariacristina; Remia, Alessandro; Rizzetto, Federica; Rovere, Marzia; Sarretta, Alessandro; Sigovini, Marco; Sinapi, Luigi; Umgiesser, Georg; Trincardi, Fabio. *High resolution multibeam and hydrodynamic datasets of tidal channels and inlets of the Venice Lagoon*. 2017. SCIENTIFIC DATA, vol. 4, pp. 170121 (ISSN 2052-4463). PUBLISHED
- Pesce, Marco; Terzi, Stefano; Al-Jawasreh, Raid Issa Mahmoud; Bommarito, Claudia; Calgaro, Loris; **Fogarin, Stefano**; Russo, Elisabetta; Marcomini, Antonio; Linkov, Igor. *Selecting sustainable alternatives for cruise ships in Venice using multi-criteria decision analysis*. 2018. SCIENCE OF THE TOTAL ENVIRONMENT, vol. 642, pp. 668-678 (ISSN 0048-9697). PUBLISHED
- Toso, Carlotta; Madricardo, Fantina; Molinaroli, Emanuela; **Fogarin, Stefano**; Kruss, Aleksandra; Petrizzo, Antonio; Pizzeghello, Nicola Marco; Sinapi, Luigi; Trincardi, Fabio. *Tidal inlet seafloor changes induced by recently built hard structures*. 2019. PLOS ONE, 14 (10). PUBLISHED

A.3. Conference contribution as presenting author

- POSTER: Madricardo, Fantina, Amos, Carl, De Pascalis, Francesca, Ferrarin, Christian, **Fogarin, Stefano**, Lorenzetti, Giuliano, Kassem, Hachem, Kruss, Aleksandra, Maicu, Francesco, Petrizzo, Antonio, Umgiesser, Georg and Zaggia, Luca (2015). *Sediment transport in a tidal inlet: the case of the Lido Inlet, Venice, Italy*. Unbounded boundaries and shifting baselines: Estuaries and coastal seas in a rapidly changing world, London, United Kingdom. 06 - 09 Sep 2015.
- POSTER: Fantina Madricardo, Federica Foglini, Aleksandra Kruss, Marco Bajo, Debora Bellafiore, Elisabetta Campiani, Francesca De Pascalis, Christian Ferrarin, **Stefano Fogarin**, Valentina Grande, Erica Keppel, Elisa Leidi, Giuliano Lorenzetti, Francesco Maicu, Giorgia Manfè, Vittorio Maselli, Alessandra Mercorella, Giacomo Montereale Gavazzi, Claudio Pellegrini, Antonio Petrizzo, Mariacristina Prampolini, Alessandro Remia, Federica Rizzetto, Marzia Rovere, Alessandro Sarretta, Marco Sigovini, Davide Tagliapietra, Fabio Trincardi. *The high resolution mapping of the Venice Lagoon tidal network*. La geologia marina in Italia-Primo convegno dei geologi marini italiani, 18 -19 February 2016, CNR Roma.
- ORAL PRESENTATION: **S. Fogarin**, F. Madricardo, L. Zaggia, A. Kruss, G. Montereale Gavazzi, C. Ferrarin, M. Sigovini, G. Lorenzetti, G. Manfè. *Benthic morphologies and habitats in a shallow highly human impacted tidal inlet*. GeoHab, Winchester, 2016.
- POSTER: Madricardo, Fantina; Foglini, Federica; Kruss, Aleksandra; Bajo, Marco; Campiani, Elisabetta; Ferrarin, Christian; **Fogarin, Stefano**; Grande, Valentina; Janowski, Lukasz; Keppel, Erika; Leidi, Elisa; Lorenzetti, Giuliano; Maicu, Francesco; Maselli, Vittorio; Montereale Gavazzi, Giacomo; Pellegrini, Claudio; Petrizzo, Antonio; Prampolini, Mariacristina; Remia, Alessandro; Rizzetto, Federica; Rovere, Marzia; Sarretta, Alessandro; Sigovini, Marco; Toso, Carlotta; Zaggia, Luca; Trincardi, Fabio. *The Challenge of High-resolution Mapping of Very Shallow Coastal Areas: Case Study of the Lagoon of Venice, Italy*, Atti del Congresso "AGU Fall Meeting 2017", American Geophysical Union – AGU.: AGU Fall Meeting 2017, 11-15 December 2017.
- POSTER: **Fogarin, Stefano**; Madricardo, Fantina; Zaggia, Luca; Ferrarin, Christian; Kruss, Aleksandra; Lorenzetti, Giuliano; Manfè, Giorgia; Montereale-Gavazzi, Giacomo; Sigovini, Marco; Trincardi, Fabio. *Benthic morphologies and sediment distribution in a shallow highly*

- human impacted tidal inlet*, Atti del Congresso "The 10th Symposium on River, Coastal and Estuarine Morphodynamics", RCEM. The 10th Symposium on River, Coastal and Estuarine Morphodynamics, September, 2017.
- POSTER: **Fogarin, S.**; Madricardo, F.; Sigovini, M.; Foglini, F.; Grande, V.; Kruss, A.; Zaggia, L.; Trincardi, F. *Benthic habitats in a highly impacted tidal inlet*, Atti del Congresso "XXVII Congresso della Società Italiana di Ecologia", Società Italiana di Ecologia S.It.E. XXVII Congresso della Società Italiana di Ecologia, September, 2017.
 - POSTER: **Fogarin, Stefano**; Madricardo, Fantina; Bosman, Alessandro; Molinaroli, Emanuela; Foglini, Federica; Kruss, Aleksandra; Romagnoli, Claudia; Correggiari, Annamaria; Remia, Alessandro; Pizzeghello, Nicola; Lamberti, Lamberto; Braga, Federica; Zaggia, Luca; Trincardi, Fabio. *Sedimentary and morphological features of a very shallow river delta: integration of high resolution multibeam bathymetry and satellite images of Po di Pila Delta (Italy)*, Atti del Congresso "GeoHab 2018 – 18th International Symposium", GeoHab. GEOHAB 2018: Marine Geological & Biological Habitat Mapping – 18th International Symposium, 2018.
 - POSTER: Madricardo, F.; Toso, C.; **Fogarin, S.**; Petrizzo, A.; Kruss, A.; Molinaroli, E.; Pizzeghello, N. M.; Foglini, F.; Trincardi, F. *Repeated multibeam surveys to assess seafloor changes induced by recently a build hard structures in a very shallow coastal environment*, Atti del Congresso GEOHAB 2018 - 18 International Symposium, GEOHAB. GEOHAB 2018 Marine Geological & Biological Habitat Mapping Conference, 18 International Symposium, May 7 - 11, 2018.